CYCLIC BEHAVIOR OF SATURATED LOW PLASTIC FINE SOILS

A THESIS SUBMITTED TO
THE GRADUATE SCHOOL OF NATURAL AND APPLIED SCIENCES
OF
MIDDLE EAST TECHNICAL UNIVERSITY

BY

SELMAN SAĞLAM

IN PARTIAL FULFILLMENT OF THE REQUIREMENTS
FOR
THE DEGREE OF DOCTOR OF PHILOSOPHY
IN
CIVIL ENGINEERING

SEPTEMBER 2011

Approval of the thesis:

CYCLIC BEHAVIOR OF SATURATED LOW PLASTIC FINE SOILS

submitted by **SELMAN SAĞLAM** in partial fulfillment of the requirements for the degree of **Doctor of Philosophy in Civil Engineering Department, Middle East Technical University** by,

Prof. Dr. Canan Özgen _____
Dean, Graduate School of **Natural and Applied Sciences**

Prof. Dr. Güney Özcebe _____
Head of Department, **Civil Engineering**

Prof. Dr. B. Sadık Bakır _____
Supervisor, **Civil Engineering Dept., METU**

Assist. Prof. Dr. M. Tolga Yılmaz _____
Co-Supervisor, **Engineering Sciences Dept., METU**

Examining Committee Members:

Prof. Dr. Haluk Sucuoğlu _____
Civil Engineering Dept., METU

Prof Dr. B. Sadık Bakır _____
Civil Engineering Dept., METU

Prof. Dr. Zülfü Aşık _____
Engineering Sciences Dept., METU

Assoc. Prof. Dr. Gürkan Özden _____
Civil Engineering Dept., DEU

Assist. Prof. Dr. Zeynep Gülerce _____
Civil Engineering Dept., METU

Date: _____

I hereby declare that all information in this document has been obtained and presented in accordance with academic rules and ethical conduct. I also declare that, as required by these rules and conduct, I have fully cited and referenced all material and results that are not original to this work.

Name, Last name: Selman Sağlam

Signature:

ABSTRACT

CYCLIC BEHAVIOR OF SATURATED LOW PLASTIC FINE SOILS

Sağlam, Selman
PhD., Department of Civil Engineering
Supervisor: Prof. Dr. B. Sadık Bakır
Co-Supervisor: Assist. Prof. Dr. M. Tolga Yılmaz

September 2011, 241 pages

Weakening and liquefaction of sands with increasing excess pore water pressures under repeated loads is well-known. Occurrence of extensive damage to the built environment also at the sites underlain by fine soils during earthquakes have led the researchers to focus on the seismic response of such soils more recently. The primary objective of this study is to investigate the factors affecting cyclic behavior of saturated low-plastic fine soils through laboratory testing. An extensive laboratory testing program including conventional soil mechanics tests, consolidation tests, reconstituted sample preparation, monotonic and cyclic triaxial tests was carried out for this purpose. Laboratory program was conducted within two parts, one of which includes the tests performed with the silt specimens reconstituted in the laboratory and the other consisting of the tests performed with the undisturbed soil samples retrieved from Adapazarı. The effects of the inherent soil properties and the effects of loading characteristics on the cyclic response of saturated low plastic silty soils were examined separately. Based on the test results, models were introduced (i) to predict the relationship between excess pore pressure ratio (r_u), number of cycles (N) and cyclic stress ratio (CSR_{tx}), (ii) to estimate the effect of initial shear stress on cyclic response, and (iii) to

show the effects of initial void ratio (e_i), initial shear stress ratio (τ_s/p'_i) and CSR_{tx} on cyclic pore pressure development.

Keywords: Cyclic Triaxial, Liquefaction, Fine Soils.

ÖZ

DOYGUN DÜŞÜK PLASTİSİTELİ İNCE ZEMİNLERİN DEVİRSEL DAVRANIŞI

Sağlam, Selman
Doktora, İnşaat Mühendisliği Bölümü
Tez Yöneticisi : Prof. Dr. B. Sadık Bakır
Ortak Tez Yöneticisi: Yrd. Doç. Dr. M. Tolga Yılmaz

Eylül 2011, 241 sayfa

Doygun zeminler tekrarli yükler altında artan aşırı boşluk suyu basınçları ile birlikte zayıflarlar. İnce taneli zeminlerin bulundugu sahalarda deprem sırasında meydana gelen zararlar, son zamanlarda araştırmacıların bu tür zeminlerin sismik davranışı üzerine odaklanmalarına sebep olmuştur. Bu bağlamda, bu calışmanın öncelikli hedefi kapsamında doygun ince taneli zeminlerin devirsel davranışını etkileyen faktörleri bir laboratuar çalışması dahilinde incelemektir. Doygun düşük plastisiteli ince taneli zeminlerin devirsel davranışını değerlendirmek üzere klasik zemin mekaniği testlerini, zemin çökeltisi oluşturma yöntemini, statik ve devirsel üç eksenli deneyleri içeren kapsamlı bir laboratuar çalışması gerçekleştirilmiştir. Laboratuar programı; laboratuarda oluşturulan silt çökeltisinden elde edilen örneklerle yapılan deneylerden ve Adapazarı'ndan alınan örselenmemiş zemin numuneleriyle yapılan deneylerden oluşan iki kısım dahilinde yürütülmüştür. Zemin ve yükleme özelliklerinin, doygun düşük plastisiteli siltli zeminlerin devirsel davranışı üzerine olan etkileri ayrı ayrı incelenmiştir. Deney sonuclarına bağlı olarak; (i) aşırı boşluk suyu basıncı oranı (r_u), devir sayısı (N) ve devirsel basınç oranı (CSR_{tx}) arasındaki ilişkiyi tahmin eden, (ii) başlangıç kesme basıncının devirsel davranışa olan etkisini tahmin eden ve (iii) başlangıç boşluk oranı (e_i), başlangıç kesme basıncı oranı (τ_s/p'_i) ve devirsel basınç

oranının (CSR_{tx}) su basıncı oluşumu üzerindeki etkisini gösteren modeller oluşturulmuştur.

Anahtar Kelimeler: Devirsel Üçeksenli, Sıvılaşma, İnce zeminler.

To My Family

TABLE OF CONTENTS

LIST OF TABLES

TABLES

LIST OF FIGURES

FIGURES

LIST OF SYMBOLS AND ABBREVIATIONS

SYMBOLS AND ABBREVIATIONS

CSR	Cyclic stress ratio
CSR_{tx}	CSR applied during cyclic triaxial test
DA	Double amplitude
D_R	Relative density
DSS	Direct simple shear
e	Void ratio
e_i	Initial void ratio
E	Young's modulus
E_1, E_N	E in the first cycle and in the N^{th} cycle
f	Frequency
FLS	Flow liquefaction surface
G	Shear modulus
G_1, G_N	G in the first cycle and in the N^{th} cycle
G_{max}	Maximum shear modulus
G_s	Specific gravity
GWT	Ground water table
K_0	Effective stress ratio
K_2	Shear modulus coefficient
K_α	The ratio of the cyclic strength under any initial shear stress to the cyclic strength without the initial shear stress
K_σ	The ratio of the CSR for a specific confining stress at the ultimate point of resistance to liquefaction to the CSR for a confining stress value of 0.1 MPa at the ultimate point of resistance to liquefaction
LI	Liquidity index
LL	Liquid limit
N	Number of cycles
NC	Normally consolidated

$N_{flexure}$, $N_{residual}$	N at flexure point and at residual point
OC	Over-consolidated
OCR	Over-consolidation ratio
p'	Mean effective stress
p'_i	Initial mean effective stress
P	Consolidation pressure
PEER	Pacific Earthquake Engineering Research Center
PGA, PGV	Peak ground acceleration and velocity
PI	Plasticity index
q	Deviator stress
r_u	Excess pore water pressure ratio
$r_{u\text{-}flexure}$, $r_{u\text{-}residual}$	r_u at flexure point and at residual point
SA	Single amplitude
SSL	Steady state line
s_u	Undrained shear strength
t	Degradation parameter
t_f	Time to failure
t_{50}	Time required for completion 50% of consolidation
USCS	Unified Soil Classification System
w_c	Water content
α	Initial shear stress ratio
δ_D	Degradation parameter
$\Delta\sigma_1$	Increase in axial stress
$\Delta\sigma_{cyc}$	Cyclic deviator stress
$\Delta\sigma_i$	Initial deviator stress
ε_a	Axial strain
γ	Shear strain
γ_c	Cyclic shear strain
γ_r	Reference shear strain
γ_t	Threshold cyclic shear strain
σ'_1, σ'_2, σ'_3	Major, intermediate and minor effective stresses
σ'_{1c}	Effective axial stress
σ'_{3c}	Effective confining stress
σ_d	Deviator stress
σ'_h	Horizontal effective stress

σ'_v	Vertical effective stress
τ	Shear stress
τ_{cyc}	Cyclic shear stress
τ_i	Initial shear stress
τ_{max}	Shear stress at failure
τ_s	Static shear stress

CHAPTER 1

INTRODUCTION

1.1 Background

It has been clearly recognized in the last 4-5 decades that the soils subjected to cyclic loads weaken or may even reach at a state of no resistance. Particularly the cyclic loads induced by the wave action affecting offshore gravity platforms and the seismic loads induced by the earthquakes have been observed as the causes which may lead soils to loose strength. The experienced cases revealed that the soils remarkably weakened due to cyclic loads were located beneath water. Seed and Lee (1966; 1967) showed that the water existing in the pores of soil grains prevails the overall cyclic response of the soils, and accordingly the term "soil liquefaction" was introduced as the state where there exists no resistance or a negligible resistance while the soil is being deformed. This definition came up as a result of observations through cyclic triaxial tests conducted over saturated sands. Subsequently, liquefaction of sands and associated damage to the structures have long been recognized as a phenomenon to be the primary concern about the structures located over high seismicity regions.

Weakening and liquefaction of sands under repeated loads is well-known. However, devastating structural damages experienced during the earthquakes occurred at the sites underlain by fine soils have led the researchers to focus on the seismic response of fine soils. Particularly, 1985 Mexico City, 1999 Izmit and 1999 Chi Chi earthquakes which have common points such as failures of shallow mat foundations underlain by silt-clay mixtures, shallow ground water table, and amplification effect due to deep alluvial basin revealed important aspects in the point of view

of geotechnical engineering, one of these is how fine grained soils behave under seismic conditions.

September 19, 1985 Mexico City earthquake was one of the most devastating ground motion caused bearing capacity failures of shallow mat foundations, which is a remarkable regard in the geotechnical engineering point of view. Many cases of demolished buildings due to excessive foundation displacements induced by tilting or settlement were observed in the city lying over deep alluvial soils. Subsoil conditions under the failed foundations are reported to be silty clays with high compressibility. The acceleration record from SCT station, located over a soft soil site, had a peak ground acceleration of 0.17g in EW and 0.091g in NS directions. The SCT ground motion records demonstrated that the motions were dominated by vibration at a period of approximately 2.0 seconds, which is near to the natural period of recording site (Seed et al., 1988; Zeevaert, 1991).

August 17, 1999 İzmit (Kocaeli) earthquake that hit Adapazarı is one of the most deadly and costly earthquakes occurred in Turkey. The affected region is the industrial vital spot and densely populated zone of the country, which makes life and economical losses more remarkable. The city of Adapazarı was one of the worst affected urban areas founded mostly on alluvial basin in the near field of the ruptured North Anatolian fault. Approximately 12 % of the total buildings in Adapazarı were heavily damaged (Yılmaz et al., 2004). The occurrence of numerous cases of displacements in various forms and levels at the foundations of three to six story reinforced concrete buildings attracted the geotechnical researchers' attention from all around the world. The studies reveal that the subsoil conditions are predominantly consisted of silt-clay mixtures at Adapazarı sites with excessive foundation displacements (Karaca, 2001; Sancio et al., 2002; Yılmaz et al., 2004). The fundamental period at the sites of silt-clay mixtures is estimated in the order of 1.8s (Bakır et al., 2002). PGA of 0.4g and PGV of 57 cm/s are obtained at a stiff site by the EW record of the earthquake. The foundation displacements occurred at the sites of silt-sand mixtures can be based on liquefaction related mechanism. However, the displacements observed on silt-clay mixtures

may not be simply attributed to the liquefaction mechanism valid for the cases of sands, although the foundation displacements on silt-clay mixtures were reported to occur due to the liquefaction of underlying soils (Bray et al., 2004; Bray and Sancio, 2006). Yılmaz et al. (2004) reported that low plastic silt clay mixtures, which dominated the studied sites of foundation displacements, did not show any tendency to be interpreted as "liquefaction" regarding stiffness and strength response, and seismic bearing capacity failure was responsible for the displacements of foundations underlain by silt-clay mixtures.

Almost one month later than the 1999 Izmit earthquake, on 21 September 1999 another earthquake with a great magnitude (M_w=7.6) hit Taiwan. The epicenter was near the small country town of Chi Chi so that the earthquake has been referred as 1999 Chi Chi Taiwan earthquake in the literature. The earthquake influenced different areas of Taiwan, and caused ground settlements and fatal structural damages all around Taiwan. Such ground settlements were reported as induced by soil liquefaction over a widespread area (Lee et al., 2001; Ku et al., 2004), and the soil underlying such liquefied areas were reported as to be consisted of sandy soils with high percentage of fine soils and silt-clay mixtures with sand.

The experiences gained via the earthquakes briefly introduced above have raised the need on identification of seismic response of fine grained soils. The cyclic response of fine soils underlying sea bed attracted scientists' interest with the need of offshore structure constructions. Accordingly, cyclic behavior of such sea bed soils was investigated and revealed as a base for design of offshore platforms with no significant discrepancy among the researchers. However, the seismic response of fine grained soils has not been clarified within a consensus. Therefore, the scope of this study is constructed on this basis.

1.2 Scope of the Study

The soils predominantly consisting of fine grained material have been reported to be liquefied and softened in the previous earthquakes (Wang 1979; Rogers et al., 1991; Boulanger et al., 1998). The identification of soil susceptibility to liquefaction and ground softening in fine grained silty and clayey soils is commonly performed using the "Chinese Criteria" (Seed and Idriss, 1982), which was constituted merely based on the data collected at sites in China by Wang (1979). Although there have been different criteria to evaluate liquefaction susceptibility of fine grained soils proposed in the last decade by Andrews and Martin (2000), Bray and Sancio (2006), and Boulanger and Idriss (2006), behavior of the soils dominated by fine grained material under repeated loading is not as clear as that of sands. Besides the background acquired through previous earthquakes, a proper testing program to be conducted over fine grained soil samples would provide a better understanding of the cyclic response in fine grained soils such that liquefaction susceptibility is evaluated and available liquefaction criteria can be revised.

Cyclic behavior of fine grained soils is relatively less studied compared to those of sandy soils. Due to the differences between the mechanisms dominating the cyclic response of fine grained and sandy soils, the procedures used to estimate the response of soils subjected to seismic loads are different for the two general soil types. Especially, the evaluation of the seismic response of silt, which is the borderline material between sand and clay in gradational order, is somewhat more complicated than that of soil that can be fairly distinguished as sand and clay (Boulanger and Idriss, 2004; Brandon et al.,2006). The experiences with ground failure in silt-clay mixtures, particularly in Mexico City and Adapazarı (Zeevaert, 1991; Hyodo et al., 1994; Yasuhara et al., 2001; Yılmaz et al., 2004), led scientists to have a profound understanding of seismic behavior of fine grained soils. Therefore, it is a strong need for advancing the knowledge on the seismic behavior of fine grained soils. Laboratory testing is a useful means that provides the researcher to control the specifications and reproduce them according to the needs. With this regard, the characteristics affecting cyclic behavior of fine

grained soils are to be elaborately investigated via laboratory testing constitute the scope of this study.

Simulation of the stress conditions existing in-situ is relatively hard to achieve in laboratory environment, especially for the case of dynamic loading. Triaxial testing is one of the most common procedures utilized to simulate either static or seismic stress conditions in laboratory conditions. In this study, the mechanisms affecting the response of the fine grained soils are investigated through triaxial with monotonic and cyclic loading tests. One of the most important reasons for selecting this type of testing is that the triaxial procedure is versatile and hence number of variables can be investigated via manipulations during testing.

The undrained shear and deformation behavior of fine grained soils are to be investigated through a series of standard and rapid monotonic loading, and stress controlled cyclic triaxial tests conducted over isotropically and anisotropically consolidated soil samples. As an objective of the study undrained monotonic tests are performed to identify any conceivable relationship between monotonic and cyclic response of fine grained soils. Performing tests on specimens having different parametric values (silt-clay mixture proportion, preconsolidation pressure, initial static shear stress,..., etc.) provide a profound understanding of cyclic behavior of fine grained soils. Based on the observations acquired from the outcome of the test series, liquefaction susceptibility of fine grained soils will be better understood, and the current liquefaction susceptibility criteria for such soils can be evaluated.

The effect of pore water pressure build up on cyclic response of saturated sandy soils has been well explained. However, the influence of pore water pressure generation on cyclic straining of saturated fine soils has not been revealed clearly. Therefore, one of the objectives of this study is to examine the pore pressure generation during cycling and to identify its effect on cyclic straining of saturated low plastic fines.

1.3 Dissertation Structure

The first chapter, which is present, includes the background that has revealed the need for such a study. It also presents the objective and scope of the subject, and the dissertation structure that briefly describes the organization of the study.

The second chapter briefly reviews the literature on seismic soil behavior investigations within a thematic heading organization. This review reveals the fundamental mechanisms involved in cyclic behavior of the soils. Therefore, the second chapter will serve as a framework to be used to examine or to enable existing approaches for progression throughout the study.

The third chapter describes general triaxial testing procedure being applied for the soils. The approach used in cyclic triaxial simulation and the limitations of triaxial testing are presented. The procedure used in preparation and placing of the triaxial specimens is included as well. All the steps implemented during monotonic and cyclic tests are described in detail. Lastly, the triaxial testing device used along the study is introduced.

In the fourth chapter, cyclic response of silt size material that was reconstituted in laboratory is investigated. The technique used during reconstitution of the silt is described. The results obtained via monotonic and cyclic triaxial tests are presented. Excess pore water pressure generation observed during cyclic tests is elaborately discussed and the relationship between r_u, N and CSR_{tx} is modeled separately for varying characteristics used during the tests. The influences induced by initial confining stress, initial shear stress, over-consolidation ratio (OCR) and loading rate are revealed in accordance with the tests performed over reconstituted silt specimens. The effect of initial shear stress on cyclic response of reconstituted silt is also modeled within this chapter. Stiffness degradation observed during cyclic tests are examined and

discussed. Lastly, existing criteria is used to examine liquefaction susceptibility of the reconstituted silt specimens.

In Chapter 5, results of cyclic and monotonic triaxial tests conducted on undisturbed soil specimens retrieved from Adapazarı are presented along with the engineering properties, sampling locations and depths. The cyclic response of Adapazarı samples are examined through the relationship between excess pore pressure and strain observed during the cyclic tests. Effects of initial characteristics of soil samples and the applied stress on the relationship between excess pore water pressure and strain are revealed by means of a statistical approach. The contributions of such factors are introduced separately. The models established in Chapter 4 are used to evaluate if the results of these tests conducted on undisturbed samples are in conformity with the models. Liquefaction susceptibility of Adapazarı soils are evaluated through existing criteria.

Chapter 6 presents a summary of overall results and conclusions of the study, and a discussion of implications for cyclic behavior of saturated fine grained soils.

CHAPTER 2

LITERATURE REVIEW

2.1 Introduction

The losses of life and property caused by seismic events have led geo-science researchers to focus on the seismic behavior of soils in the last 4-5 decades. A particular form of damage due to seismic activity is the foundation settlement and/or collapse. Nevertheless, it must be noted that developments in the soil testing technology makes it possible to investigate the seismic soil behavior in laboratory, and the models used to simulate in-situ conditions is getting better with the improvement of soil testing technology. In this chapter, the literature on the investigation of seismic soil behavior will be overviewed within a thematic heading organization. This review will serve as a framework to examine or to enable the existing approaches for progression throughout the study.

2.2 General Characteristics of Soil Behavior

At the outset, any mass of soil is classified to reveal its identity that would significantly dominate the behavior from the engineering point of view. Soil classification systems commonly used in civil engineering practice emphasize the differences essentially in terms of the particle size and size distribution characteristics for coarse grained soils, and in terms of the plasticity for fine grained soils. Although the soils are categorized into a variety of types by classification systems, sand and clay are the representatives of two distinct mechanical soil behaviors. Holtz and Kovacs (1981), and Mitchell (1993) have discussed the essential differences between sand and clay behavior in detail. Boulanger and

Idriss (2004) have itemized these basic behavioral differences in brief. Some key features for sands are reported in that study as:

- Relative density (D_R) and confining stress strongly affect the stress-strain behavior of the sand. However, there is no typical relationship between D_R and confining stress history. D_R of sand is generally dependent on the environmental factors determining deposition of the sand grains.
- Compressibility of sands is generally small enough to keep D_R almost unaltered under increasing effective stress.
- Sands are rather susceptible to disturbance during steps involved in recovering samples from field to a laboratory test device. Therefore, in situ penetration tests and use of corresponding correlations have become common practice to characterize sand deposits.

Some key features of clays are reported by Boulanger and Idriss (2004) as:

- The relationship between void ratio and confining stress history can be specific for the clays. Due to the high compressibility of clays, their void ratio or density considerably depends on the effective consolidation stress and consolidation stress history. Therefore, preconsolidation stress information of a clay deposit is the most important data in characterizing the strength and the compressibility of that clay deposit.
- Clays are less susceptible to disturbance during sampling process if it is done properly. They are impermeable enough to remain undrained during sampling, and therefore they are capable to retain their in situ effective confining stress. Nevertheless, the minor disturbance effects can also be diminished by reconsolidation of the sample to the levels suitable for the aim of evaluation. It is commonly accepted that the laboratory testing gives good results in characterizing of clay deposit in collaboration with an in situ testing program.

Obviously, as indicated by Wang et al. (2010), the behavioral properties of mixed soil types are more complicated. Nevertheless, it has been recognized that the features of silt which is the borderline material between sand and clay are not that clear and simple as those briefed above. The studies on silty soils will be referred in the proceeding review of literature.

2.3 Cyclic Behavior of Sands

The intensity of seismically induced damage at the sites underlain by loose granular soil deposits led researchers to focus on the investigation of contributing phenomena. The deposits of loose granular soils display a tendency of volumetric contraction under seismically induced ground shaking. Moreover, if the deposit is saturated or wet enough to provide development of excess pore pressures to sufficient levels due to compaction tendency, the deposit can undergo strength reduction and softening, which is the phenomenon termed as *soil liquefaction.*

The term *soil liquefaction* has remained as a hot topic because of the description complicity of the term. The term 'spontaneous liquefaction' was introduced and defined by Terzaghi and Peck in 1948. They used this term to indicate the sudden change of loose sands into a viscous fluid, which is triggered by a disturbance. The occurrence of slope failures in saturated sand deposits was explained as a result of this phenomenon.

The earthquake occurred in Niigata, Japan in 1964 became a milestone in recognition of the liquefaction phenomena by the geotechnical engineering community. An unprecedented scale of damage occurred due to liquefaction related phenomena affecting hundreds of buildings in the City of Niigata (Ohsaki, 1966). Peculiarity of the case from the point of engineering led numerous researchers to investigate the basic mechanism and the associated problems of soil liquefaction.

Under strong ground shaking, the soil deposits may be subjected to a variety of phenomena, like the onset of liquefaction and consecutive

settlements or the flow failure involving large movements of soil masses. Ishihara (1993) presented a flowchart regarding the pertinent phenomena and the associated problems in which the level and sloping ground cases are considered (Figure 2.1). In the case of level ground, after clarifying that the liquefaction will be triggered due to a specific earthquake with a given intensity, estimation of possible settlements is the next step. Whereas in the case of sloping ground, the post-seismic stability is evaluated for the liquefied soil and an assessment is made consequently whether the flow type failure is possible. Residual strength or steady state strength of the liquefied soil is used in this analysis.

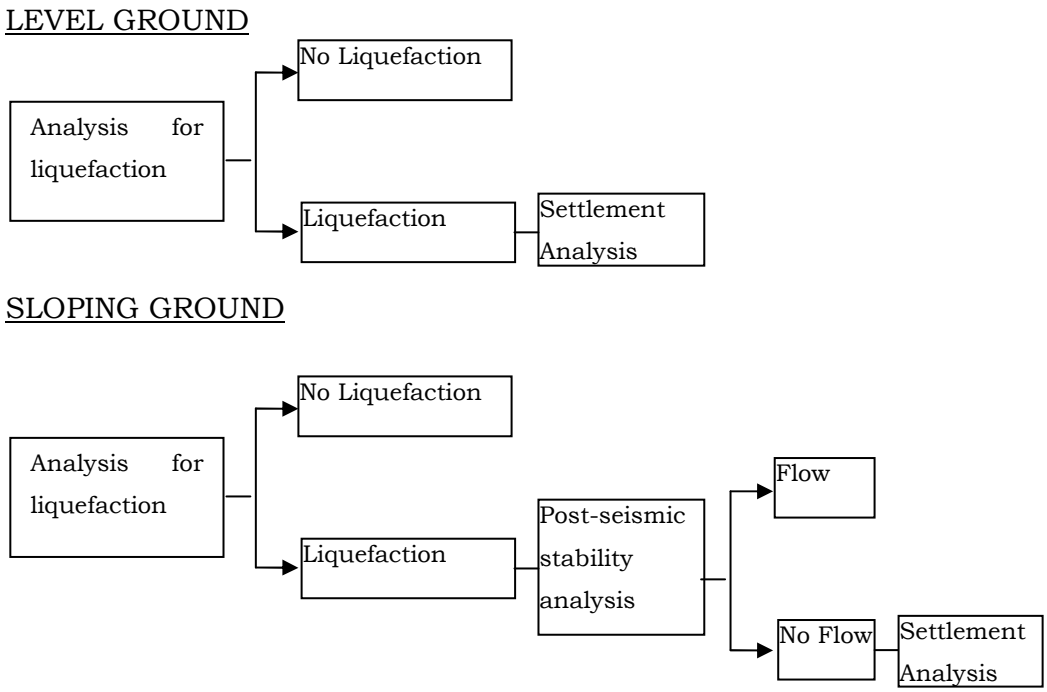

Figure 2.1 Flow chart of the problems associated with liquefaction (Ishihara, 1993)

2.3.1 Steady state of sands

During undrained shearing of sandy soils if the deformation takes place continually at constant volume and under constant shear and confining stresses, the sand is called at steady state (Castro, 1975; Castro and Poulos, 1977). The shear stress mobilized at the steady state is defined as the steady state strength or residual strength. Castro (1969) performed static and cyclic triaxial tests on isotropically and anisotropically consolidated sand specimens. From static tests, three different types of stress-strain behavior were observed as given in Figure 2.2. In the figure loose, medium-dense and dense specimens are represented by behavioral tracks of A, B and C, respectively. Loose specimens, depicted by A in Figure 2.2, initially display a peak undrained strength and then deteriorate rapidly to lower stresses with increasing strain. This type of behavior was defined as "liquefaction" earlier. However, it is recently delineated as "flow liquefaction" (Kramer, 1996). Medium-dense specimens (depicted by B) show a peak undrained strength at low strain where a strain-softening behavior starts and continues through a limited period. Then, the lowest shear stress reached at strain softening phase is followed by dilation providing a higher shear strength at large strains. The point where the state of minimum shear stress is reached by behavioral change from contractive to dilative was named as "phase transformation point" by Ishihara et al. (1975). This type of behavior was described as "limited liquefaction". Dense specimens (depicted by C), although, show a slight contraction initially then dilate until a considerably high shear strength value is reached at large strain.

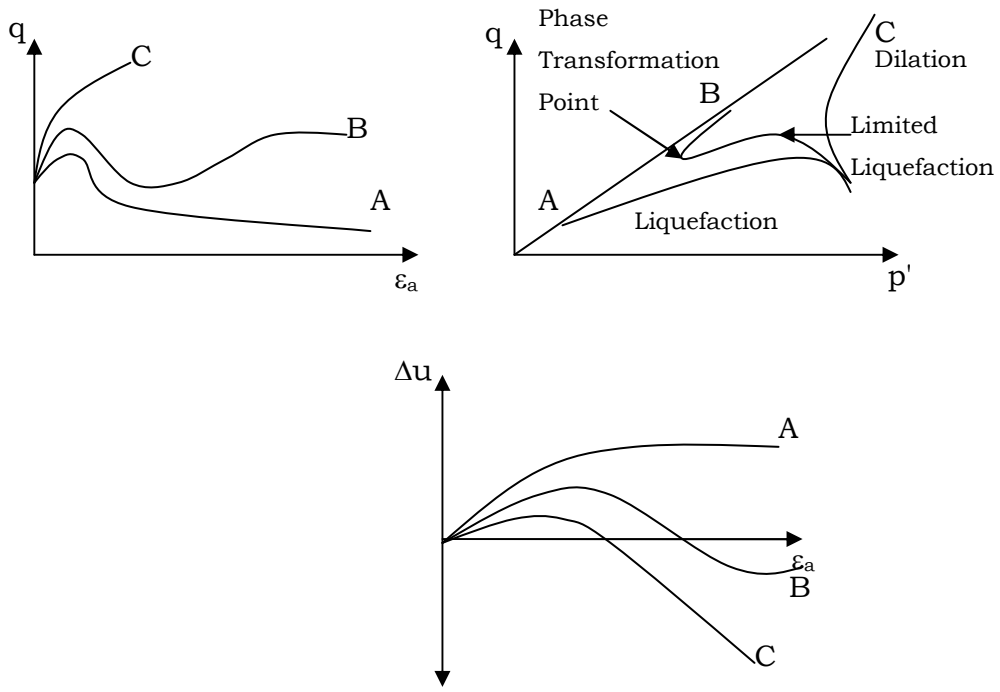

Figure 2.2 Representative types of undrained behavior of sands (after Castro, 1969).

Dilatancy is defined as an increase in volume as the soil deposit is subjected to shearing. Casagrande (1936; 1938), explained dilative and contractive behavior of sands, as well as the critical void ratio which is the void ratio at which the soil deforms without any change in volume. It was also showed by Casagrande that the critical void ratio is a confining pressure dependent parameter. The importance of volume change on stress-strain behavior of sand was also confirmed by Taylor (1948) through laboratory testing.

It has been shown that the steady state condition is dependent on stress paths in compression and extension (Vaid et al., 1990; Vaid and Thomas, 1995; Reimer and Seed, 1997). Vaid and Thomas (1995) reported that the sands reconstituted by water deposition technique do not show contractive behavior in triaxial compression, even in the loosest state of sands, and it is also reported in that study that in order to make realistic simulations, water deposition technique is a necessity in the reconstitution process. Therefore, during laboratory testing of sands,

great care must be given on depositional, stress and loading conditions that would be applied.

The locus of steady state points describing the relationship between void ratio and effective confining stress is called the steady state line (SSL). However, the general form of SSL is viewed as a tri-dimensional curve in the void ratio (e)-effective confining stress (σ'_{3c})-shear stress (τ) space. The SSL displayed in Figure 2.3a is a projection of the tri-dimensional SSL onto a plane of constant τ. The SSL can be used as a boundary to identify whether sand is susceptible to flow liquefaction or not, as indicated in Figure 2.3c. If state of the sand plots above the SSL and if the available static stress is higher than the steady state strength, the sand is specified as susceptible to flow liquefaction. On the other hand, if it plots below the SSL, the sand is specified as not susceptible to flow liquefaction. Although the SSL can be a useful tool to identify flow liquefaction susceptibility of sands and to understand basic concepts of liquefaction, it must be noted that determination of the position of the SSL is not that easy in practice.

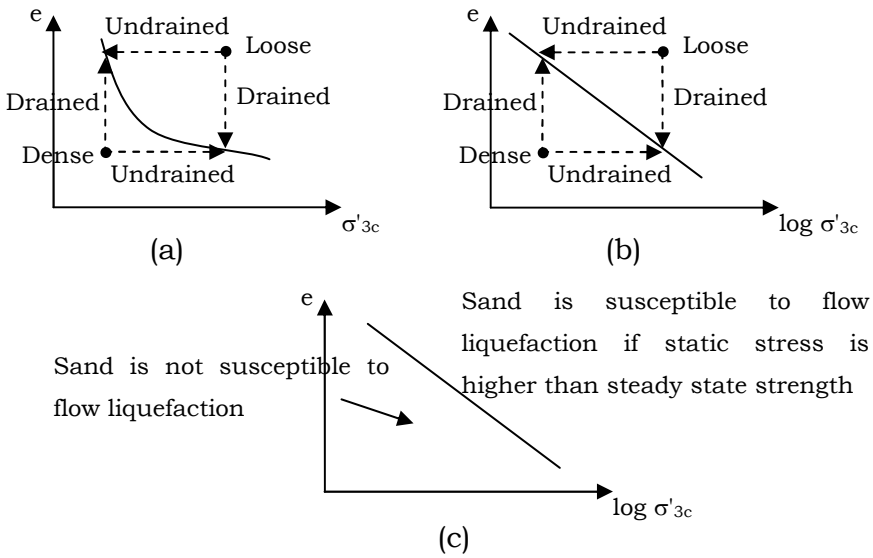

Figure 2.3 Behavior of initially loose and dense sands under drained and undrained conditions

2.3.2 Mechanism of Liquefaction

Saturated sands imposed to seismic loads are prone to contraction. If drainage conditions of those sand deposits do not permit to let the pore water out during the interval of ground vibration, decrease in volume causes the pore water pressures to increase in the saturated mass. If the excess pore water pressure generation continues so as to be equal to the overburden pressure, the effective overburden pressure becomes zero, which means a complete loss of strength of the sand deposit. The sand, thus, behaves as a liquid (Seed and Idriss, 1982). In order to illustrate the general behavior of sand subjected to cyclic loading, the results of an undrained cyclic simple shear test conducted on Monterey sand are given in Figure 2.4.

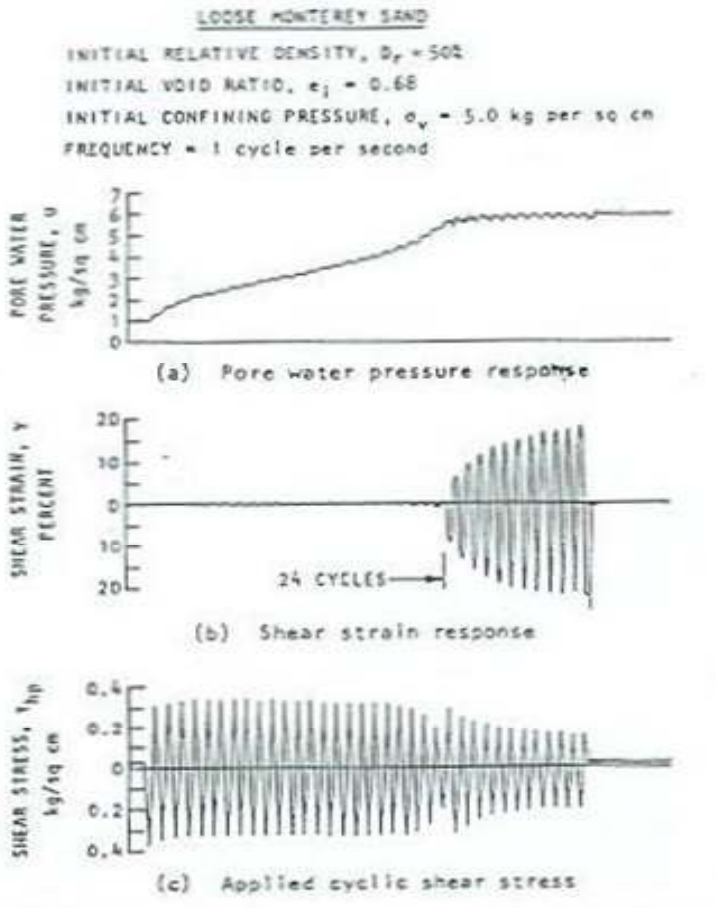

Figure 2.4 Results of an undrained cyclic simple shear test on Monterey sand (Seed and Idriss, 1982).

Basically, cohesionless soils undergo liquefaction as a result of excess pore water pressure build up due to cyclic shear stresses induced by ground shaking. Those shear stresses are imposed as being identical to the nature of wave propagation form. Therefore, the stresses occur in a cyclic random pattern during earthquakes. Nevertheless, as emphasized by Seed and Idriss (1982), the pore water pressure buildup mechanism can be quantified. The pore pressure increase and corresponding cyclic strength at any cycle of applied stresses can be approximated or computed based on the relevant information of the stress-strain characteristics and the volume change characteristics of the soil under cyclic strain conditions (e.g. Finn et al. 1977; Liou et al., 1977; Martin and Seed, 1979; Seed et al. 1976; Haldar and Miller, 1984).

The loose saturated sands exposed to cyclic loads begin to undergo large deformations with a sudden increase in pore water pressure build up. The pore pressure development during cyclic loading depends on the applied stress conditions, sample stress history as well as the soil type. Nevertheless, it is known that the accumulation rate of pore water pressure is a function of applied cycles. The pore pressure accumulation and the representative stress path for a saturated soil contracting under repeated loading were presented by Hyde and Ward (1985) as shown in Figure 2.5.

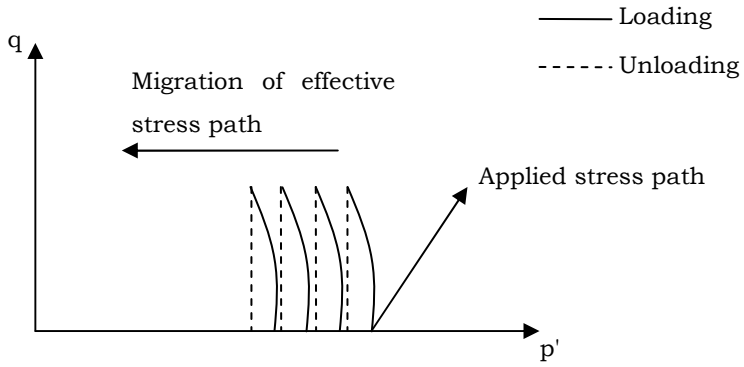

Figure 2.5 Effective stress path for a saturated soil contracting during repeated loading (Hyde and Ward, 1985)

Liquefaction susceptibility of soil deposits are evaluated by means of the approaches that are principally based on the simplified procedure proposed by Seed and Idriss (1971). Those methodologies are briefed by Youd et al. (2001). It must be pointed out that the susceptibility of a soil deposit to liquefaction does not necessarily imply that it will liquefy during a given earthquake. Therefore, it is important to understand the state of liquefaction initiation which requires a strong enough triggering disturbance.

Kramer (1996) explained the liquefaction initiation by means of the stress path of a soil subjected to monotonically increasing stresses. A stress-controlled triaxial compression test carried out on an isotropically consolidated saturated loose sand specimen was considered in that study. The stress path, stress- strain curve, pore pressure development curve and SSL of a specimen that is initially consolidated under isotropic conditions is given in Figure 2.6. Since sand is loose and plots a state well above the SSL, the specimen exhibits a contractive behavior. During shearing, depending on contraction tendency a positive pore water pressure starts to build up. However, when the specimen reaches the peak resistance state at point B the developed pore water pressure is not at its peak yet. Then the strain starts to increase dramatically similar to the trend observed in pore water pressure during the ongoing shearing following the peak resistance state. At point C and beyond, the specimen deformation takes place in the steady state and the effective confining pressure is quite less compared to that of the initial. In fact, the collapse state mechanism discussed here occurs also during liquefaction of soil induced by seismic shaking.

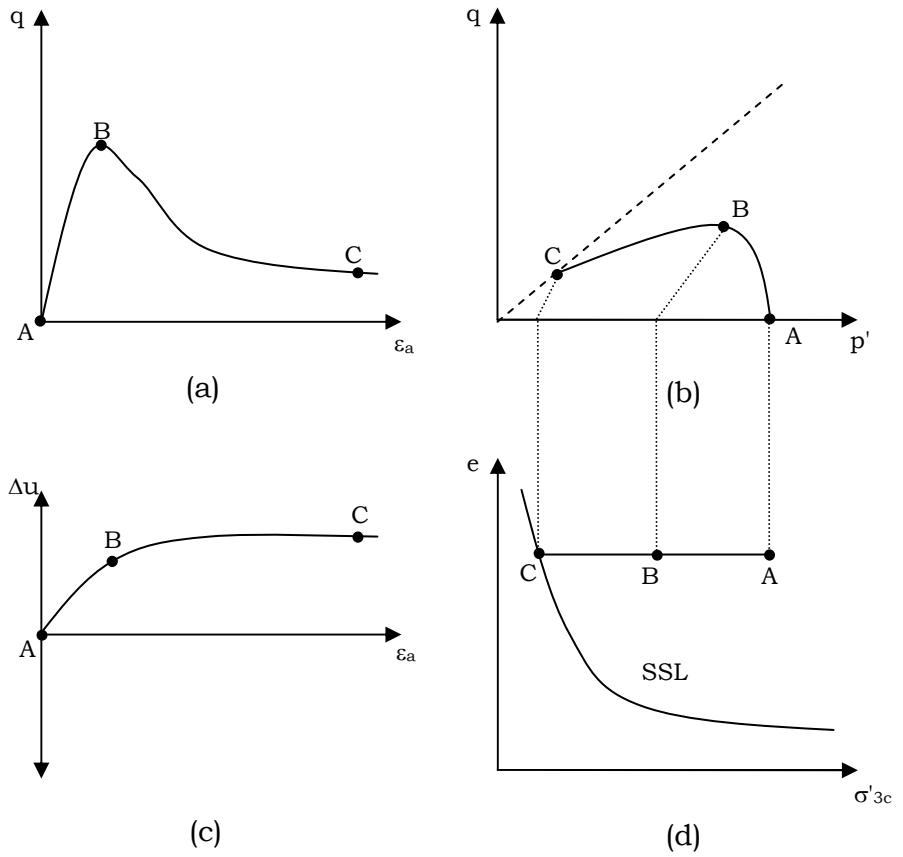

Figure 2.6 Triaxial compression behavior of loose saturated sand (a) stress-strain curve, (b) effective stress path, (c) excess pore water pressure, (d) SSL (Kramer, 1996)

If different specimens initially consolidated to the same void ratio are subjected to different effective confining pressures, they all reach the same effective stress conditions at steady state as illustrated in Figure 2.7. As the initial states of the specimens A and B plot below the SSL, they dilate during shearing. The other specimens, namely, C, D and E display contractive response as they plot above the SSL. Consequently, all the effective paths combine at steady state point. Hanzawa et al. (1979), and Vaid and Chern (1983a) reported that the locus of points corresponding to the maximum resistance states form a straight line passing through the origin. Since the soil undergoes collapse state following the mobilization of maximum resistance during undrained shearing, that straight line defines a boundary surface between the stable and unstable states in the stress path space. As the dense soils exhibit

dilation below the steady state point in stress path space, the boundary surface is truncated at steady state point level to construct a surface, named as "flow liquefaction surface (FLS)" by Kramer (1996). If the stress conditions reach the FLS during monotonic or cyclic loading, flow liquefaction is triggered (Vaid and Chern, 1983a). The FLS, thus, expresses the conditions at which the flow liquefaction is initiated.

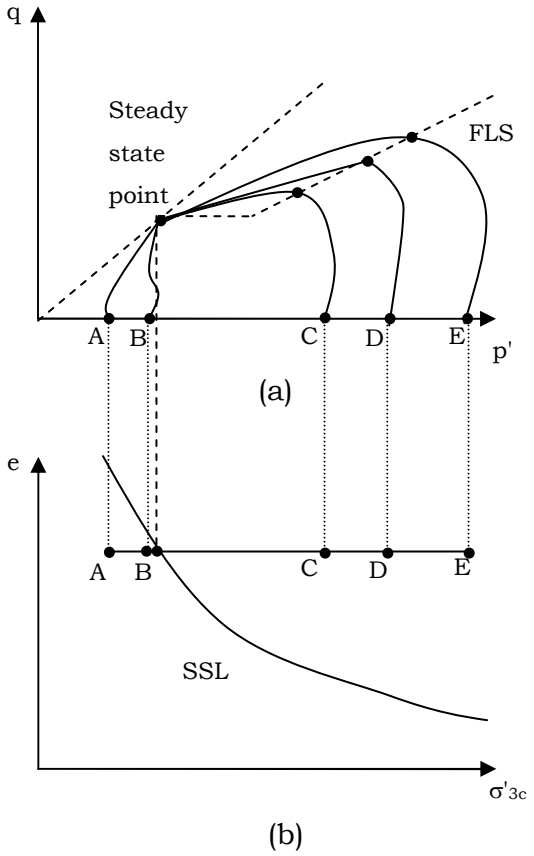

Figure 2.7 Triaxial compression behavior of loose saturated specimens isotropically consolidated to the same void ratio at different effective confining pressures (a) effective stress path, (b) SSL (Kramer, 1996)

Figure 2.8 shows two loose saturated sand specimens consolidated unisotropically to an initial shear stress τ_i and having the same void ratio. Then, one of the specimens is subjected to undrained monotonic loading while the other is cyclically loaded. The specimen loaded monotonically displays a peak resistance at point B on FLS after which it undergoes a

collapse state and reaches to steady state at point C as introduced previously. The cyclically loaded specimen, on the other hand, follows an effective stress path, moving toward left in the p'-q plot due to positive pore water pressure build up and strain accumulation. Subsequently it reaches the FLS at point D that corresponds to a lower shear stress mobilization compared to that of monotonically loaded specimen. Eventually, however, it also fails and reaches the steady state at the same point indicated by C in Figure 2.8.

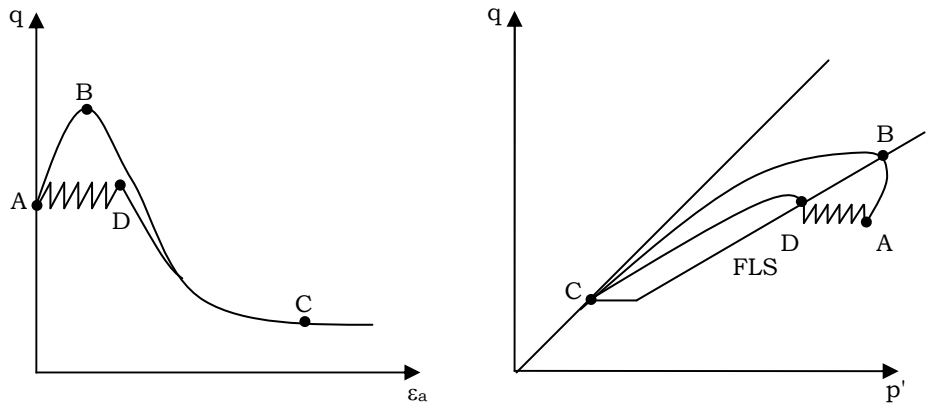

Figure 2.8 Initiation of flow liquefaction by cyclic and monotonic loading (Kramer, 1996)

2.3.3 Cyclic Mobility

Seed and Idriss (1982) pointed out that if sand that is in a loose state deforms virtually unlimited without mobilizing a significant strength to deformation, the sand is said to be liquefied. On the other hand, if the sand is in a dense state at the beginning, a high pore pressure level even equal to confining pressure (pore pressure ratio r_u of 100 %) would also occur. However, this pore water pressure would be transient due to dilation that would occur in the next cycle or in a following monotonic loading. This decrease in pore water pressure prevents the strength reduction in the sand. Due to the fact that sand does not show a full

dilation instantly, it continues to deform during mobilization of the sufficient strength against deformation. After all, there appears a cyclic strain level at which the soil will be able to withstand further deformation (DeAlba et al., 1976). This type of liquefaction related phenomenon is termed as “cyclic mobility”.

Wu (2002) explained cyclic behavior of Monterey 0/30 sand with different relative densities by using cyclic simple shear testing. The results of tests conducted over specimens having D_R values of 54 % and 77 % are given in Figure 2.9 and Figure 2.10, respectively. Figures 2.9a and 2.10a show the relationship between normalized shear stress and normalized effective vertical stress. This relationship is comparable with that of described in q-p' space. As it is seen, this plot shows the decrease in effective vertical stress with shear stresses cycling during the test. The stress-strain behavior of specimens is presented in Figures 2.9b and 2.10b. It is clearly understood from both the shear stress-effective vertical stress and stress-strain plots that both specimens show dilation at some point during cyclic behavior. The looser one exhibits a contractive behavior at first, but the dilation becomes clearer at the last few cycles. In the case of dense specimen, however, the dilation takes place even at the first cycle. Nevertheless, although the strain accumulates in almost a constant rate for the dense specimen, a significant trend of increase is observed in the last few cycles for the looser specimen. Figures 2.9c and 2.10c show the pore water pressure generation with increasing number of cycles. Figures 2.9d and 2.10d show the development track of strains with increasing number of cycles. The strain accumulation trends for loose and dense sands are more clearly seen in these plots. The pore water pressure accumulation rate and the difference between the pore pressures in extension and compression sides of a cycle dramatically increase beyond excess pore pressure ratio of 65 % for the looser specimen. However, the pore water pressure and the difference between the pore pressures in extension and compression sides of a cycle constantly increase starting from the beginning. These two figures show the difference between cyclic mobility and flow liquefaction as defined above.

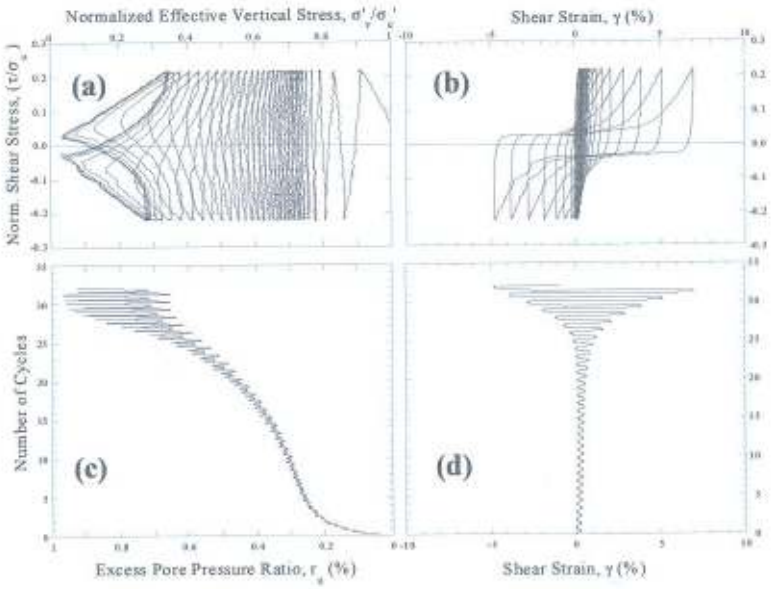

Figure 2.9 Cyclic simple shear test results for Monterey sand with D_R of 54 %, effective vertical stress of 95 kPa and CSR of 0.20 (Wu, 2002)

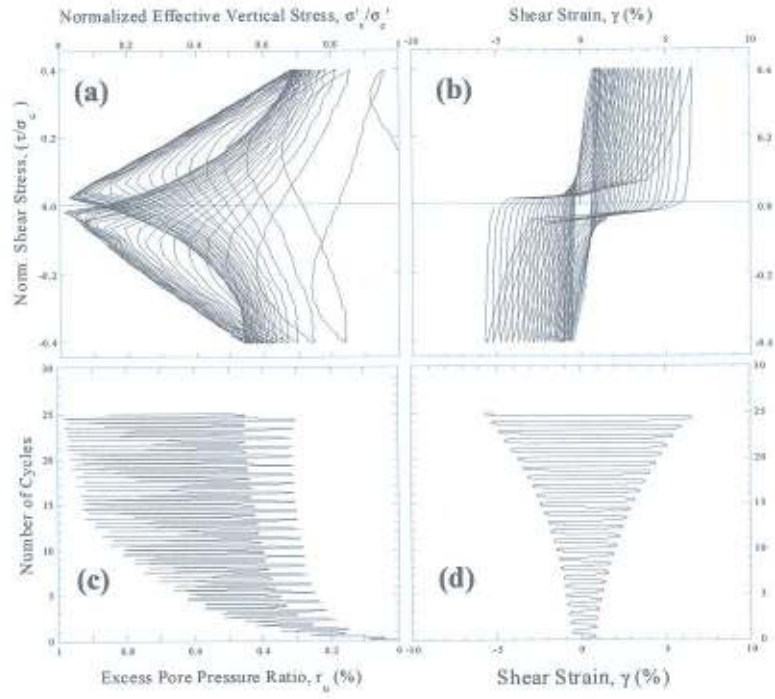

Figure 2.10 Cyclic simple shear test results for Monterey sand with D_R of 77 %, effective vertical stress of 77 kPa and CSR of 0.36 (Wu, 2002)

2.4 Factors Affecting Cyclic Behavior of Sands

Cyclic response and corresponding liquefaction susceptibility of sands are affected by certain soil properties. Those properties have been examined a number of times so far. Relative density, confining stress, initial shear stress, percentage of fine grained material and soil fabric (that results from depositional features) are those mostly mentioned in the literature. As stated previously, relative density D_R is the significant parameter in understanding both cyclic and monotonic stress-strain behavior of sands. The lower D_R values are indicator of looser state of sands, and the denser state of sands is implied with increasing D_R. Therefore, the higher D_R the sand has, the more dilative it is. Thus, the liquefaction resistance of sands increases with increasing density. Sitharam et al. (2004) showed that the shear modulus of sands clearly show an increasing trend with increasing initial density, and also reported that an increase in initial density results in a reduced susceptibility to liquefaction. The other factors that have significant influences on the cyclic behavior of sands are dealt with in the following.

2.4.1 Effect of Confining Stress

All laboratory based studies so far have indicated that cyclic strength of sands has a tendency of decrease with increasing confining stress (Ishihara, 1996). Such an influence of confinement is addressed especially for the case of high dams and tall buildings which cause substantial increases in confining stress within underlying soil deposits. This effect has been examined by means of a factor K_σ which is defined as the ratio of the cyclic stress ratio (CSR) for a specific confining stress at the ultimate point of resistance to liquefaction (the point after which the soil is presumed as liquefied) to the CSR for a confining stress value of 0.1 MPa at the ultimate point of resistance to liquefaction. The effect of confining stress was investigated by Rollins and Seed (1988), and Seed and Harder (1990). They assumed the point of 5 % double amplitude (DA) strain in 20 cycles as the ultimate point of resistance to liquefaction. Seed and Harder (1990) compiled test data on materials of earth dams and

clean sands, and presented the relationship between K_σ and effective confining stress as depicted in Figure 2.11. As it is seen in that figure, an increase of 0.1 MPa to 0.8 MPa in confining stress causes the K_σ to decrease from 1.0 to a level of 0.4, which indicates a reduction of about 40 % in cyclic strength.

Laboratory studies on reconstituted samples of a variety of sands were carried out by Vaid and Thomas (1995) in the same manner, the results of which are compiled and given by Vaid and Sivathayalan (1999) as in Figure 2.11. The results in general indicate that K_σ has a decreasing trend with increasing confining stress. Besides, it is seen that the nature of decreasing trend is dependent on the D_R value as well as the type of sand. Also, Hynes and Olsen (1999) studied the factors affecting K_c and they concluded that K_σ was strongly dependent on the method of deposition, aging properties, stress history and density of sands. It was suggested by Ishihara (1996) that the relationship between K_σ and confining stress is better to be determined separately for different materials under consideration.

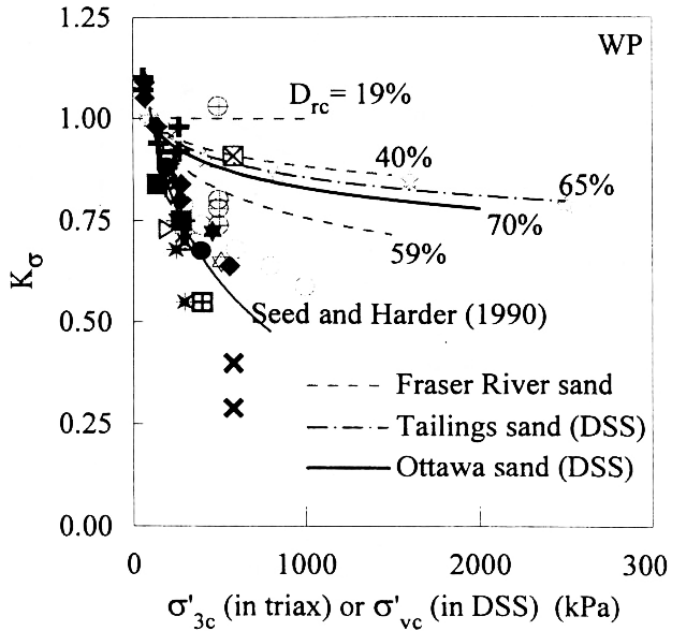

Figure 2.11 Influence of confining stress on cyclic strength of sands (adapted from Vaid and Sivathayalan, 1999)

Although Youd et al. (2001) stated "*Cyclically loaded laboratory test data indicate that liquefaction resistance increases with increasing confining stress*", they inconsistently showed that cyclic strength decreases with increasing confining stress through the curve and corresponding equation given for the relationship between K_σ and effective confining pressure. Nevertheless, as also indicated by Steedman et al. (2000), who conducted centrifuge tests on Nevada sand to investigate the effect of high confining stress on cyclic strength of sands, that increased confining stress is expected to broadly improve the resisting capacity of a soil against liquefaction, not reduce it. It was concluded in that study that the excess pore water pressure levels remain well below the initial vertical effective stress levels for the high confining stress values. Accordingly, the potential for liquefaction beneath dams was concluded as not to be hazardous as perceived to be.

2.4.2 Effect of Initial Shear Stress

Shear stress initially existing on the plane of cyclic shear stress application reveals a remarkable influence on the cyclic behavior and liquefaction susceptibility of sands. Thus the cyclic resistance of the soils underlying a structure is different from those in free field condition. Castro (1975) and Castro and Poulos (1977) performed cyclic triaxial tests on anisotropically consolidated sands. From both of these studies, it has been reported as a basic finding that anisotropic consolidation causes a decrease in the resistance to liquefaction. However, a contradictory finding was reported by Lee and Seed (1967b). This contradiction on cyclic response of sands with initial shear stress has been clarified by the proceeding studies. Vaid and Chern (1983a, 1983b), and Mohamad and Dobry (1986) showed that the cyclic strength of sands can be positively or negatively affected by the initial shear stress. The effect of initial shear stress on cyclic strength of sands was reported in detail as follows:

For the anisotropically consolidated contractive specimens (i.e. those in the loose state):

- In the case of no shear stress reversal, increasing initial shear stress decreases the cyclic strength if the sum of initial shear stress and cyclic shear stress exceeds the undrained steady-state strength.
- In the case of shear stress reversal, increasing initial shear stress increases the cyclic strength if the sum of initial shear stress and cyclic shear stress is less than the undrained steady-state strength.

For the anisotropically consolidated dilative specimens (i.e. those in the dense state), it was indicated that the increasing initial shear stress always increases the cyclic strength.

Ishibashi et al. (1985) conducted cyclic tests with hollow cylindrical torsional simple shear device using loose and dense specimens of Ottawa sand. The tests were strain-controlled and performed using uniform cyclic shear strains. It was concluded that the level of initial static shear application does not have a significant effect on resultant volumetric strains. Meanwhile, the pore pressure was found as irresponsive to the existence of initial static shear application.

Rollins and Seed (1988), and Seed and Harder (1990) also studied the effect of existing initial shear stress by means of compiled cyclic triaxial test data on sands. It was found that the cyclic strength of dense sands shows an increasing trend with increasing initial shear stress. However, the opposite tendency, a decreasing trend with increasing initial shear stress, was also reported for the loose sands in those studies.

The effect of initial stress is generally investigated by means of the plot showing the relationship between initial shear stress ratio α and the correction factor K_α. The α parameter is defined as the ratio of initial shear stress τ_i and the effective confining stress σ'_{3c}. The correction factor

K_α is defined as the cyclic strength under any initial shear stress normalized to the cyclic strength without the initial shear stress.

Vaid and Sivathayalan (1999) presented the relationship between K_α and α for the data of Fraser River sand, tailings sand and Ottawa sand. This relationship is illustrated in Figure 2.12. In the plot K_α factors suggested by Seed and Harder (1990) were superimposed with the results from the study by Vaid and Sivathayalan (1999). It was concluded that the factors proposed by Seed and Harder (1990) may be too conservative, particularly for the loose sands which are more liquefaction prone. It was also pointed out that the cyclic response of sands do not just depend on the factors individually, therefore the correction factors K_σ and K_α, at a given relative density, cannot be independent of each other and applied sequentially. The sequential application of those factors may result a great underestimation of cyclic resistance, particularly for the loose sands. The superimposed shaded zones in Figure 2.12 indicate the cyclic resistance predicted by Seed and Harder (1990) corrections.

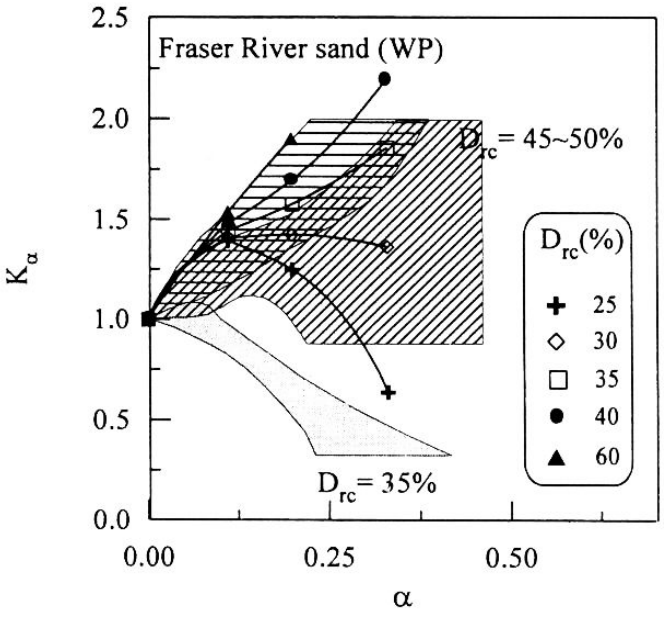

Figure 2.12 Influence of initial shear stress on cyclic strength of sands (Vaid and Sivathayalan, 1999).

2.4.3 Effect of Fines Content

The liquefied sands observed at different earthquake case histories have been reported to include silt up to high levels (e.g., Wang, 1979; Yasuda et al., 1994). Therefore, the effect of fines content has been pointed out mostly in terms of silt which is less cohesive than clay. Chang et al. (1982) performed laboratory tests to investigate the effect of silt content on cyclic strength of clean sands. It was reported that the cyclic strength increases with increasing silt content. The cyclic strengths were compared in terms of the void ratio, and the void ratio of the silty sand samples was arranged as to be the same with those of clean sand samples. Kuerbis et al. (1988) reported an opposite tendency in cyclic resistance of silty sands for a given relative density or void ratio. Nevertheless, it must be noted that the relative density has been reported as not to be a convenient index for characterizing the behavior of silty sands (Ishihara et al., 1980). Void ratio instead of relative density was preferred for comparison of silty sand behavior by Ishihara et al. (1980). However, Vaid (1994) suggested on the basis of the monotonic test results conducted on Brenda silty sands that the use of void ratio may also be inadequate for characterizing of silty sands. In that study, no significant behavioral difference was observed although the void ratio substantially decreased with increasing silt content. The use of void ratio of the sand skeleton instead of total void ratio is recommended as an alternative index for characterizing behavior of silty sands. It is concluded that the cyclic strength increases slightly with increasing silt content when the sand skeleton void ratio remains fixed.

Koester (1994) conducted five hundred undrained cyclic triaxial tests on reconstituted sand, silt and clay mixtures. The samples were prepared corresponding to 50% relative density of the sand fraction before addition of fines. It is concluded that the cyclic strength is reduced by increasing amount of fines up to 24% to 30% of the total specimen dry weight. Addition of fines beyond this fractional weight is concluded to render cyclic response of the samples as being dominated by fines content.

Accordingly, the cyclic strength of the samples is reported to increase with increasing amount of fines beyond 24% to 30% fractional weight. Thevanayagam et al. (2000) reached similar conclusions with those reported by Koester (1994) regarding the cyclic response of silty sands. However, the threshold silt content at which the cyclic response begins to increase was not reported; it was stated that the threshold content was dependent on the characteristics of fine and coarse particles and the total void ratio.

The experimental studies carried out by Lade and Yamamuro (1997), Yamamuro and Lade (1999), and Yamamuro et al. (1999) reveal that the sands with significant silt content are more liquefiable than clean sands. Nevertheless, Yamamuro and Covert (2001) performed tests on specimens composed of Nevada 50/200 sand with 40% silt content. It is concluded that the undrained behavior of these specimens with high silt content is highly contractive; accordingly, the observed axial strains are much greater than those of clean sands or sands with lower silt contents.

Sitharam and Dash (2008) performed undrained cyclic triaxial tests on specimens composed of Ahmedabad sand with different fines percentage. The cyclic resistance is found to reach the lowest value for a silt content of 20%, and with further increase in silt content the cyclic resistance increases and reaches a value almost twice the cyclic resistance of clean sand at a silt content of 75% (Figure 2.13). It is indicated that below limiting silt content the response of the soil is dominated by the sand matrix, and beyond, by the silt.

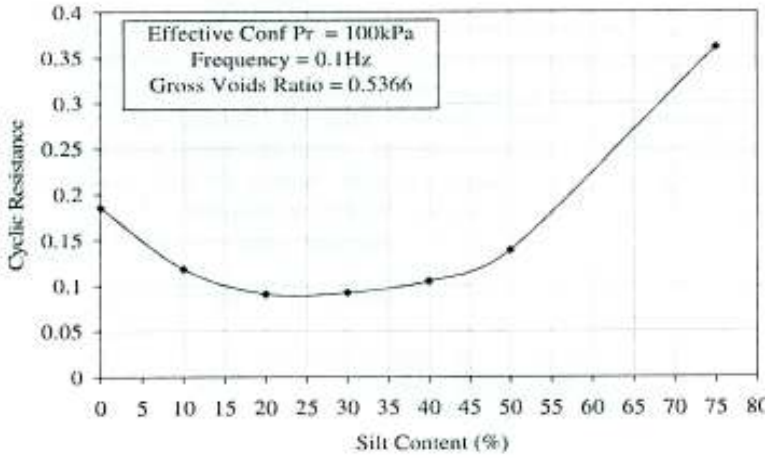

Figure 2.13 Cyclic resistance of Ahmedabad sand with increasing silt content (Sitharam and Dash, 2008).

2.4.4 Effect of Soil Fabric

The need for the test repeatability and investigation of the effects of particular factors on soil behavior necessitates the use of reconstituted samples in laboratory. Fundamental studies of soil behavior also require homogeneous specimens to obtain uniform stress-strain states. In-situ conditions of soil are presumably well simulated in the laboratory utilizing the methods of reconstitution. A variety of reconstitution techniques have been developed and reported as having significant influence on the behavior of samples being tested in the laboratory (Mulilis et al., 1977; Tatsuoka et al.,1986; Vaid et al., 1995; Vaid and Sivathayalan, 1999; Yamamuro and Wood, 2004;). Moist tamping, air pluviation, water pluviation, and slurry deposition are the commonly used techniques of reconstitution.

Vaid et al. (1995) performed undrained direct simple shear tests on Syncrude sand reconstituted by moist tamping, air pluviation and water pluviation. The stress-strain behaviors of the specimens reconstituted to identical initial states by different methods obtained in that study are presented in Figure 2.14. Moist tamped specimen shows a pronounced strain softening behavior, which reaches to steady state eventually. Air

pluviated specimen also shows strain softening behavior but not as distinctive as the moist tamped sand. The water pluviated specimen, on the other hand, displays dilative behavior. Similar tendencies for the air and water pluviated sand specimens tested by triaxial compression are reported by Vaid et al. (1999) as well. Water pluviation technique has been considered the most useful technique to simulate the fabric of fluvial and hydraulic fill sands (Oda et al., 1978; Vaid and Sivathayalan, 1999).

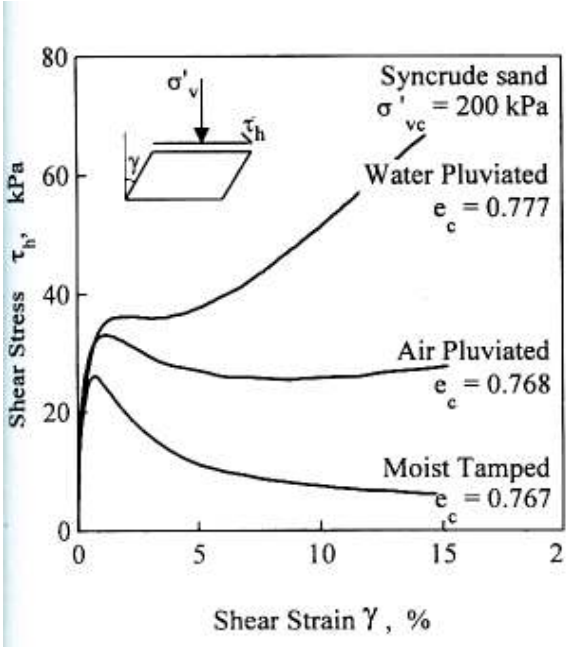

Figure 2.14 Effect of sample reconstitution technique on undrained response of sand (Vaid et al. 1995)

2.5 Cyclic Behavior of Fine Grained Soils

The behavior of deposits composed of fine grained soils subjected to loads induced by earthquakes, ocean storms (i.e. off-shore structures), pile driving, traffic or other causes has been attracting the interest of researchers and scientists for many decades. As indicated previously, the cyclic response of sands and relatively clean sandy soils under seismically induced loads has been comprehensively documented within a scientific consensus. On the other hand, the fine grained deposits have also been reported either as liquefied or underwent severe strength or bearing

capacity loss during past earthquakes (Tohno and Yasuda, 1981; Youd et al., 1985; Boulanger et al., 1998; Yılmaz et al. 2004). Still, however, there exist contradictory issues to be resolved regarding the seismic response of fine grained soils.

It is widely known that the silt deposits are prone to earthquake damage. Based on the reported case histories of liquefied silts in the past earthquakes, Youd et al. (2001) evaluated the liquefaction susceptibility of silts in the series of the workshops sponsored by the National Center for Earthquake Engineering Research (NCEER). However, as also indicated by Sanin and Wijewickreme (2006), no clear consensus was reached as regards the assessment of liquefaction potential of silts in those workshops. Hence, the need for further research is clear to improve the present level of knowledge and the available database on the seismic behavior of silts as emphasized by Sanin and Wijewickreme (2006), and Boulanger and Idriss (2004).

Although the cyclic response of fine grained soils is controlled by a number of parameters, Sanin and Wijewickreme (2006) reported, in a general sense that the low plastic, deltaic silt (Fraser River silt) deposit does not show a behavior that can be interpreted as flow liquefaction. The behavior observed in their study was cyclic mobility type strain softening which is independent of the applied CSR or the level of pore pressure ratio developed during the tests. The same authors reported in another study that the progressive stiffness degradation with gradual excess pore pressure development the Fraser River silt displayed is more similar to dense sand behavior rather than that of the relatively loose sand in terms of cyclic response (Wijewickreme and Sanin, 2010).

Bray and Sancio (2006) stated that the undisturbed non-plastic silts recovered from Adapazarı-Turkey also show cyclic mobility type response as indicated by Sanin and Wijewickreme. The soils tested in that study were composed of fine contents greater than 70% with plasticity index (PI) ranging between 0 and 25. It is indicated that even loose silt specimens resulting pore pressures close to initial effective confining stress dilate during shearing and produce a dramatic increase in stiffness, and

consequently they show a constant strain accumulation for each cycle. Bray and Sancio (2006) concluded that cyclic response of fine grained soils are typically manifested as cyclic mobility, and hence, their seismic response is less likely to cause large deformations like those observed at the sites of saturated loose clean sands.

Boulanger and Idriss (2006; 2007) categorized the seismic behavior of fine grained soils based on their plasticity. The fine grained soils having plasticity indeces below a particular value are presumed to behave like sands, whereas those having plasticity indices above are presumed to behave like clays. The difference between the cyclic responses of sand and clay is pointed out in association with the liquefaction susceptibility of these soil types. The sand-like fine grained soils are accepted as susceptible to liquefaction under analogous conditions required to cause liquefaction in sands. The potential for strength loss in clay-like fine grained soils is interpreted depending on the soil's sensitivity and the magnitude of seismically induced shear strains (Boulanger and Idriss, 2007). The sensitivity of the soil is expressed as the ratio of peak shear strength to remolded shear strength. Normally consolidated (NC) or lightly overconsolidated clays generally have higher water contents, higher liquidity index (LI) and higher sensitivities. Therefore, these types of clays are reported as being more prone to strength loss during earthquakes than the well-compacted or heavily overconsolidated clays. However, it is also noted that the significant earthquake induced ground deformations are less frequently encountered in clays than in sands.

The cyclic behavior of clays attracted interest of geotechnical researchers particularly due to the need for design criteria of offshore structures (e.g. Andersen et al., 1980; 1988; Andersen and Lauritzsen, 1988; Azzouz et al., 1989; Hyodo et al., 1992). The foundation clays at the seabed are imposed to cyclic loads induced by the wave action during storms. As the duration of storm loading is much longer than the duration of loading during an earthquake, the effects of long-term cyclic loading on clays had to be clarified for the design of foundations of offshore structures. Yasuhara et al. (1992) stated that although saturated clay does not fail

easily like saturated loose sand under earthquake loads, it behaves differently when imposed cyclic load continues for a long period of time.

Andersen et al. (1988) elucidate the simplified stress conditions along a potential failure surface beneath a structure as shown in Figure 2.15. As it is seen in that figure, the combination of cyclic and static shear stresses varies point to point along a potential failure surface. Therefore, it is stated that in order to investigate the cyclic loading effects on foundation soils it was necessary to perform both direct simple shear (DSS) and triaxial tests on specimens with a range of initial shear stresses. Having performed cyclic DSS and triaxial tests, Andersen et al. (1988) formed diagrams displaying cyclic response of marine clay called Drammen clay. The diagrams show the relationships between applied cyclic shear stress, initial shear stress, overconsolidation ratio (OCR) and number of cycles. The diagrams are aimed to provide a general knowledge about the behavior of clay for preliminary design of offshore structures. Since the tests were conducted with constant amplitude cyclic stresses, the equivalent number of load cycles with constant cyclic stress that will provide the same effect as the real irregular cyclic history of a storm is required to be determined. The equivalent number of cycles is reported to be determined using shear strain or pore water pressure expected to develop during a storm. These characteristics are reported as “memory” characteristics of clays.

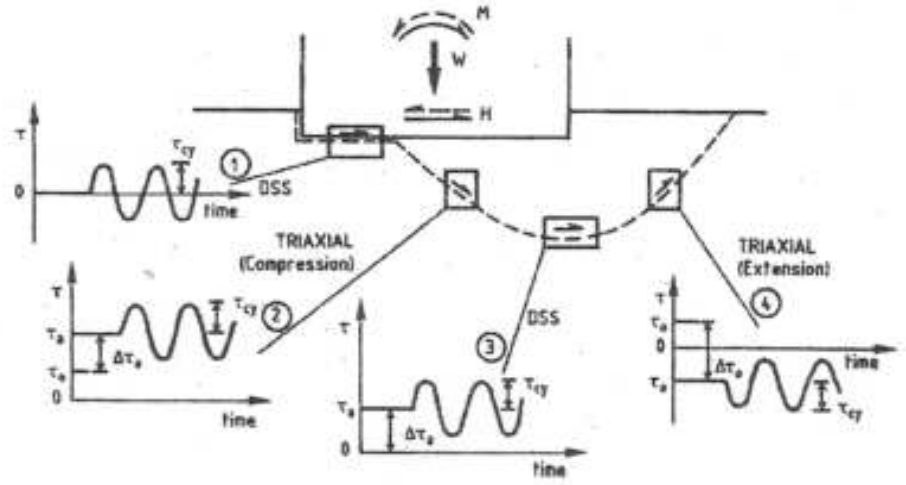

Figure 2.15 Simplified stress conditions for soil elements along a potential failure surface beneath a structure (adopted from Andersen et al., 1988).

As the excess pore water pressure development induced by the cyclic loading causes a reduction in the effective stress, the initially sustained effective stress over the specimen is altered. As a result, the specimen becomes overconsolidated during cyclic loading. This type of behavior, which is termed as “apparent overconsolidation”, is reported to manifest the cyclic response of clays (Azzouz et al., 1989; Yasuhara et al., 1992). Apparent overconsolidation occurs without a change in the water content and volume, unlike the mechanical overconsolidation. A hypothesis based on apparent overconsolidation is proposed to predict undrained cyclic response of slightly overconsolidated clays using results of NC clays by Azzouz et al., 1989.

The information relating to the cyclic behavior of fine grained soils cited in literature is stated briefly in the preceding paragraphs. The significant characteristics governing the cyclic response of fine grained soils and in part still being searched are discussed comprehensively in the following sub-headings.

2.5.1 Pore Water Pressure Generation

Under cyclic loading conditions, progressive of pore water pressure generation may result in saturated soils. This additional pore water pressure is referred to as the excess pore water pressure. As it is stated by Polito et al. (2008), the excess pore water pressure build-up during cyclic loading can be separated into two components as the transient and residual excess pore pressures. Increment in total stress applied to the soil develops transient pore pressures equal to the applied stress increment (Lambe and Whitman, 1979). Those transient excess pore pressures have little influence on the effective stresses acting over the soil. The residual excess pore pressures develop as a result of irreversible deformation of the soil skeleton. Therefore, the residual excess pore pressures are those dominating the change in effective stress acting on the soil. The excess pore pressures built-up at the state of zero cyclic deviator stress during stress-controlled cyclic tests are residual excess pore pressures (Dobry et al., 1982).

Matasovic and Vucetic (1995) conducted cyclic undrained direct simple shear tests on clays to investigate the pore pressure generation during cyclic loading. It is stated that the pore pressure generation occurs in each cycle of loading, independent of applied cyclic shear strain amplitude γ_c. However, if the applied cyclic shear strain (γ_c) is smaller than a value of threshold cyclic shear strain γ_t, there will be no residual excess pore water pressure remaining after cyclic loading ceased. In the same manner, if γ_c is larger than γ_t, excess residual pore pressure progressively builds up and remains even after ceasing of the cyclic loading. Hsu and Vucetic (2006) reported that γ_t in cohesive soils is larger than in cohesionless soils. According to the results of cyclic direct simple shear tests conducted on silts and clays having PI values between 14 and 30, Hsu and Vucetic (2006) concluded that γ_t ranges between 0.024 and 0.06%, while it varies between 0.01 and 0.02% for sands and gravels. As another outcome of the study, γ_t in silts and clays does not seem to significantly depend on applied vertical consolidation stress during the tests.

Vucetic (1994) reported that the threshold cyclic shear strain (γ_t) depends on the PI of the soil and there is no significant relation with OCR. Nevertheless, it has been shown that the excess pore water pressure generation is always positive during shearing of NC clays, whereas it may be negative for OC clays (Anderson et al., 1980; Matsui et al., 1980; Ohara and Matsuda, 1988; Vucetic, 1988). Figure 2.16 presented by Vucetic (1988) shows that negative pore water generation increases with increasing OCR. It also observed that the pore water pressure generation tends to be positive with increasing number of cycles in general.

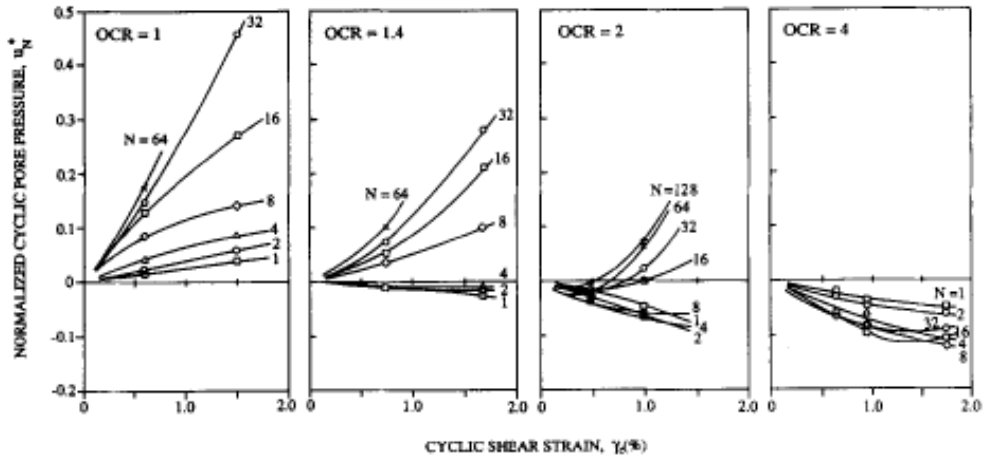

Figure 2.16 Pore water pressure generation tendency during cyclic shearing (Vucetic, 1988)

Ohara and Matsuda (1988) performed strain controlled cyclic simple shear tests on NC and OC kaolinite. The relationship between cyclic shear strain γ_c applied and pore water pressure ratio obtained in that study is given for NC clay in Figure 2.17. The pore water pressure ratio increases with increasing cyclic shear strain. As also indicated by many researchers, it is observed that no excess pore pressure generation occurs below a threshold value of applied cyclic shear strain. It is also concluded in the study that the excess pore water pressure generation decreases with increasing OCR, and γ_t increases with increasing OCR.

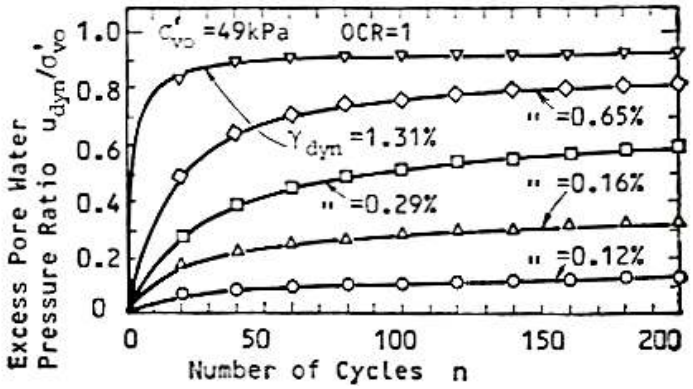

Figure 2.17 Excess pore water pressure variation with applied cyclic shear strain, γ_c (Ohara and Matsuda, 1988).

Okur et al. (2008) conducted stress controlled dynamic triaxial and dynamic hollow torsional tests on fine grained soils having PI values ranging between 9% and 45%. The tests were conducted under a low loading frequency of 0.001 Hz. It is shown in the study that pore water pressure generation begins more rapidly in the specimens having lower values of PI. Another outcome of the study is that, the pore pressure ratio (r_u) reaches the peak value of about over 90% under double amplitude (DA) strain of 5% where shear modulus (G) decreases to the levels of 10% of the maximum (G_{max}), where G_{max} was defined as the shear modulus during the first cycle. The peak r_u value is stated to be reached at relatively high number of cycles which is unlikely to occur during a seismic loading. The variation of shear modulus ratio (G/G_{max}) as a function of the excess pore water pressure ratio derived in the study is presented in Figure 2.18. In the figure, the effect of PI on generation of pore water pressure and stiffness degradation can also be observed. For a given degradation degree of stiffness, the generated excess pore water pressure increases with increasing PI.

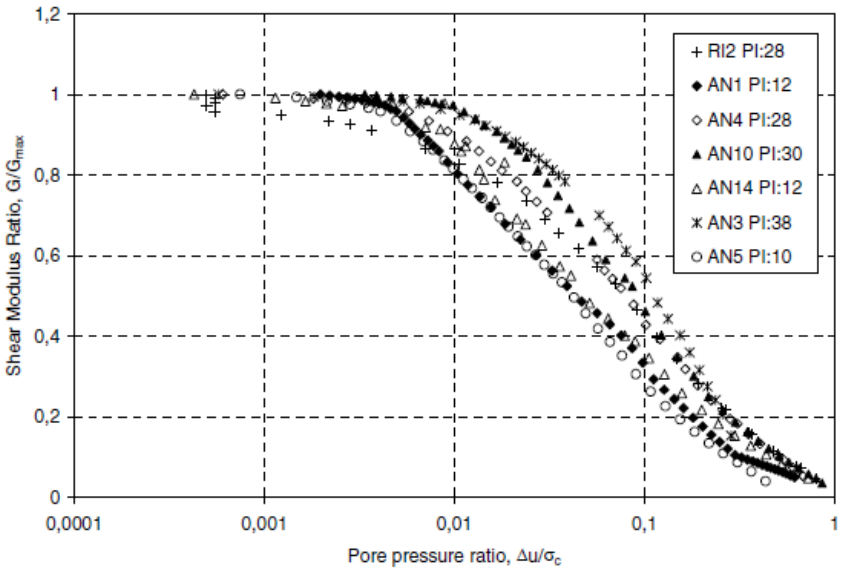

Figure 2.18 Variation of stiffness degradation with respect to excess pore water pressure (Okur et al., 2008)

Hyodo et al. (1992) performed cyclic triaxial tests on clay specimens with a loading frequency of 0.1 Hz. The CSR values used in tests ranged between 0.35 and 0.60. It was observed that the generated excess pore water pressure ratio decreased with increasing CSR as shown in Figure 2.19. However, Hyde and Ward (1985) reported an increasing tendency of pore water pressure generation with CSR in cyclic triaxial tests performed on silty clay with a loading frequency of 0.1 Hz.

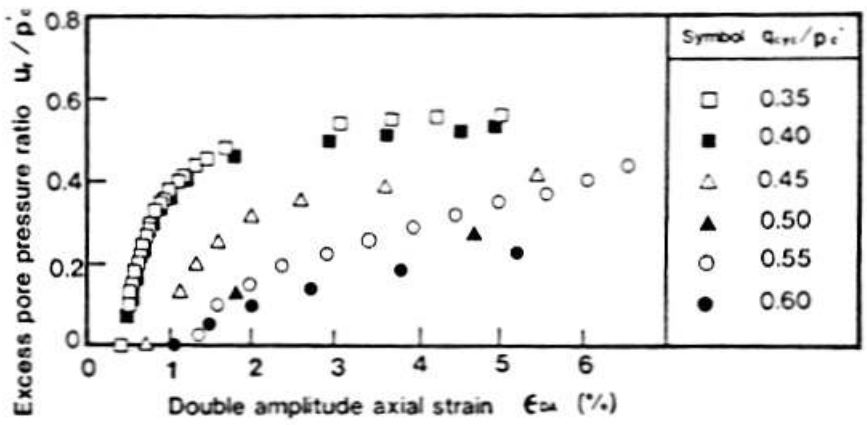

Figure 2.19 Variation of excess pore water pressure with DA axial strain corresponding to different CSR values (Hyodo et al., 1992).

A series of cyclic triaxial tests were conducted on soft marine clay by Jiang et al. (2010). The excess pore water pressure ratio was found to increase with decreasing loading frequency. It was also observed that the excess pore pressure ratio did not exceed 0.18 even after 3000 number of cycles in any test conducted with a CSR value of around 0.20. The rate effect on pore water pressure generation was also observed in monotonic triaxial tests on clayey silts performed by Konrad and Wagg (1993). Both isotropically (abbreviated as CIU) and anisotropically (abbreviated as CAU in the Figure 2.20) consolidated specimens were tested in the study, and the pore pressure was measured at middle and bottom end of the specimens during the tests. The monotonic tests were carried out with different axial strain rates (%/s) for which the maximum differences between the pore water pressure measurements at base and middle are shown in Figure 2.20. As it can be seen, the pore pressures measured at the base of the specimens are higher than those at the middle. It is conluded that during the test the difference between pore pressures at the base and middle reaches a peak and remains constant afterwards. As it is seen in the figure, the difference becomes greater with increasing strain rate. Also, the maximum difference occurs at negligible levels for the tests conducted with a strain rate lower than 0.001 %/s. Ten years earlier than the study by Konrad and Wagg (1993), Kimura and Saitoh (1983) conducted much slower monotonic triaxial tests on cohesive soils. They observed that at low strains the pore pressure at the center of the specimen was greater than that of at the bottom while at high strains the difference occurred at negligible levels. The difference between pore pressures at the center and bottom of the specimens is reported to get smaller by decreasing strain rate.

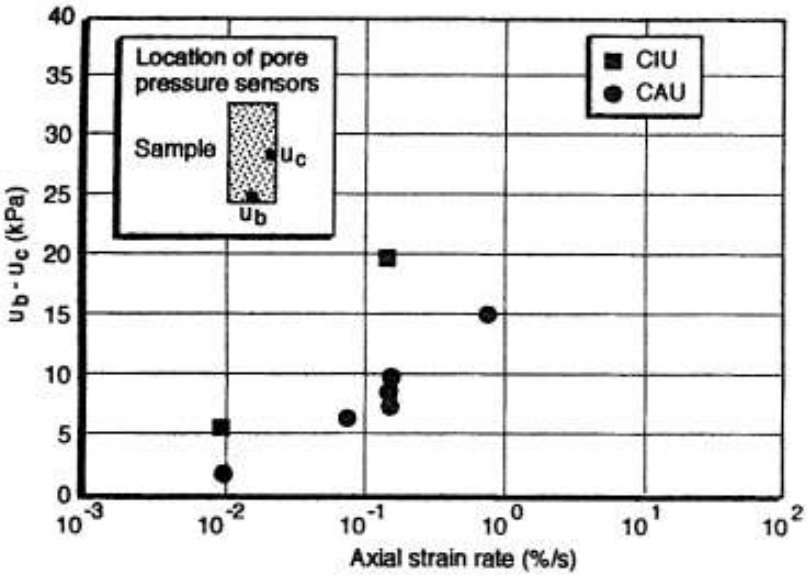

Figure 2.20 Maximum differences between pore water pressure measurements at the base and middle of the specimens tested monotonically (Konrad and Wagg, 1993)

2.5.2 Effect of Initial Confining Stress

The initial state of stress of fine grained soils has been investigated and reported as a significant characteristic influencing the cyclic behavior by many researchers.

Mitchell and King (1977) carried out stress controlled cyclic triaxial tests on Champlain Sea clay at effective confining stress levels less than the preconsolidation pressure (170 kPa) of the samples. It is shown in the study that the pore water pressure increases at early cycles of the loading, followed by decreases for the samples with low initial confining stresses as shown in Figure 2.21. The initial confining stress used in the tests ranged between 10 and 150 kPa. As it can be observed in the figure, excess pore water generation increases with increasing initial confining stress. Interestingly, it is also observed that the samples having initial confining stresses between 50 and 100 kPa reach failure earlier than the samples with lower confining stress. The larger cyclic strength observed for the samples with lower confining stress is attributed to the generated

excess pore water pressure level which is almost zero. The zero level of excess pore water pressure is due to applied cyclic deviatoric stress that is lower than a threshold level required for the generation of excess pore water pressure. On the other hand, the larger cyclic strength observed for the samples with confining stresses higher than 100 kPa is attributed to the reduction in dilation due to the increasing confining stress approaching to NC state of stress.

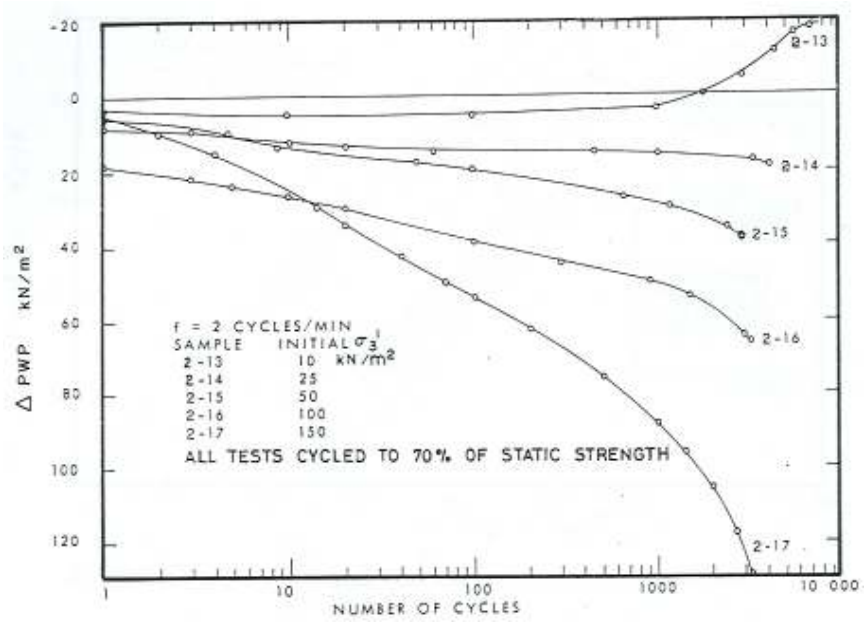

Figure 2.21 Excess pore water pressure response observed for different initial confining stresses (Mitchell and King, 1977).

In order to examine the effect of confining stress on cyclic response of fine soils, Ishihara (1996) carried out cyclic triaxial tests on volcanic clay samples under confining stresses of 20, 50 and 80 kPa. Real earthquake loading histories were utilized during the tests. In each test series, the specimens were consolidated under a specific confining stress. Subsequently, an initial shear stress equal to 70% of the static strength of the clay was applied. The curves showing the average trend of stress-residual strain behavior obtained for the confining stresses are displayed in Figure 2.22. As it can be seen, the ratio of cyclic strength and static strength decreases as the confining stress increases. The dashed lines in

the figure represent the static stress-strain behavior of the specimens. It is concluded that the trends observed in Figure 2.22 reveal that during dynamic loading both stiffness and ultimate strength of the samples increase.

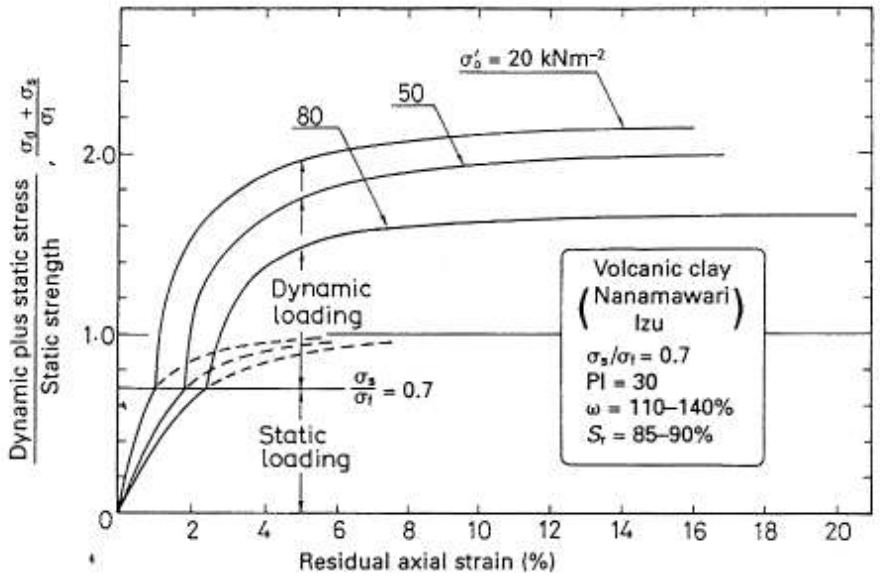

Figure 2.22 Effects of confining stress on the shear stress-residual strain relationship (Ishihara, 1996)

Axial strain accumulation with number of cycles for the clay specimens tested in cyclic triaxial device is studied by Voznesensky and Nordal (1999). The results of their study is presented in Figure 2.23, where three specimens consolidated under different initial confining stresses with a constant effective stress ratio K_0, are represented by letters a, b and c according to the initial confining stresses of 92.4, 180 and 258.5 kPa, respectively. Considering the specimens represented by the curves a (92.4 kPa) and b (180 kPa), stress states of which are in OC range, the cyclic strength of clay increases with increasing confining stress. However, a dramatic decrease occurs in cyclic strength when the preconsolidation pressure is exceeded. Thus, it can be concluded that the cyclic strength increases with increasing confining stress in OC range, and the cyclic strength of OC clays are significantly greater than that of NC clays.

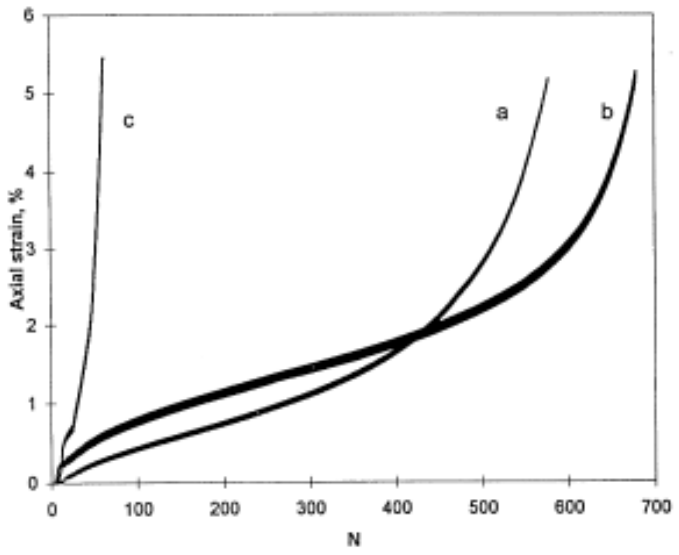

Figure 2.23 Axial strain accumulation in cyclic tests of clay with initial confining stresses of (a) 92.4 kPa, (b) 180 kPa, (c) 258.5 kPa (Voznesensky and Nordal, 1999).

Bray and Sancio (2006) conducted cyclic triaxial tests on fine grained soils recovered from Adapazarı, Turkey. From the indications of the study (Figure 2.24), it is clear that cyclic strength decreases with increasing confining stress. The high cyclic resistance of the samples tested with low initial confining pressures (<75 kPa) is attributed to slight OCR those specimens have.

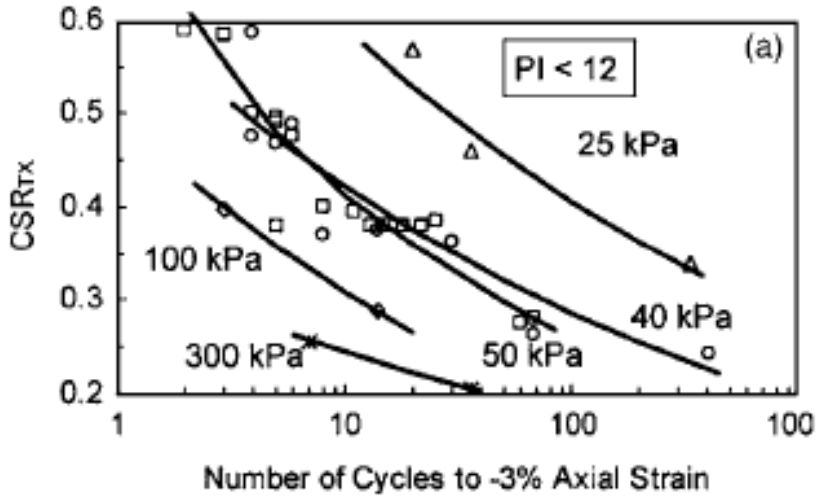

Figure 2.24 Relationship between applied CSR values and number of cycles to 3% axial strain for varying initial confining pressures (Bray and Sancio, 2006).

2.5.3 Effect of Initial Shear Stress

The soil elements beneath existing structures or in slopes are subjected to initial shear stresses previous to a potential cyclic loading. In order to simulate the in-situ stress states of such elements, the specimens are anisotropically consolidated previously in cyclic triaxial testing, and subjected to initial static shear stresses in cyclic simple shear testing. Cyclic strength of fine grained soils has been reported as displaying both decreasing and increasing trends with increasing initial shear stress. Andersen et al. (1980) and Yasuhara et al. (1992) reported that imposed initial shear stress increases the cyclic shear strength of normally consolidated clays. For overconsolidated clays, Andersen et al. (1980) reported that cyclic strength seems to be independent of initial shear stress. Konrad and Wagg (1993) also observed the increasing trend of cyclic resistance with increasing initial shear stress for 20% clay and 80% silt mixture.

Hyodo et al. (1994) performed monotonic and cyclic triaxial tests on normally consolidated clay. The monotonic tests were carried out both in

compression and extension. The monotonic tests in compression were conducted with specimens consolidated under different anisotropic stress states, whereas the tests in extension were carried out only on isotropically consolidated specimens. As it can be observed in Figure 2.25a, the stress-strain traces on compression side display strain softening behavior after reaching a peak deviator stress. The strain softening becomes more significant with increasing initial shear stress, and the critical strength is reached even at smaller values than the initial deviator stress for those specimens sustaining higher initial shear stresses. Although the peak strength increases with increasing initial shear stress, the softening behavior occurs more rapidly for the specimens with high initial shear stresses. On the other hand, cyclic strength of the tested specimens is reported to decrease with increasing initial shear stress. The relationship shown in Figure 2.25b is plotted as a function of the number of cycles causing total axial strain of 10% for different cyclic deviator stress ratios. Another interesting point of the study is that the cyclic strength of sands with relative densities of 50% and 70% are compared to that of clay with reference to the sustained initial shear stresses. The cyclic strength of clay is almost twice of that of sands for isotropically consolidated states of stress, whereas the cyclic strength of clay is reduced well below those of sands with increasing initial shear stress.

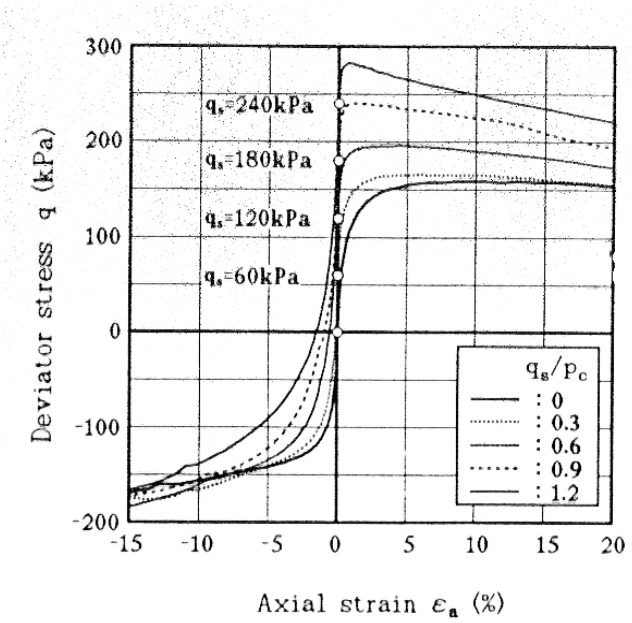

(a)

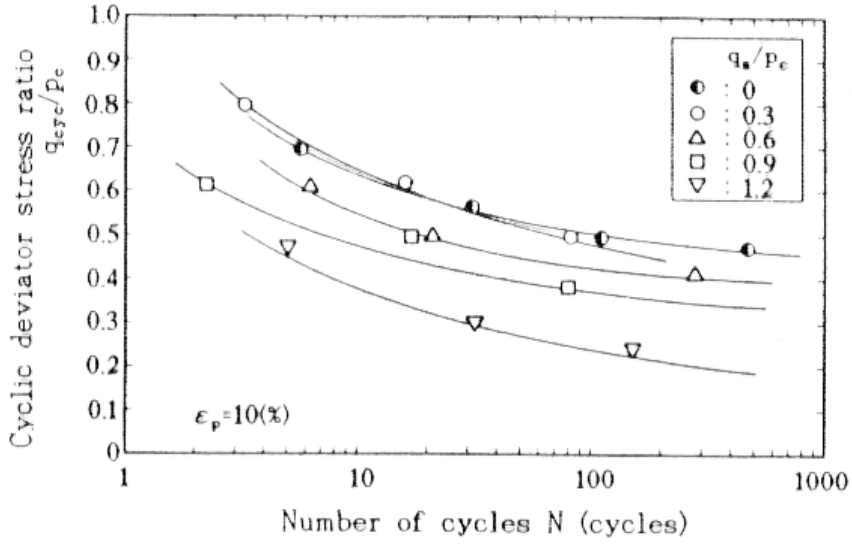

(b)

Figure 2.25 Relationship between (a) deviator stress and axial strain, (b) cyclic deviator stress ratio and number of cycles to cause peak axial strain of 10% with various deviator stresses (Hyodo et al., 1994).

The tests conducted with volcanic clay by Ishihara (1996) shows that if the applied initial shear stress exceeds 90% of static strength of the clay, the cyclic strength is prone to severe decrease with increasing initial shear stress. On the other hand, an initial shear stress ranging between 50% and 80% of the static strength is reported as not having an

appreciable influence on the cyclic strength of the clay tested in the study. Same tendency is also showed by Lefebvre and Pfendler (1996) for soft clay specimens with initial shear stresses ranging between 0 and 80% of undrained static strength. As it is seen in Figure 2.26, although increase in sustained initial shear stress reduces cyclic resistance of clay, the overall strength of clays subjected to undrained cyclic loading is greater than undrained monotonic strength as emphasized by Ishihara (1996) as well. Such an increase in undrained strength for clays is mostly related to loading rate effect on which the studies committed will be reviewed in detail under another heading.

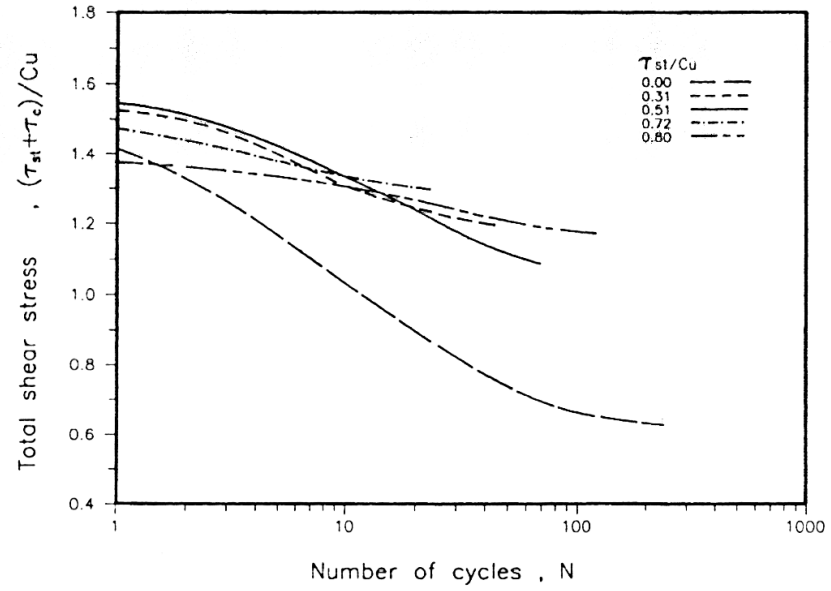

Figure 2.26 Relationship between total undrained shear stress and number of cycles for various initial shear stress levels (Lefebvre and Pfendler, 1996).

Hyde et al. (2006) performed cyclic and monotonic triaxial tests over a low plastic silt. The specimens were consolidated so as to have initial shear stresses ranging between 0 and 100% of initial mean effective stresses. In the monotonic tests, the excess pore water pressure generated during shearing was observed to increase as the initially sustained shear stress decreased. The monotonic strength on compression side is reported as being increased with increasing initial shear stress, whereas it is

independent of initial shear stress in extension side. The cyclic behavior of silt is reported to be dependent on whether there exists stress reversal or not during cycling. The relationship between cyclic deviator stress ratio and initially sustained deviator stress with respect to the number of cycles required to reach 5% total axial strain is given in Figure 2.27. The curves representing cyclic response of silt is recommended based on the results of the tests conducted in the study. As it is seen, the increasing initial shear stress decreases the cyclic resistance of the specimens subjected to stress reversals during cycling. The cyclic response of those specimens subjected stress reversals is defined by flow liquefaction whereas it is defined as cyclic mobility for the cases of no reversal. After the specimens reach the lowest cyclic strength at no reversal case, where initially sustained deviator stress is 50% of initial mean effective stress, the cyclic resistance of the specimens displays an increasing trend with additional increase in the initial deviator stress.

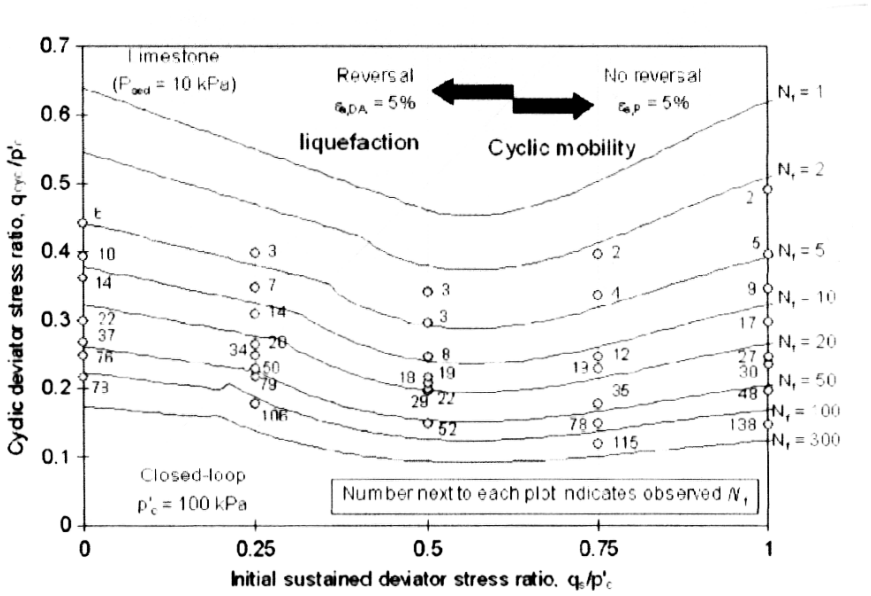

Figure 2.27 Relationship between cyclic deviator stress, initial deviator stress and number of cycles to 5% total axial strain (Hyde et al., 2006).

Bray and Sancio (2006) stated that although the specimens with initial shear stress reach 5% shear strain in fewer cycles than those isotropically consolidated, the excess pore pressure built-up during cycling in the tests

with anisotropically consolidated specimens is less than that developed in the isotropically consolidated specimens. It is emphasized in the study that the cyclic simple shear testing would be preferred rather than the triaxial testing to examine the effect of initial shear stress. This is due to the fact that during testing of anisotropically consolidated specimens, the strains in extension are minimized and consequently a greater number of cycles are required to reach at a specified strain level in cyclic triaxial testing. The cyclic simple shear tests conducted by Kodaka et al. (2010) on clay also confirm this finding that the cyclic strength is decreased with increasing initial shear stress.

Boulanger and Idriss (2007) suggested an equation formulating the relationship between K_α (ratio between cyclic strength under any initial shear stress and cyclic strength without the initial shear stress) and α (initial shear stress ratio) with varying OCR values for claylike soils. The relationship is given in Figure 2.28. As it is seen from the figure, cyclic strength decreases with increasing initial shear stress, and the effect of initially sustained shear stress on cyclic strength becomes more unfavorable with decreasing OCR.

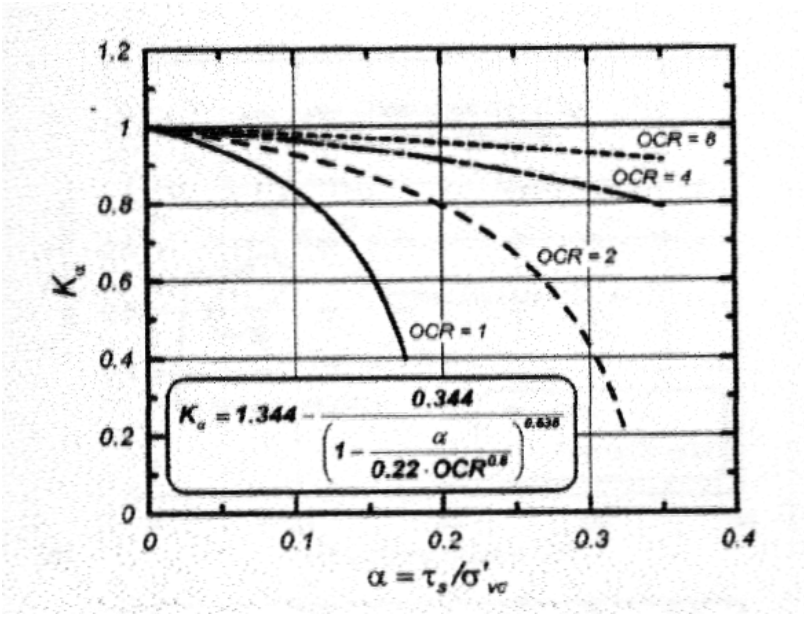

Figure 2.28 Relationship between K_α and α for clay at various OCR (Boulanger and Idriss, 2007).

2.5.4 Effect of OCR

Stress history of soils is known as one of the characteristics significantly affecting cyclic response particularly of fine grained soils which are believed to have a stress memory. Andersen et al. (1980) conducted monotonic and cyclic triaxial, and simple shear tests on Drammen clay specimens with OCR ranging between 1 and 50. In order to simulate preconsolidation stress state of in-situ deposits, the samples were initially consolidated with a specified maximum effective stress (σ'_v = 400 kPa) and a horizontal effective stress (σ'_h = 200 kPa) half of the vertical one (i.e. K_0=0.5). Such K_0 value was reported as closely corresponding to no lateral strain for saturated normally consolidated Drammen clay. The OC specimens were then obtained by decreasing vertical effective stress while preventing lateral straining. As it is seen in Figure 2.29, the undrained shear strength (s_u) of the clay is observed to decrease with decreasing vertical effective stress (i.e. increasing OCR). The decreasing trend becomes more obvious with increasing OCR. However, it is also stated in the study that the ratios of s_u/σ'_v increase with increasing OCR. Such a relationship indicates that if two specimens are subjected to the same σ'_v, the s_u is greater for the specimen having higher OCR.

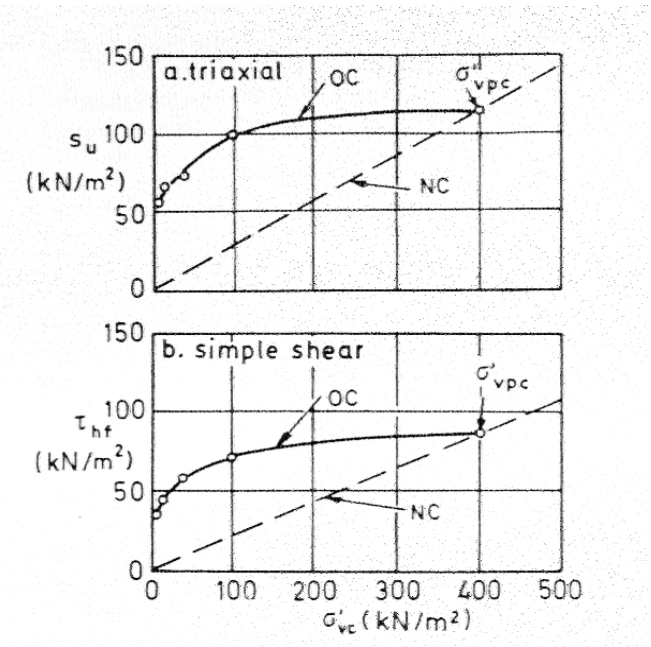

Figure 2.29 Relationship between undrained shear strength and vertical effective stress (Andersen et al.,1980).

It is concluded by Andersen et al. (1980) that OC specimens reach 3% shear strain in earlier cycles than NC specimens under a certain cyclic shear stress level, which reveals that cyclic resistance of NC clay is greater than that of OC clay. According to the results of cyclic tests performed by Azzouz et al. (1989), the cyclic resistance apparently decreases with increasing OCR for some specimens, whereas the opposite tendency was observed for other specimens.

As indicated previously under the heading of pore water pressure generation, although negative excess pore water pressure generation increases with increasing OCR, the pore water pressure generation turns out to be positive with increasing number of cycles (Azzouz et al., 1989). Nevertheless, Hyde and Ward (1985) reported that the generation of excess pore water pressure decreases with increasing OCR, but it does not take negative values and therefore significant excess pore water pressures are generated in lightly OC soils (OCR=4). Besides, this observation is stated as being in contrast with the results of monotonic tests where excess pore pressure generation is found to be negative for OC soils.

Sanin and Wijewickreme (2006), and Wijewickreme and Sanin (2010) carried out cyclic direct simple shear (DSS) tests on low plastic silt. It is indicated that OC silt specimens take more cycles of loading to reach a certain shear strain level compared to those of NC specimens. Such response is related to dilation tendency which increases with OCR. The cyclic behavior of representative NC and OC silt specimens that was observed during cyclic DSS tests is presented in Figure 2.30. The effect of OCR on number of cycles to reach 3.75% shear strain is given by Sanin and Wijewickreme (2006) (Figure 2.31).

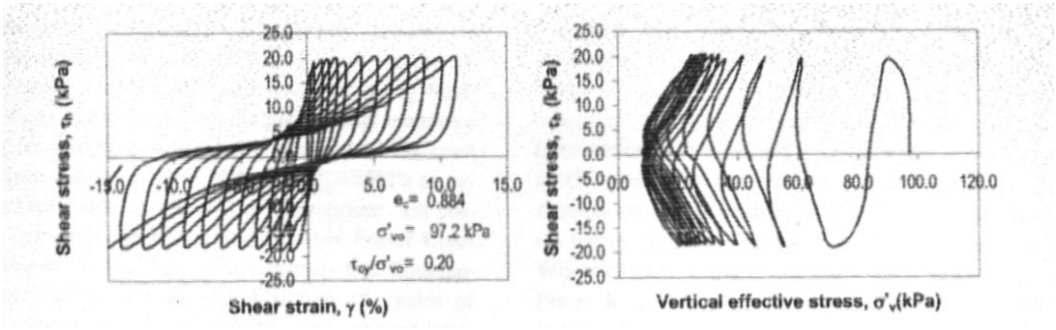

(a)

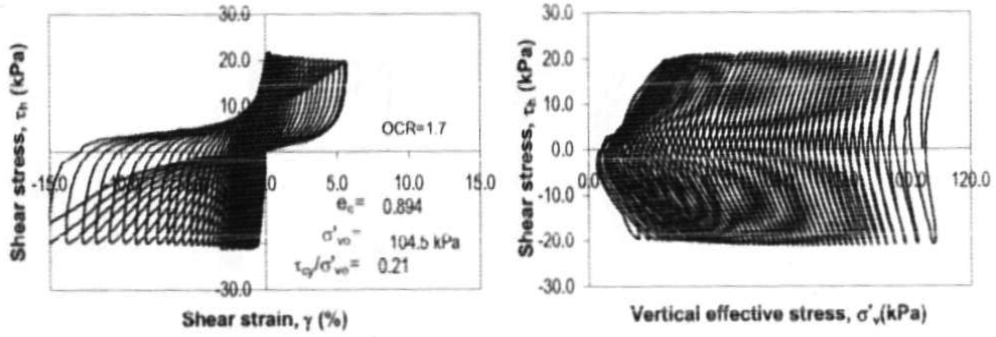

(b)

Figure 2.30 Typical stress-strain and stress path diagrams during cyclic tests for (a) NC and (b) OC silt specimens (Wijewickreme and Sanin, 2010).

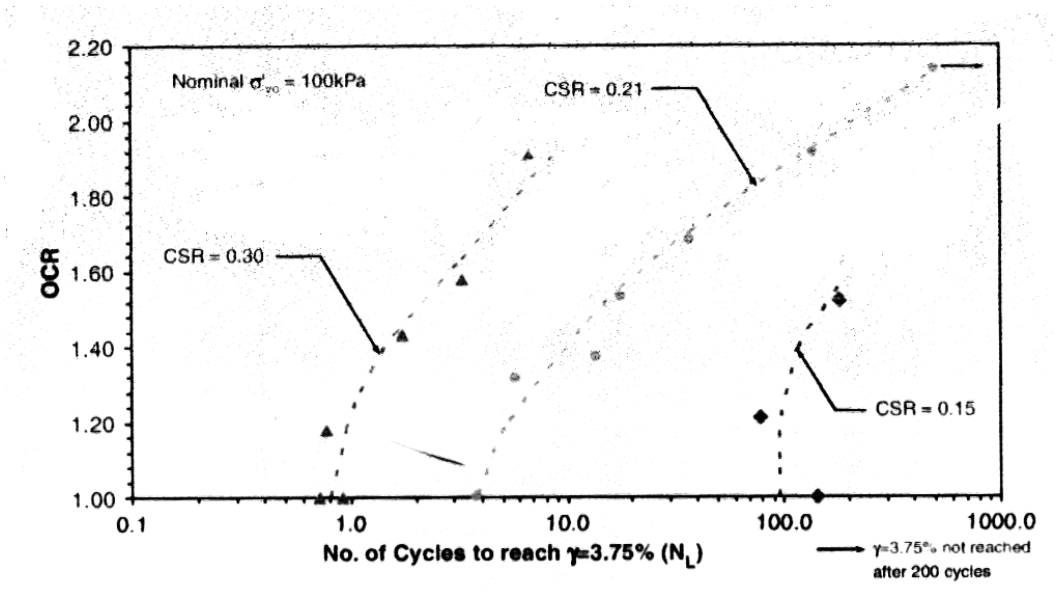

Figure 2.31 Relationship between OCR and number of cycles required to reach 3.75% shear strain with various CSR values (Sanin and Wijewickreme, 2006).

Vucetic and Dobry (1988), and Zhou and Gong (2001) showed that fine grained soils with high OCR have high strength, and cyclic degradation of shear modulus is reported as being reduced with increasing OCR. Yasuhara et al. (2003) determined reduction in the initial Young's modulus and undrained shear strength of low plastic silt imposed to cyclic loading. It is stated that after undrained cyclic loading, reduction in Young's modulus is more remarkable than that in undrained shear strength, and this tendency becomes more obvious with increasing OCR.

2.5.5 Effect of Loading Rate

Another important aspect in cyclic response of fine grained soils is the speed of the loading. It has been well known that increasing speed of loading derives soil to exhibit a greater resistance to deformations in monotonic loading. The influence of loading speed observed during monotonic loading tests provides a profound understanding on response of soils subjected to cyclic loading with various speeds during earthquakes, off-shore wave loads, traffic loads.. etc. The loading speed is arranged based on either strain rate for monotonic tests or loading frequency in cyclic tests.

Ladd and Foott (1974) reported on the basis of the information provided in literature that each log cycle decrease causes a reduction in the undrained shear strength of clayey soils about 10% in triaxial compression tests. Although Yasuhara et al. (1982) stated that the loading frequency does not significantly affect the cyclic undrained strength of NC clays, Procter and Khaffaf (1984) revealed that a frequency change from 1/120 to 1 Hz results approximately 30% increase in cyclic resistance of clays (Figure 2.32).

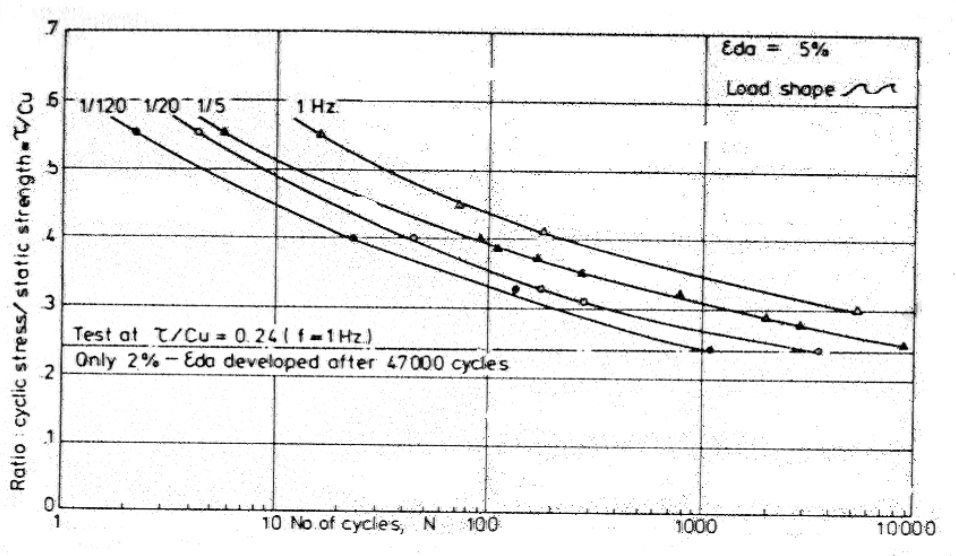

Figure 2.32 Relationship between CSR and number of cycles causing 5% DA strain for various loading frequencies (Procter and Khaffaf, 1984).

It is also stated by Procter and Khaffaf (1984) that the greater loading rates inhibit the development of strains that would emerge due to creep effect in tests with low loading rate. In other words, increased frequency retards the weakening process of soil for a certain period of loading. Accordingly, it is emphasized in the study that the laboratory tests on clays should be carried out by the actual frequency to be experienced in the field. Furthermore, Procter and Khaffaf (1984) gave a plot showing an adjustment on undrained shear strength of clays for the testing rate effect (Figure 2.33). As it is observed, the modification line for strain controlled test behavior is given together with the line for stress controlled test behavior based on Craig (1982).

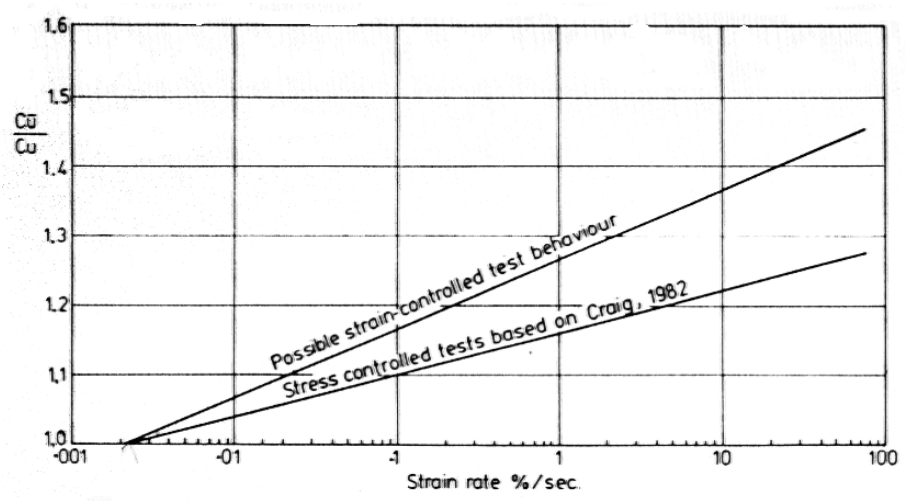

Figure 2.33 Ratio of fast to static shear strengths with varying strain rate (Procter and Khaffaf, 1984).

Lefebvre and LeBoeuf (1987) performed monotonic and cyclic triaxial tests on sensitive NC and OC clays. It is indicated in the study that in order to obtain pore pressure equalization of 95%, it is required to apply a strain rate at most 15%/hour for OC clays whereas 1%/hour for NC clays. However, the strain rate used in the study has been ranged between 1 and 132%/hour. Excess pore water pressure generation is reported as being unaffected with a change in strain rate for OC clays. On the other hand, for NC clays, the pore pressure generation significantly increases with decreasing strain rate. This tendency is attributed to incomplete pore pressure equalization. It is also concluded that the gain in strength for a log cycle increase in strain rate is about 10% on average for both NC and OC clays. Ansal and Erken (1989) conducted cyclic tests on NC clays as well. The pore pressure generation is reported as being significantly increasing with decreasing strain rate at earlier cycles of loading. However, this tendency was observed to decrease at high number of cycles where the pore pressure is believed to be equalized even for high frequencies. Accumulated shear strain and generated pore pressure ratio becomes almost the same at higher number of cycles for the specimens tested with different frequencies. Therefore, it is indicated by Ansal and Erken (1989) that frequency of cyclic loading does not have an effect on cyclic response for NC clays subjected to large number of cycles such as wave cycles acting on off-shore structures.

The static and dynamic direct simple shear tests carried out by Vucetic and Dobry (1988) revealed that the clay specimens show higher strength when imposed to dynamic loading. Figure 2.34 shows both static strength and cyclic strength of the clay for various OCR values. It is seen that the strength is also increasing with increasing OCR. In Figure 2.34, each static curve is obtained by just one direct simple shear test whereas each dynamic curve is constructed by means of at least two points each of which represents the tip of first cycle loop recorded in one cyclic test. The cyclic tests were strain controlled and they were conducted with various strain rates under a constant frequency of 0.2 Hz. Hence, the change in strain rate directly reflects the change in loading speed. It can be also seen in each dynamic curve for a specific OCR that increasing cyclic strain rate (i.e. increasing loading rate) results in an increase in cyclic strength.

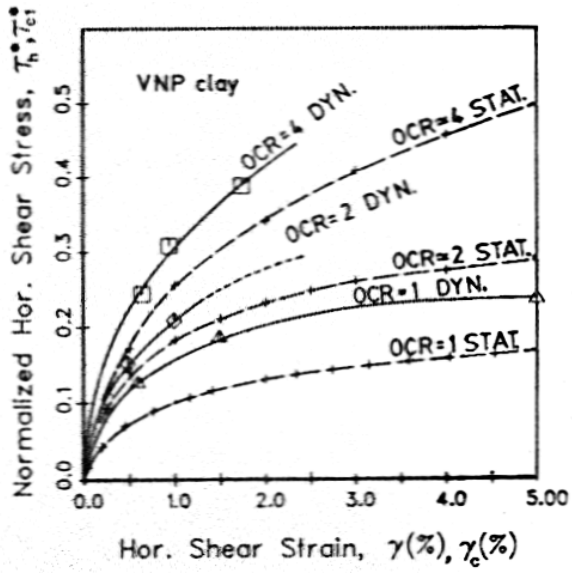

Figure 2.34 Relationship between applied shear stress and applied shear strain rates during static and cyclic direct simple shear tests (Vucetic and Dobry, 1988).

Konrad and Wagg (1993) reported that the undrained strength of silt-clay mixtures increases with increasing strain rate based on the results obtained by monotonic triaxial tests. It is shown that the strength envelopes obtained for different strain rates are all parallel to each other,

and just the cohesion is increasing for the specimens tested with higher strain rates. The pore pressures were measured at both midheight and bottom of the specimens during the tests. As shown in Figure 2.20, the difference between pore pressures measured at midheight and bottom increases with increasing strain rate. Accordingly, it is concluded in the study that non-uniform pore pressure distribution observed for higher strain rates may affect the position of the dynamic failure envelope as well.

Ishihara (1996) reported that loading speed affects the modulus of fine grained soils after reaching strain level of 1% of the strain at failure. The modulus is reported to have a tendency to decrease as the duration of loading gets longer. The difference between the modulus of soils subjected to rapid and slow loading becomes more remarkable as the level of strain increases. Such increase in modulus is attributed to viscous nature of deformation characteristics prevailing in cohesive soils. Figure 2.35 illustrates the elastic modulus degradation with axial strain accumulation during cyclic tests obtained for various numbers of cycle. As it is seen, the degradation is dependent on the number of cycles as well as the strain level. The gain in modulus due to speed of loading is being gradually reduced by degradation effect of loading repetition. After reaching 20 cycles the modulus becomes equal to that corresponding to the static conditions, and afterwards as the number of cycles increases, the modulus is further reduced.

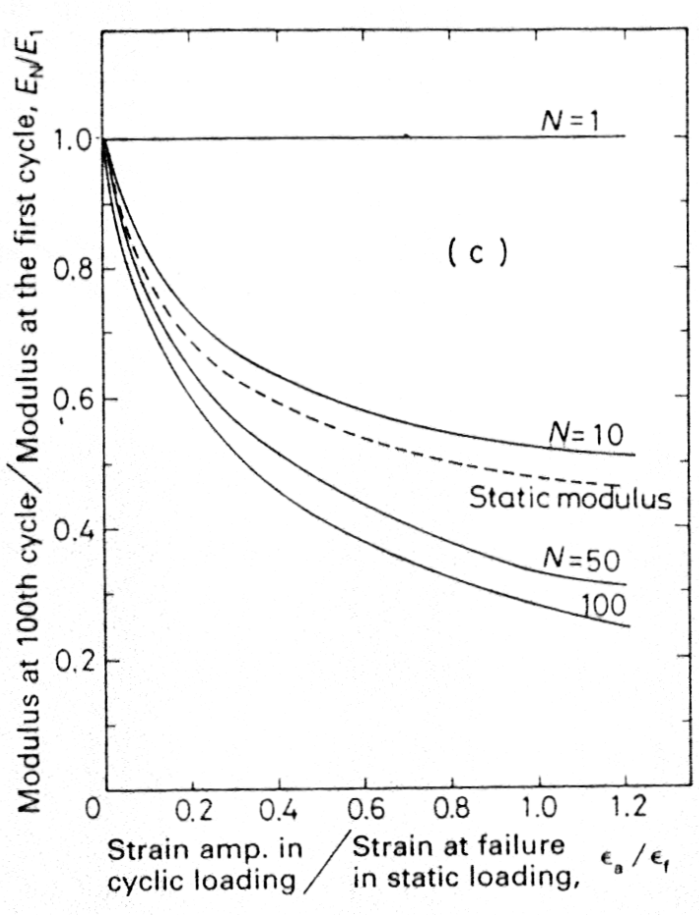

Figure 2.35 Modulus degradation with increasing strain at the 10th and 100th cycles of load application (Ishihara, 1996).

The increase in resistance to degradation with increasing loading rate is attributed to viscous nature of deformation by Matesic and Vucetic (2003). The viscosity is simply expressed as resistance showed by liquid or gaseous systems to shear stresses imposed and more viscous materials exhibit greater resistance to flow. The mechanism behind the observation of lower strength due to lower loading rates is associated to more time allowed for the soil to creep and relax. It is also stated in the study that the rate effect is more pronounced in clays than in sands because clays are more susceptible to creep and relaxation than sands. Accordingly, it can be concluded that the sands are more viscous than clays if both are loaded at low loading rates. It is also concluded in the study that although the shear modulus is increased with increasing loading rate, the increase in modulus becomes less for high loading rates in clays.

2.5.6 Cyclic Stiffness Degradation of Fine Grained Soils

Stiffness degradation of soils is quantitatively expressed by means of a parameter called degradation index (δ_D) that is introduced by Idriss et al. (1978). This index defines the relative variation of secant Young's modulus (E) or shear modulus (G) by the ratio of modulus in the first cycle (E_1 or G_1) to the modulus in the N^{th} cycle (E_N or G_N). Idriss et al. (1978) obtained the relationship between secant Young's modulus and number of cycles (N) in strain controlled cyclic triaxial tests on clay samples. It is observed that G decreases linearly with increasing N on the logarithmic scale of both axes. For each cyclic strain level there is one straight line representing the relationship between the soil modulus and N. Ishihara (1996) illustrated some straight lines for various cyclic strain amplitudes compiled from different studies as given in Figure 2.36.

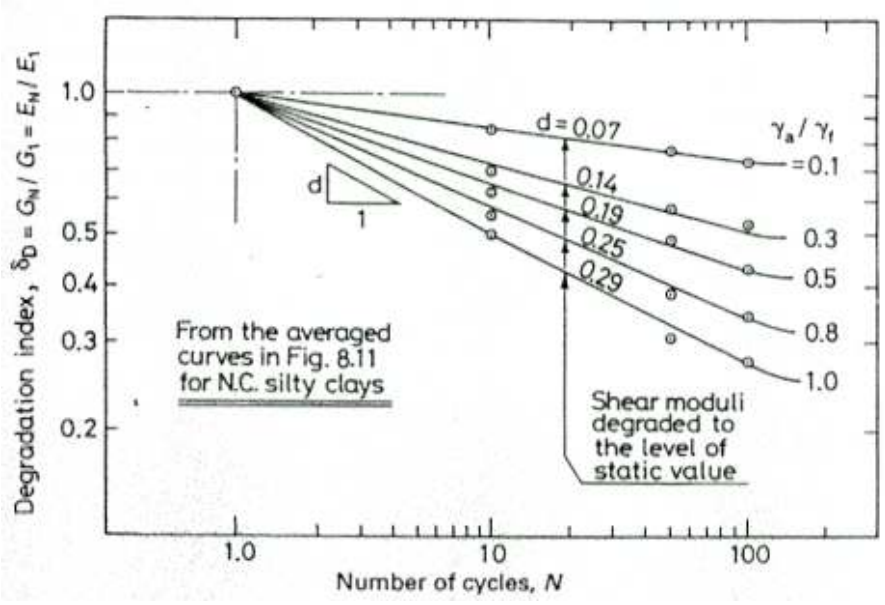

Figure 2.36 Modulus degradation with increasing cycles (Ishihara, 1996)

In log-log scale plot, the relationship represented by straight line can be expressed as:

$$\log E_1 - \log E_N = t \log N \qquad (2.1)$$

which can be expressed as:

$$\frac{E_N}{E_1} = N^{-t} \qquad (2.2)$$

where t indicates the slope of the straight line and is called degradation parameter by Idriss et al. (1978). Accordingly, degradation index (δ_D) becomes as:

$$\delta_D = \frac{G_N}{G_1} = \frac{E_N}{E_1} = N^{-t} \qquad (2.3)$$

The value of t is observed to increase with increasing cyclic strain. It is also indicated by Idriss et al. (1978) that the parameter t seems to be essentially independent of initial confining stress and water content for the clay samples used in the study.

Vucetic and Dobry (1988) investigated a number of factors affecting degradation parameter among which OCR seems to have great effect on cyclic degradation of clays. As shown in Figure 2.37, even with a small increase in OCR the degradation is reduced significantly. The same conclusions were also reached by Zhou and Gong (2001). The results by Vucetic and Dobry (1988) suggest that the plasticity of clay is another substantially influential factor on the degradation parameter. High plasticity clays were observed as degrading at a much slower rate than low plasticity clays.

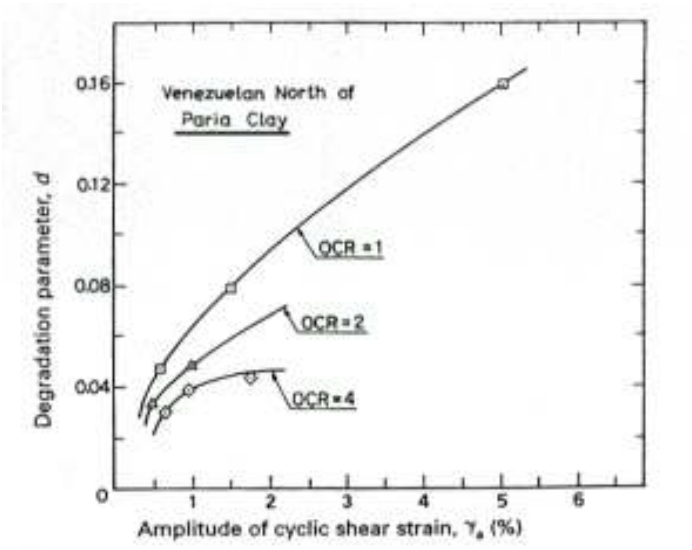

Figure 2.37 OCR effect on degradation parameter for clays (Vucetic and Dobry, 1988)

In another study by Vucetic and Dobry (1991) the effect of plasticity on stiffness degradation was investigated in detail. The plasticity effect was again displayed by means of strain-controlled cyclic tests. As shown in Figure 2.38, the degradation index is greater for higher PI at a given cyclic strain value. Thus, it is concluded that degradation is reduced with increasing PI for NC clays as well as OC clays.

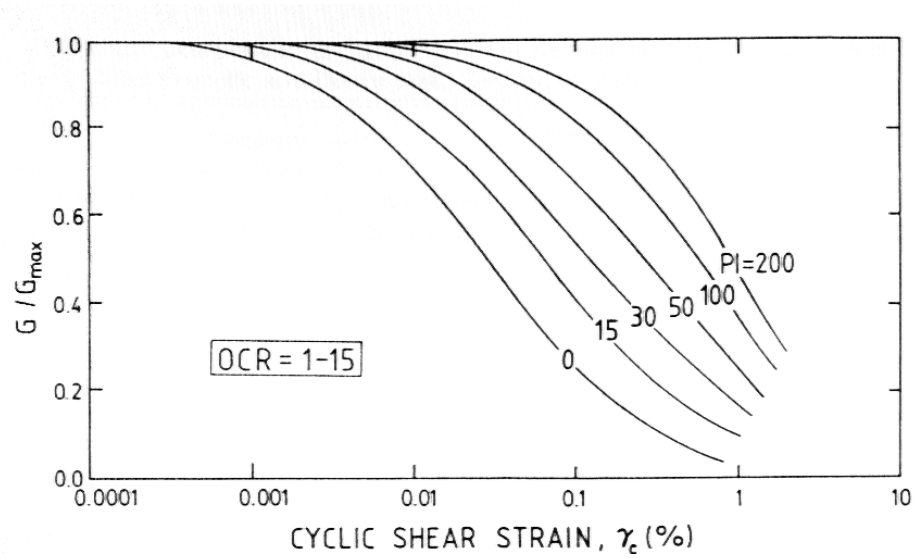

Figure 2.38 The effect of PI on degradation index for clays (Vucetic and Dobry, 1991).

The studies conducted by Yasuhara et al. (2001; 2003) show that stiffness degradation is much more pronunced than that of undrained strength for the silts which are previously imposed to cyclic loading. The tendency seen in post-cyclic state of silts is reported as more clear for OC samples rather than NC samples.

There is a threshold strain value below which stiffness degradation will be negligible and this lower limit threshold strain would be dependent on the pore water pressure generation (Ishihara, 1996; Okur and Ansal, 2007). Okur and Ansal (2007) also indicated that confining stress and PI are important factors affecting the threshold strain for stiffness degradation, and the threshold strain becomes smaller with decreasing confining stress and PI. On the other hand, Li and Huang (2010) stated that cyclic stiffness degradation increases with increasing confining stress for off-shore soft clays which were mostly tested with high number of cycles (around 5000).

2.6 Procedures for Evaluating Liquefaction Susceptibility of Soils

A wide range of phenomena involving loss of strength induced by pore pressure increase and accompanying large shear strains under dynamic loading of saturated granular soils have historically been defined by the term “liquefaction”. In fact, the definition has come about on the basis of field and laboratory observations relating to the response of sands. As indicated by Youd et al. (2001), loose sands subjected to undrained cyclic loading may undergo large shear deformations or even flow failure as a result of shear strength loss. In dense sands, however, excessive strength loss and consecutive large ground deformations are prevented due to dilation tendency of dense sand, although transient softening and shear strain accumulation occur during undrained cyclic loading. This kind of softening response is commonly defined as cyclic mobility.

There have been numerous definitions of soil liquefaction and liquefaction susceptibility criteria, and unavoidably inconsistencies among researchers over the years. The evaluation of liquefaction susceptibility of fine grained soils began with the criteria introduced on the basis of the data observed after large earthquakes in China (Wang, 1979). Seed and Idriss (1982) interpreted Wang's findings and stated that clayey soils meeting the conditions of (a) percent of particles less than 0.005 mm < 15%, (b) liquid limit (LL) < 35, and (c) the ratio of initial water content (w_c) to the LL (w_c/LL) > 0.9 could be sensitive to severe strength loss as a result of seismic loading. The conditions as a whole are known as the "Chinese criteria". Koester (1992) later noted that LL values determined by means of fall cone device used in China are about four points higher than those values determined by means of Casagrande cup used in U.S. Hence, Koester suggested appropriate corrections to LL values of Chinese criteria if Casagrande cup is to be used to determine LL values.

Andrews and Martin (2000) reviewed the observations of a few earthquake case histories, and discussed the properties of the soils that were documented as liquefied. Clay content and LL were regarded as "key" parameters on liquefaction susceptibility evaluation of silty soils, and it was concluded that the soils are susceptible to liquefaction if they have LL < 32 and clay content < 10%, and are not susceptible if they have LL ≥ 32 and clay content ≥ 10% both. If the soil meets only one of the conditions mentioned above, further studies were suggested by Andrews and Martin. LL values determined by Casagrande cup and clay regarded as grains finer than 2 μm are the points expected to be paid attention during utilization of the criteria.

More recent criteria, which was primarily based on the observations and laboratory work regarding ground failure sites in Adapazarı following the 1999 Kocaeli (Turkey) earthquake, was proposed by Bray et al. (2004). It has been proposed in the criteria that fine grained soils are susceptible to liquefaction or cyclic mobility if the ratio of w_c/LL ≥ 0.85 and the plasticity index (PI) ≤ 12. Nevertheless, the soils satisfying the conditions of 0.8 ≤ w_c/LL ≤ 0.85 and 12 < PI ≤ 20 have been introduced as moderately susceptible to liquefaction or cyclic mobility. In a later study, in which the

field data observed after earthquakes were evaluated in addition to those of Kocaeli earthquake, Bray and Sancio (2006) stated that clayey silts and silty clays having PI values between 12 and 18, and $w_c/LL > 0.8$ could undergo liquefaction whereas sensitive soils with PI >18 might undergo severe strength loss as a result of seismic loading.

Boulanger and Idriss (2004) recommended that the evaluation of the liquefaction potential of fine grained soils depended on the behavior characteristically dominated by either clay (clay-like behavior) or sand (sand-like behavior). Fine grained soils of PI < 7 have been classified as "sand-like" (i.e. susceptible to liquefaction), and soils of PI ≥ 7 have been classified as "clay-like". Boulanger and Idriss (2006) later stated that if a soil plots on plasticity chart as CL-ML the PI criterion may be reduced to PI ≥ 5, and the soils with PI values of 3-6 are better to be tested in-situ and in laboratory in addition to liquefaction correlations based on standard penetration test (SPT) and cone penetration test (CPT).

The criteria reviewed above are the tools proposed to determine whether the soil has a tendency to liquefy under capable loading conditions. However, the definition of "soil liquefaction" has been subject of discussion amongst researchers regarding the criteria to be used to define initiation of the liquefaction. As stated by Wu et al. (2004), liquefaction initiation criteria are commonly based on one of the factors of pore pressure, shear strength and shear deformation. Lee and Seed (1967a) defined "initial liquefaction" as when the soil first exhibits none or negligible resistance to deformation over a wide strain range during cyclic loading, which is based on the strength of soil. This type definition commonly requires that liquefied soils behave like a viscous fluid, which implies the loss of shear strength completely. Silver et al. (1976) and Vessely et al. (1996) suggested "initial liquefaction" as the point at which the excess pore pressure generated during the test equals the initial confining stress, irrespective of the strength of the soil. However, recent laboratory studies indicate that it is doubtful whether a full equalization of the excess pore pressure and initial confining stress can be achieved in all liquefiable soils. Although there is no universally accepted criteria for selecting a specific strain level referred as "initial liquefaction",

liquefaction initiation has been mostly identified within a specified strain level and used by researchers, some of which are: 3% single amplitude (SA) axial strain (Boulanger et al., 1998), 5% SA axial strain (Campanella and Lim, 1981), 10% double amplitude (DA) axial strain (Silver et al., 1976), 15% DA axial strain (Andersen et al., 1988), 6% DA or 6% SA shear strain (Wu et al., 2004). The selection of a particular strain level for the onset of liquefaction seems to depend on deformation mode (e.g. triaxial or simple shear) and characteristics of the soil tested.

The loss in strength during cyclic loading is generally evaluated with either excess pore pressure level or maximum strain level developed during cycling. It is well known that the stiffness of soils subjected to cyclic loads also degrades. The stiffness of soils is quantified by means of elastic modulus (E) or shear modulus (G). Hardin and Drnevich (1972), Krizek et al. (1974) and Kuribayashi et al. (1974) reported that the modulus of sands is considerably influenced by three main factors: (i) the confining pressure, (ii) the strain level, and (iii) the relative density (D_R or the void ratio). Hardin and Drnevich (1972) expressed the degradation in shear modulus by Equation 2.4.

$$\frac{G}{G_{\max}} = \frac{1}{1+\frac{\gamma}{\gamma_r}} \qquad (2.4)$$

where γ is a given shear strain and γ_r is reference shear strain calculated by:

$$\gamma_r = \frac{\tau_{\max}}{G_{\max}} \qquad (2.5)$$

where τ_{max} is the shear stress at failure (i.e. shear stress obtained from result of a monotonic test or from the first cycle of cyclic test). τ_{max} is expressed by the equation given below :

$$\tau_{\max} = \left\{ \left(\frac{1+K_0}{2} \sigma'_v \sin\phi' + c' \cos\phi' \right)^2 - \left(\frac{1-K_0}{2} \sigma'_v \right)^2 \right\}^{1/2} \qquad (2.6)$$

where K_0 is the lateral stress coefficient at rest and σ'_v is the vertical effective stress at failure. Thus, the influences of shear strain level and the excess pore water pressure (i.e. effective stress state) are included in the proposed formulae for stiffness degradation. Another convenient formulae showing the relationship between the shear modulus and the confining pressure is provided by Seed and Idriss (1970).

$$G = 1000 K_2 (p')^{1/2} \qquad (2.7)$$

where K_2 is shear modulus coefficient and p' is the effective mean principal stress. Seed et al. (1986) reported that K_2 value is mainly a function of particle size, relative density and shear strain level. It is clear that the p' becomes a function of excess pore water pressure accumulation during cycling. Equation 2.7, thus, takes the influences of shear strain level and excess pore water pressures into account in designation of G. Based on these relationships, the excess pore water generation and strain accumulation are related to each other.

CHAPTER 3

OVERVIEW OF TRIAXIAL TESTING PROCEDURE

3.1 Introduction

The existing soil conditions or the conditions that would emerge as a result of probable repetitive loading upon a soil formation are investigated by means of simulation setups in the laboratory. The simulation setups are attempted to model either an element or a system. Unlike the setups which aim to simulate a system with proper boundary condition, element level tests simulate merely a soil element with specific boundary conditions. Instrumentation and application of element level tests are in general easier and cheaper than those of the model tests. These factors make them attractive particularly for the studies concerning the fundamental soil behavior.

3.2 Triaxial Testing

Cyclic triaxial testing has been widely used due to widespread availability of the testing equipment, and ease in performing the test. A sectional view of a typical triaxial test apparatus is given in Figure 3.1.

In order to check the consistency of cyclic triaxial testing, a testing program was carried out cooperatively in eight laboratories in the United States (Silver et al., 1976). This cooperative investigation showed that sample preparation techniques, dry unit weight and wave shape of loading can influence the cyclic strength of sands used in triaxial tests. It was also shown that the behavior of sand specimens tested in different laboratories was in good agreement if the tests were performed properly. A

similar conclusion was reached for a cyclic triaxial testing program carried out by Japanese researchers (Tatsuoka et al., 1986).

Seed and Lee (1966) utilized cyclic triaxial test to study the liquefaction of saturated sands under free field conditions for the first time. They carried out stress and strain controlled cyclic triaxial as well as simple shear tests on sands. The idealized stress states convenient for application in cyclic triaxial testing to simulate the free field conditions, introduced by Seed and Lee (1966), are depicted in Figure 3.2. They concluded that the deformations happening in a soil element in free field during earthquake can be best simulated by cyclic simple shear testing. Nevertheless, Tatsuoka (1988) stated that major deformation and strength characteristics which take place in soils during earthquake can be quite realistically captured in the cyclic triaxial testing as well.

There exist a number of disadvantages of cyclic triaxial testing due to stresses developing during cyclic phase. During testing, the intermediate principle effective stress σ'_2 is equal to either major principle effective stress σ'_1 or minor principle effective stress σ'_3 inherently. While the principle stresses of a soil element imposed to earthquake loading rotate continuously, the orientation of principle stresses changes 90° instantaneously during cycling. In addition, since the shear plane within the specimen is not horizontal and its direction cannot be controlled during shearing, implementation of K_0 consolidation is not possible on failure plane.

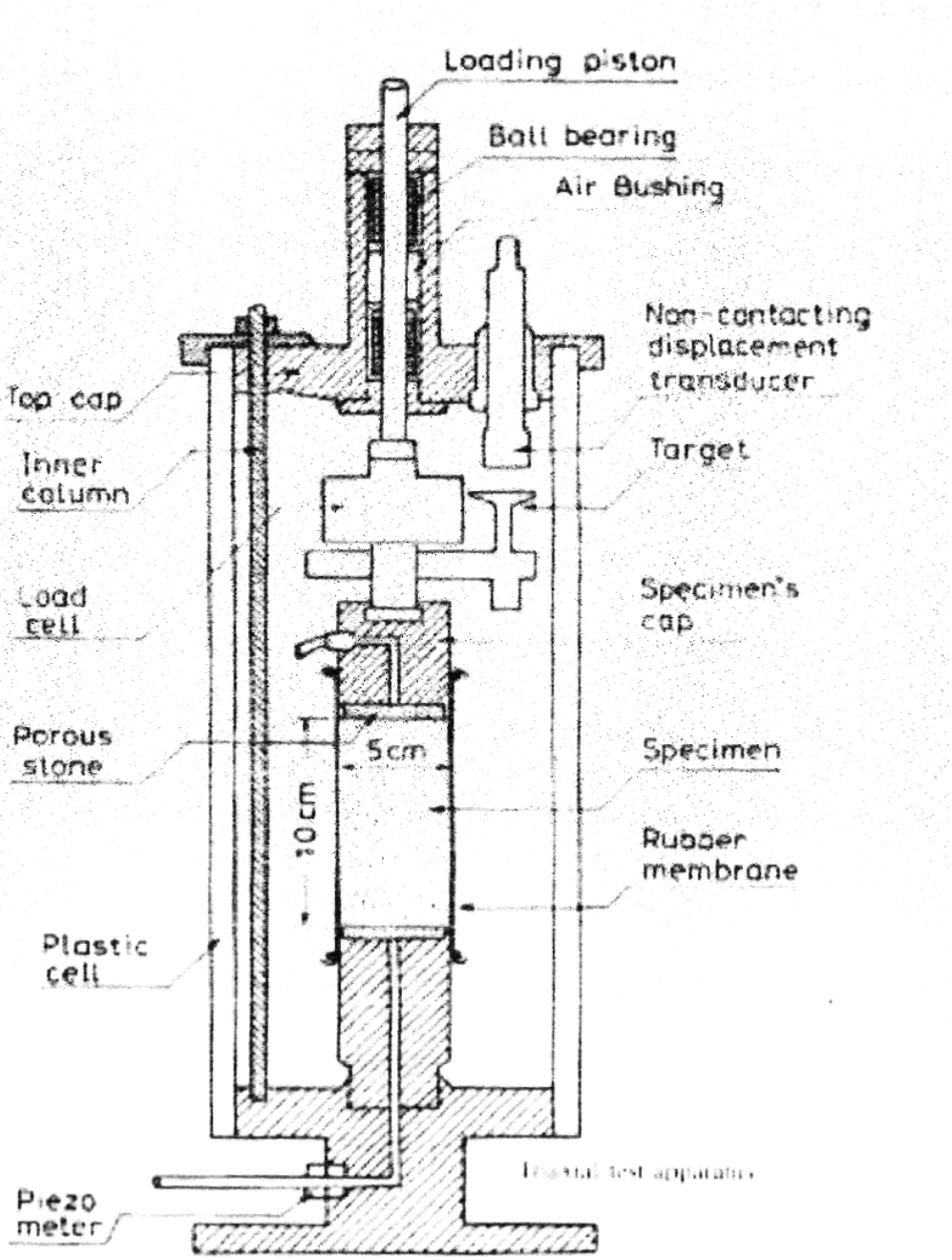

Figure 3.1 General scheme of triaxial apparatus (Ishihara, 1996).

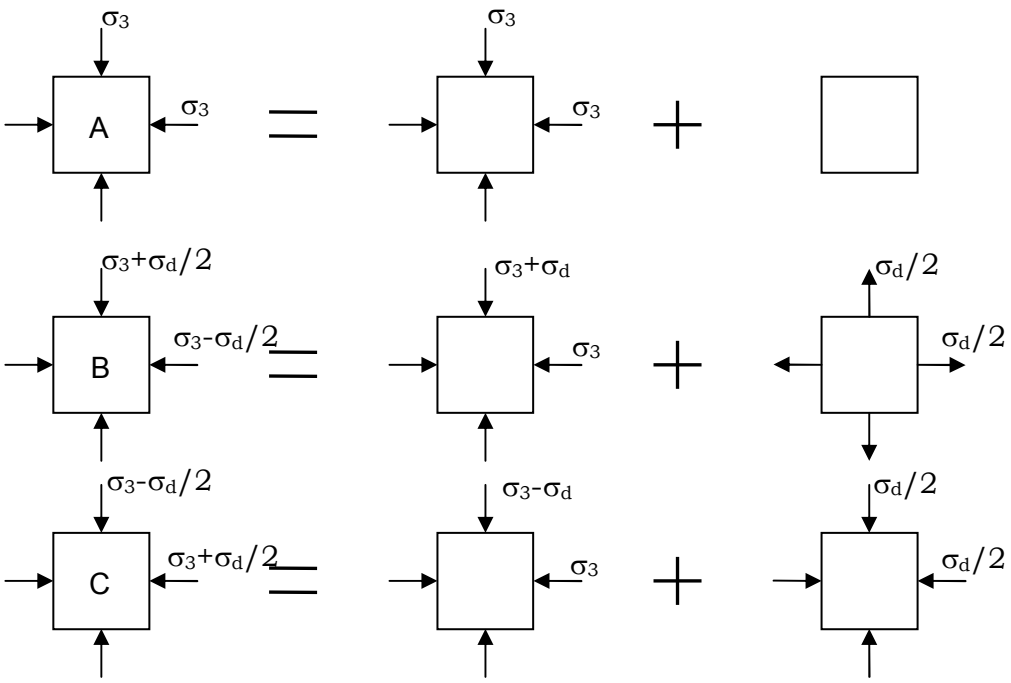

Figure 3.2 Equivalent stress conditions used to simulate free field during a cyclic triaxial test (Seed and Lee, 1966).

3.2.1 Simulation in Cyclic Triaxial Testing

Cyclic triaxial test is one of the major cyclic tests utilized to simulate the stress conditions existing in real deposits of free field or under a structure during shaking. The stress conditions and simulation of the conditions by cyclic triaxial test are reviewed in this section.

A soil element at a specific depth under a horizontal surface is subjected to a vertical effective stress, σ'_v, and a horizontal effective stress, σ'_h. In normally consolidated soils, the horizontal effective stress exists as a proportion of the vertical effective stress such that the ratio between horizontal and vertical effective stresses is defined as the earth pressure coefficient at rest, K_0. The soil element beneath a foundation is subjected to a vertical effective stress increase due to the load imposed by the structure. As a result of the increase in the vertical effective stress, the horizontal effective stress is also increased by the amount of vertical

effective stress multiplied by K_0 (Figure 3.3). Beneath an existing structure the distribution of stress increase is not uniform. The effect of the imposed weight decreases with increasing distance from the center of the loaded area ($\sigma_{edge} < \sigma_{center}$). The general stress state acting over an element of soil located beneath a structure is depicted in Figure 3.3.

The soil element would be deformed by the shear stresses developing due to propagation of shear waves induced by a seismic event. Due to the random nature of earthquake induced loading, irregular shear stresses are imposed on the soil element. Seed et al. (1975) developed a weighting procedure to convert irregular shear stress time histories to an equivalent number of harmonic stress cycles so as to produce an equivalent increase in pore pressure to that of the irregular time history. In that study, uniform harmonic stress cycles were arranged at an amplitude of 65% of the peak cyclic stress ($\tau_{cyc}=0.65\ \tau_{max}$), and the procedure was developed considering reconstituted clear sand samples. Accordingly, the pore pressure generation effect induced by an earthquake can be effectively simulated in the laboratory through application of uniform harmonic stress cycles to the soil specimens.

The vertical and horizontal stresses acting on the soil element will vary instantaneously due to the additional stresses induced by the oscillating structure.Hence, the mean total stress will also vary throughout the cyclic loading. Due to the difficulties involved in simulation of this loading pattern in the laboratory, the inertial effects of a building imposed by the seismic load are neglected for practicality. Accordingly, the vertical and horizontal stresses are assumed to remain uniform throughout the cyclic loading. Thus, the mean total stress remains unchanged during cyclic loading.

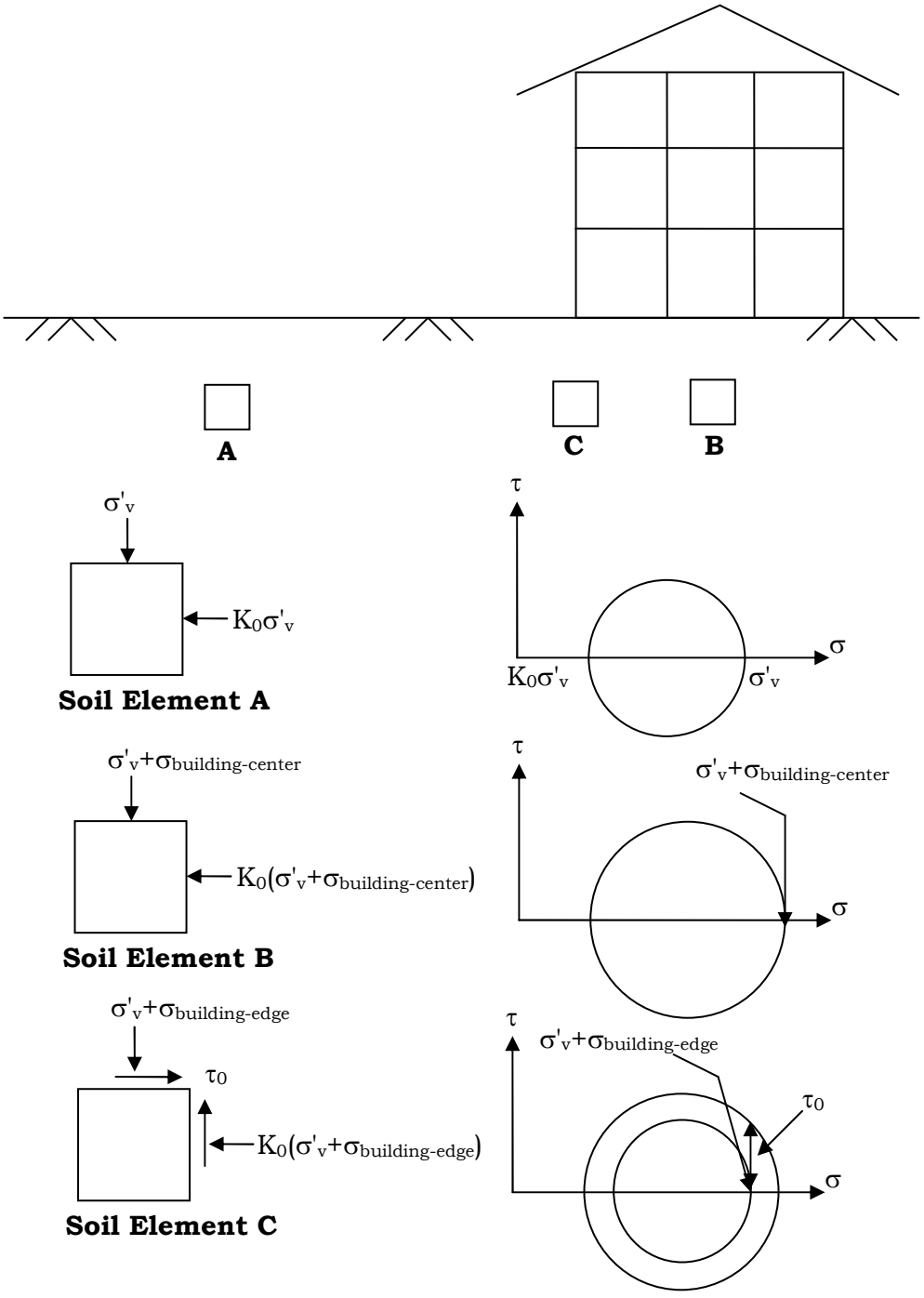

Figure 3.3 Idealized stress conditions in free-field, beneath the center and beneath the corner of a structure

In situ stresses corresponding to the free field conditions are simulated in the triaxial test via a specimen initially loaded to a hydrostatic stress equal to σ_3, and then the load is increased to obtain a vertical stress of $\sigma_3+\sigma_d/2$, and simultaneously decreased to obtain a horizontal stress of $\sigma_3-\sigma_d/2$. Subsequently the vertical stress is reduced to $\sigma_3-\sigma_d/2$ while horizontal stress is increased to $\sigma_3+\sigma_d/2$. The major and the minor principal stresses are the horizontal and vertical stresses respectively, and the cycle is completed when the stresses return back to an isotropic condition of σ_3. The ideal stress conditions are equivalent to the superposition of the conditions displayed in Figure 3.2. The stress combination consists of simultaneous application of an axial vertical stress of σ_d and an isotropic stress reduction of $\sigma_d/2$. In saturated soils, however, an isotropic stress change would only cause an increase or decrease of the pore water pressure by the same magnitude. There would be no change in effective stress, which makes it unnecessary to apply an isotropic change in stress in cyclic triaxial testing of saturated soils. Therefore, free field cyclic loading conditions can be satisfied only by cyclic application of an axial vertical deviator stress (σ_d) while the isotropic stress is maintained constant at σ_3.

The Mohr circles corresponding to the loading conditions during a consolidated-undrained triaxial test are illustrated in Figure 3.4. The specimen is initially consolidated to a hydrostatic confining stress equal to σ_3, then if it is necessary (for the case of an existing structure load), an additional axial stress ($\Delta\sigma_1$) is applied to consolidate the specimen anisotropically. Subsequently, the axial load is cycled symmetrically around the initial axial load at a given frequency until a predetermined axial strain is reached or until a specific number of cycles have been applied.

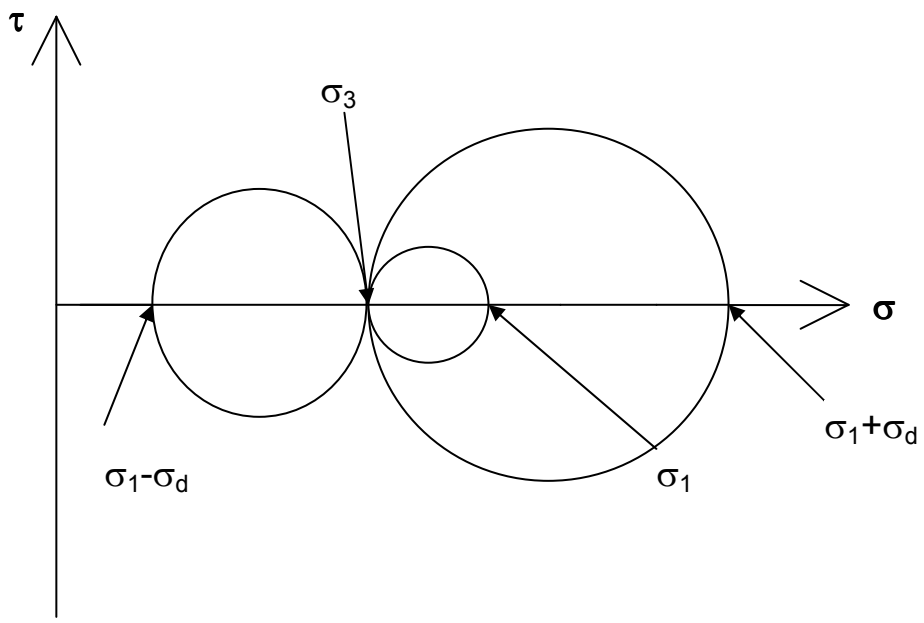

Figure 3.4 Applied stress conditions during an undrained triaxial test over a saturated soil sample.

It is important to note that the principal stresses have different orientation at maximum and minimum axial stress if the initial deviator load is not high enough to ensure the stress state to remain in compression side during the test. In the tests conducted under the stresses having no reversal during cycling, the load pattern becomes a one-way loading; contrarily, it becomes a two-way loading for the tests stress reversals occurred. The principal stresses rotate 90^{o} during each cycle of a two-way loading test.

In cyclic triaxial test, the compressive and extensional response of the soil is evaluated within the same test. Since the extensional strength of the natural soils is smaller than the compressive strength, the measured axial strains are not symmetric and are primarily due to deformation in extension. This condition is expected to be taken into consideration during evaluation of the results of a cyclic triaxial test.

The applied cyclic stress ratio (CSR) is commonly used to describe the amplitude of loading. CSR is defined herein as the ratio of half the applied

cyclic deviator stress ($\Delta\sigma_{cyc}$) to the initial mean effective stress (p'_i) for triaxial conditions.

$$CSR_{tx} = \frac{\Delta\sigma_{cyc}}{2p'_i} \qquad (3.1)$$

Although triaxial testing is relatively easy to perform and inexpensive, there are some limitations exist. These limitations are summarized in the following (Bishop and Henkel, 1962):

- Intermediate principal stress is equal to the minor principal stress in compression and the major principal stress in extension type of triaxial test, while it is formed by the conditions of plain strain in the field.
- In triaxial test, the principal planes are fixed in as related to the axis of the specimen, and principal stresses can rotate only 90^o whereas the rotation angle of principal stresses is not fixed at 90^o in the field.
- Friction between the ends of the specimen and the rigid end caps prevents formation of uniform stress and strain conditions throughout the specimen.

3.3 Specimen Preparation and Placement

In the study, as it is indicated previously, the cyclic behavior of fine grained soils is investigated via triaxial tests conducted over reconstituted and undisturbed samples. Therefore, the specimens tested throughout the study were extruded from either reconstitution box (the reconstitution process will be addressed in following chapter) or shelby tubes acquired from various locations in Adapazarı, Turkey. The procedure used to prepare specimens is described in proceeding paragraphs.

From the reconstitution box or from a shelby tube, the specimens are extruded by utilizing the samplers of 36 mm in diameter and 100 mm in height. The specimens are kept in moisture room under ideal conditions until to be tested, and replaced from the sampler to the mould just before testing. The mould has dimensions of 35 mm in diameter and 71 mm in height. Portions of the specimen in excess of the mould at top and bottom are trimmed gently. The specimen is then taken out of the mould and mounted on the pedestal of the triaxial device.

In order to reduce the duration of consolidation and to accelerate the equalization of pore pressures during shearing, the specimen is surrounded by filter paper. The filter paper is cut according to the dimensions of the specimen, and it is slotted to minimize restriction of sample deformations. The slots are arranged to obtain 6 drains each having 1cm width. In order to prevent absorption of moisture from the specimen, filter paper is saturated by de-aired water just before wrapping around the specimen. Slight finger pressures are then applied to smooth out the filter paper and to release trapped air bubbles between the filter paper and the specimen.

The cell pressure and back pressure connections are primarily tightened to the bottom plate which is already placed on the loading platform. The pressure systems are checked against leakage under high pressures while the valves on the bottom plate are closed (Figure 3.5).

Figure 3.5 View of bottom plate with connections

The volumetric change and pore pressure measurement connections linked to the top of the pedestal should be saturated prior to mounting of the specimen. The burette is filled sufficiently (about 30-35 milliliters) with de-aired water, and then connected to the relevant valve on the bottom plate while the valve is closed. The filter stone, which has previously been boiled in water, is placed directly on the pedestal. The volume change valve is then opened and de-aired water is circulated through the system until the pore pressure channel is saturated.

The rubber membrane is placed in the mounting cylinder and a slight suction is applied to hold the membrane tight against the wall of the cylinder while the membrane is being adjusted to remain smooth and free from twists. The mounting cylinder is then placed directly over the pedestal and the specimen surrounded by filter drains is mounted carefully into the cylinder (still holding the membrane tight with vacuum). Then, another filter stone is placed over the specimen and the membrane is released out of the mounting cylinder such that the bottom end of the membrane is pushed down over the pedestal and the top end of the membrane is pushed up to stand freely. At this stage, the volume change valve is closed after the pore pressure line is connected to the pore

pressure transducer. To prevent the leakage between the cell and the specimen two O-rings are placed around the rubber membrane at the pedestal and top cap respectively. The back pressure mechanism is saturated before the top cap is placed over the top filter stone. Care should be taken not puncture the rubber membrane.

The diameter at both ends and middle of the sample and the height of the sample are measured with taking into account of the thicknesses of filter paper and membrane. The top section of triaxial cell is then lowered over the specimen carefully such that the piston must be held up not to press on the specimen. The upper cell section is rotated until the three wing bolts line up with the holes in the bottom plate. Having tightened these bolts as keeping the top and bottom plates are parallel. The piston is let to fall into the socket on the top cap; it may be necessary to tilt the entire cell in order to assure this alignment. Then, the cell is filled with water after opening the screw valve to allow the entrapped air exit the cell.

3.4 General Testing Procedure

Earthquake loading, which is of mostly interest in this study, is generally applied so rapidly that the saturated soils are loaded under undrained conditions, and the behavior of those soils are primarily based on pore pressure response under such rapid loads. Therefore, full saturation of specimens is essential for accurate and reliable measurement of pore pressure response during an undrained triaxial test.

During the beginning of triaxial testing process it was observed that the pore pressure of the specimens had risen at least to value of 90% of the applied confining pressure. However, it was aimed to obtain Skempton's B value of 95% at least. The degree of saturation was measured using Skempton's B value, which is defined as the ratio of the increase in pore water pressure and the increase in confining pressure ($B=\Delta u/\Delta\sigma_3$). Additionally, the air trapped in the porous stones, drainage lines and between the soil and the membrane must be removed and replaced with

de-aired water. Therefore, back pressure procedure is used to achieve B values greater than 0.95.

Before applying the back pressure, the specimens were consolidated either isotropically or anisotropically to achieve the desired stress histories. Consolidation process was performed before the back pressure process due to high values of B (B ≥ 0.90) at the beginning.

After achieving satisfactory values of B, the specimens are tested either monotonically or cyclically. In the study, monotonic compression tests were performed by strain controlling with strain rate of 0.07%/min in general. Cyclic tests were performed by applying stress controlled sinusoidal loading at a frequency of both 0.5 Hz and 0.05 Hz. The loading amplitude was characterized in terms of the Cyclic Stress Ratio (CSR), which for the cyclic triaxial test is defined as the ratio of the maximum cyclic shear stress ($\Delta\sigma_d/2$) to the initial mean effective consolidation stress. The CSR values are ranging between 0.3 and 0.8. The cyclic loading was mostly applied until axial strains in excess of 10% were reached. However, in some tests although the cycle numbers exceeded 100, axial strain of even 5% was not reached. In such cases, the tests were terminated at an axial strain value between 3% and 5%.

3.4.1 Specimen Consolidation

The desired pressure is achieved by adjusting the screw control and the weights to be hung on the yoke underside the control table simultaneously. Before applying the cell pressure, the cell pressure valve on the bottom plate of triaxial system is closed against a possible pressure fluctuation. The connection valve between the screw control and the tap water is opened, and then the reservoir of the screw control is filled by turning it almost all the way out. The tap water connection is then closed. The pressure caused by the weights is checked after the piston is given a slight movement by the screw control. The load applied through the weights hung on is adjusted and the pressure is checked again until the desired pressure is reached. The valve to the constant

pressure cell is then opened and the system is ready for isotropic consolidation.

The lock preventing the movement of the rod, which connects the load cell to the specimen, is opened to allow the volumetric expansion or consolidation. Having all these steps completed, the volumetric change and the cell pressure valves are opened to start consolidation. To measure the change in void ratio of the specimen, the water level in the burette is recorded at the start and the end of the consolidation.

Due to prolonged consolidation process, cell pressure may slightly drop because of leakage in the system. In such cases, the connection to the triaxial cell is closed and the constant pressure piston is raised up again by means of the screw control. The valve to the triaxial cell is opened as soon as the pressure is stabilized at the desired level.

The specimens to be consolidated anisotropically are loaded by the weights hung on the yoke mounted on the rod, thus anisotropic conditions are achieved by increasing the stresses acting vertically on the specimens. Anisotropic consolidation phase is conducted after the completion of isotropic consolidation.

3.4.2 Specimen Saturation

The state of "full saturation" is generally achieved by a procedure called back pressure saturation. The saturation process is conducted by increasing the pore water pressure and the confining pressure incrementally such that the effective stress of the specimen is maintained constant. The term of "back pressure" is used to explain the pressure applied to increase the pore water pressure of the specimen. An increase in back pressure causes a reduction in volume of the trapped air (Boyle's law), and the sustained pressure causes dissolution of air into the water by the time (Henry's law). Thus the time needed to saturate a specimen depends on the amount of air in the system, the initial degree of specimen

saturation and the maximum back pressure that can be applied by the testing system.

After the completion of the consolidation the lock of the rod used to apply vertical deviator load is tightened to prevent the movement of the rod which is to be caused by the increase in cell pressure. The system then becomes ready to conduct back pressure saturation. The confining pressure and the back pressure are increased by means of the relevant screw controls so that the effective stress remains constant. The back pressure is applied through the pipe connected to the cap mounted on upper part of the specimen, and the pore water pressure of the specimen is measured by the transducer connected to the pedestal. Each pressure increment, therefore, is applied after enough time been allowed for the pore water pressure to equilibrate with the back pressure. This time period depends on the height of the specimen and on the permeability of the soil.

Specimens were saturated under back pressures ranging between 100 to 200 kPa. Having applied enough back pressure, the degree of saturation is measured using Skempton's B value. For this, the valve of the back pressure is closed and the all-round pressure is then increased by an amount of $\Delta\sigma_3$, while the change in pore water pressure (Δu) is being monitored. In all cases of this study, $B > 0.95$ ($B=\Delta u/\Delta\sigma_3$) was achieved at the back pressure levels greater than 2 bars.

3.4.3 Cyclic Phase

All the valves excluding the one connecting the cell pressure, which are on the pedestal, are closed just before starting the test. Permanent cell pressure provides a constant level of pressure in the cell. The rod transferring load to the specimen is adjusted at a level that the movement of the rod must not be limited during cycling. The rod is kept as locked until the start. The power function generator is set to "run" position while keeping the magnitude of the load at zero. Then, the pressure transferred through actuator is adjusted to the desired value by the screw on the

control unit. That screw is used to adjust initial pressure to a level of either zero (i.e. isotropically consolidated) or another positive pressure (i.e. anisotropically consolidated). The rod is unlocked, after which the cyclic deviator stress ($\Delta\sigma_{cyc}$) is set to desired magnitude and frequency and the test is started at the same time of cyclic stress application. Pore pressure, cell pressure, axial pressure and axial displacement variations are recorded during the test.

3.5 Testing Equipment

The monotonic traixial tests were carried out by a standard triaxial test device produced by ELE. The cyclic tests were performed by Norwegian cyclic triaxial apparatus which was connected to a data acquisition system produced by TDG. The other relevant soil mechanics tests required to identify the characteristics of the samples used in the study were performed by standard soil testing equipments available in the soil mechanics laboratory of the Middle East Technical University (METU). The equipment used for the cyclic triaxial tests is introduced below.

3.5.1 Norwegian Cyclic Triaxial Apparatus

The cyclic triaxial test system used in this study was produced by Geonor under supervision of the Norwegian Geotechnical Institute. The equipment can be utilized to perform load controlled monotonic and cyclic tests under both drained and undrained conditions. A general view of the apparatus is presented in Figure 3.6

Figure 3.6 General view of the Norwegian Cyclic Triaxial Test Device

The system is an electropneumatic cyclic triaxial testing system, the instrumentation consists of an external load cell and external LVDT to monitor the axial load and vertical displacement respectively, and two pressure transducers to measure cell pressure and pore water pressure. The system is controlled by a personal computer through the CODA software, and allows open-loop stress controlled cyclic loading.

3.5.2 TDG AI8b Data Acquisition System

AI8b is basically a desktop voltage measurement device. It is capable to measure the exit voltages of the static sensors that do not change rapidly with time. The measured voltages are then transferred to the computer in which the software of CODA is used to store the data collected. The data acquisition system of TDG AI8b transfers the collected data to the computer by means of universal serial bus (USB) device gate. The data collected through USB port is recorded and plotted by the software of TDG CODA. There exist 8 channels on the device, each of which has its own signal processing unit. Due to the 16-Bit CMOS SAR ADC, it is also capable to provide a high measurement resolution of 65536 steps in full scale of voltage range (±10V). The voltage applied to each channel can be increased according to the gain values about 150/247/396/494/ 643/740/890. The deviation due to measurement error is at the level of 0.1% of the full scale.

CHAPTER 4

CYCLIC RESPONSE OF RECONSTITUTED LOW PLASTIC SILT

4.1 Introduction

It has been long recognized that fine grained soils can also undergo high deformations and strength degradation during cyclic loading. Such behavior is evident from post earthquake observations and numerous laboratory studies conducted over fine grained soils. Although results based on the laboratory tests conducted over undisturbed samples provide information about the soils at a specific site, it is difficult to make generalizations on the cyclic response of fine grained soils. The sample characteristics influencing the cyclic response can not be controlled during studies with undisturbed samples, and typically it is difficult to provide sample uniformity. Accordingly, reconstituted samples are preferred in numerous studies to achieve a profound understanding of the factors affecting the soil behavior.

The primary purpose of the testing program in this study is to provide a systematic and controlled investigation of the factors affecting fine grained soil behavior on a comparative basis. For this purpose, to be able to eliminate the inherent variability of naturally deposited soils, and to provide control over sample characteristics, reconstituted specimens are used in the study. Many researchers reported that reconstitution procedure may have a great effect on the behavior of sands (Mulilis et al., 1977; Tatsuoka et al., 1986; Yamamuro and Wood, 2004). However, the information concerning the effect of reconstitution method on the behavior of fine grained soils in literature is rather limited. Common reconstitution methods are briefly discussed in section 4.2

4.2 Reconstitution Techniques

There are four methods considered within the study. These are the most widely used reconstitution methods, therefore each method is briefly discussed in the following.

4.2.1 Moist Tamping

The technique consists of compacting moist material in layers, in which each layer is tamped with a specified force and frequency to obtain a prescribed dry unit weight (Ladd, 1974; Silver et al., 1976). The method best models the soil fabric for the compacted fills, for which the method was originally designed (Kuerbis and Vaid, 1988). Moist tamping is not useful to produce specimens representing naturally deposited soils and it is known that the specimens prepared via this technique can exhibit non-uniformity in the layer boundaries. The method is also reported to be convenient for preparation of sand samples as it can provide specimens with a wide range of void ratios, which is quite difficult to achieve in finer soils (Zlatovic and Ishihara, 1997).

4.2.2 Air Pluviation

In the air pluviation method, dry soil is pluviated into a mold from the nozzle of a tube placed at a controlled height. The major factors affecting relative density of the air-pluviated samples are reported as the height of particle fall (Vaid and Negussey, 1988) and rate of deposition (Miura and Toki, 1982). Increasing height of particle fall results in a denser soil specimen. The method best models the natural deposition process of wind blown aeolian deposits, which mostly consists of well-sorted soils. It is reported that the well-graded soils cannot be reconstituted by air-pluviation as efficiently as the well-sorted soils due to the occurrence of segregation (Kuerbis and Vaid, 1988).

4.2.3 Water Pluviation

Water pluviation is similar to the air pluviation technique with a difference that the soil particles are pluviated through de-aired water, which ensures the sample saturation. The velocity of the soil particles falling in the water is lower than that of the particles falling in the air, thus air-pluviated soils mostly have higher relative densities than those of water-pluviated soils (Kuerbis and Vaid, 1988; Vaid and Negussey, 1984). It is reported that fabric and behavior of naturally deposited alluvial soils display similarities with those of soils reconstituted via water pluviation (Oda et al., 1978). The technique can be used to produce homogeneous samples with the exception of utilizing well-graded soils. Segregation due to particle size range is a problem in water pluviation of well-graded soils. The technique forms initially saturated samples having fabric most like that of natural alluvial soils. However, the technique requires a large amount of sample and long time to prepare specimens.

4.2.4 Slurry Deposition

Slurry deposition is a technique mainly utilized to obtain homogeneous samples regardless of grain size. There has been different implementation of slurry deposition techniques due to sample properties and the test device used. The specimen preparation technique described by Kuerbis and Vaid (1988) is developed primarily for preparation of silty sand samples. The sample is mixed with de-aired water and boiled to de-air the mixture after which the mixing tube is vigorously rotated to obtain completely homogeneous samples. The sample is then deposited in the mould located in the load cell. Donahue et al. (2007) utilized a different technique of slurry deposition of silts to be used in cyclic triaxial and cyclic simple shear devices. Soil and water are mixed with a specific water content providing optimum mixing and workability. The mixture is deposited by applying vacuum and vertical load combination in which it becomes able to stand freely under its own weight. The ability to provide

homogeneous samples is one of the important advantages of slurry deposition techniques.

Among those mentioned above, slurry deposition technique appears to be the most convenient for the reconstitution of saturated fine grained soils consisting of a wide range of particle sizes.

4.3 Properties of the Reconstituted Material

The tests are programmed to investigate the soils within a wide range of particle sizes, dominated by fine grained material (i.e. % of particles less than 0.075mm is greater than 50% of the sample by weight). The soil used in the tests was supplied in powdered form from Balad, Iraq. The grain size distribution of the light brown colored soil is determined using both sieve and hydrometer analyses. As it is seen in Figure 4.1, the material consisted of 68.5% silt, 4.5% clay, and 27% fine sand particles. The basic characteristics of the material are as follows: G_s=2.69; LL=31; PL=24; PI=7. The LL was determined by means of Casagrande cup. Koester (1992) reported that the LL values determined by Casagrande cup and fall cone test can be different for the same soil. Accordingly, LL value is 35 according to fall cone test applying the corrections proposed by Koester (1992) when considering Chinese liquefaction assessment criteria. The material is classified as low plasticity silt (ML) according to the Unified Soil Classification System (USCS), and plots adjacent to the A-line on the plasticity chart as shown in Figure 4.2.

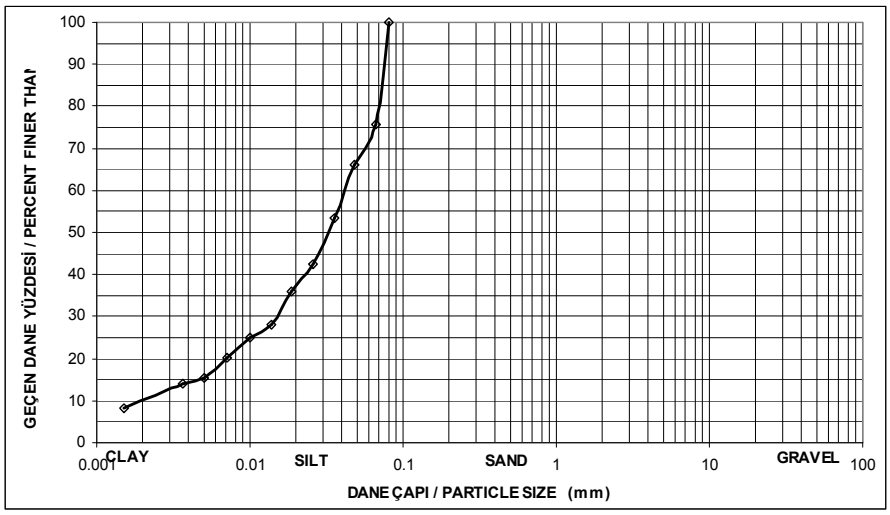

Figure 4.1 Grain size distribution curve of the soil utilized in the study

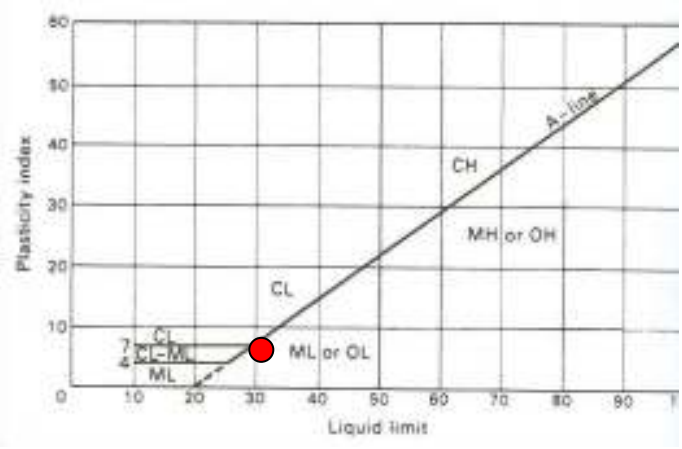

Figure 4.2 The location of the reconstituted material on plasticity chart

4.4 Reconstitution Procedure

The material was mixed with de-aired water of an amount required to bring the water content to about 2 to 3 times of the liquid limit. In that specific water content the soil was experienced to increase in workability during the mixing process, and consequently a homogeneous slurry is provided. The slurry was then placed into a cubic box inside of which was covered with a woolen tissue. The box which has the dimensions of 19.5,

19.5 and 21 cm and narrow holes on the top and bottom cover, was then placed in a container having dimensions of 32, 32 and 25 cm. The container was then filled up with de-aired water such that the box was submerged totally in the water. The slurry was then consolidated under a vertical pressure of 40 kPa, which was imposed by means of a pneumatic piston as shown in Figure 4.3. The applied pressure was sufficient to obtain specimens that are able to stand freely under their own weight. After having consolidated the slurry, it was possible to extrude 16 specimens from one slurry box.

Figure 4.3 View of oedometric consolidation during reconstitution process

4.5 Monotonic Triaxial Compression Tests

A series of undrained monotonic triaxial tests were conducted over the reconstituted samples to examine the static response, and to identify if any conceivable relationship between monotonic and cyclic responses exists. An important issue during triaxial testing of fine grained soils is the rate at which the load is applied. Due to the friction at the two ends, distribution of the stress and strain is non-uniform along the specimen. Sufficient time should be allowed during loading to provide stabilization of the pore water pressure within the specimen. Otherwise, the strength of the soil is affected by the non- uniformity of pore pressure.

Proper loading rates ensure 95% of pore pressure stabilization in the specimen, assuming that the time to failure $t_f \geq 4t_{50}$ in undrained tests, where t_{50} is the time required for completion 50% of consolidation (Bishop and Hengel, 1957; Germaine and Ladd, 1988). t_{50} values of the reconstituted material were obtained from oedometric consolidation test for different consolidation pressures (P) as presented in Table 4.1. The pore pressure within the specimen tested under a loading rate should be in equilibrium when the failure is reached after minimum t_f. That is, if a soil is found to reach peak strength at 1% strain and if t_f value for that soil is 1 minute, then uniform pore pressure distribution is provided when the triaxial test is conducted at a strain rate of 1% per minute or slower. The peak strength of the reconstituted specimens were reached at strain levels ranging between 6% and 10% for different triaxial stress conditions. As it can be seen in Table 4.1, the longest time required to reach failure is almost 10 minutes. The static triaxial tests were conducted at strain rate ranging between 0.05 and 0.1%/min, which is, thus, quite low than those required for pore water pressure equilibrium of the soil tested.

Table 4.1 Minimum time to failure (t_f) obtained with different oedometric stresses

P (kPa)	t_{50} (min)	$t_f=4t_{50}$ (min)
25	2.52	10.09
50	1.34	5.37
100	0.09	0.36
200	0.15	0.60

Results of 25 strain controlled monotonic triaxial tests conducted on the reconstituted specimens are listed in Table 4.2. In addition to the tests performed with loading rates between 0.05 and 0.1%/min, two more tests were performed at a loading rate of 1.4%/min and 1%/min on the specimens isotropically consolidated under 100 kPa. Based on the test results, the average values of internal friction angle and cohesion were determined as 37^o and 5 kPa, respectively.

Two specimens with OCR of 2 and 4 were monotonically tested as well. State of OC was achieved through unloading the specimens isotropically consolidated under 200 kPa. Accordingly, the OC specimens sustained 100 kPa and 50 kPa effective initial confining stresses just before getting sheared. Those specimens were tested with loading rate of 0.07%/min.

The initial stress conditions of the specimens were arranged to provide a wide range of representative in-situ stress states that may exist beneath the foundations as well as at the free field. Prior to testing, the specimens were first subjected to certain confining pressures (σ'_{3c}), and then the axial stress was increased incrementally by allowing drainage of the specimen until a particular stress state was reached. Variation in the axial stress applied at this stage imposed an initial sustained deviator stress ($\Delta\sigma_i$). To remove the influence of initial stress state, the deviator stress ($\Delta\sigma$) is normalized by initial mean effective stress (p'_i). Accordingly, the stress ratio ($\Delta\sigma_i/p'_i$) sustained initially ranges between 0 and 1.5. Here, $\Delta\sigma_i$ is the initial deviator stress and p'_i is the initial mean effective stress.

Table 4.2 Initial states and loading rates of monotonic tests

Test	σ'_{1c} (kPa)	σ'_{3c} (kPa)	Initial p'_i (kPa)	Rate of ε_a (%/min)	OCR	$\Delta\sigma_i/p'_i$
ST1	35	35	35	0.1	1	0
ST2	50	50	50	0.07	1	0
ST3	50	50	50	0.07	2	0
ST4	50	50	50	0.07	4	0
ST5	80	80	80	0.07	1	0
ST6	75	75	75	0.05	1	0
ST7	100	100	100	0.07	1	0
ST8	100	100	100	1	1	0
ST9	100	100	100	1.4	1	0
ST10	80	50	60	0.07	1	0.50
ST11	100	50	66.67	0.1	1	0.75
ST12	100	50	66.67	0.1	1	0.75
ST13	120	50	73.33	0.1	1	0.95
ST14	90	60	70	0.07	1	0.43
ST15	120	60	80	0.07	1	0.75
ST16	140	50	80	0.1	1	1.13
ST17	150	50	83.33	0.07	1	1.20
ST18	160	50	86.67	0.1	1	1.27
ST19	200	50	100	0.07	1	1.50
ST20	120	80	93.33	0.1	1	0.43
ST21	150	80	103.33	0.1	1	0.68
ST22	120	100	106.67	0.1	1	0.19
ST23	150	100	116.67	0.1	1	0.43
ST24	180	100	126.67	0.1	1	0.63
ST25	200	100	133.33	0.1	1	0.75

4.6 Cyclic Triaxial Tests

When studying the liquefaction resistance of soils, it is a common practice to report the number of cycles required for the specimen to reach the state "liquefaction". The proper use of the term "liquefaction" has been a subject of discussion among researchers for over the last three decades. Lee and Seed (1967a) defined the "liquefaction" as when the soil exhibits resistance at negligible levels to deformation over a wide strain range during cyclic loading. This definition is based on the strength of the soil during cyclic loading. Alternatively, Silver et al. (1976) and Vessely et al. (1996) proposed that the "liquefaction" is initiated during cyclic testing when the generated excess pore water pressure becomes equal to the

initial confining stress irrespective of the strength and the strain levels developed.

Although there exists no universally accepted criteria for a specific strain level referred to as failure or as "liquefaction", different definitions have been proposed. These include: 3% single amplitude axial strain (Boulanger et al., 1998), 5% single amplitude axial strain (Campanella and Lim, 1981), 10% double amplitude axial strain (Silver et al., 1976), 15% double amplitude strain (Andersen et al., 1988). Single amplitude (SA) strain refers to peak strain in compression (positive side) or extension (negative side) for a given cycle, while double amplitude (DA) refers to the addition of the absolute values of the peak single amplitude strain in compression and extension for a given cycle. In this study, the definition of SA strain is considered to be more convenient when evaluating the results of the tests performed with anisotropically consolidated specimens in which the strain levels in compression and extension are significantly different, and the strain accumulation occurs at the side where the stresses dominate the behavior. On the other hand, DA strain values are used in comparison of the results of the tests performed with isotropically consolidated specimens.

Total of 69 cyclic tests were conducted over isotropically and anisotropically consolidated silt specimens. The consolidation pressures were intended to be representative of the stresses over the soil elements at depths critical for structures during seismic events. The applied cyclic stress ratio (CSR) commonly represents the amplitude of loading. A range of CSR_{tx} values between 0.30 and 0.72 were used in the tests, and the corresponding amplitudes of cyclic stress were applied in a load controlled manner. The stresses applied during cycling, the loading frequencies, stress states previous to the cyclic phase, void ratio and the ratio of water content to LL at the beginning of cyclic shearing for the tested samples are given in Table 4.3.

Majority of the tests were conducted at a frequency of 0.5 Hz, which is considered as representative of the typical frequency range of seismically induced loading. However, such a loading rate is too fast to ensure excess

pore water pressure dissipation throughout the specimen. In order to examine the influence of loading rate on the response, 11 of the tests were performed at a frequency of 0.05 Hz, which is a rate considered to be slow enough to ensure pore water pressure homogeneity in such a silty soil.

In order to investigate the influences of stress history and initial stress state on the cyclic response of silt, the tests were carried out with the specimens having various OCR and initial shear stress ratios (τ_s/p'_i). The OC state was reached by unloading the specimens to a confining stress which provides OCR values between 1 and 4. The specimens having OCR greater than 1 were isotropically consolidated under a specified confining stress. After the initial consolidation phase, the drainage valve is closed and the confining pressure was reduced so as to obtain the specified OCR. Having reduced the confining pressure, the drainage valve was then opened and the specimens are consolidated for 2 hours in OC state. All the OC specimens, thus, had just isotropic initial stress states before getting cycled. Nevertheless, the specimens in NC state were consolidated under various ratios of initial shear stress to initial mean effective stress (τ_s/p'_i). As indicated in Table 4.3, the initial shear stress ratio sustained by the specimens ranges between 0 and 0.75. It should be noted that $\tau_s/p'_i=0$ condition refers to the isotropic consolidation. The sustained initial shear stresses were provided by application of axial deviatoric stresses ($\Delta\sigma$) after consolidation under confining pressures (σ'_{3c}). All the specimens were consolidated 24 hours under isotropic conditions although a few hours were generally sufficient for consolidation. Then, consolidation was continued under applied major axial stress ($\sigma'_{1c}=\sigma'_{3c}+\Delta\sigma$) and σ'_3 for 5 to 6 hours. Therefore, the duration for the second consolidation phase following loading to impose an initial shear stress or unloading to create an OCR was limited with a few hours.

Table 4.3 Initial conditions of cyclic triaxial tests carried out with reconstituted silt

Test	σ'_{1c} (kPa)	σ'_{3c} (kPa)	τ_s/p'_i	CSR_{tx} ($\Delta\sigma_{cyc}/2p'_i$)	e_i	w/LL	OCR	f (Hz)
C1	50	50	0	0.35	0.74	0.84	1	0.5
C2	50	50	0	0.3	0.74	0.843	1	0.5
C3	50	50	0	0.55	0.75	0.849	1	0.5
C4	50	50	0	0.6	0.75	0.851	1	0.5
C5	45	45	0	0.72	0.72	0.82	1	0.5
C6	75	50	0.21	0.34	0.74	0.835	1	0.5
C7	75	50	0.21	0.51	0.72	0.812	1	0.5
C8	75	50	0.21	0.69	0.75	0.846	1	0.5
C9	75	50	0.21	0.69	0.75	0.852	1	0.5
C10*	95	50	0.35	0.35	0.75	0.851	1	0.5
C11	95	50	0.35	0.54	0.75	0.848	1	0.5
C12	90	50	0.32	0.71	0.74	0.844	1	0.5
C13*	120	60	0.38	0.41	0.75	0.857	1	0.5
C14*	120	60	0.38	0.5	0.77	0.875	1	0.5
C15	120	60	0.38	0.59	0.74	0.839	1	0.5
C16	80	80	0	0.31	0.75	0.854	1	0.5
C17	80	80	0	0.41	0.74	0.838	1	0.5
C18	80	80	0	0.5	0.75	0.848	1	0.5
C19	80	80	0	0.59	0.74	0.842	1	0.5
C20	80	80	0	0.59	0.73	0.825	1	0.5
C21	80	80	0	0.59	0.73	0.833	1	0.5
C22	90	60	0.21	0.36	0.74	0.841	1	0.5
C23	90	60	0.21	0.54	0.75	0.85	1	0.5
C24	90	60	0.21	0.64	0.72	0.821	1	0.5
C25*	150	50	0.6	0.45	0.75	0.851	1	0.5
C26*	150	50	0.6	0.6	0.74	0.845	1	0.5
C27	50	50	0	0.3	0.73	0.828	2	0.5
C28	50	50	0	0.5	0.73	0.827	2	0.5
C29	50	50	0	0.6	0.73	0.825	2	0.5
C30	50	50	0	0.6	0.73	0.83	2	0.5
C31	50	50	0	0.65	0.73	0.826	2	0.5
C32	50	50	0	0.35	0.7	0.789	4	0.5
C33	50	50	0	0.35	0.7	0.79	4	0.5
C34	50	50	0	0.5	0.69	0.781	4	0.5
C35	50	50	0	0.55	0.7	0.797	4	0.5
C36	50	50	0	0.6	0.68	0.773	4	0.5
C37	50	50	0	0.8	0.69	0.778	4	0.5

Table 4.3 (continued)

Test	σ'_{1c} (kPa)	σ'_{3c} (kPa)	τ_s/p'_i	CSR_{tx} ($\Delta\sigma_{cyc}/2p'_i$)	e_i	w/LL	OCR	f (Hz)
C38	95	95	0	0.45	0.72	0.814	2	0.5
C39	75	75	0	0.47	0.72	0.822	2.5	0.5
C40	50	50	0	0.55	0.72	0.817	2	0.5
C41	100	100	0	0.55	0.7	0.797	2	0.5
C42	100	100	0	0.48	0.72	0.813	1.5	0.5
C43	100	100	0	0.3	0.7	0.796	2	0.5
C44*	95	50	0.35	0.4	0.76	0.858	1	0.5
C45	90	60	0.21	0.48	0.73	0.829	1	0.5
C46	90	60	0.21	0.61	0.74	0.837	1	0.5
C47*	150	50	0.6	0.7	0.74	0.838	1	0.5
C48*	200	50	0.75	0.39	0.73	0.829	1	0.5
C49*	195	50	0.74	0.6	0.74	0.841	1	0.5
C50	100	100	0	0.34	0.74	0.843	1	0.5
C51	75	50	0.21	0.4	0.72	0.817	1	0.5
C52*	95	50	0.35	0.42	0.76	0.858	1	0.5
C53	50	50	0	0.5	0.74	0.843	3	0.5
C54	50	50	0	0.62	0.72	0.82	4	0.5
C55	50	50	0	0.7	0.72	0.82	3	0.5
C56	50	50	0	0.53	0.72	0.812	4	0.5
C57	50	50	0	0.52	0.74	0.843	2	0.5
C58	50	50	0	0.58	0.74	0.843	2	0.5
C59	50	50	0	0.53	0.72	0.812	1	0.05
C60	50	50	0	0.85	0.71	0.804	1	0.05
C61	120	60	0.38	0.54	0.72	0.812	1	0.05
C62	80	80	0	0.54	0.74	0.843	1	0.05
C63	150	50	0.6	0.6	0.73	0.827	1	0.05
C64	50	50	0	0.3	0.72	0.82	1	0.05
C65	100	50	0.38	0.37	0.72	0.82	1	0.05
C66	120	60	0.38	0.44	0.72	0.82	1	0.05
C67	80	80	0	0.44	0.73	0.827	1	0.05
C68	150	50	0.6	0.48	0.71	0.804	1	0.05
C69	100	50	0.38	0.56	0.71	0.804	1	0.05

*Number of cycles was calculated considering SA axial strains

Number of cycles (N) required for the axial strains of 3%, 5% and 10% reached in each test are listed in Table 4.4. In the case of stress reversal, double amplitude (DA) axial strains; and for non-reversal stress conditions, single amplitude (SA) axial strains were taken into consideration to calculate the values of N.

Table 4.4 Number of cycles (N) and excess pore pressure ratio reached at the axial strains of 3%, 5%, and 10%.

	Number of Cycles (N)			Excess Pore Pressure Ratio, r_u					
Test	**3% Ax.St.**	**5% Ax.St.**	**10% Ax.St.**	**3% Ax.St.**	**5% Ax.St.**	**10% Ax.St.**	**Max. Ax.St. (%)**	**N at Max. Ax.St.**	**r_u at Max. Ax.St.**
C1							0.6	220	0.42
C2	130	150		0.92	1		4.1	147	1
C3	1	7	21	0.16	0.63	1.13	12	49	1.34
C4	2	3	5	0.4	0.58	0.95	18	14	1.34
C5	13	25		0.5	0.73		4.4	25	0.73
C6							0.5	360	0.08
C7	12	21	34	0.57	0.72	0.91	13	45	1
C8	2	3	6	0.28	0.42	0.72	11	9	0.88
C9		1	5		0.39	0.7	12	5	0.73
C10*	110			0.68			4	217	0.72
C11	2	4		0.23	0.48		6.7	9	0.8
C12		1	4		0.35	0.65	10.7	5	0.73
C13*	22	54	300	0.56	0.72	0.82	10	300	0.82
C14*	4	7	12	0.36	0.54	0.74	30	23	0.98
C15	1	2	4	0.17	0.3	0.5	17	13	0.88
C16	50	56	68	0.62	0.72	0.92	10	68	0.92
C17	4	8	12	0.25	0.52	0.74	17	19	1
C18	2	3	4	0.15	0.27	0.37	21	19	1
C19		1	3		0.28	0.38	12	5	0.55
C20		1	2		0.27	0.47	14.5	4	0.68
C21		1	2		0.27	0.49	15	4	0.72
C22	110	134	154	0.85	0.92	1	13	160	1.08
C23	2	3	8	0.2	0.31	0.72	13	10	0.9
C24		1	2		0.22	0.4	23	10	0.88
C25*	43	116		0.45	0.55		5.5	147	0.57
C26*	5	10	35	0.31	0.41	0.54	30	83	0.63
C27	14	30		0.63	0.82		5.3	32	0.83
C28		1	5		0.1	0.44	14	11	0.75
C29	4	11		0.23	0.55		8.5	19	0.81
C30	1	3	13	0.18	0.4	0.9	11.6	15	1
C31		1	2		0.14	0.2	19	19	0.6
C32	22	32		0.31	0.46		7.5	44	0.58
C33							0.7	140	0.1

Table 4.4 (continued)

Test	3% Ax.St.	5% Ax.St.	10% Ax.St.	3% Ax.St.	5% Ax.St.	10% Ax.St.	Max. Ax.St. (%)	N at Max. Ax.St.	r_u at Max. Ax.St.
C34		1	3		0.1	0.15	13	7	0.32
C35	4	5	9	0.06	0.1	0.25	15	13	0.55
C36	1	2	5	0.08	0.1	0.22	14	7	0.34
C37	2	4	13	0.1	0.12	0.48	10	13	0.48
C38	1	2	5	0.22	0.33	0.57	15	13	0.86
C39	1	2	6	0.11	0.26	0.55	13	13	0.77
C40	10	34		0.37	0.8		6.7	63	0.96
C41		1	3		0.1	0.4	19.5	17	0.86
C42		1	2		0.5	0.67	24	16	0.95
C43	13	22		0.28	0.6		0.7	33	0.83
C44*	75	314		0.66	0.78		5	314	0.78
C45	3	6	14	0.35	0.58	0.87	20	21	1.02
C46	2	3	6	0.34	0.48	0.79	16	11	1.08
C47*	5	9	20	0.33	0.48	0.58	20	54	0.58
C48*	57	85	225	0.12	0.16	0.24	10.5	245	0.24
C49*	8	14	30	0.08	0.12	0.12	30	135	0.31
C50	3	4	7	0.22	0.33	0.67	18	20	0.97
C51	4	10	20	0.08	0.2	0.31	13	28	0.45
C52*	8	13	25	0.45	0.6	0.69	26	60	0.8
C53	7	8	13	0.16	0.22	0.6	12	17	0.72
C54	7	9	15	0.21	0.35	0.65	20	35	0.99
C55	2	4	7	0.12	0.2	0.51	16	12	0.8
C56	14	20	27	0.28	0.45	0.64	12	31	0.74
C57	5	8	14	0.25	0.42	0.85	15	19	1
C58		1	3		0.08	0.2	24	14	0.86
C59	1	2	3	0.53	0.75	0.85	39	10	1.27
C60	1		2	0.37	0.4	0.63	40	12	0.97
C61	1	2	4	0.14	0.42	0.66	30	11	0.95
C62		1	2	0.1	0.57	0.71	30	10	0.92
C63*	1	2	7	0.08	0.27	0.45	20	20	0.55
C64							0.2	97	0.29
C65*							2.3	116	0.8
C66*	25	92		0.64	0.76		5.5	115	0.8
C67		1	2	0.1	0.47	0.65	30	10	1
C68*	24	40		0.46	0.5		8	90	0.56
C69*	1	2	80	0.24	0.33	0.74	10	124	0.77

*Number of cycles was calculated considering SA axial strains

Cyclic response is observed to depend on whether the specimens are subjected to stress reversal or not during cyclic loading. In the case of no stress reversal, plastic strains accumulate with almost a constant rate in each cycle. As it can be seen in Figure 4.4, the plastic strain accumulation rate tends to decrease after having reached the point where the peak cyclic stress becomes lower than the monotonic strength. The greater the ratio of the applied peak cyclic stress to the monotonic strength, the greater strain accumulation rate is observed, which is consistent with the observed trends cited in literature (Andersen et al., 1980; Yılmaz et al., 2004). No significant cyclic degradation was observed in stiffness of the specimens under loading without stress reversals, although the axial strains exceeded 5%.

In the case of stress reversal, the strain accumulation is predominant either in compression or in extension depending on the initial stress state. In the tests conducted with isotropically consolidated specimens, the incremental strains developed in each additional cycle are added to the maximum past strains in compression and extension respectively. The strain accumulation rate becomes more pronounced in extension with increasing N, which is attributed to lower strength of soils in extension.

Figure 4.5 shows the test results of isotropically consolidated specimens subjected to different CSR_{tx} and p'_i values. The axial strain accumulation rate is observed to increase for the specimen subjected to CSR_{tx} value of 0.31. There is no sudden increase in strain to be interpreted as flow liquefaction. At relatively high CSR_{tx} of 0.5, strain accumulation rate decreases with increasing N although the strain accumulates particularly in the earlier cycles of loading. In most of the isotropically consolidated cyclic tests, a high loading rate of 0.5 Hz was used. The r_u values were, however, observed to reach, and even exceed 0.9 at different cycles. Although the excess pore water pressure reaching initial confining stress led to the loss in effective stress and to cyclic strain softening as a consequence, the tendency of dilation of the silt prevented excessive loss of strength.

In the tests with anisotropically consolidated specimens subjected to higher cyclic demands (higher CSR_{tx} values), the stress reversals also occurred. Figure 4.6 shows the test results of anisotropically consolidated specimens imposed to stress reversals. The strains predominantly accumulate in the compression side of loading. Accumulation rate increases with the increasing extent of peak stress exceeding the monotonic strength and also with increasing CSR_{tx}. The pore water pressure ratio r_u generated in the specimen having an initial shear stress ratio τ_s/p'_i of 0.21 approaches to 0.8, whereas it approaches to 0.5 for τ_s/p'_i of about 0.35. However, majority of DA axial strains of the tests exceed 10% regardless of r_u values.

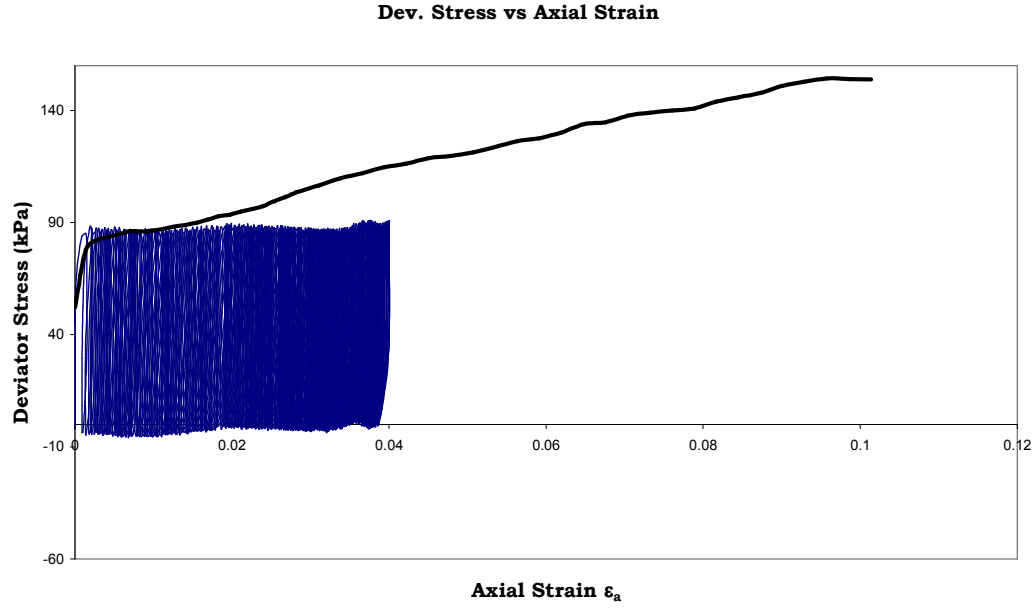

(a)

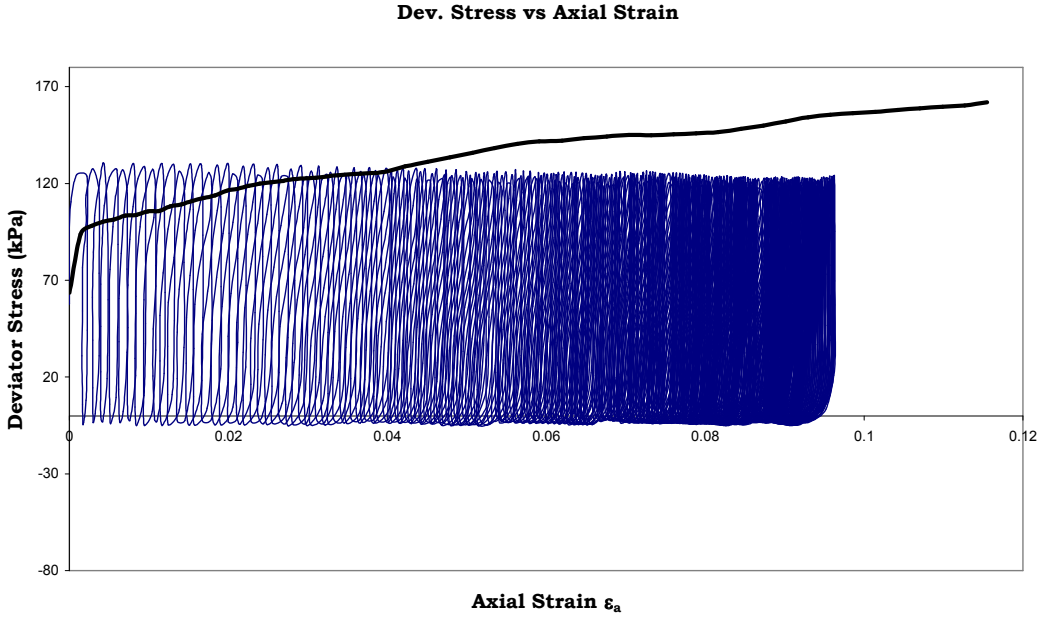

(b)

Figure 4.4 Stress-strain behavior for the case of non-reversal stress conditions observed for the tests of (a) C10 where CSR_{tx}=0.35 and τ_s/p'_i=0.31, and (b) C13 where CSR_{tx}=0.41 and τ_s/p'_i=0.33.

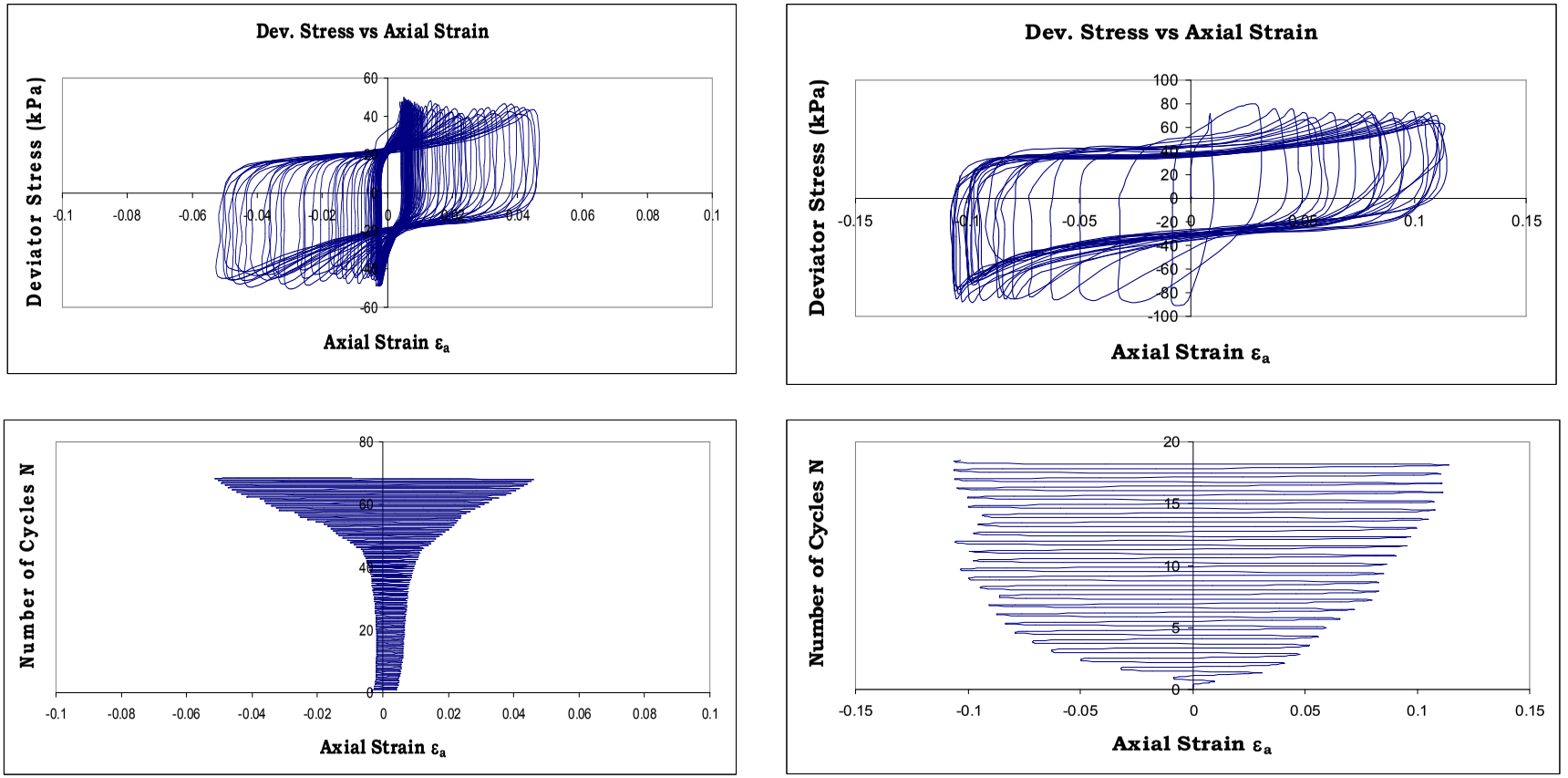

Figure 4.5 Stress-strain behavior of the specimens subjected to (a) CSR_{tx} of 0.31 and p'_i of 80 kPa (C16), (b) CSR_{tx} of 0.50 and p'_i of 80 kPa (C18).

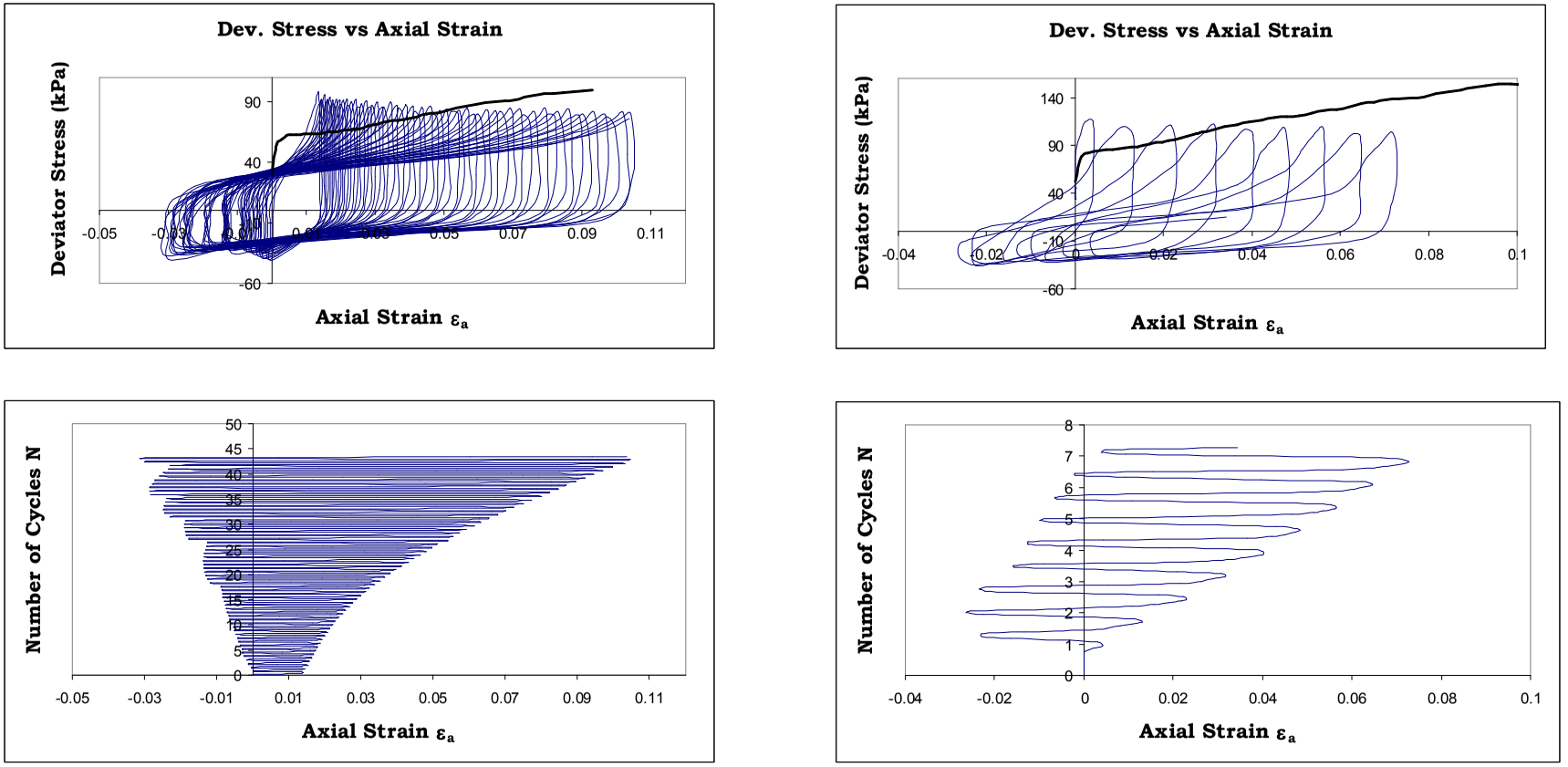

Figure 4.6 Stress-strain behavior and pore water pressure generation in the specimens subjected to (a) CSR_{tx} of 0.51 and τ_s/p'_i of 0.21 (C7), (b) CSR_{tx} of 0.54 and τ_s/p'_i of 0.35 (C11)

4.7 Pore Water Pressure Generation

As indicated by Polito et al. (2008), the excess pore water pressure generation during cyclic loading can be taken into consideration as separate components of transient and residual excess pore pressures. The residual component is described as the excess pore water pressure built up at the state of zero cyclic deviator stress in a cycle while the transient one is the offset of the excess pore pressure around residual excess pore water pressure in a cycle. In this study, the maximum excess pore pressure generated during cyclic tests will be called total excess pore water pressure (residual + transient).

The reconstituted silt specimens were mostly tested under CSR_{tx} values causing large strains that are greater than threshold strains beyond which the excess pore water pressure begins to generate (Matasovic and Vucetic, 1995). Therefore, the excess pore water pressure generation was observed even at the initial cycles in great majority of the tests. However, there are two tests in which the total excess pore water pressure ratio observed during cyclic straining remained at level of 10% although N exceeded 100. The DA axial strains observed during tests of C6 and C33 are 0.5% and 0.7%, respectively, as can be seen in Figure 4.7. These low strain values constantly occurred in each cycle of loading without any accumulation. Although the strain levels are higher than the threshold values (shear strain γ_t of 0.02-0.06%) reported for fine grained soils in literature (Hsu and Vucetic, 2006), the excess pore water pressure generated during the tests remained at negligible levels.

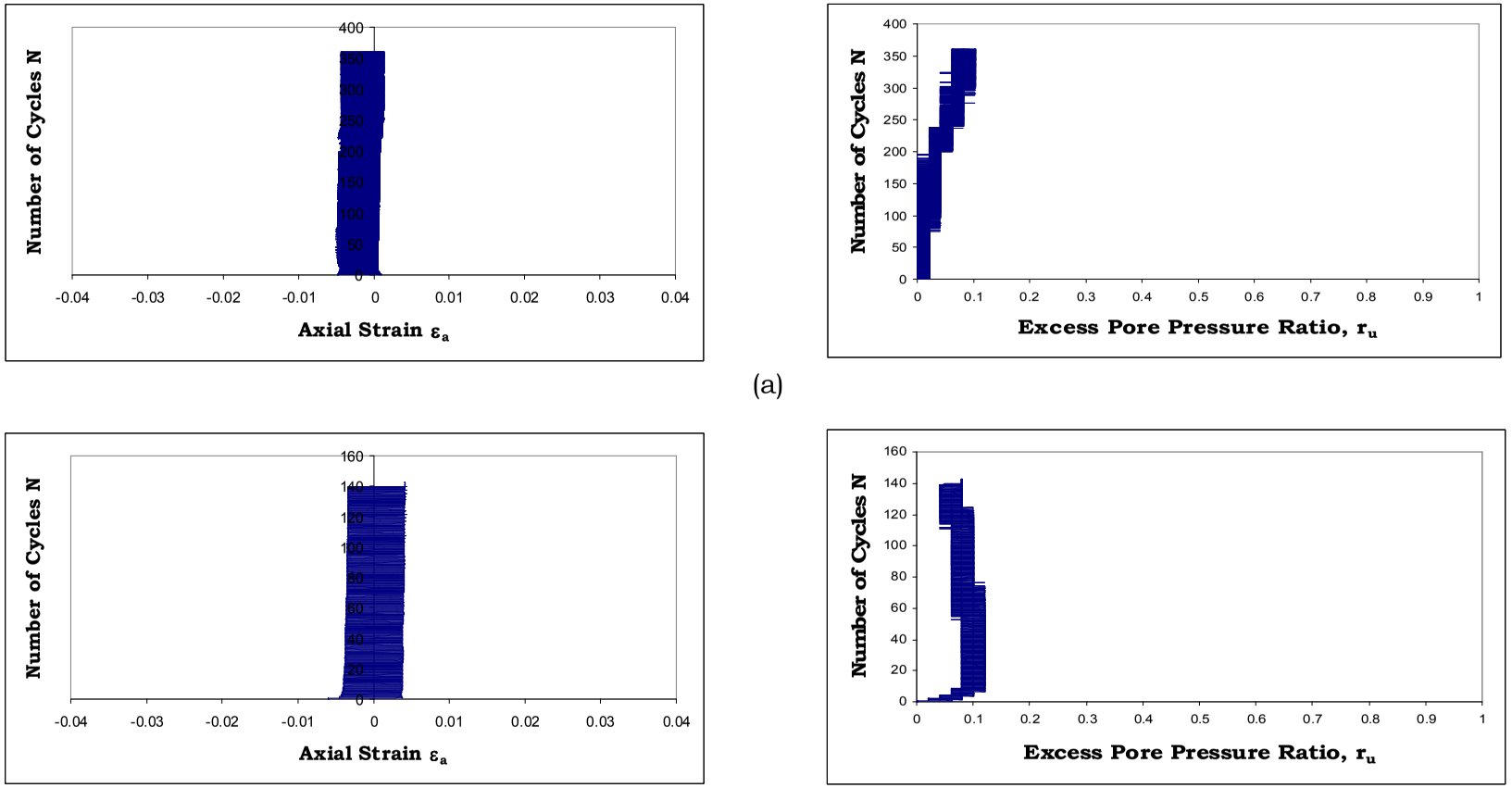

Figure 4.7 Axial strain and excess pore pressure ratio generated with number of cycles in the tests of (a) C6 and (b) C33

The excess pore water pressure generation during cyclic tests is examined through the relationship between total excess pore water pressure and increasing axial strain as shown in Figure 4.8. The logarithmic variation of total excess pore water pressure is observed to increase gradually with increasing axial strain up to a point beyond which the excess pore water pressure increase slows down and finally reaches a constant residual value while the axial strain increases to higher levels. This characteristic point is to be used as a reference point to discuss the effect of pore water pressure generation on cyclic straining, and it is referred as flexure point hereafter. This point is approached empirically with the method described below.

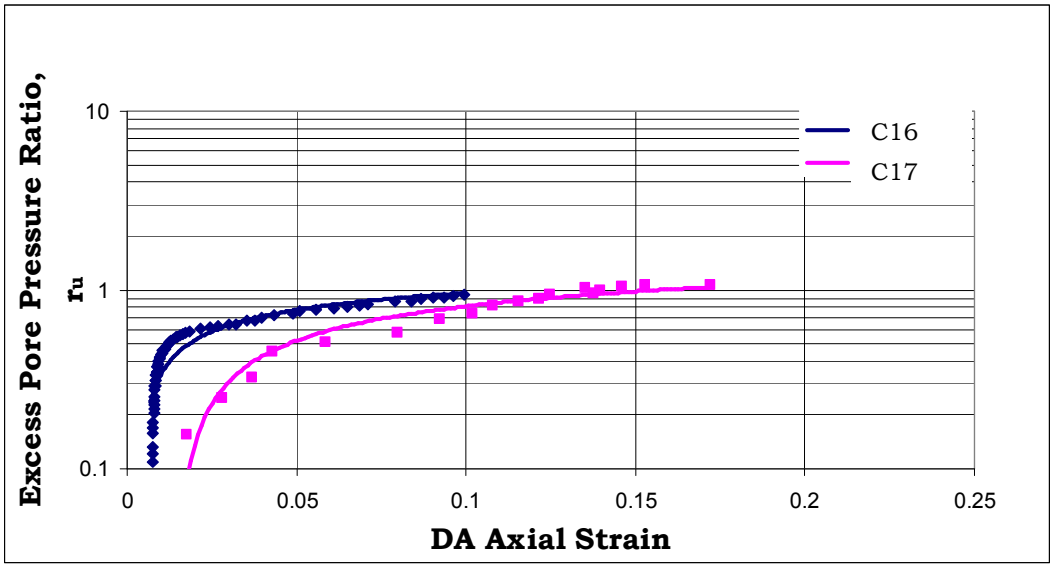

Figure 4.8 The relationship between total excess pore water pressure and axial strain observed in the tests C16 and C17

The relationships shown in Figure 4.8 are fitted by means of least squares method using logarithmic functions. In order to determine the flexure point, firstly a tangent is drawn to the fitted curve at r_u of 0.1 (Figure 4.9). Since the curvature at the earlier stage of the curve is relatively small, the tangent at r_u of 0.1 almost coincides with that part which is practically linear. Then, a horizontal line passing through maximum r_u value is drawn. The vertical drawn through the point of intersection of the tangent

and the horizontal lines gives the approximate axial strain of the flexure point.

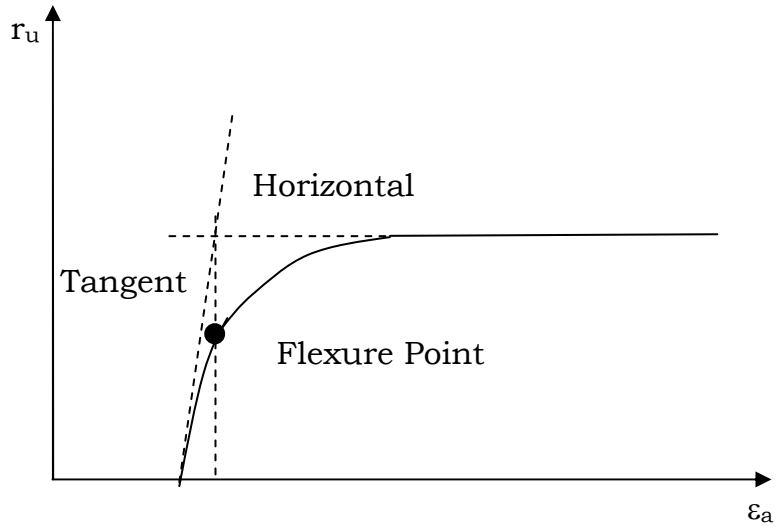

Figure 4.9 Determination of flexure point

It can be concluded from Figure 4.8 that at the flexure point of the test C16, the r_u is 0.50 and the DA axial strain is 1.8% whereas the r_u is 0.56 and the DA axial strain is 5.6% at the flexure point of the curve for the test C17. The r_u is increasing beyond negligible levels after 0.5% to 1% axial strain which is not seen in log scaled r_u axis. Nonetheless, it must be remembered that beyond the flexure points the r_u value of 1 is not necessarily reached, and it may even remain well below 1. Therefore, to be able to observe the effects of test conditions on the pore water pressure generation, the cyclic tests were separated into groups, the relevant conditions of which are given in Table 4.5.

Nevertheless, it should be kept in mind that the flexure point is a specific point based on the relationship between the pore pressure and axial strain. Therefore, a change in skewness degree of the curve would be indicating a change either in excess pore pressure generation rate or in axial strain accumulation rate.

Table 4.5 The test groups used to evaluate pore water generation in reconstituted silt

Group No	τ_s/p'_i	Frequency	OCR
1	0	0.5	1
2	0.21	0.5	1
3	0.35	0.5	1
4	0.60 & 0.75	0.5	1
5	0	0.5	2
6	0	0.5	3
7	0	0.5	4
8	0	0.05	1
9	0.38	0.05	1
10	0.60	0.05	1

The r_u values and the axial strains at the observed flexure points vary in a wide range. Accordingly, the corresponding values at the flexure points are evaluated within each test group separately. The tests included in each group and the flexure points after which the gradient of the curve decreases are presented in Table 4.6. It must be noted that the axial strain accumulated during cycling are taken into consideration in terms of DA axial strains for the tests with stress reversals and SA axial strains for the tests without stress reversals.

The r_u values at flexure points for the tests in group 1 range between 40% and 60% whereas the DA axial strains range between 0.2% and 11.4%. The average r_u at flexure and DA ε_a values for the first group are 50.18% and 5.70%, respectively. The data observed for other groups are given in Table 4.6. The cyclic loading amplitudes (i.e. CSR_{tx} values) and initial confining stresses (σ'_{3c}) for the tests in each group are by and large different from each other. Hence, the influence of CSR_{tx} on pore pressure generation is also examined through the plot shown in Figure 4.10. As can be observed in Figure 4.10, r_u values observed at flexure points gently decrease with increasing CSR_{tx}. Although the plot is obtained just for the tests in group 1, the tendency is also the same for the tests in the groups 5 and 8. The tests in these groups were conducted with isotropically consolidated specimens. This tendency implies that the axial strain accumulation begins to increase at levels of lower r_u with increasing CSR_{tx} for the specimens sustaining no initial shear stress.

Table 4.6 The r_u and ε_a values observed at flexure point in the cyclic tests

Group 1	**At flexure point**		**Group 2**	**At flexure point**		**Group 3**	**At flexure point**		**Group 4**	**At flexure point**		**Group 5**	**At flexure point**	
Test No	**r_u (%)**	**ε_a (%)**	**Test No**	**r_u (%)**	**ε_a (%)**	**Test No**	**r_u (%)**	**ε_a (%)**	**Test No**	**r_u (%)**	**ε_a (%)**	**Test No**	**r_u (%)**	**ε_a (%)**
C1	No flexure	No flexure	C6	No flexure	No flexure	C10	40	0.9	C25	32	1.2	C27	55	2.6
C2	40	0.2	C7	52	2.8	C11	39	2.1	C26	32	2.7	C28	52	10.8
C3	57	4	C8	62	7.2	C12	50	8.3	C47	32	2.7	C29	52	4.4
C4	50	3.6	C9	56	9.6	C13	43	1.6	C48	No flexure	No flexure	C30	61	6
C5	48	2.7	C51	31	9.8	C14	47	3.7	C49	No flexure	No flexure	C31	44	15.7
C16	50	1.8	C22	46	0.8	C15	53	8.5				C57	58	6.2
C17	56	5.6	C23	59	7.7	C44	43	1.2				C58	60	16.8
C18	60	10.6	C24	59	11.8	C52	41	2.8				C40	63	4
C19	42	10.4	C45	58	5.4							C38	56	8.5
C20	53	11.4	C46	54	5							C39	56	9.4
C21	40	5										C41	60	13.4
C50	56	7.4										C43	62	5.4
Average	50.18	5.70	**Average**	53.00	6.68	**Average**	44.50	3.64	**Average**	32	2.20	**Average**	56.58	8.60
Group 6	**At flexure point**		**Group 7**	**At flexure point**		**Group 8**	**At flexure point**		**Group 9**	**At flexure point**		**Group 10**	**At flexure point**	
Test No	**r_u (%)**	**ε_a (%)**	**Test No**	**r_u (%)**	**ε_a (%)**	**Test No**	**r_u (%)**	**ε_a (%)**	**Test No**	**r_u (%)**	**ε_a (%)**	**Test No**	**r_u (%)**	**ε_a (%)**
C53	42	6	C32	35	3.2	C59	45	2	C61	45	3.7	C63	35	7.7
C55	51	8.7	C33	No flexure	No flexure	C60	52	10.3	C65	36	0.2	C68	30	1.1
			C34	29	13.7	C64	No flexure	No flexure	C66	44	1.4			
			C35	33	10.3	C62	46	4.2	C69	50	5			
			C36	27	11.6	C67	56	11						
			C37	33	9									
			C54	55	8.3									
			C56	43	5.2									
Average	46.50	7.35	**Average**	36.43	8.76	**Average**	49.75	6.88	**Average**	43.75	2.58	**Average**	32.50	4.40

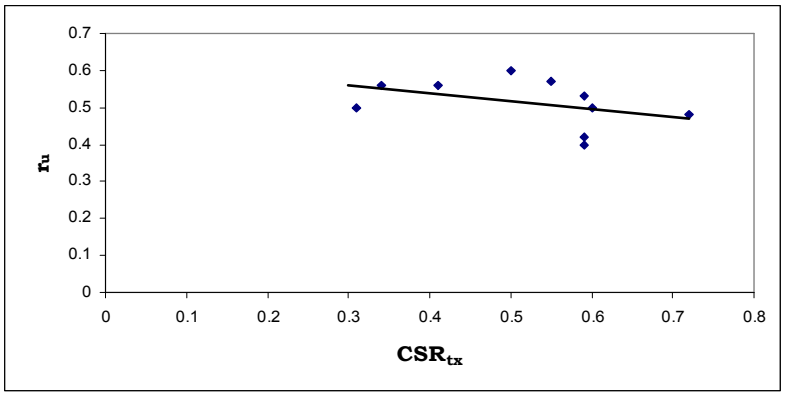

Figure 4.10 The relationship between r_u at flexure point and CSR_{tx} for the first group of tests

The tests in the second group were anisotropically consolidated so as to provide an initial shear stress ratio (τ_s/p'_i) of 0.21. As all the specimens sustaining an initial shear stress had an OCR of 1, the specimens tested in this group were also in NC state. The loading frequency used in this group is 0.5 Hz. The r_u values at flexure point varied between 31% and 62%, with an average of 53%. The axial strains at flexure point range between 0.8% and 11.8%, and the average is 6.68%. As it is seen in Figure 4.11, the r_u values observed at flexure points increase with increasing CSR_{tx}. Although the plot is obtained just for the tests in group 2, the tendency is also the same for the other groups in which the tests conducted with specimens having an initial shear stress.

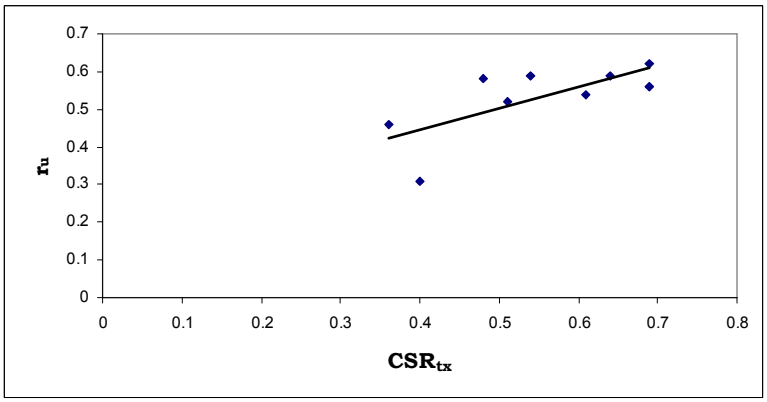

Figure 4.11 The relationship between r_u at flexure point and CSR_{tx} for the second group of tests

The tests carried out with CSR_{tx} values around 0.30 exhibit higher r_u values at flexure points. It means that the pore water pressure generation rate starts to decrease following the peak values of r_u observed in cyclic tests. The relationship between r_u and ε_a for the tests of C2, C10, C16 and C22 is depicted in Figure 4.12. The value of r_u reaches at 1 eventually for all the tests shown in the figure. As it is observed, ε_a values at flexure points are conversely the lowest (around 1%) observed in cyclic tests. Thus, the highest r_u values are attained at lowest ε_a values for the tests with lower CSR_{tx} values. Nevertheless, it must be stated that the number of cycles to flexure points for these tests are relatively high as compared to the tests with higher CSR_{tx}. The tests presented in Figure 4.12 were performed with a loading frequency of 0.5 Hz. Such a high loading rate prevents equalization of pore water pressure throughout the specimen at early cycles, and as it is stated previously the pore pressures are measured at the bottom of the specimens. Accordingly, it can be stated that the pore pressures measured at higher number of cycles are in equilibrium to a large extent. Such high r_u values observed at flexure points, thus, can be attributed to equalized residual excess pore water pressures.

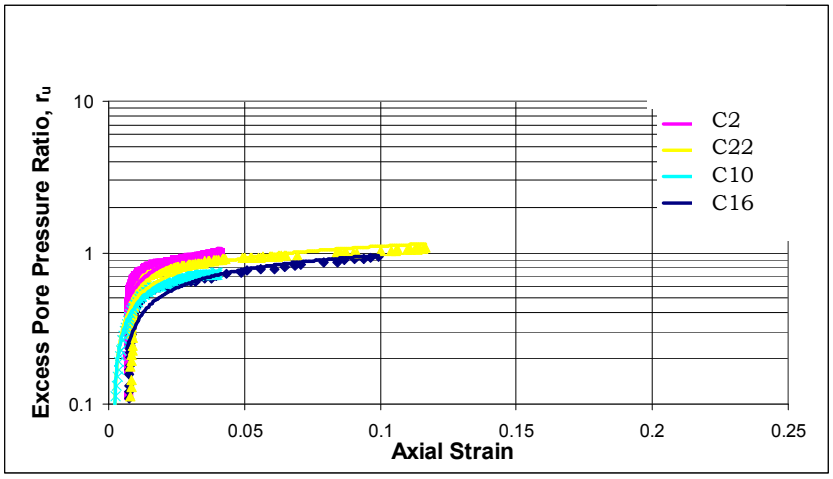

Figure 4.12 The relationship between total excess pore water pressure and axial strain observed at the tests C2, C10, C16 and C22.

The groups 8, 9 and 10 consisted of the tests performed with a loading frequency of 0.05 Hz. The strain developing during cycling significantly

depends on the loading amplitude (i.e. CSR), and the strain developed in a certain time interval is the indicator of the loading rate. The loading frequency of 0.05 Hz is to be evaluated whether it is low enough to provide a homogeneous distribution of pore pressure in the specimen during cycling. In Table 4.7 the loading rates used in cyclic tests conducted under 0.05 Hz and the limiting loading rates which should not be exceeded to obtain equalized pore pressure are calculated and compared. The ε_a value reached at the end of first cycle of each test is used to calculate the cyclic loading rate. As the strain accumulation is not constant during cycling, a reference strain is required to calculate the cyclic loading rate. The residual pore water pressure during cycling increases with increasing number of cycles, and the transient pore water pressure becomes relatively negligible compared to the residual. Hence, the equalization of residual pore water pressure continues throughout the cycling process and improves with increasing number of cycles. Accordingly, the strains developed in the first cycles of the tests are taken into consideration to calculate the cyclic loading rate.

The loading rate ensuring 95% of pore pressure equilibration in the specimen is calculated by the procedure introduced previously. Corresponding t_f values are determined considering the peak deviator stresses and the relevant axial strains reached in static tests. The t_f values for the peak deviator stresses suitable to the oedometer stresses (P) given in Table 4.1 are calculated through interpolation of the values given in the same table. Then, the limit values of strain rates for the corresponding tests are eventually calculated (Table 4.7).

Table 4.7 Loading rates for the tests conducted under loading frequency of 0.05 Hz.

Test No	ε_a% at the end of first cycle	ε_a%/sec	Peak Static Deviator Stress (kPa)	ε_a% static	t_f (min)	Max. ε_a%/sec for Pore Pressure Equalization
C59	4	0.2	68	8.5	3	0.047
C60	11.4	0.57	68	8.5	3	0.047
C61	6.9	0.345	100	10	0.36	0.463
C62	6.5	0.325	165	9.8	0.5	0.327
C63	3.3	0.165	61	10	4	0.042
C64	0	0	68	8.5	3	0.047
C65	0.07	0.0035	100	10	0.36	0.463
C66	0.6	0.03	100	10	0.36	0.463
C67	7.4	0.37	165	9.8	0.5	0.327
C68	0.25	0.0125	61	10	4	0.042
C69	0.4	0.02	100	10	0.36	0.463

The cyclic loading rate of tests C59, C60 and C63 is higher than that required to obtain homogeneous pore pressure distribution in the specimen, whereas the rest of the tests performed under a loading frequency of 0.05 Hz have cyclic loading rates allowing pore water pressure equalization from the beginning of the cycling. The tests in group 8 are conjugate with those in group 1 in terms of initial stress conditions and applied CSR_{tx} values. As it is shown in Table 4.6, although the loading frequency of group 1 tests is ten times of that of group 8, the average r_u values at flexure point are almost the same for both groups (the average ε_a values at flexure point are 5.7% and 6.88% for the groups 1 and 8, respectively). Representative r_u responses are given in Figure 4.13 for the tests C3 from group 1 and the test C59 from group 8, both of which performed under close CSR_{tx} values (0.55 and 0.53, correspondingly). The r_u values at flexure point are 57% and 45%, and the corresponding ε_a values are 4% and 2%, respectively. The decrease in gradient with increasing axial strain begins at the points close to each other for both tests. However, this point is reached in the first cycle in test C59 whereas it is reached in the fourth cycle in test C3.

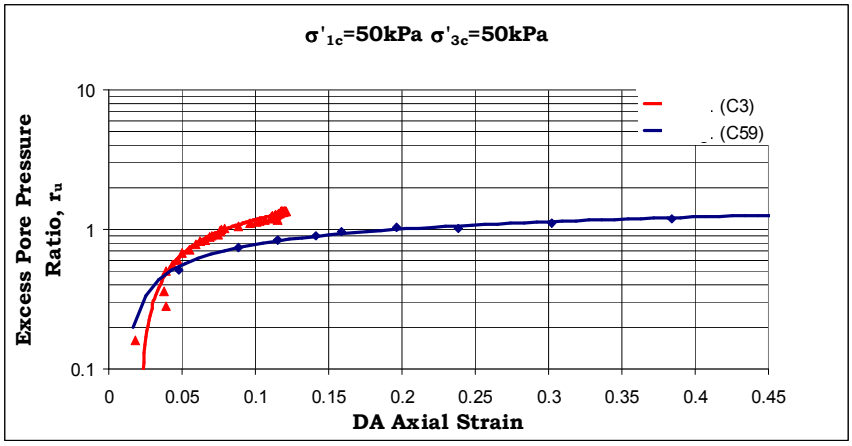

(a)

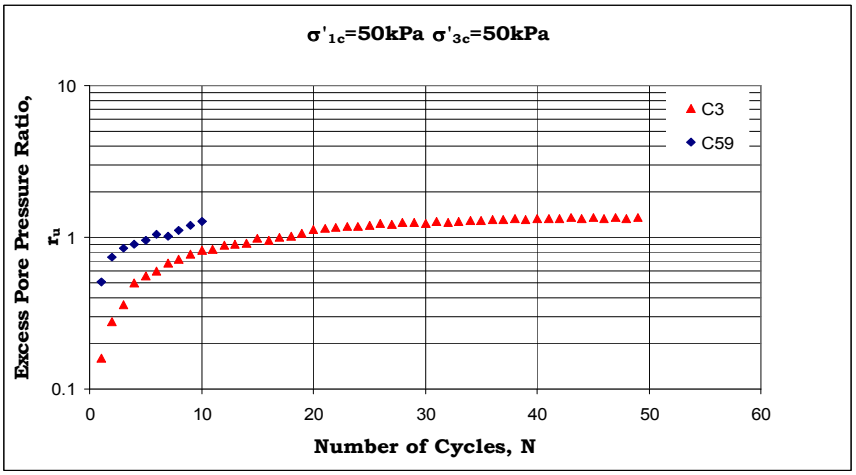

(b)

Figure 4.13 Total pore water pressure response of the tests C3 and C59

The effect of loading frequency on total pore water pressure response is significant for the specimens having an isotropic stress state initially. Although r_u values at flexure point is almost the same for the tests C3 and C59, r_u and ε_a values observed at flexure points for the other conjugate specimens with no initial shear stress are quite different. The r_u, ε_a and number of cycles (N) observed at flexure points of the conjugate tests are given in Table 4.8. In the tests in which the specimens have an initial shear stress, loading frequency does not have a significant effect on the pore water pressure generation. As it is illustrated in Figure 4.14, the curves representing the relationship between r_u and ε_a for the conjugate tests with initial shear stress are very similar. Particularly, the tests with no stress reversals yield almost overlapping r_u response curves. Thus, the loading rate effect on excess pore water pressure generation is significant

for the tests with stress reversals during cycling. Based on the observations, it can also be concluded that the effect of loading rate becomes more significant on pore water pressure generation with the increasing stress on extension side

N values observed at flexure points of the conjugate tests conducted with 0.5 and 0.05 Hz are also almost same for the case of no stress reversals. However, the corresponding N values of the tests conducted with 0.5 Hz varies between 3.5 to 5.5 times of those of the tests carried out with 0.05 Hz over isotropically consolidated specimens. Thus, a 10 fold increase in loading frequency results in significant decrease in the excess pore water pressure generation for isotropically consolidated specimens.

Table 4.8 The r_u, ε_a and N values observed at flexure points of conjugate tests conducted with 0.5 and 0.05 Hz.

Conjugate Tests	σ'_{1c} (kPa)	σ'_{3c} (kPa)	τ_s/p'_i	CSR_{tx}	f (Hz)	At flexure point		
						r_u (%)	ε_a (%)	N
C3	50	50	0	0.55	0.5	57	4	4
C59	50	50	0	0.53	0.05	45	2	1
C5	45	45	0	0.72	0.5	48	2.7	11
C60	50	50	0	0.85	0.05	52	10.3	2
C18	80	80	0	0.5	0.5	60	10.6	5
C62	80	80	0	0.54	0.05	46	4.2	1
C17	80	80	0	0.41	0.5	56	5.6	7
C67	80	80	0	0.44	0.05	56	11	2
C10*	95	50	0.35	0.35	0.5	40	0.9	23
C65*	100	50	0.38	0.37	0.05	36	0.2	22
C13*	120	60	0.38	0.41	0.5	43	1.6	10
C66*	120	60	0.38	0.44	0.05	44	1.4	7
C11	95	50	0.35	0.54	0.5	39	2.1	3
C69	100	50	0.38	0.56	0.05	50	5	5
C15	120	60	0.38	0.59	0.5	53	8.5	4
C61	120	60	0.38	0.54	0.05	45	3.7	5
C26*	150	50	0.60	0.6	0.5	32	2.7	4
C63*	150	50	0.60	0.6	0.05	35	7.7	3
C25*	150	50	0.60	0.45	0.5	32	1.2	14
C68*	150	50	0.60	0.48	0.05	30	1.1	10

*Number of cycles was calculated considering SA axial strains

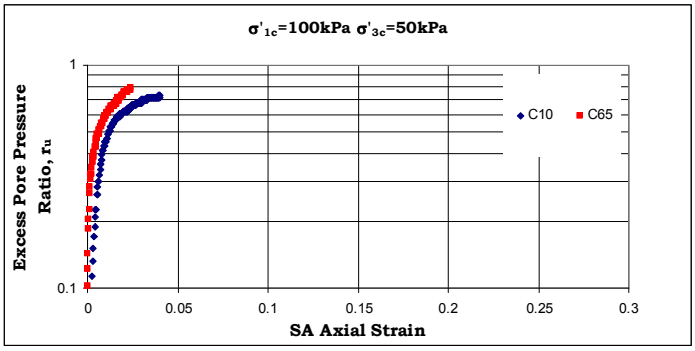

(a)

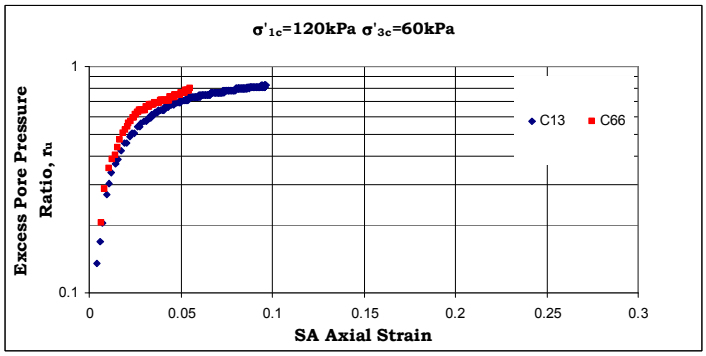

(b)

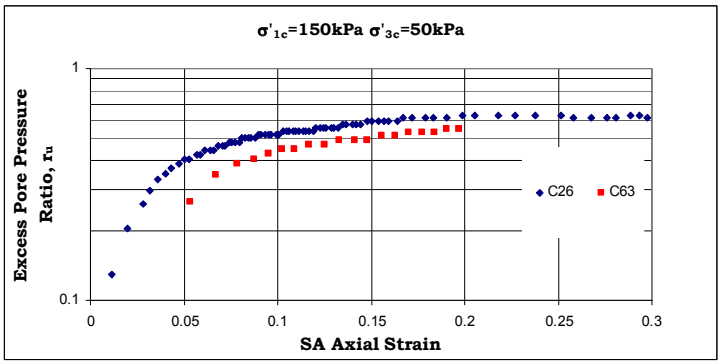

(c)

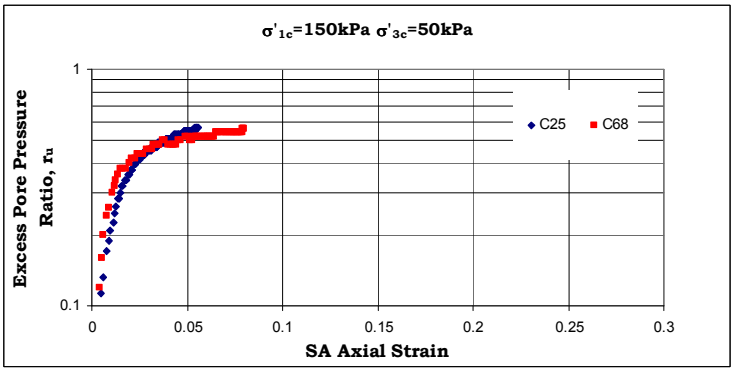

(d)

Figure 4.14 Loading rate effect on r_u response of tests with no stress reversals

The pore pressure generation during cyclic tests is observed to depend on the level of overconsolidation (OCR) of the silt specimens. Representative total excess pore water pressure responses obtained from tests of group 1, 5, 6 and 7 are given in Figure 4.15. The response of isotropically consolidated specimens having OCR values of 1, 2, 3 and 4 are compared in the figure. The data presented in Figure 4.15 is from tests that were carried out with a sustained isotropic pressure of 50 kPa prior to the cyclic shearing. The OCR values of the tests C3, C28, C53 and C34 are 1, 2, 3 and 4, correspondingly. As it is observed in Figure 4.15, pore pressure generation decreases in general with increasing OCR as pointed out by Ohara and Matsuda (1988). On the other hand, straining tendency increases with increasing OCR. Thus, with increasing OCR the specimens exhibit higher axial strain with lower excess pore water pressure generation.

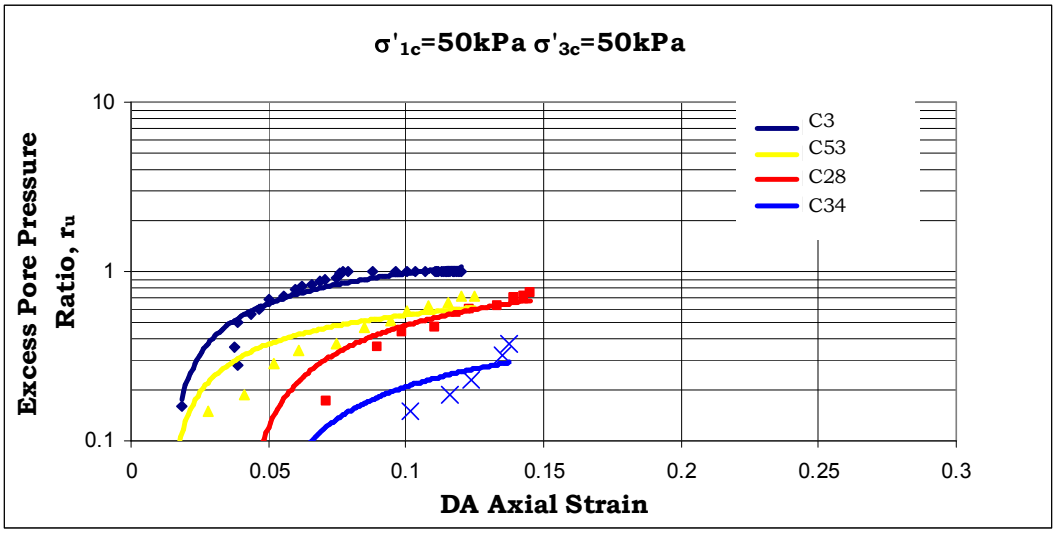

Figure 4.15 Response of excess pore water pressure for the tests with OCR of 1 (C3), 2 (C28), 3 (C53) and 4 (C34).

The pore pressure response of reconstituted silt, so far, has been examined in parallel with the axial strain accumulated during cycling. As reported by Wu et al. (2004), the initiation of soil liquefaction has been attributed either to a specific state of the excess pore water pressure or to a specific amount of strain. It is observed that the excess pore water

pressure ratio increases rapidly within initial levels of axial strain, mostly up to about 5-6% DA for the tests with stress reversals, and 2-4% SA for the tests without stress reversals. Following these axial strain levels, the gradient of the curve representing the relationship between excess pore water pressure ratio and axial strain begins to decrease. At the point referred to as the flexure point, the excess pore pressure ratio is observed to be between 40-60% in general. This range of excess pore water pressure ratio is well below those reported as a criterion for initiation of liquefaction in the literature. As mentioned in the chapter on literature review, the initiation of liquefaction is defined at the state where excess pore water pressure ratio reaches a value of 100% for sands, and r_u between 70 to 90% is reported as the maximum value at failure for the fine grained soils. As it is seen in Figure 4.13b, the curve showing the relationship between r_u and N has a similar shape with that between r_u and ε_a. The relationship between r_u and N indicates that the pore water pressure keeps building up to r_u values between 60 to 90% with almost a constant rate, while the pore pressure generation rate begins to decrease after r_u reaching a value within a range between 60 to 90%. On this basis, it can be concluded that the axial strain accumulation rate increases when r_u reaches a value between 40 to 60%. Therefore, if the failure, which is commonly defined as the state where strain accumulation substantially increases, the value of r_u between 40 and 60% can be attributed as failure initiation. However, as the total pore pressure generation keeps developing with a uniform rate up to r_u values of 60 to 90%, referring an r_u value within a range of 40 to 60% as the failure point is contradictory to the liquefaction or cyclic mobility phenomenon introduced in the literature.

4.7.1 Pore Pressure Generation Modeling

Both, the excess pore water pressure and strain built up during cyclic tests depend on the amplitude and duration of cyclic loading. As indicated previously, the cyclic behavior, and hence the excess pore water pressure generation do actually depend on numerous factors some of which are related to the soil characteristics and the stress history.

However, all soils display a cyclic response, and undergo failure sooner or later under reasonably demanding loading conditions. In the literature, liquefaction susceptibility of soils has been evaluated by and large based on the soil response under loading conditions simulating seismic shaking. In such assessments, clays are typically delineated as insusceptible to liquefaction. However, the studies on sea bed clay show that the clays display a substantial loss of strength and stiffness when subjected to cycles in the order of thousands. Since the amplitude and duration of the loading have significant effect on the cyclic response of soils, the total excess pore pressure generation is also investigated via examination of effects of CSR_{tx} and N on r_u. Then, a generalized model to represent the relationship between r_u and CSR_{tx} as a function of N, based on the observations of the test results, is presented.

In order to remove the effects of initial stress state on the behavior, the cyclic loading amplitude is defined as CSR in most of cyclic tests. As introduced in the third chapter, CSR is expressed as the ratio of applied cyclic deviator stress ($\Delta\sigma_{cyc}$) to initial mean effective stress (p'_i).

The change in r_u is plotted as a function of N for each cyclic test. The gradient of the curve showing the relationship between r_u and N decreases after a certain r_u value, and eventually becomes almost zero. Two of such curves are presented in Figure 4.16. The curves in the figure are fitted as trendlines of power functions which provide appropriate R-squared values. R-squared value is a measurement indicating the compatibility between the trendline and the modeled relationship. R-squared values obtained for fitting functions of the relationships between r_u and N are calculated to be between 0.80 and 0.99 for all the cyclic tests. The relationship between r_u and N is modeled with the function given below:

$$r_u = a * N^b \qquad (4.1)$$

where a and b are the coefficients depending on the loading frequency, CSR_{tx} and the soil characteristics. Hence, the relationship between r_u, N and CSR_{tx} is modeled separately according to the loading frequencies of

0.5 and 0.05 Hz. Nevertheless, since the behavior is influenced by the initial stress state as well, the models are formed according to the initial stress ratios (τ_s/p'_i).

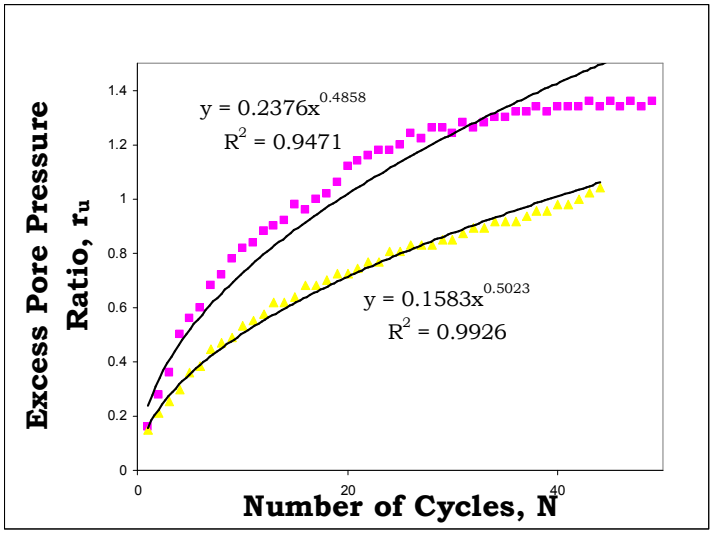

Figure 4.16 Representative curves (C3, C7) showing the relationship between r_u and N for reconstituted silt.

The pore pressure response of all OC specimens cannot be modeled. This is due to the fact that the specimens having an OCR of 4 do not display a consistent relationship, hence the effect of CSR_{tx} cannot be interfered appropriately. Nevertheless, an interesting point regarding the specimens having OCR of 4 is that the relationship between r_u and N is linear. . Another interesting point is that the r_u values observed in the tests with OCR of 4 are relatively lower, although the axial strains are significantly high (Figure 4.15). It seems that the stress-strain response of such OC specimens is not influenced by the excess pore water pressure generation.

Firstly, the relationship between r_u, N and CSR_{tx} is modeled for the tests conducted with NC specimens which do not sustain an initial shear stress ($\tau_s/p'_i=0$). After determining the function representative of r_u-N relationship for each test, the CSR_{tx} effect is taken into account by correlations between CSR_{tx} values and the coefficients obtained from r_u-N

functions. As given in Table 4.3, such specimens were tested under loading frequencies of 0.5 and 0.05 Hz. In the relationship obtained through the tests carried out under loading frequency of 0.5 Hz, the coefficients of a and b are correlated with CSR_{tx} as given in equations 4.2 and 4.3.

$$a = 0.01e^{5.7CSR_{tx}} \tag{4.2}$$

$$b = e^{-2.5a} \tag{4.3}$$

All the correlations obtained between the coefficients and CSR_{tx} are represented by exponential functions which yield R-squared values between 0.60 and 0.80. Accordingly, for a given CSR_{tx} value it is possible to calculate the coefficients a and b; then, using these coefficients it is possible to find the value of r_u corresponding to a specific N. In other words, a curve representing the response of r_u as a function of CSR_{tx} can be obtained by means of the functions given above for a specific N value. Such curves obtained for the tests conducted under 0.5 Hz and initial stress states of τ_s/p'_i=0 and OCR=1 are given in Figure 4.17 together with the test results to illustrate the consistency of the model.

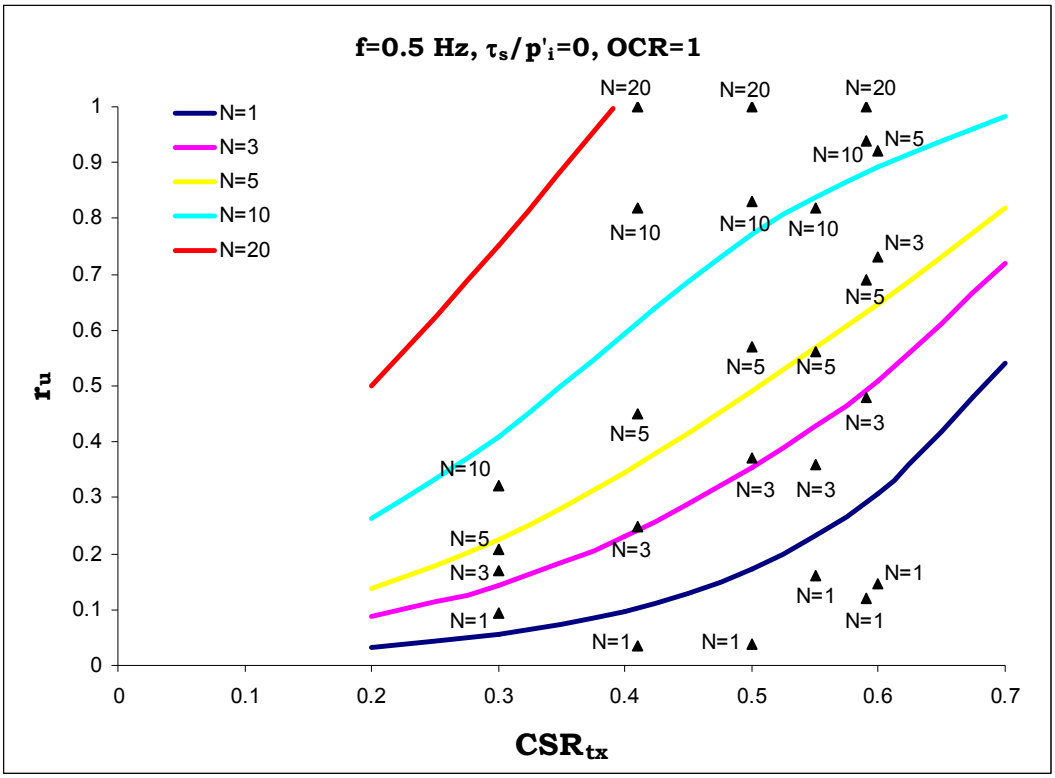

Figure 4.17 Modeling of pore water pressure for the tests conducted under 0.5 Hz, and stress states of τ_s/p'_i=0 and OCR=1.

In the relationship obtained through the tests carried out under loading frequency of 0.05 Hz, the coefficients of a and b are correlated with CSR_{tx} as given in equations 4.4 and 4.5. The specimens in the tests used to obtain such functions had initial stress states of τ_s/p'_i=0 and OCR=1. The curves obtained using the equations and the measured pore pressures are illustrated in Figure 4.18.

$$a = 0.02e^{6.3CSR_{tx}} \qquad (4.4)$$

$$b = 0.18e^{1.2a} \qquad (4.5)$$

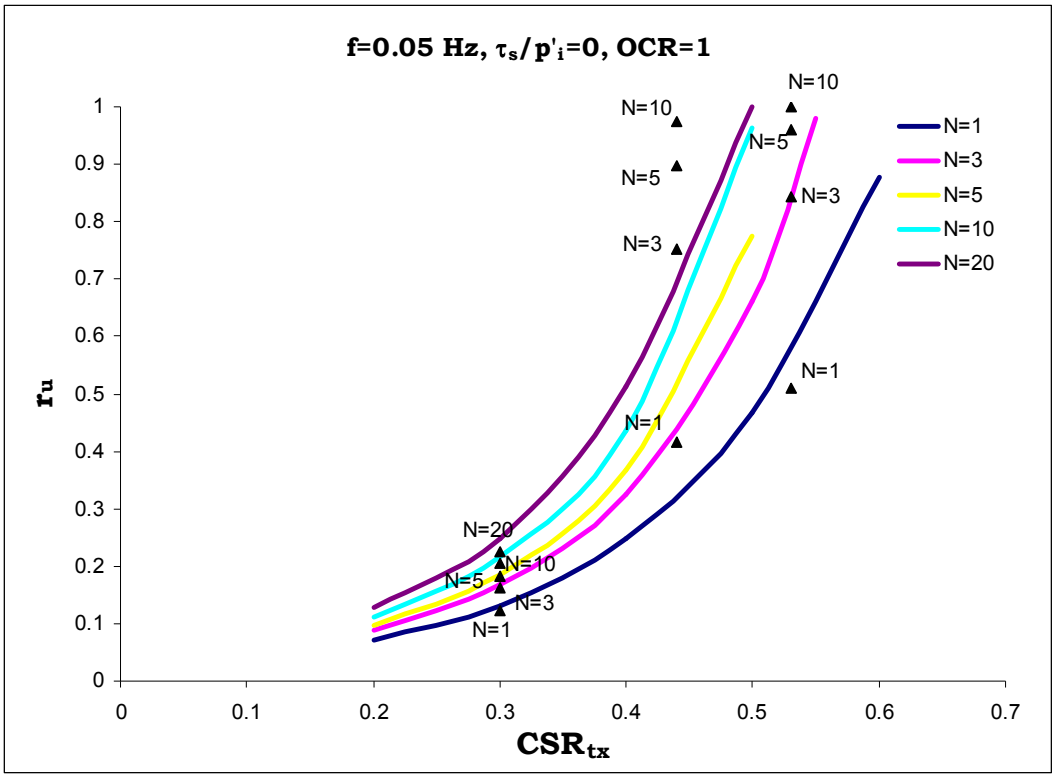

Figure 4.18 Modeling of pore water pressure for the tests conducted under 0.05 Hz, and stress states of τ_s/p'_i=0 and OCR=1.

In Figures 4.17 and 4.18, it is observed that the r_u is remarkably low at all cycles for CSR_{tx} values between 0.2 and 0.3. The r_u for the tests of 0.5 Hz can reach values over 40% even under CSR_{tx} of 0.2. Nevertheless, it displays a sharp increase after CSR_{tx} of 0.4 for the tests of 0.05 Hz, whereas the increase rate in r_u is moderate for the tests of 0.5 Hz. In both cases, r_u value reaches 1.0 after 10 cycles for the CSR_{tx} values greater than 0.5. The difference between the pore pressure responses obtained for the tests conducted with 0.5 and 0.05 Hz is significant for CSR_{tx} values lower than 0.4. Interestingly, the excess pore pressure built up in the specimens tested under 0.05 Hz is lower than that observed in the tests with 0.5 Hz for CSR_{tx} values up to 0.4. This observation can be attributed to the non-uniform pore pressure distribution throughout the specimen. Konrad and Wagg (1993) reported that the pore pressure measured at the bottom of the specimen is higher than at the center of the clayey silts, especially in the tests with higher loading rates. Accordingly, since the pore pressures were measured at the bottom of the specimens, the

measured r_u values in the tests conducted with 0.5 Hz are likely to be higher than those measured in the tests with 0.05 Hz.

It is realized that the pore pressure response during cyclic loading significantly depends on whether stress reversals are applied or not in the tests. Accordingly, the pore pressure responses observed in the specimens with varying τ_s/p'_i values are modeled separately. The model constituted for the specimens of τ_s/p'_i=0.35 which were loaded with a frequency of 0.5 Hz is given by the equations 4.6 and 4.7.

$$a = 0.0045e^{9CSR_{tx}} \tag{4.6}$$

$$b = 0.5e^{-2.5a} \tag{4.7}$$

The model established for the specimens of τ_s/p'_i=0.60 which were loaded with a frequency of 0.5 Hz is given with equations 4.8 and 4.9.

$$a = 0.04e^{2.3CSR_{tx}} \tag{4.8}$$

$$b = 0.5e^{-2.5a} \tag{4.9}$$

The model constituted for the specimens of τ_s/p'_i=0.75 which were loaded with a frequency of 0.5 Hz is given with equations 4.10 and 4.11.

$$a = 0.003e^{4.3CSR_{tx}} \tag{4.10}$$

$$b = 0.5e^{-2.5a} \tag{4.11}$$

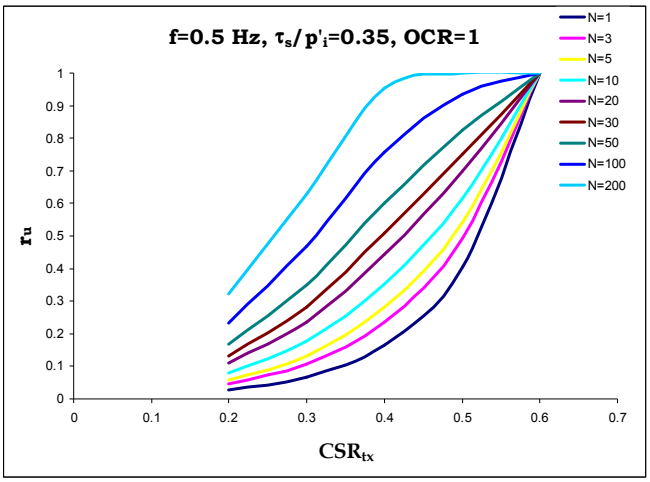

(a)

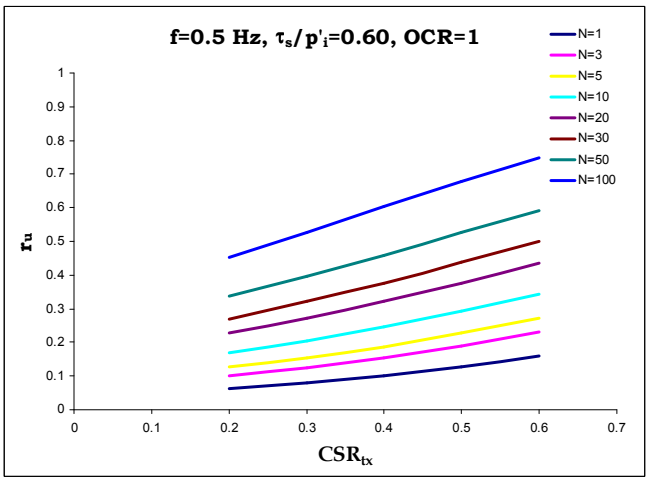

(b)

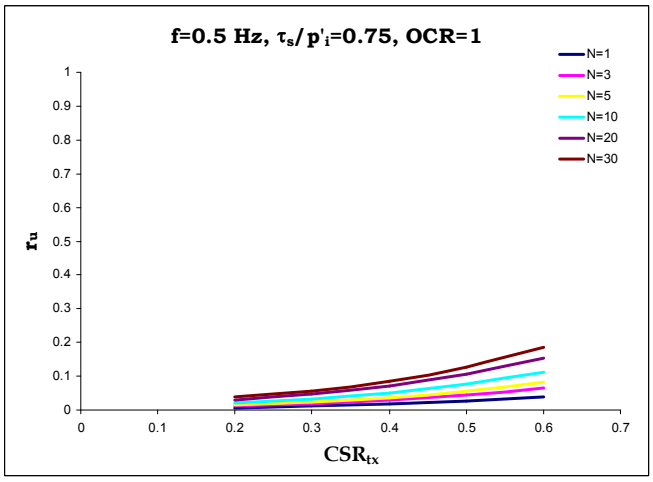

(c)

Figure 4.19 Modeling of pore water pressure for the tests conducted under 0.5 Hz and initial shear stress states of τ_s/p'_i=0.35, 0.60 and 0.75.

The models constituted for specimens having τ_s/p'_i of 0.35, 0.60 and 0.75 are given in Figure 4.19. As it is seen from the model curves, the pore pressure generation decreases with increasing τ_s/p'_i. In the tests conducted over specimens with τ_s/p'_i of 0.35, the cyclic stress-strain behavior develops on both the compression and extension side, particularly under high CSR_{tx} values. Therefore, r_u generation is similar to that observed for the specimens with no initial shear stress. Increasing τ_s/p'_i reveals that the stress-strain response is further dominated by the compression side. There was no stress reversal for all the specimens having τ_s/p'_i of 0.60 and 0.75 within the CSR_{tx} range applied in the study. Hence, the r_u values observed for these one way loading tests remained well below 1 as reflected by the models.

The effect of loading frequency on the pore pressure response is also investigated by models suited for the specimens having τ_s/p'_i of 0.35 and 0.60 tested under 0.05 Hz. The functions given by equations 4.12 and 4.13 suitably fit to the relationship observed for the case of τ_s/p'_i=0.38.

$$a = 0.0003e^{13.5CSR_{tx}} \tag{4.12}$$

$$b = 0.7e^{-3a} \tag{4.13}$$

The model constituted for the specimens of τ_s/p'_i=0.60 which were loaded with a frequency of 0.05 Hz is given with equations 4.14 and 4.15.

$$a = 0.003e^{6.5CSR_{tx}} \tag{4.14}$$

$$b = 0.7e^{-3a} \tag{4.15}$$

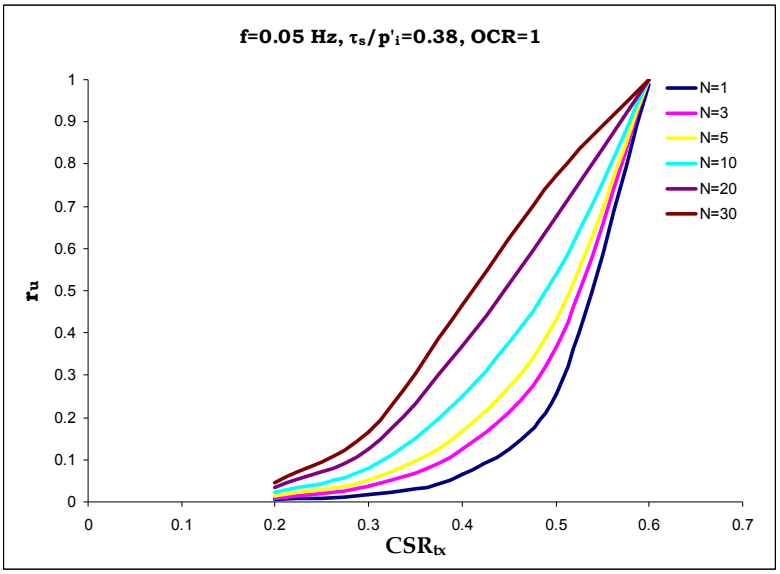

(a)

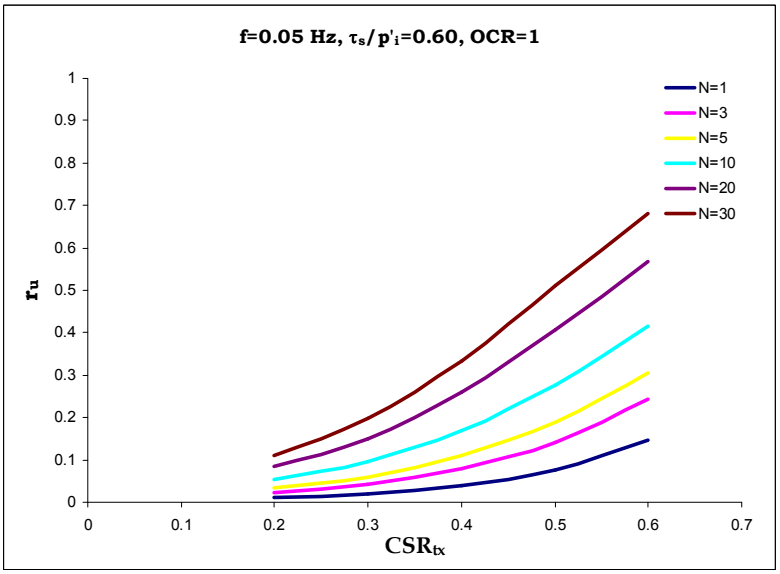

(b)

Figure 4.20 Modeling of pore water pressure for the tests conducted under 0.05 Hz, and initial shear stress states of τ_s/p'_i=0.38 and 0.60.

The pore pressure response of the specimens with initial shear stress is very similar for both loading frequencies. Particularly, if there is no stress reversal during cycling the pore pressure generation is not affected by the loading frequency.

Stress history of the reconstituted silt has been realized to have influence on the pore pressure response during cyclic loading. The excess pore

pressure response, thus, is correlated to CSR_{tx} and N through equations 4.16 and 4.17. The models given by these equations apply to the specimens having an OCR value of 2. Cyclic stress-strain behavior of the specimens has been observed to be significantly affected by increasing OCR. The excess pore pressure generation is reduced by increasing OCR, whereas the cyclic strain accumulation persists at a high rate. Consequently, as indicated before, the pore pressure response observed in the tests performed with the specimens having OCR of 4 could not be suitably correlated to CSR_{tx} and N.

$$a = 0.003e^{6CSR_{tx}} \tag{4.16}$$

$$b = e^{-3a} \tag{4.17}$$

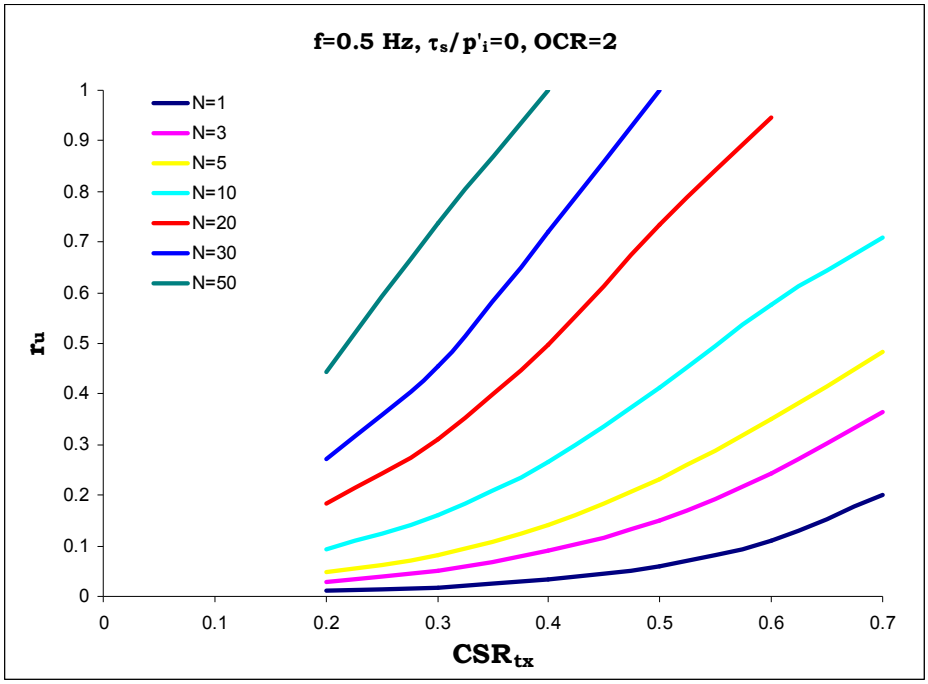

Figure 4.21 Modeling of pore water pressure for the tests conducted under 0.5 Hz, and stress states of τ_s/p'_i=0 and OCR=2.

The curves of the model for the case of OCR=2 are given in Figure 4.21. The r_u generation within the cycles up to 10 is very similar with that obtained for the case of OCR=1. For greater cycles the pore pressure

seems to increase more rapidly with increasing CSR_{tx}. Although the pore pressure generation at the cycles lower than 10 appears similar to that for the case of OCR=1, it must be noted that the cyclic strain values observed in the tests of OCR=2 are considerably higher than those observed in the tests of OCR=1.

4.8 Effect of Initial Confining Stress

Initial confining stress sustained by soil elements has been investigated and reported as a significant factor affecting cyclic response of soils in the literature. In free field, soil elements are imposed to horizontal and vertical stresses which are not equal to each other, and the ratio of horizontal stress to vertical stress is termed as lateral earth pressure coefficient (K_0). However, as indicated in Chapter 3, stress condition initially existing in free field is simulated through application of isotropic confining stress only. Therefore, it is also of concern to distinguish the effects of initial shear stress and the effects induced by the confining stress.

Isotropic consolidation phase during triaxial tests were carried out mostly with confining pressures of 50, 80 and 100 kPa. The effect of confining stress on the relationship between DA axial strain and N can be observed in Figure 4.22. The responses presented in Figure 4.22a belong to the tests performed with NC specimens. The specimens in the tests C2, C16 and C50 were consolidated under isotropic confining stresses of 50, 80 and 100 kPa, respectively, and were loaded with a CSR_{tx} of 0.30. As it can be inferred from the figure, cyclic straining tends to increase in the earlier cycles with increasing confining stress. In Figure 4.22b, the responses obtained in tests C4 and C19 which were consolidated under σ'_{3c} of 50 and 80 kPa are given. The CSR_{tx} used in these tests was 0.60. Even if the decreasing resistance is not as much as clear that for the case CSR_{tx} of 0.30, the cyclic resistance decrease with increasing confining stress.

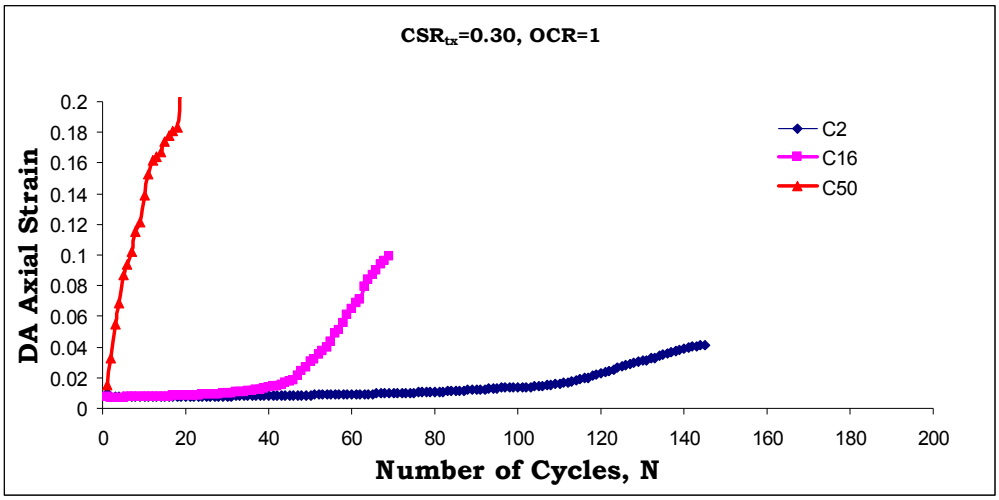

(a)

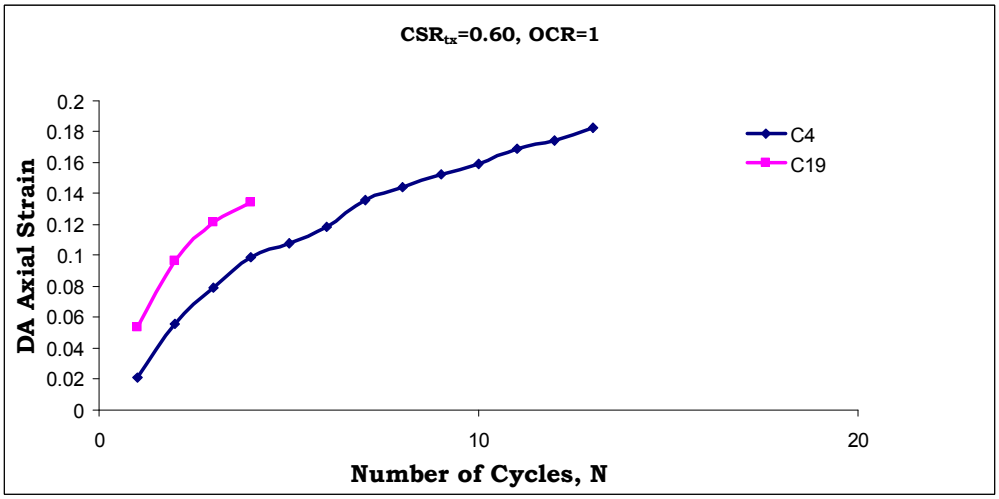

(b)

Figure 4.22 The relationship between DA axial strain and N for reconstituted NC specimens conducted with CSR_{tx} of (a) 0.30 and (b) 0.60.

The influence of confining stress on the cyclic response of NC specimens is shown by the plots given in Figure 4.23. The plots shows the relationship between CSR_{tx} and N to reach 5% DA axial strain for the tests conducted with σ'_{3c} of 50 and 80 kPa. It is seen that N required to reach 5% DA axial strain is greater for the tests conducted with σ'_{3c} of 50 kPa compared with those conducted with σ'_{3c} of 80 kPa.

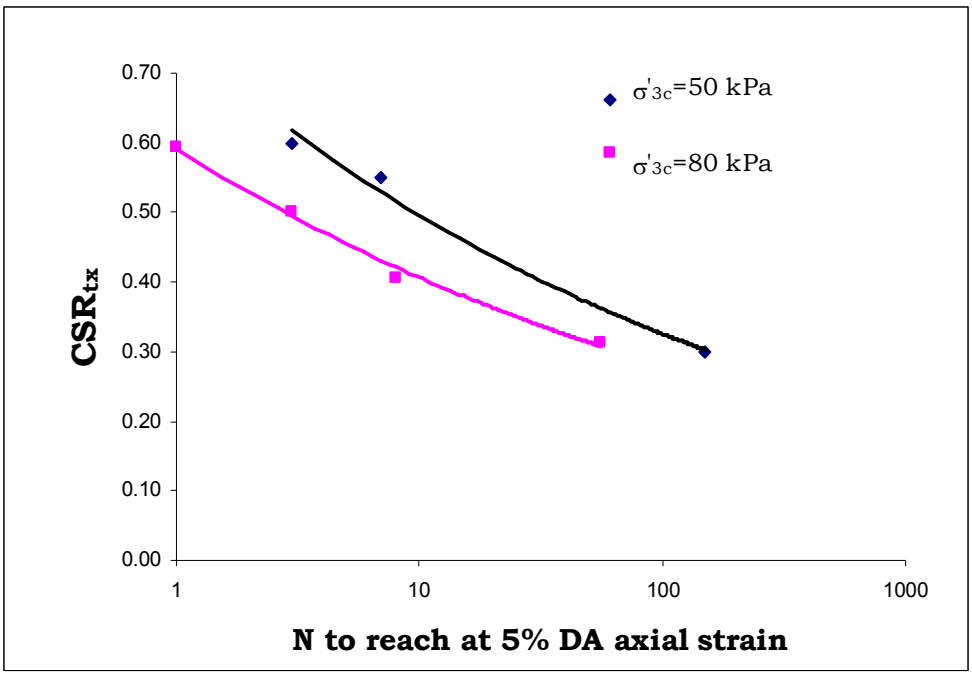

Figure 4.23 Relationship between CSR_{tx} and N to reach at 5% DA axial strain for reconstituted NC specimens consolidated under σ'_{3c} of 50 and 80 kPa.

The strain responses of two OC specimens tested with CSR_{tx} of 0.55 are illustrated in Figure 4.24 as a function of N. The tests C40 and C41 with OCR of 2 were consolidated under σ'_{3c} of 50 and 100 kPa, respectively. The specimen tested with σ'_{3c} of 100 kPa undergoes high strains earlier than that tested with σ'_{3c} of 50 kPa. In Figure 4.25, it is seen that CSR_{tx} is greater for the specimens consolidated under σ'_{3c} of 50 kPa. Thus, it can be concluded that increasing confining stress has a detrimental effect on the cyclic resistance of reconstituted NC and OC silt with OCR of 2. The tests performed with specimens having OCR values greater than 2 were carried out with only σ'_{3c} of 50 kPa, therefore the effect of confining pressure of specimens with OCR greater than 2 can not be evaluated. Nevertheless, it must be pointed out that Voznesensky and Nordal (1999) showed that the cyclic resistance of clays increases with increasing confining stress for the samples in OC state, whereas it is opposite for NC samples.

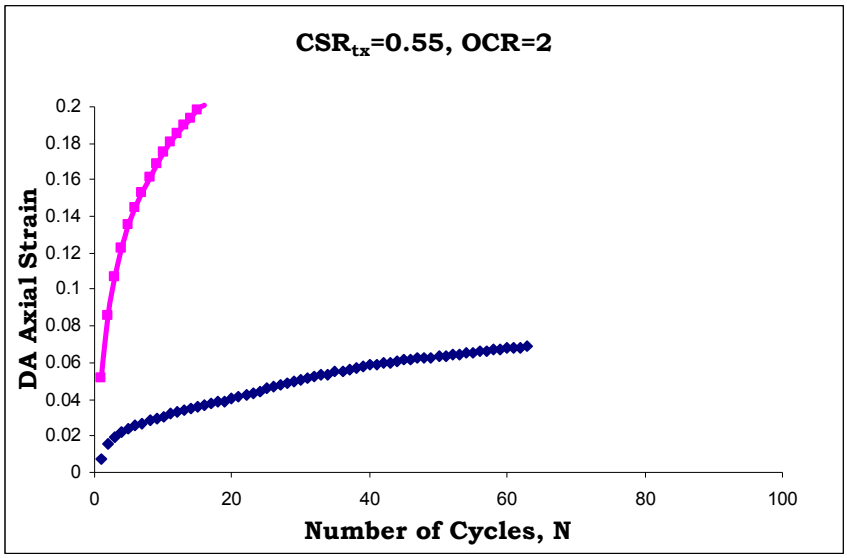

Figure 4.24 Relationship between DA axial strain and N for reconstituted specimens having OCR of 2 that were loaded with CSR_{tx} of 0.55.

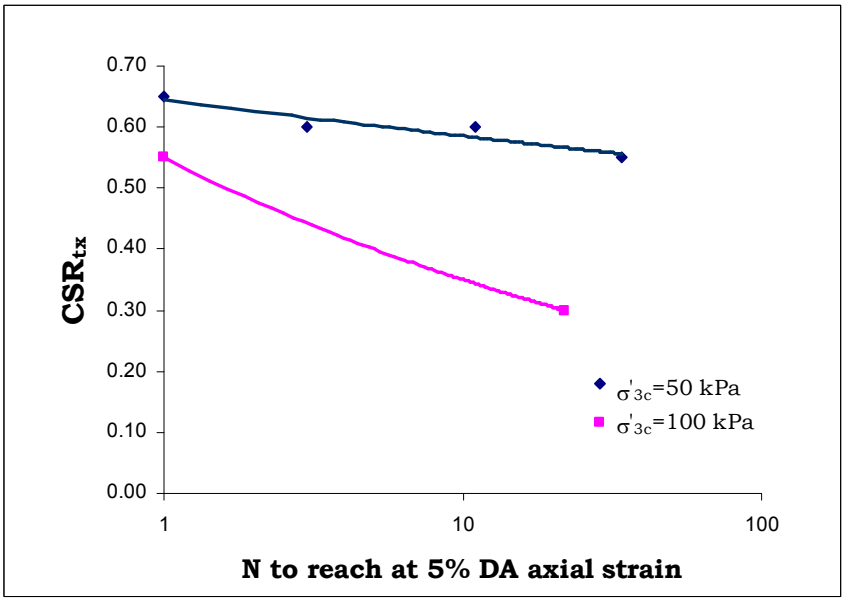

Figure 4.25 Relationship between CSR_{tx} and N to reach at 5% DA axial strain for reconstituted specimens with OCR of 2 that were consolidated under σ'_{3c} of 50 and 100 kPa.

4.9 Effect of Initial Shear Stress

The soil elements beneath or around existing foundations sustain a shear stress induced by the weight of structures. The investigations so far have revealed that the initially sustained shear stress has a significant effect on the cyclic behavior of soils. Magnitudes of the initial shear stress and cyclic load jointly designate whether the soil is to be imposed to stress reversals or not. As stated previously, the cyclic response of soils is substantially varies depending on the amount of strain and stress at the extension side.

The tests conducted with frequency of 0.5 Hz are to be taken into consideration for examination of initial shear stress effect, because the number of tests with 0.05 Hz is rather limited in the study compared to that of tests with 0.5 Hz. However, in order to understand how the initial shear stress affects the basic stress-strain relationship of the reconstituted silt, the monotonic tests performed with specimens consolidated to different initial shear stresses are to be examined firstly. As presented in Table 4.2, monotonic tests were carried out with different initial shear stress states and loading rates. The static stress-strain responses yielded by the monotonic tests conducted with a loading rate of 0.05%/min are given in Figure 4.26. As it is clear in the figure, the strength increases with increasing initial shear stress. The same tendency is observed for the tests performed under different loading rates as well.

The pore water pressure generating during monotonic shearing is also an important aspect of the stress-strain response. The pore pressure generation revealed that the reconstituted silt is highly dilative. This tendency becomes more pronounced with increasing initial shear stress. The pore pressures begins to decrease after reaching a certain value and can even get negative values in the tests performed with high initial shear stresses. The peak pore pressures observed during tests correlate to τ_s/p'_i as depicted in Figure 4.27. The maximum pore pressure ratio observed during monotonic shearing significantly decreases with increasing τ_s/p'_i. The observed effect of the initial shear stress over the monotonic tests is in agreement with those reported in literature.

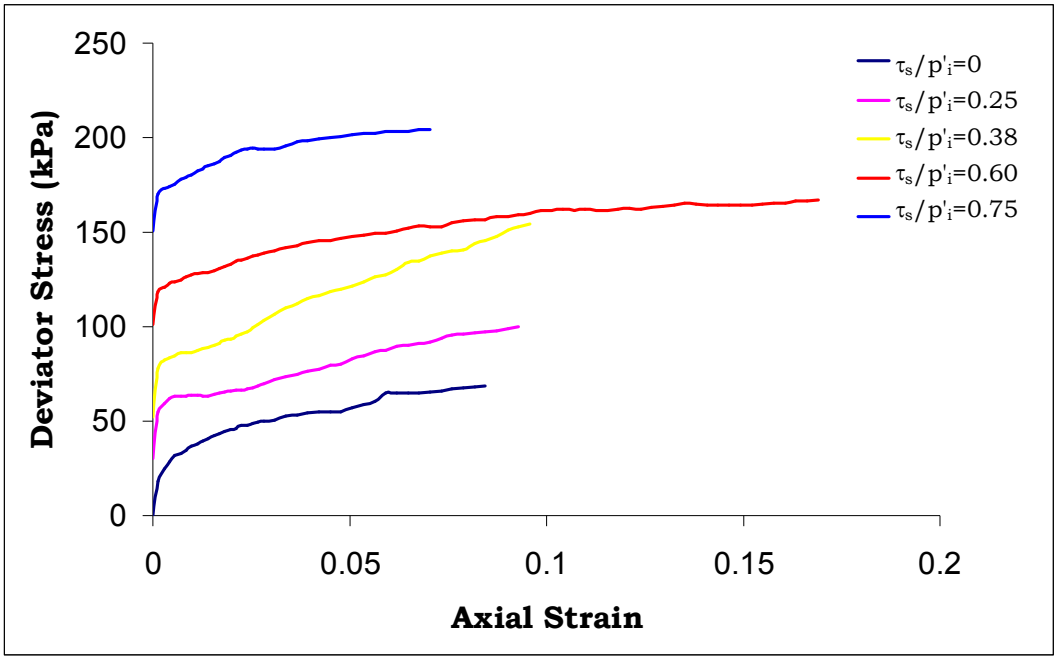

Figure 4.26 Monotonic stress-strain response for the tests conducted with τ_s/p'_i values of 0 (ST2), 0.25 (ST10), 0.38 (ST11), 0.60 (ST17), 0.75 (ST19).

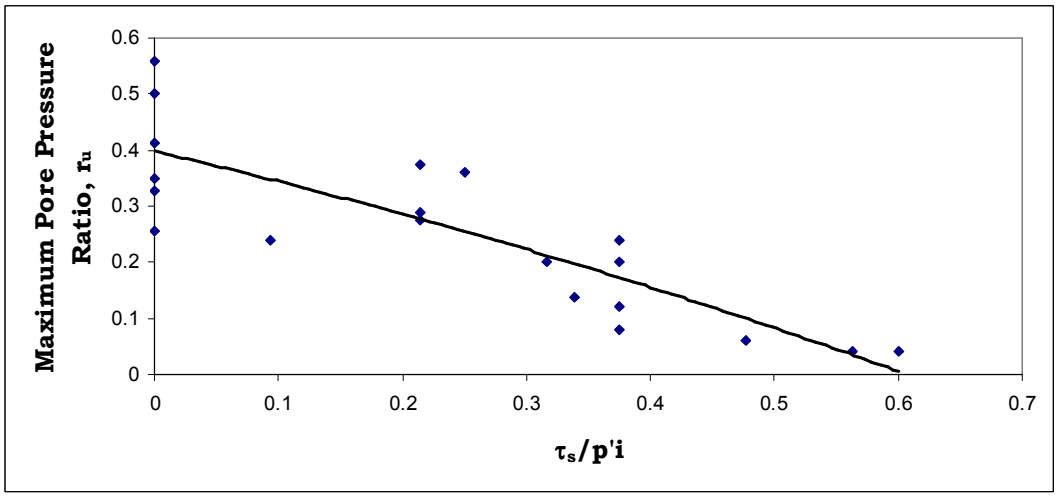

Figure 4.27 Maximum pore pressures observed in monotonic tests with varying τ_s/p'_i.

In literature, cyclic strength of the fine grained soils has been reported to decrease or increase with increasing initial shear stress. Hyodo et al. (1994) reported that cyclic strength of the clay used in that study tended to decrease with increasing initial shear stress, although the monotonic strength was conversely reported to increase. The effect of initial shear stress on cyclic strength is examined by means of the relationship between CSR_{tx} and N needed to reach ε_a of 5%. In the cyclic tests the axial strains mostly reach or exceed 10%. In some of the tests, however, the cyclic strain remains below a certain value, and even below 5%. Therefore as an optimal value reached overall in the tests ε_a of 5% is chosen as a reference strain when examining the initial shear stress effect. As it is seen in Figure 4.28, N needed to reach ε_a of 5% is increases with increasing τ_s/p'_i for a given value of CSR_{tx}. Nevertheless, the specimens having τ_s/p'_i of 0.75 display a reduced cyclic strength compared to those having τ_s/p'_i of 0.60. It must be noted, however, that the curve for τ_s/p'_i of 0.75 is plotted by means of only two tests.

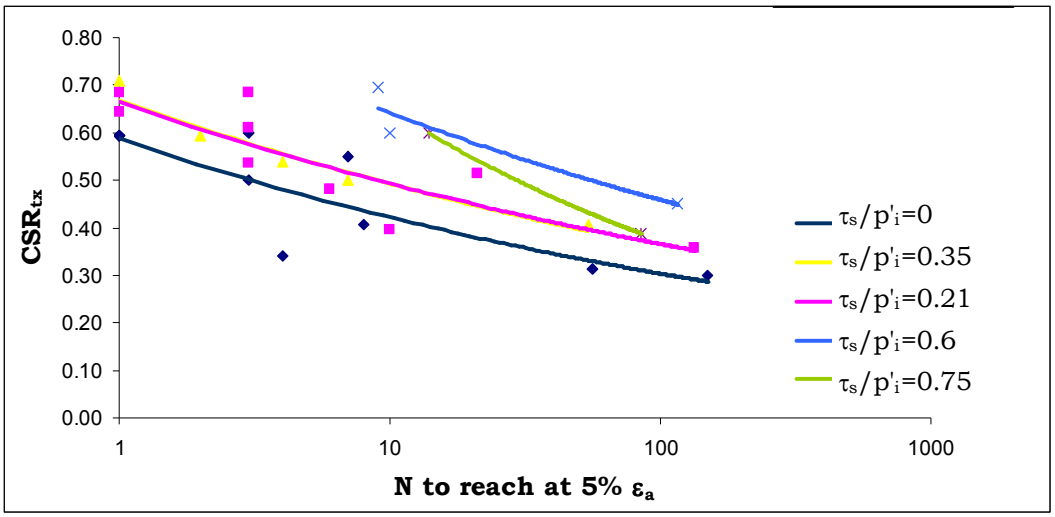

Figure 4.28 The relationship between CSR_{tx} and N to reach at 5% ε_a for different τ_s/p'_i values.

Ishihara (1996), and Lefebvre and Pfendler (1996) reported that the cyclic strength of clays is reduced by increasing initial shear stress if the initial shear stress exceeds 80% of the undrained static strength. However, as it

is to be discussed in detail under the proceeding heading, the loading rate has a significant influence on the undrained strength of fine grained soils. Therefore, an initial shear stress exceeding 80% of undrained static strength would be a subjective way to evaluate initial shear stress effect on cyclic response. Instead of the undrained static strength, which can significantly depend on the monotonic loading rate, initial mean effective stress (p'_i) is considered to be a better choice to interpret the effect of initial shear stress on the cyclic response of fine grained soils. Accordingly, it can be said that the initial shear stress exceeding 60-70% of p'_i causes a decrease in the cyclic strength of the silt used in the study. The observed tendency of cyclic strength to increase with increasing initial shear stress is identical with the data for sands having relative densities greater than 50% as reported by Ishihara (1996). The increase in strength becomes more evident when the results are interpreted in terms of maximum total undrained shear stress ratio ($(\tau_s+\tau_{cyc})/p'_i$). In Figure 4.29, it is seen that the total shear stress ratio required to reach an axial strain of 5% increases with a given N. The specimens having τ_s/p'_i of 0.75 are observed to have a greater total undrained shear stress ratio than those having 0.6.

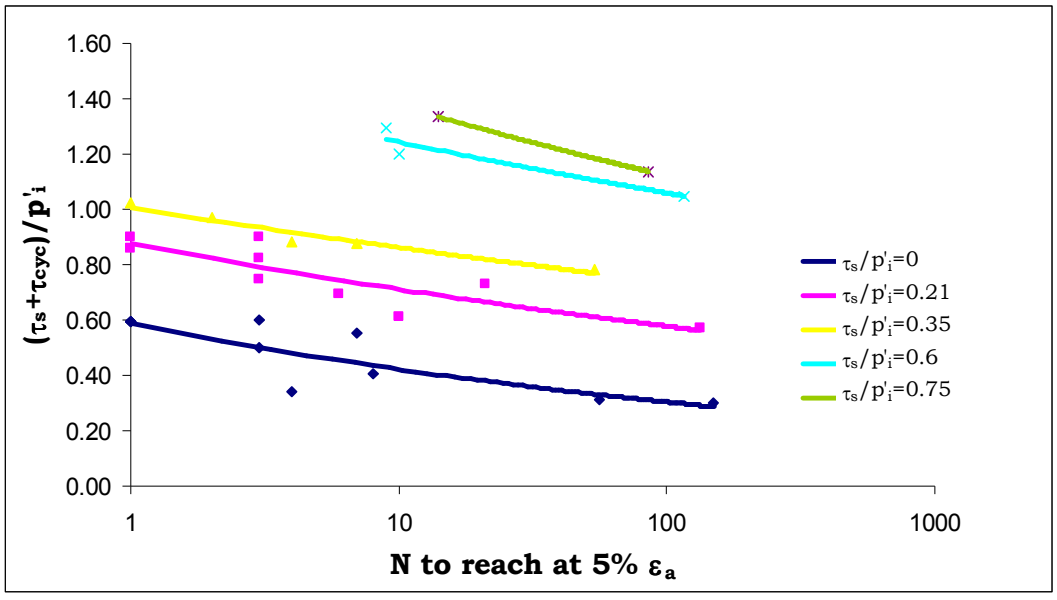

Figure 4.29 The relationship between $(\tau_s+\tau_{cyc})/p'_i$ and N to reach at 5% ε_a for different τ_s/p'_i values.

The relationship between pore pressure generation and τ_s during cyclic tests is similar with that observed in the monotonic tests. The change in excess pore pressure ratio with increasing initial shear stress is given in Figure 4.30. The excess pore pressure decrease becomes more pronounced for values of τ_s/p'_i beyond 0.38.

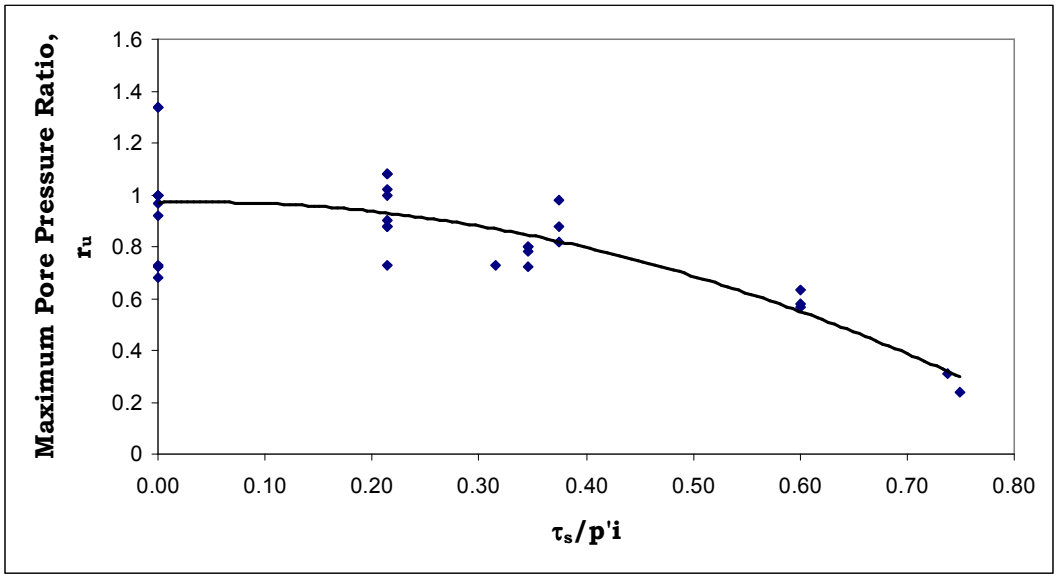

Figure 4.30 Maximum pore pressures observed in cyclic tests with varying τ_s/p'_i.

Hyde et al. (2006) reported that the cyclic behavior is dependent on whether there exists stress reversal or not during cycling, and modeled the relationship between cyclic deviator stress ratio and initial shear stress ratio as a function of N needed to reach 5% ε_a as given in Figure 2.27. The increasing initial shear stress decreases the cyclic resistance of the specimens subject to stress reversal, and the cyclic resistance exhibits an increasing trend with increasing initial shear stress for the tests with no stress reversal for the low plastic silt investigated by Hyde et al. (2006). The behavior observed in the tests conducted in this study shows almost an opposite trend for both stress reversal and no stress reversal cases. It is observed that the cyclic resistance increases more apparently for the tests with stress reversal, and no significant influence

of increasing initial shear stress is detected for the case of no stress reversal. This behavior modeled by using the relationships plotted in Figure 4.28. The fitted curves demonstrate that CSR_{tx} correlates to N to reach at 5% ε_a by the equation given below:

$$CSR_{tx} = c * N^{d} \tag{4.18}$$

where c and d are the coefficients depending on the τ_s/p'_i values. The relationships between the coefficients and τ_s/p'_i are given by the equations 4.19 and 4.20.

$$c = 0.7\,\tau_s / p'_i + 0.5 \tag{4.19}$$

$$d = -0.18(c + 0.1) \tag{4.20}$$

The relationships modeled by the equations given above are plotted in Figure 4.31. The observed effect of initial shear stress on cyclic response of reconstituted silt is in good agreement with the model given in the figure. This effect appears like that indicated for loose sandy soils in literature.

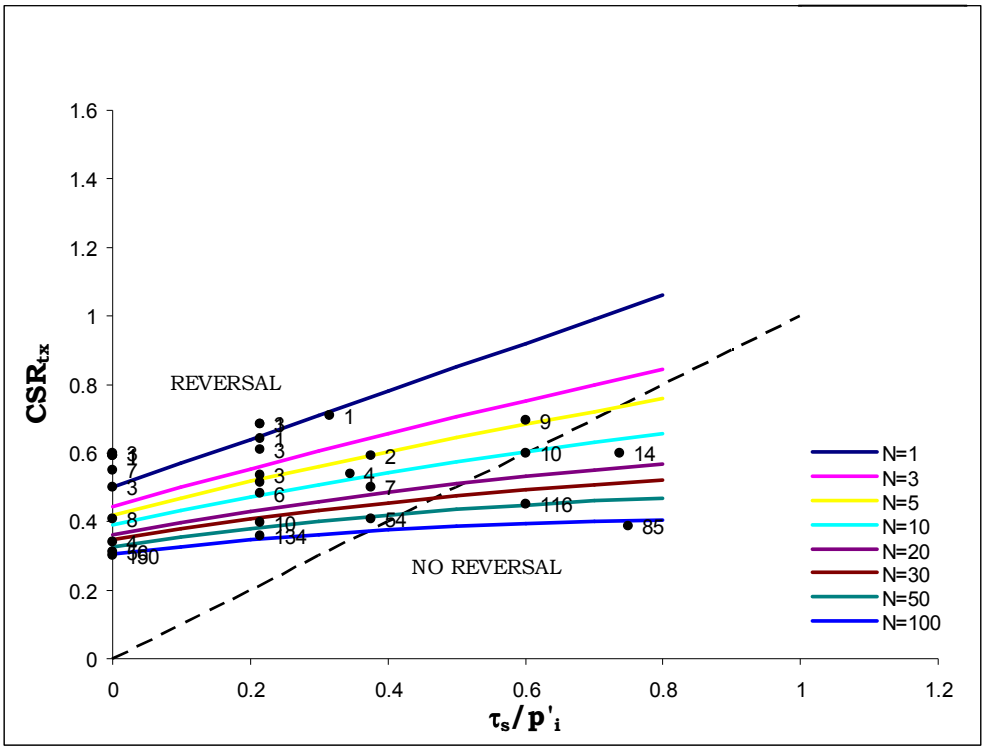

Figure 4.31 The model representing the effect of initial shear stress on cyclic response of reconstituted silt

4.10 Effect of Overconsolidation Ratio

Stress history of the soils is an important factor influencing stress-strain response under both monotonic and dynamic loading. This effect is more obvious for saturated fine grained soils, since the fine grained soil behavior is intrinsically dependent on the stress history. Although increasing OCR has generally been reported as causing an increase in the monotonic strength of fine grained soils, there exist studies with contradictory finding regarding the cyclic strength.

In the study, OC states were obtained by modification of σ'_{3c} following an isotropic consolidation phase. In the tests OC states were obtained typically by reloading to σ'_{3c} of 50 kPa. Thus, the specimens with OCR of 1, 2, 3 and 4 were initially consolidated under 50, 100, 150 and 200 kPa, respectively. Accordingly, effect of OCR on the monotonic and cyclic behavior of reconstituted silt would be investigated for the specimens sustaining no initial shear stress.

The effect of OCR on monotonic stress-strain response is explored with monotonic tests with OCR of 1, 2 and 4. As indicated in Table 4.2, a greater part of the monotonic tests were conducted with NC specimens. Additionally two more tests were conducted with specimens having OCR of 2 and 4. As illustrated in Figure 4.32, undrained shear strength (s_u) is increase with increasing OCR. The results of the tests of ST2, ST3 and ST4 are presented in the figure. These tests had a σ'_{3c} of 50 kPa at the beginning of shearing. Therefore, there is no influence of confining stress on the plotted relationship. The pore water pressure generation during monotonic tests decreases with increasing OCR. As it is plotted in Figure 4.33, the pore water pressure takes negative values with increasing OCR. Thus it can be stated that the dilation tendency becomes more prevalent with increasing OCR.

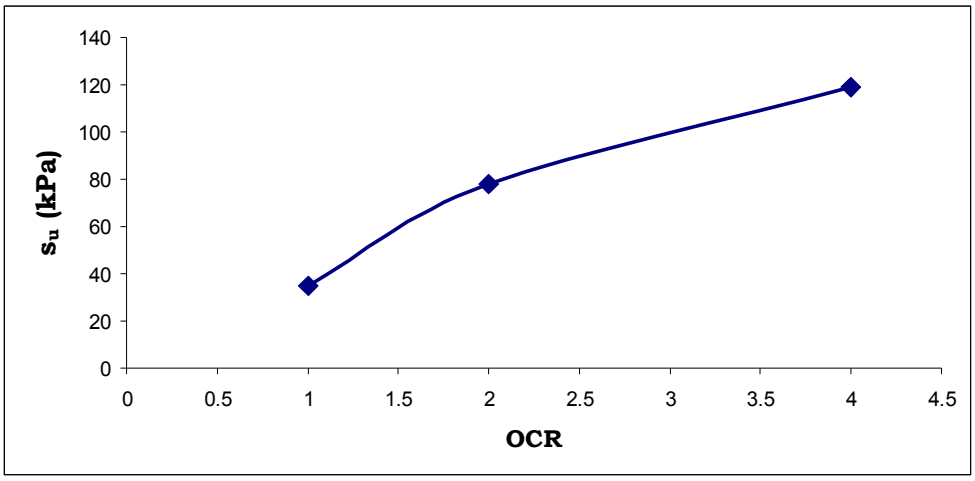

Figure 4.32 Monotonic undrained shear strength versus OCR for reconstituted silt.

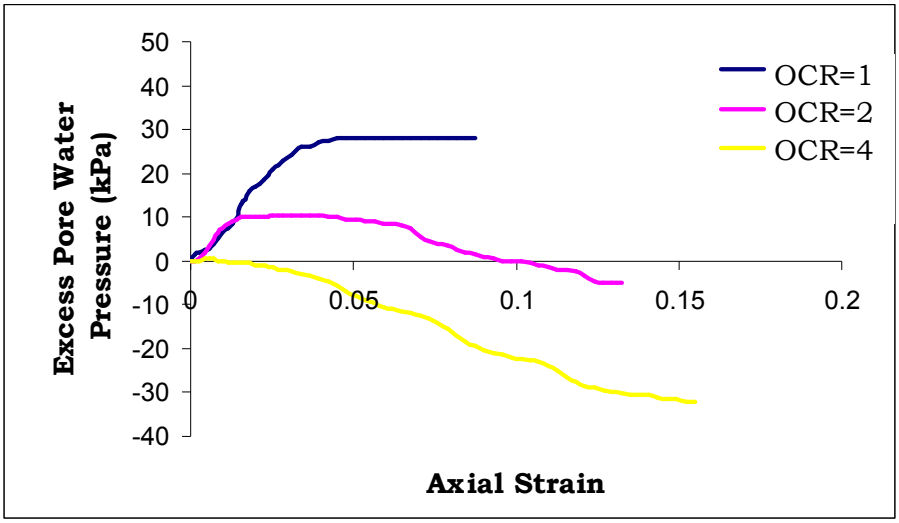

Figure 4.33 Monotonic excess pore water pressure change with axial strain for different OCR values.

The effect of OCR on cyclic response is examined via relationship between CSR_{tx} and N to reach at 5% ε_a. Again, ε_a of 5% is chosen as a reference value to compare the resistance of the specimens having different OCR values. As it can be seen in Figure 4.34, the CSR_{tx} that would cause a certain value of N required to reach at 5% ε_a increase with increasing OCR. However, the increase in resistance is not as significant as that observed in monotonic tests. Even for some specific tests, it is observed that increasing OCR causes a decrease in N required to reach at 5% ε_a.

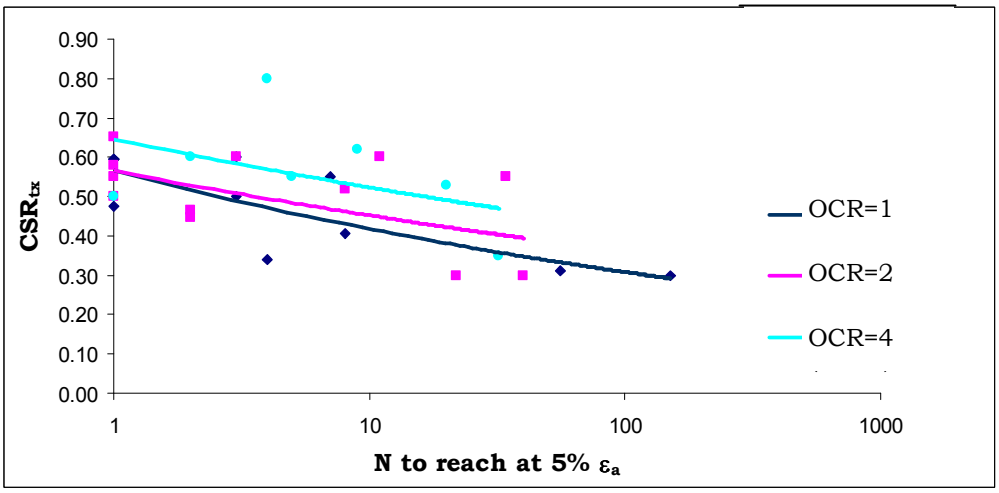

Figure 4.34 The relationship between CSR_{tx} and N to reach at 5% ε_a for different OCR values.

The excess pore water pressure generation during cyclic tests is displayed in Figure 4.35. As it is seen, maximum r_u is decrease with increasing OCR. Interestingly, however, certain axial strains are reached at lower excess pore water pressures with increasing OCR. In a way, if the cyclic resistance is evaluated by means of axial strain accumulation, OCR effect on cyclic resistance is not that clear as observed in monotonic tests. On the other hand, if the cyclic resistance is evaluated by means of pore water pressure generation, cyclic resistance more clearly increases with increasing OCR. As it is seen in Figure 4.35, straining progress independent of excess pore water pressure.

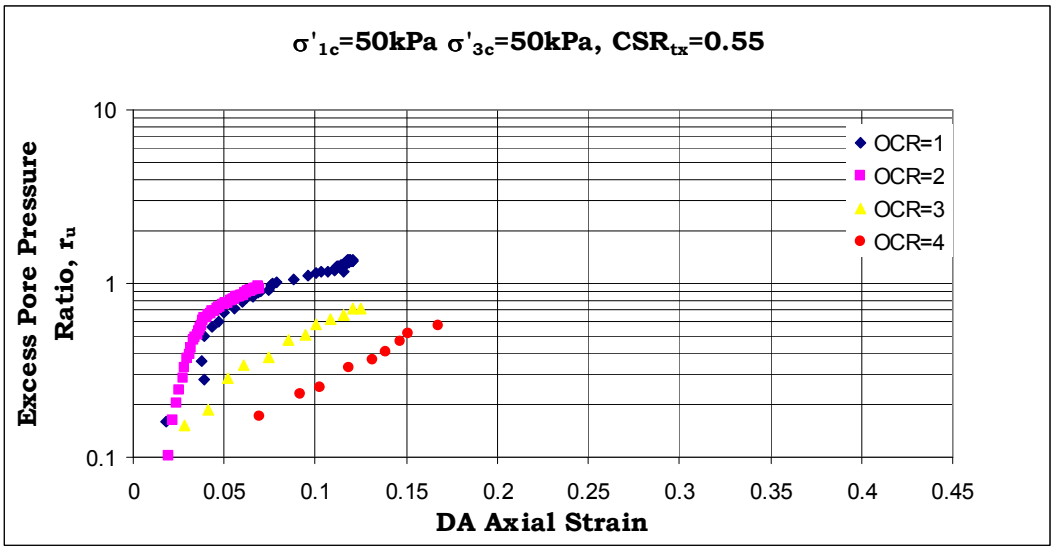

Figure 4.35 Excess pore pressure generation with axial strains for different OCR levels.

4.11 Effect of Loading Rate

Loading rate is another factor that has been frequently pronounced in literature as a significant effect on the stress-strain behavior of particularly fine soils. Loading speed is based on strain rate for strain controlled monotonic tests, and it is based both on loading frequency and the loading magnitude for cyclic tests. Monotonic tests carried out with different strain rates have provided a profound understanding of cyclic

response of soils. Monotonic strength of fine grained soils is increase with increasing loading rate.

The influence induced by loading rate has been mostly attributed to the pore pressure generation. As discussed under the heading of pore water pressure generation, pore water pressure is significantly affected by the loading rate. Due to the rather low hydraulic conductivities of fine grained soils, the pore water pressure along the specimen would not be uniformly distributed under high speed loading.

The effect of loading rate on stress-strain response observed during monotonic tests of isotropically consolidated specimens is given in Figure 4.36. Although the relationship between p'_i and monotonic strength is not linear, in order to evaluate the loading rate effect within a similar basis, the deviator pressure ($\Delta\sigma$) is normalized with p'_i. It can be generalized from the figure that the resistance of the silt increases with increasing loading rate. Nevertheless, it is interesting to observe a decrease in resistance for the test with a loading rate of 1%/min, which is ten times the loading rate of the test showing highest strength. There is no clear reason for such a behavior other than a possible mistake involved during testing.

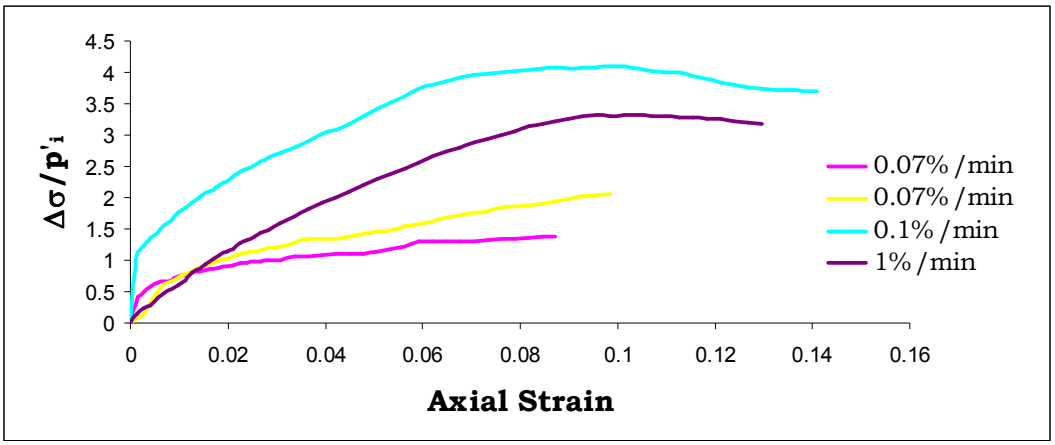

Figure 4.36 Relationship between normalized deviator stress ($\Delta\sigma/p'_i$) and axial strain for isotropically consolidated specimens tested with different loading rates

The pore water pressure generation observed during the tests illustrated in Figure 4.36 is given in Figure 4.37. As it is seen, the excess pore water pressure tends to decrease after a certain value, and this tendency is more pronounced with increasing loading rate. Since the pore water pressure is measured at the bottom end of the specimen, the nonequivalent pore pressure distribution along the specimen might be the reason for measureing lower excess pore water pressures with increasing loading rate.

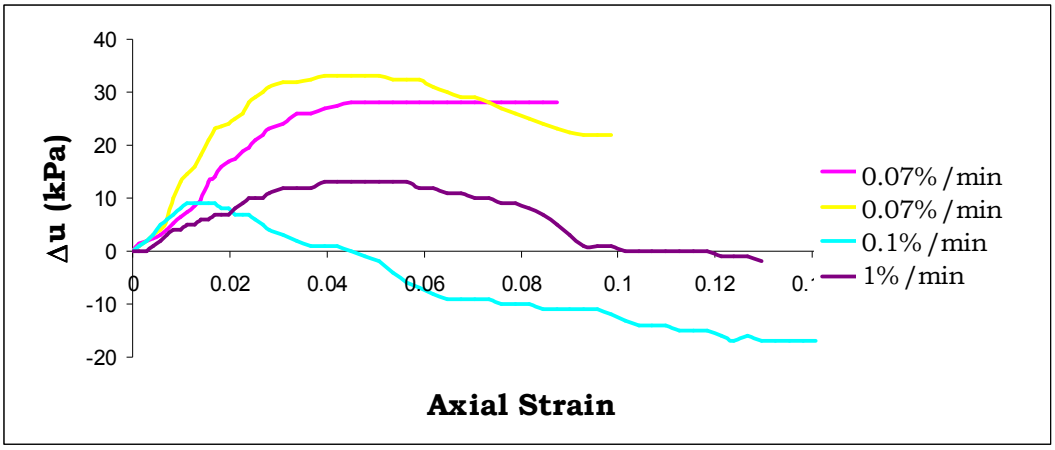

Figure 4.37 Relationship between excess pore water pressure (Δu) and axial strain for isotropically consolidated specimens tested with different loading rates

The tests with initial shear stress were carried out with just loading rates of 0.07%/min and 0.1%/min. Therefore, loading rate effect is examined with separate figures for τ_s/p'_i values of 0.38 and 0.60. As it is seen in Figure 4.38, the resistance is also increasing with increasing loading rate for anisotropically consolidated specimens. The excess pore pressure is decreasing after reaching a certain value and getting negative values. The pore pressure observed in the tests of 0.1%/min is getting negative values earlier than those of 0.07%/min. The more initial shear stress that specimen sustains the earlier excess pore water pressure is getting negative values. This response is actually resulting of the increasing dilation tendency with increasing initial shear stress.

Loading rate effect on cyclic behavior is to be examined via tests conducted under two different frequencies of 0.5 and 0.05 Hz. Cyclic pore water pressure response for different loading rates were investigated in detail under the heading of pore water pressure generation. Accordingly, the effect of loading rate is evaluated here based on cyclic stress and strain responses only.

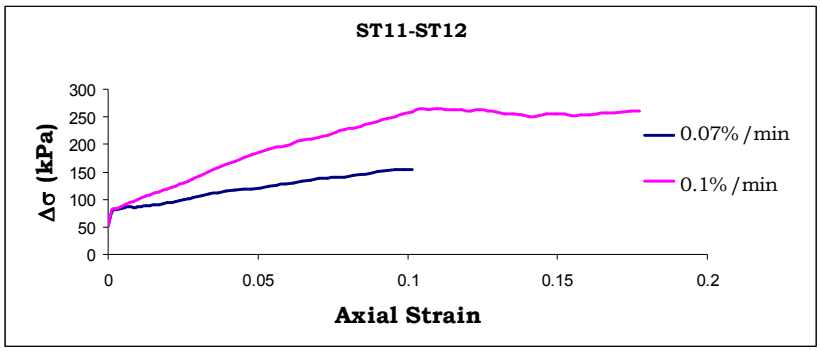

(a)

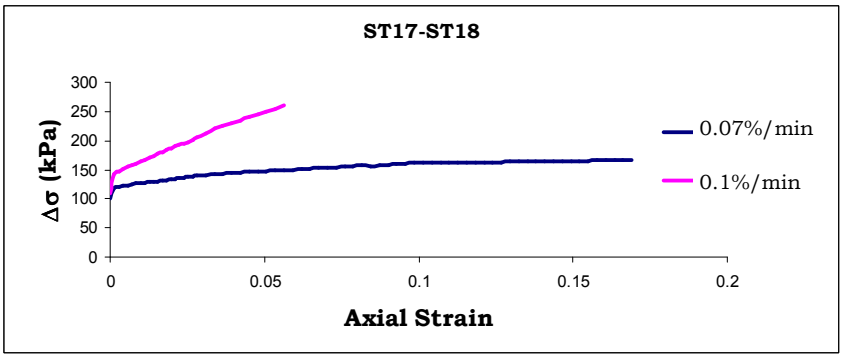

(b)

Figure 4.38 Loading rate effect for specimens with τ_s/p'_i values of (a) 0.38 and (b) 0.60.

Table 4.9, which is similar to Table 4.8, shows the r_u and N values at an ε_a value of 5% for the conjugate tests conducted with different frequencies. The loading rate effect differs depending on whether there exists initial shear stress or not. As it can be observed ε_a of 5% is reached by the first cycle for the tests with 0.05 Hz, whereas it is reached at N between of 2 and 25 for the tests with 0.5 Hz when compared to the conjugate tests carried out with no initial shear stress. Thus, an increase

in loading rate obviously causes an increase in cyclic resistance of the silt specimens that do not sustain initial shear stress. On the other hand, N values observed at 5% ε_a for conjugate tests conducted with specimens having an initial shear stress do not display a significant difference, and N observed for a test of 0.5 Hz is even lower than that observed in the conjugate test with 0.05 Hz. Therefore, in the general sense the loading rate does not influence the cyclic resistance if the cyclic behavior is dominated on the compression side.

Table 4.9 The r_u and N values observed at ε_a of 5% for conjugate tests conducted with 0.5 and 0.05 Hz.

Conjugate Tests	σ'_{1c} (kPa)	σ'_{3c} (kPa)	τ_s/p'_i	CSR_{tx}	f (Hz)	At 5% ε_a	
						r_u (%)	N
C3	50	50	0	0.55	0.5	68	7
C59	50	50	0	0.53	0.05	51	1
C5	45	45	0	0.72	0.5	73	25
C60	50	50	0	0.85	0.05	35	1
C18	80	80	0	0.5	0.5	25	2
C62	80	80	0	0.54	0.05	55	1
C17	80	80	0	0.41	0.5	51	6
C67	80	80	0	0.44	0.05	40	1
C10*	95	50	0.31	0.35	0.5	-	-
C65*	100	50	0.33	0.37	0.05	-	-
C13*	120	60	0.33	0.41	0.5	71	46
C66*	120	60	0.33	0.44	0.05	76	91
C11	95	50	0.31	0.54	0.5	48	3
C69	100	50	0.33	0.56	0.05	46	3
C15	120	60	0.33	0.59	0.5	30	2
C61	120	60	0.33	0.54	0.05	58	2
C26*	150	50	0.5	0.6	0.5	41	9
C63*	150	50	0.5	0.6	0.05	27	2
C25*	150	50	0.5	0.45	0.5	55	113
C68*	150	50	0.5	0.48	0.05	52	39

*Number of cycles was calculated considering SA axial strains

Interestingly, the r_u values observed at 5% ε_a are also higher for the tests conducted with 0.5 Hz and no initial shear stress. The r_u values obtained from the tests with initial shear stress are very similar to those for the conjugate tests as indicated under pore water pressure generation heading. The pore water pressure generation during cyclic loading is not influenced by the loading rate.

4.12 Cyclic Stiffness Degradation

Degradation during cyclic loading in soils occurs with regards to strength and stiffness. The change in strength is mostly assessed through the soil resistance based on the relationship between N and CSR_{tx} for a specific value of ε_a. Nevertheless, the change in stiffness can as well be observed at every cycle of loading as indicated by Idriss et al. (1978).

Cyclic degradation in soils is measured by means of the degradation index (δ_D) as introduced in Chapter 2. The index defines the relative variation of secant modulus (E) or shear modulus (G) by the ratio of the modulus in the first cycle (E_1 or G_1) to the modulus at the N^{th} cycle (E_N or G_N). Idriss et al (1978) and Ishihara (1996) showed that δ_D decreasing linearly with increasing N. The inclination of this straight line increase with increasing cyclic loading amplitude. The slope of this line is termed as the degradation parameter (t) and associated to stress history of fine grained soils as discussed in Chapter 2.

The cyclic degradation observed in the reconstituted silt specimens in this study is quantified based on tests conducted with isotropically consolidated specimens. Since the stiffness degradation diminishes with increasing initial shear stress ratio and becomes negligible with increasing N for the tests with no stress reversal. The cyclic degradation is measured in this study through the ratio of secant modulus (E) calculated at the first and N^{th} cycles. Calculation of E values for the first and the second cycles of a two way test is depicted in Figure 4.39. As it is seen, E is calculated considering the peak $\Delta\sigma_{cyc}$ and ε_a observed at that peak stress for the relevant cycle. Then, δ_D is calculated for each cycle by considering SA ε_a values observed at compression side.

The relationship between δ_D and N is plotted as a function of the applied CSR_{tx}. Cyclic degradation for the silt specimens with different OC states were evaluated with separate plots. As would be expected, it is observed

that the cyclic degradation increases with increasing CSR_{tx} for all OCR values.

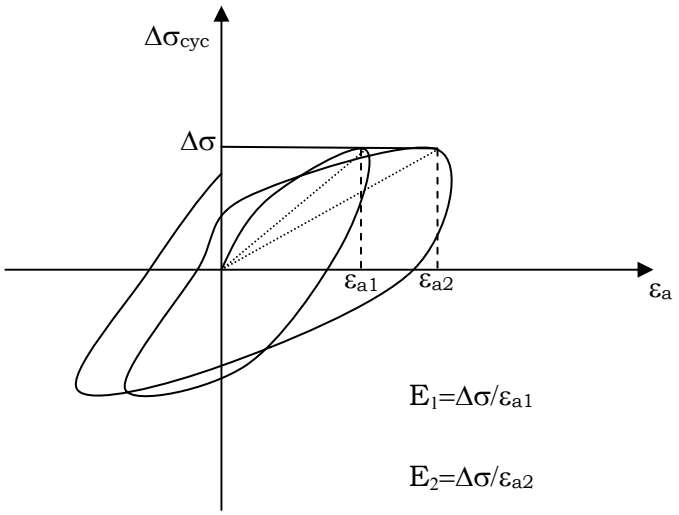

Figure 4.39 Illustration for secant Young's modulus calculation

The cyclic degradation observed in the tests performed with specimens having OCR values of 1, 2 and 4 is presented in Figure 4.40. The increasing CSR_{tx} causes a faster stiffness degradation in all the specimens. The relationships between δ_D and N were fitted by trendlines. It is observed that the relationships deviate from being linear with increasing CSR_{tx}, although it was observed and modeled as a straight line by Idriss et al. (1978). The trendlines observed for the tests conducted with a CSR_{tx} around 0.30 are linear for OCR values of 1 and 4. Interestingly, each trendline plots a curve rather than a line for the specimens having OCR value of 2. In order to evaluate the effect of stress history on degradation tendency, the degradation parameter (t) was calculated for the linear part of the trendlines shown in Figure 4.40. The relationships between t and CSR_{tx} for OCR values of 1, 2 and 4 are given in Figure 4.41. It is observed that an increase in OCR causes reduction in the stiffness degradation as indicated by Vucetic and Dobry (1988). However, this reduction is not as much significant as that for clays shown by Vucetic and Dobry (1988).

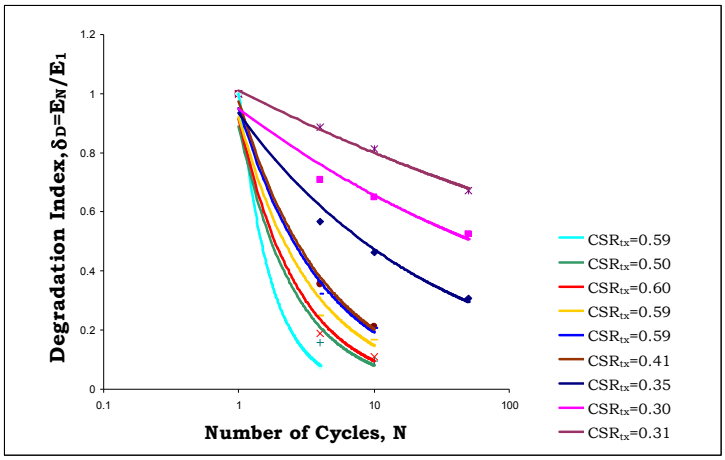

(a)

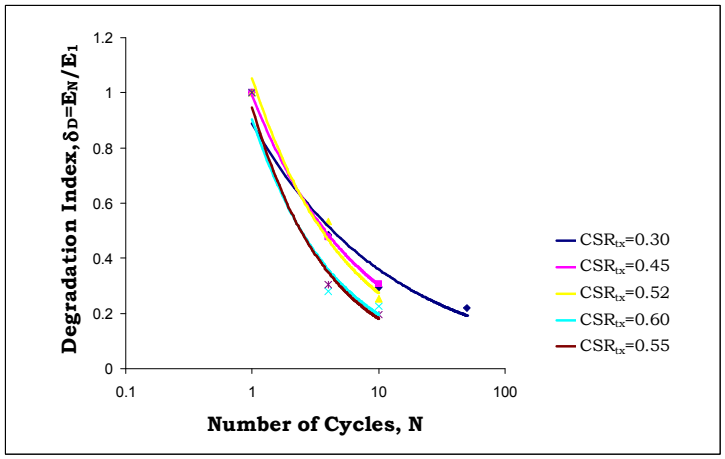

(b)

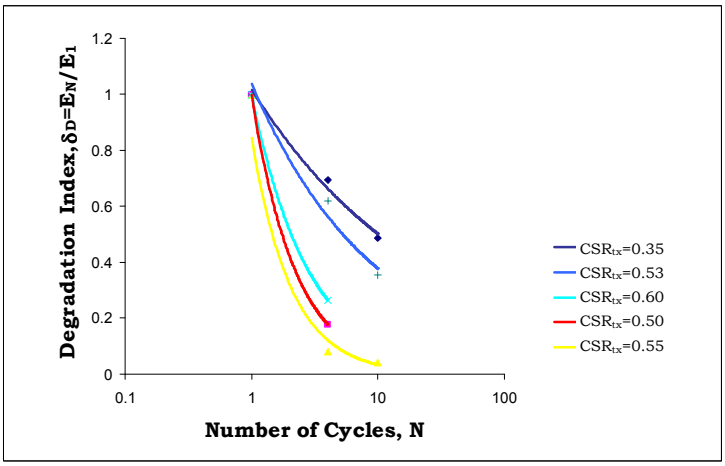

(c)

Figure 4.40 Stiffness degradation with increasing cycles for the silt specimens with OCR of (a) 1, (b) 2 and (c) 4.

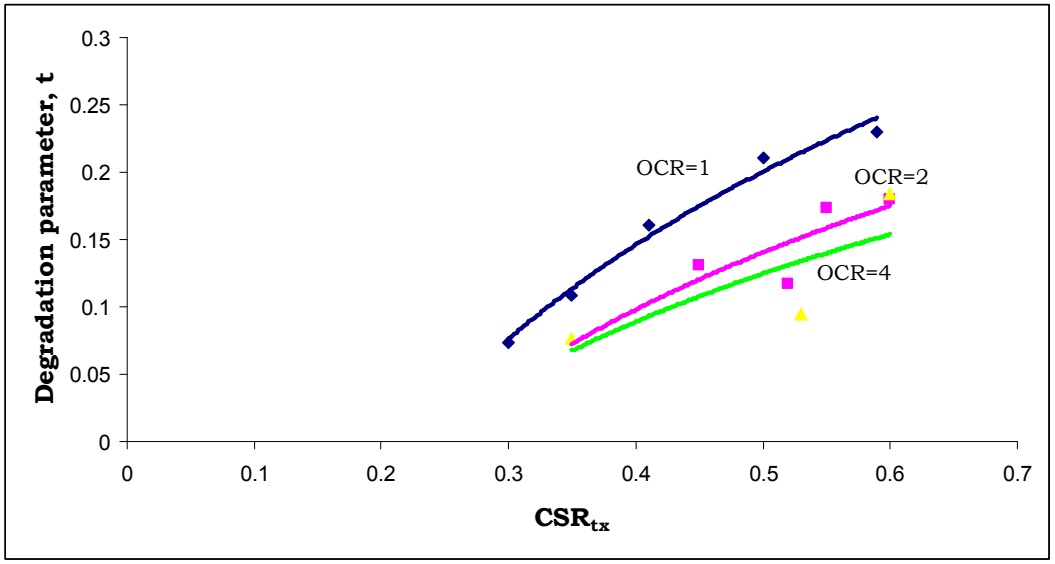

Figure 4.41 Effect of OCR on stiffness degradation of reconstituted silt

4.13 Examination of the Liquefaction Susceptibility of Reconstituted Silt via Existing Criteria

Chinese criteria is represented graphically in Figure 4.42 for the soils having 0.005 mm and smaller particle sizes less than 15%. The percent of particles less than 0.005 mm is about 9 % for the silt used in the study. The relevant data for the cyclically tested 69 specimens of the reconstituted silt are plotted on the same figure. It is to be mentioned that the modification for LL, suggested by Koester (1992), is applied for the silt. As it is observed in Figure 4.42, the silt plots on the "not susceptible to liquefaction" side. The assessment of the criteria meets the test results when considering that no flow liquefaction has been observed throughout the tests. However, this assessment can be regarded as somewhat conservative when considering the response of cyclic mobility that has frequently occurred during the cyclic tests. It should also be noted that the representative points are adjacent to the boundary defining potential susceptibility to liquefaction.

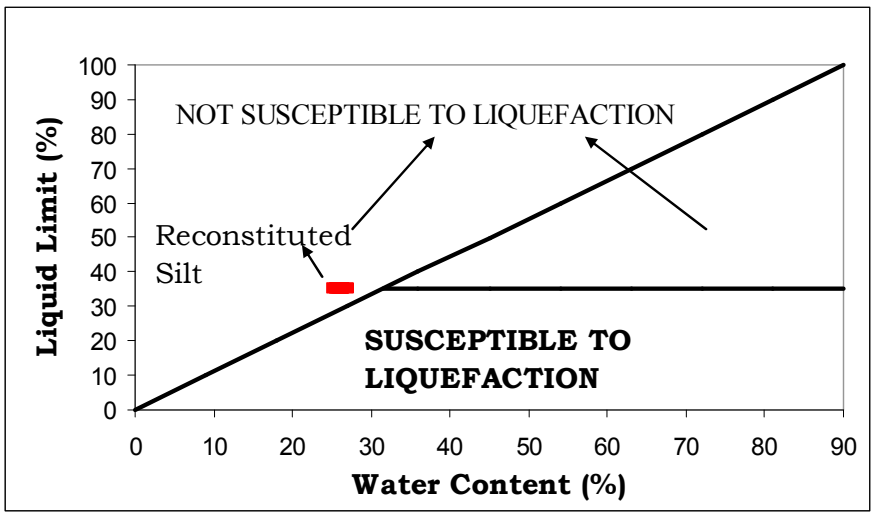

Figure 4.42 Chinese criteria for the soils having 0.005 mm and smaller particle sizes less than 15 %.

The data of the reconstituted silt are also plotted on the graphical representation of the criteria proposed by Andrews and Martin (2000). As it is seen in Figure 4.43, even though the silt plots in the area defined as "susceptible to liquefaction", the parameters are almost on the borderline separating the "susceptible" and "not susceptible" sides.

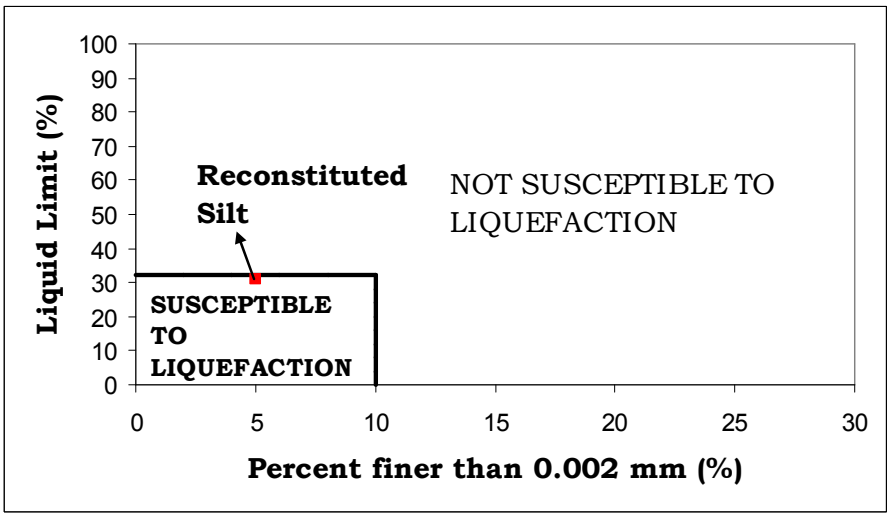

Figure 4.43 Liquefaction susceptibility criteria proposed by Andrews and Martin (2000)

The test data for the reconstituted silt are plotted with respect to the criteria proposed by Bray et al. (2004) (Figure 4.44). The silt is classified as in the range from "moderately susceptible to liquefaction or cyclic mobility" to "susceptible to liquefaction or cyclic mobility". This assessment is in conformity with the "cyclic mobility" observed for the reconstituted silt during cyclic triaxial tests. The area defined as "moderately susceptible to liquefaction or cyclic mobility" gives a room for evaluation of liquefaction susceptibility of borderline materials, especially for low plasticity silts. However, the criteria do not provide a clear distinction between the "liquefaction" and "cyclic mobility".

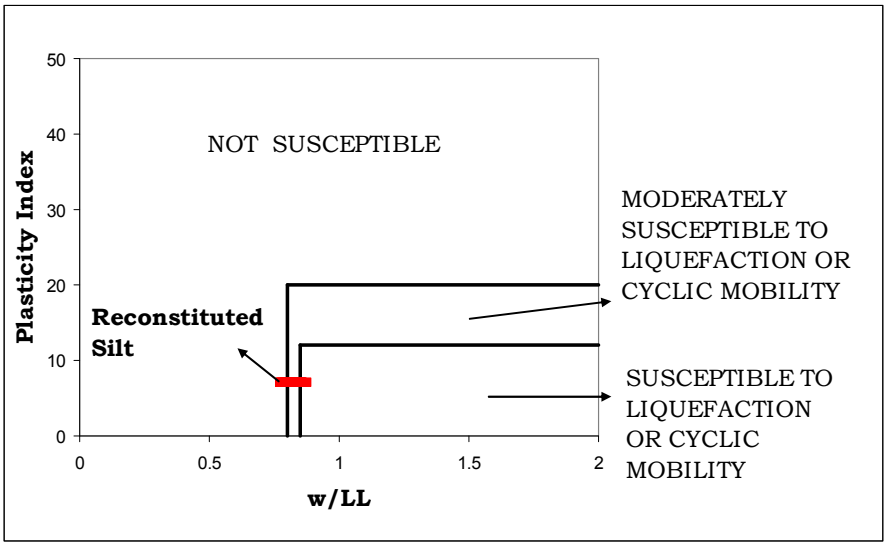

Figure 4.44 Liquefaction susceptibility criteria proposed by Bray et al. (2004)

Boulanger and Idriss (2004) suggested that fine-grained soils of PI < 7 are to be classified as "sand-like" (i.e. susceptible to liquefaction) and soils of PI ≥ 7 classified as "clay-like" materials. In accordance with this characterization, the silt of PI = 7 would be classified as "clay-like" material. However, attention should be payed on the accuracy of the measured parameters which becomes quite critical during liquefaction susceptibility evaluation of such borderline materials.

CHAPTER 5

CYCLIC RESPONSE OF FINE-GRAINED SOILS RECOVERED FROM ADAPAZARI,TURKEY

5.1 Introduction

The City of Adapazarı, which is the provincial capital of Sakarya, was one of the hard hit cities during the August 17 1999 İzmit (Kocaeli) earthquake (M_w=7.4). The surface rupture of the fault emerged during the earthquake was at a mere average distance of 5 km to the south of the City. Building damage in the city was remarkably concentrated over the central districts during 1999 earthquake. The city is situated at the edge of an alluvial basin, and the deposits composed of alluvial soils reaching depths in excess of 200 m beneath the central districts. The ground water table fluctuates between 0.5 m and 2.0 m seasonally below the ground surface in the city. As it was stated by Bakır et al. (2005), there two entirely different and mutually exclusive modes of building damage was observed over reinforced-concrete buildings with similar characteristics situated over deep alluvial sites .

The damage was either due to structural system failures or foundation displacements of various forms and levels. At first the foundation displacements and settlements observed in the city were primarily attributed to soil liquefaction by many researchers. However, the surface soils at the sites where the foundation displacements were commonly observed have been reported be consisting of fine-grained soils (CL/ML) which are conventionally regarded as non-liquefiable (Karaca, 2001; Pekcan, 2001; Yılmaz and Bakır, 2009). Nevertheless, Bakır et al. (2005), and Yılmaz and Bakır (2009) reported that the seismic bearing capacity of

the shallow mat foundations, which are commonly utilized in the reinforced concrete buildings in the City with a few exceptions, were exceeded during 1999 earthquake.

5.2 Geology of Adapazarı

The City of Adapazarı is located over a sedimentary basin, which was a lake bed formerly. The main geological characteristics are presented in Figure 5.1 adapted from Bakır et al. (2005). The older part of the City is to the south, underlain by stiff and shallow sedimentary soils, while the City later developed through north underlain by Quaternary alluvia deposited by Sakarya River and its tributaries. The alluvia are underlain by deep clay layers which are lake sediments. Depth to bedrock rapidly increases through south reaching levels in excess of 200 m within the city limits. The river deposits consist of normally consolidated or lightly overconsolidated fine sand and silt-clay mixtures with varying proportions. Majority of the fine-grained soils is of low plasticity. Although the river deposits display rapid variations within, the lake deposits are by and large dominated by clays.

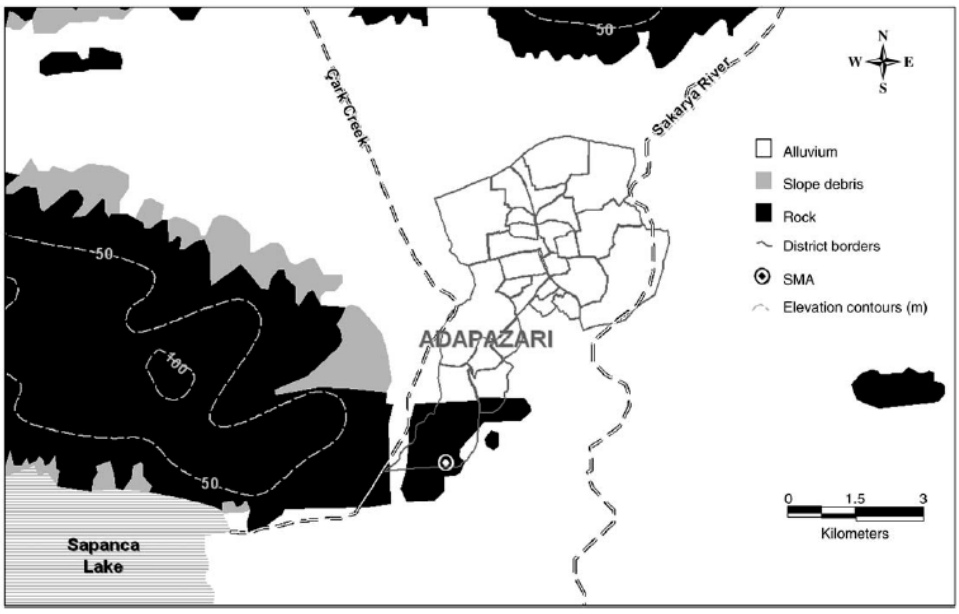

Figure 5.1 Surface geology of Adapazarı (Bakır et al., 2005).

5.3 Seismicity of the Region

The North Anatolian fault system is the primary source of the seismic activity in the region. During the earthquake that occurred in 1894, 840 houses collapsed and 3000 were damaged out of existing 4000 houses in the City at that time.

In 20th century, two destructive earthquakes other than 1999 earthquake, also induced by the North Anatolian fault system, influenced Adapazarı. In 1943, the city was hit by the Adapazarı earthquake with a magnitude of 6.6, the epicenter of which was 10 km to the east of the city. It was particularly severe, causing destruction of 70% of the houses in the City and loss of over 300 lives in the area (Ambraseys and Zapotek, 1969).

The other, Mudurnu Valley earthquake with a magnitude of 7.1 occurred within an epicentral distance of 27 km to the City in 1967. Its impact over the City was relatively less as compared to that happened in 1943. Liquefaction was reported to occur along the Sakarya River (Ambraseys and Zapotek, 1969). Nevertheless, there was no evidence of liquefaction within the city limits according to the reconnaissance reports.

The most devastating at the region, however, was the 17 August of 1999 earthquake. According to a comprehensive survey conducted by the Adapazarı Municipality, 2844 buildings, constituting about 12% of the total, either collapsed or were eventually demolished due to heavy damage in the City, while 3694 lives, almost 2% of the City's population, were lost. Only the east-west horizontal component of the acceleration was recorded by the strong motion station in Adapazarı, at a 3 mere km distance from the surface rupture. The recorded component, which is also almost fault-parallel, had a peak ground acceleration of 0.4g, and integration of the component gives a peak ground velocity of 57 cm/s (Anderson et al., 2000). However, the station is situated at the southern part of the City, underlain by stiff and shallow residual soils, where overall damage was strikingly low. As a general trend, concentration of damage increased

rapidly to the north, underlain by the soft, thick alluvial soils, with multistory reinforced concrete building structures receiving the greatest impact. The ground water table over the alluvial sediments in the city is reported to fluctuate within 0.5 and 2.0 m of the ground surface seasonally.

5.4 Characteristics of the Sites under Investigation

In order to evaluate the cyclic behavior of fine-grained surface soils overlying the alluvial basin to the north of Adapazarı, a number of sites, where foundation displacements occurred during 1999 earthquake, were documented for detailed investigations. The sites, which are dominated by fine soils at the ground surface, were selected based on an evaluation of the earlier investigations including drillings, conducted by other researchers in the City following the 1999 earthquake (i.e. Karaca, 2001; Pekcan, 2001; Yılmaz, 2004). Accordingly, the selected sites consist of previously drilled boreholes as well.

Eventually a total of 5 sites at two different districts (Tığcılar and Yenigün) of the city were selected. The two districts, namely, the Tığcılar and Yenigün districts (indicated by numbers 12 and 13, respectively), are illustrated on the map of the City presented in Figure 5.2. Table 5.1 provides general information about the boreholes, including location, depth and position of ground water table (GWT). Undisturbed soil samples were recovered by means of Shelby tubes during opening of the boreholes within the framework of this study.

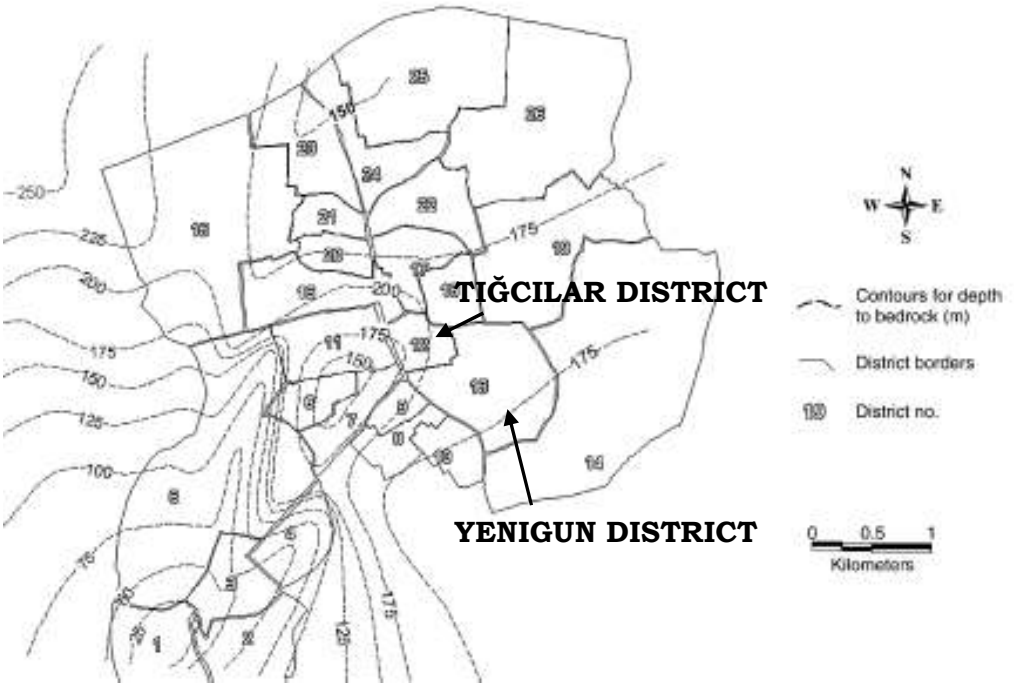

Figure 5.2 Central districts of the city of Adapazarı (adapted from Bakır et al., 2005).

The boreholes were drilled to depths ranging between 6 m and 8 m from ground surface, and 1 to 3 tubes of undisturbed samples were retrieved from each borehole. The tubes used in sampling had external diameters of either 6.35 or 7.6 cm with 1.5 mm wall thickness. The heights of the sampled soil in the tubes were around 65 cm. Two triaxial specimens, each 3.6 cm in diameter, could be extruded side by side from a tube having 7.6 cm diameter, whereas only one specimen could be sampled from a specific interval from a tube with 6.35 cm external diameter. The specimens were extruded at 2 or 3 sequential levels along the sample height of 60-65 cm. In addition, a specimen was taken from each tube for determination of consolidation characteristics. Atterberg limits, specific gravities and gradational distributions of each sample were determined and soil classification was made based on USCS.

Table 5.1 General information about boreholes

Borehole No	Street	District	Borehole Depth (m)	GWT Depth (m)
SK-1	Hasırcılar	Yenigün	8	2.10
SK-2	Çırak	Yenigün	7	1.60
SK-3	Sönmez	Yenigün	7	2.60
SK-4	Yazar	Yenigün	8	1.80
SK-6	Backyard of Vocational School for Girls	Tığcılar	6	2.10

5.4.1 Hasırcılar Street (SK-1)

Hasırcılar Street is located in the Yenigün District. During the earthquake the adjacent buildings of Teverler and Bahadır, which were situated over Hasırcılar street, tilted towards opposite sides as shown in Figure 5.3. Pacific Earthquake Engineering Research Center (PEER) conducted an extensive investigation over the entire area that was affected during the earthquake and drilled boreholes around these buildings. Accordingly, the soil profile at the site can be roughly generalized as given in Table 5.2.

Figure 5.3 View of the tilted buildings of Teverler and Bahadır after 1999 Kocaeli (İzmit) earthquake (adopted from PEER web-site).

Plan of the site is depicted in Figure 5.4. The borehole drilled at the site was at 10 m away from the southern corner of the building of Bahadır. The depth of the borehole was 8 m, and GWT was observed at a depth of 2.10 m from the ground surface. Two tubes were recovered from between depths of 2.00 m - 2.70 m and 6.00 m - 6.70 m. Since the soil mostly consisted of silty sand, the sample representative of 2.00 m - 2.70 m was not suitable for triaxial and consolidation testing

Table 5.2 Generalized soil profile of the site at Hasırcılar Street

Depth Interval (m)	Soil Description
0-1.5	Fill
1.5-4.0	Low plasticity silt to sandy silt
4.0-5.0	High plasticity silty clay
5.0-7.0	Clayey silt to sandy silt

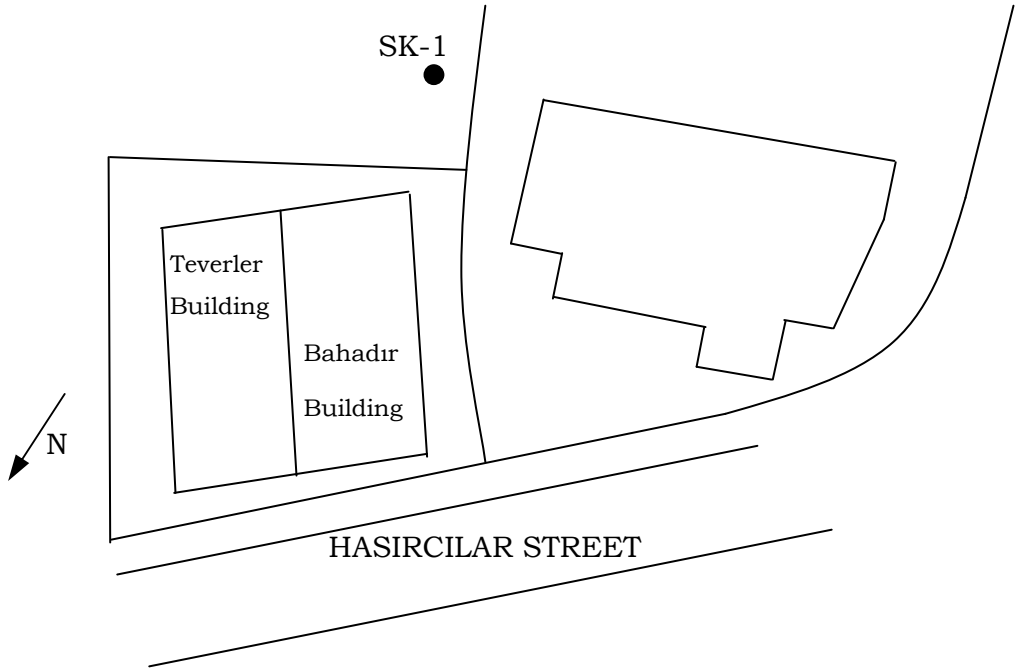

Figure 5.4 Plan of the site around Hasırcılar Street

5.4.2 Çırak Street (SK-2)

The Street of Çırak is also located in the Yenigün District. Plan of the site is given in Figure 5.5. The settlement observed in the Buildings of Yıldız Apartments during 1999 earthquake is shown in Figure 5.6a. The sand ejected from the northwestern corner of the block A is also to be noted. This site was explored by PEER as well. Generalized soil profile around Çırak Street is described in Table 5.3.

Table 5.3 Generalized soil profile of the site around Çırak Street

Depth Interval (m)	Soil Description
0-1.0	Fill
1.0-3.5	Clayey silt
3.5-5.0	High plasticity silty clay
5.0-9.0	Silty fine sand

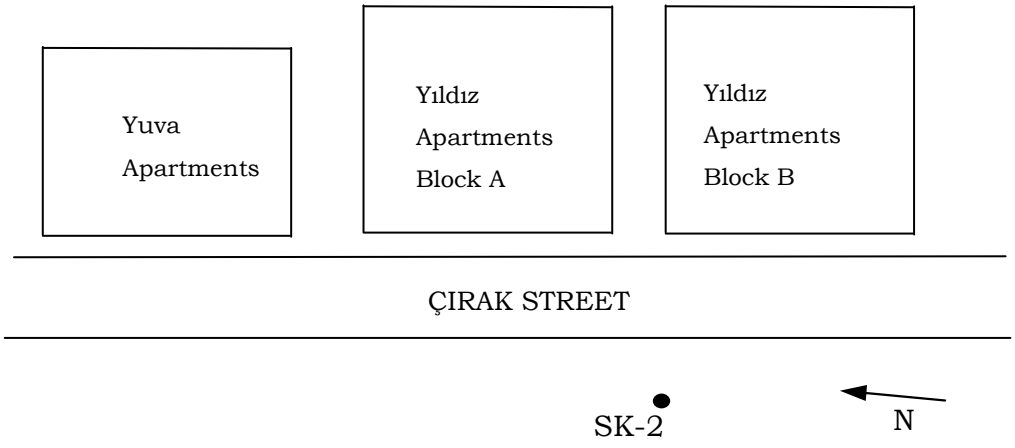

Figure 5.5 Plan of the site around Çırak Street

The borehole SK-2 was drilled at a 20 m distance from block B on the west side of the building. The depth of the borehole was 7 m, and GWT was at a depth of 1.60 m from the ground surface. Three Shelby tubes were retrieved from the depth intervals of 1.50 m - 2.20 m, 4.00 m - 4.70 m and 5.50 m - 6.20 m of the borehole.

(a)

(b)

Figure 5.6 View of (a) northeastern corner of Yıldız Apartments Block A just after the 1999 Kocaeli earthquake (adopted from PEER web-site), (b) Çırak Street from south.

5.4.3 Sönmez and Yazar Streets (SK-3, SK-4)

The streets of Sönmez and Yazar are parallel two streets in the District of Yenigün, and Yazar is a dead end. Borehole SK-4 was drilled 3 m north of the dead end of the street. As it is seen on the plan given in Figure 5.7, boreholes SK-3 and SK-4 are drilled to investigate the same site where the building shown in the figure underwent a severe foundation settlement, and another 3 stories building marked in the figure as house A, collapsed totally during the earthquake.

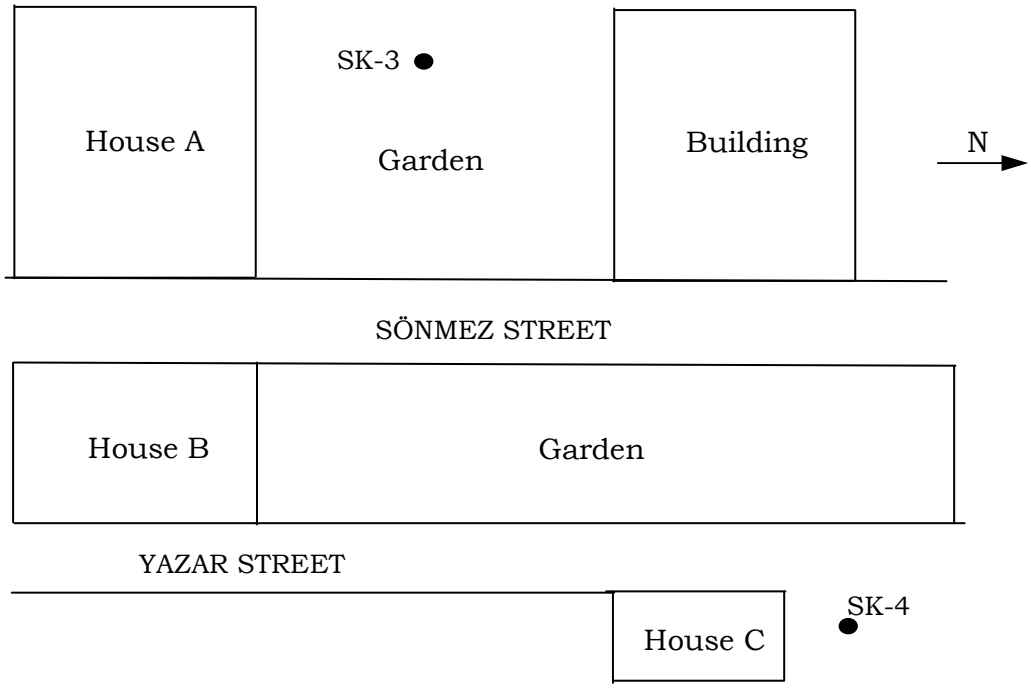

Figure 5.7 Plan of the site comprising Sönmez and Yazar streets

In association with the investigation performed by PEER, the soil profile prevailing this site can be generalized as that given in Table 5.4. However, boreholes of the investigation conducted by PEER were drilled over the area closely surrounding the building seen on the plan. Therefore, the soil profile represented by means of SK-4, which was drilled 25 m east of the building, would be different than the one introduced in Table 5.4.

Table 5.4 Generalized soil profile of the site around Sönmez Street

Depth Interval (m)	**Soil Description**
0-1.0	Fill
1.0-3.0	Low plasticity sandy silt
3.0-5.0	Low plasticity silty clay
5.0-8.5	Sandy silt to silty sand

The borehole SK-3 was drilled in the middle of the garden existing on west side of the Sönmez Street, and at 10 m south of the building settled during 1999 earthquake, as shown in Figure 5.8. The depth of SK-3 was 7 m and the GWT was at a depth of 2.60 m. Three Shelby tubes were retrieved from the depths of 2.50 m - 3.20 m, 4.00 m - 4.70 m and 6.00 m - 6.70 m of SK-3. The borehole SK-4 was drilled at north of house C given on the plan. Its depth was 8 m and the GWT was at 1.80 m. Only one tube was retrieved from 3.00 m - 3.70 m depth range of SK-4.

Figure 5.8 The location of SK-3 and view of the building settled during the earthquake

5.4.4 Vocational School for Girls (SK-6)

The vocational school for girls in Adapazarı is located in the District of Tığcılar. SK-6 was drilled in the backyard or the school. Although there was no significant damage on the school building, settlements were observed in numerous building foundations in the District of Tığcılar. The subsoil conditions of Tığcılar district was comprehensively investigated by Karaca (2001). Accordingly, the borehole that was drilled at almost 20 m southwest of the school building within the framework of the study by

Karaca (2001) roughly represents the soil profile around the school, which is presented in Table 5.5.

Table 5.5 Representative soil profile of the site around vocational school for girls

Depth Interval (m)	Soil Description
0-1.5	Fill
1.0-4.0	Silt with fine sand
4.0-6.0	Silty clay
6.0-12.0	Very dense silty sand

The depth of SK-6 was 6 m, and the GWT in the borehole was at a depth of 2.10 m. Only one Shelby tube was recovered from between the depths of 2.50 m - 3.20 m. The location of the borehole is given in Figure 5.9.

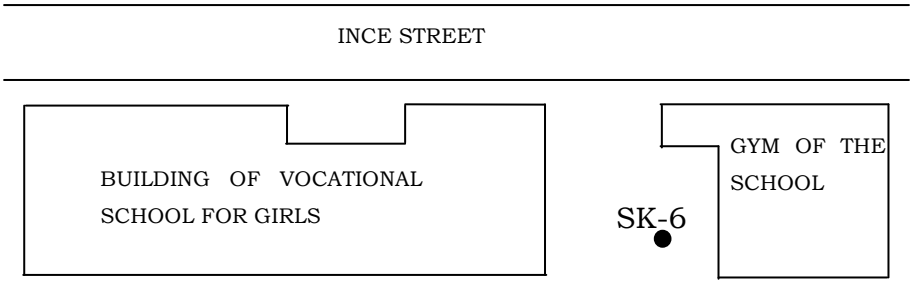

Figure 5.9 Plan of the vocational school for girls in Adapazarı

5.5 Properties of the Soil Samples Recovered from Adapazarı

The index properties of the samples recovered from Adapazarı were determined through laboratory tests. The sample heights in Shelby tubes were around 60 cm - 65 cm. Although soils displayed rapid variations vertically, the soil at middle part of each tube was considered as

representative of the tube and used to determine the index properties, which are given in Table 5.6.

Table 5.6 Index properties of the soil samples recovered from selected sites in Adapazarı

SAMPLE		w_c (%)	Gs	ATTERBERG LIMITS			PARTICLE SIZE, mm (Passing Percentage)			USCS
BORING NO	DEPTH (m)			LL	PL	PI	2	0.063	0.002	
SK-1	6.00-6.70	38.37	2.64	35.5	23.45	12.05	100	85.9	15	CL
SK-2	1.50-2.20	33.85	2.63	29.7	26.21	3.49	100	53.6	5	ML
	4.00-4.70	38.1	2.57	30.3	24.21	6.09	100	56	8.5	ML
	5.50-6.20	31.55	2.58	28.9	22.87	6.03	100	68	10.5	ML
SK-3	2.50-3.20	32.06	2.62	29.8	26.01	3.79	100	69.1	7	ML
	4.00-4.70	29.43	2.64	26.6	23.68	2.92	100	44.7	6.5	SM
	6.00-6.70	22.8	2.68	NP	NP	NP	100	23.1	1.5	SM
SK-4	3.00-3.70	30.98	2.63	33.2	22.27	10.93	100	76.2	14.5	CL
SK-6	2.50-3.20	23.74	2.65	NP	NP	NP	100	28	1	SM

As it is seen in Table 5.6, the percentage passing 0.063 mm is generally greater than 50% in the samples. The exceptions are the samples recovered from 6.00 m - 6.70 m depths in SK-3 and from 2.50 m - 3.20 m depths in SK-6. The samples, which consisted of low plastic silt-clay mixtures and fine sand with silt, were classified according to the Unified Soil Classification System. As it is given in Figure 5.10, the samples plot adjacent to A-line at low plasticity side of the chart. It is to be pointed out that the cyclic behavior of such low plastic fines is the subject matter of the present study.

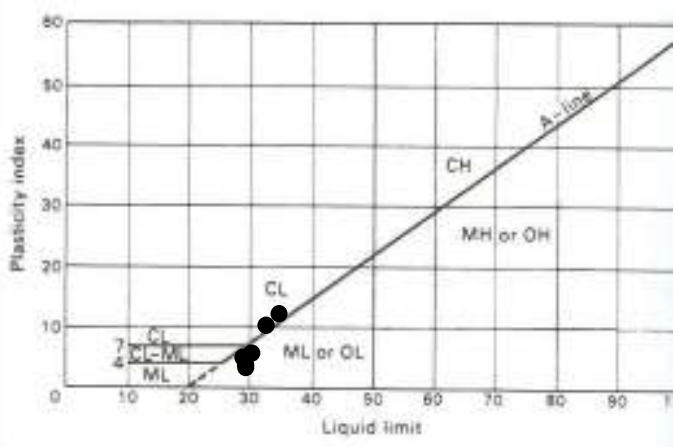

Figure 5.10 The locations of the samples recovered from Adapazarı on the plasticity chart

5.6 Monotonic Triaxial Compression Tests on Adapazarı soils

A series of undrained monotonic tests were conducted over Adapazarı samples to examine the static response of those soils, and to identify any conceivable relation between responses under monotonic and cyclic loading. As indicated in Chapter 4, the frictional ends cause the stress inhomogenity throughout the specimen, and the strains occur non-uniformly along the specimen as a result. Thus, due to both, stress concentrations and low permeability of fine grained soils a certain duration of time is required for equilibration of pore water pressure within the specimen, and the loading rate becomes an important aspect during loading. In order to eliminate the effect of loading rate on monotonic strength, the method suggested by Bishop and Hengel (1957) was again used to determine the loading rate so as to provide 95% equilibrium in pore pressure within the triaxial specimen. The procedure is given in detail in Chapter 4. Accordingly, the loading rates to be applied are calculated for the samples as shown in Table 5.7. The t_{50} values were determined by means of the consolidation tests conducted for each tube recovered.

Table 5.7 Loading rates required to ensure pore water pressure equilibrium during monotonic tests

Test No	Peak Strength (kPa)	Strains at Peak Strength (%)	SAMPLE		$t_f=4t_{50}$ (minute)				Max. Loading Rate (%/min)
			BORING NO	DEPTH (m)	P=25 kPa	P=50 kPa	P=100 kPa	P=200 kPa	
STA1	135	9.6	SK-4	3.00-3.70	0.52	0.67	0.23	0.39	41.74
STA2	178	14.3	SK-2	1.50-2.20	0.23	0.59	0.28	0.33	43.33
STA3	194	14.1	SK-2	1.50-2.21	0.23	0.59	0.28	0.33	42.73
STA4	260	13.5	SK-3	4.00-4.70	0.67	0.59	0.33	0.45	30.00
STA5	567	11	SK-3	6.00-6.70	NA	NA	NA	NA	NA
STA6	179	11	SK-2	5.50-6.20	0.32	0.43	0.73	0.62	17.74
STA7	180	12.7	SK-2	4.00-4.70	0.28	0.39	0.75	0.59	21.53
STA8	236	9	SK-2	5.50-6.20	0.32	0.43	0.73	0.62	14.52
STA9	126	9.3	SK-3	2.50-3.20	0.3	0.37	0.65	0.67	14.31
STA10	526	7.6	SK-3	6.00-6.70	NA	NA	NA	NA	NA
STA11	245	7.6	SK-6	2.50-3.20	NA	NA	NA	NA	NA
STA12	405	10.4	SK-4	3.00-3.70	0.52	0.67	0.23	0.39	26.67

As it is seen in Table 5.7, maximum loading rate required to ensure pore water pressure equilibrium was calculated according to the axial strain value reached at peak strength. The consolidation tests on the samples were carried out under four different axial loads. Naturally, however, the peak strength observed during monotonic tests does not coincide with the stresses applied in consolidation tests. Therefore, during calculation of the maximum loading rate the strain is divided by t_f value observed at the nearest axial stress (P) to the corresponding peak strength of the specimen. As it is seen, the loading rates that should not be exceeded to provide pore water pressure equilibrium are quite high depending on the tendency of rapid consolidation observed for the samples recovered from Adapazarı. The loading rates used in monotonic tests of Adapazarı soils are 0.07 and 1.4%/min. Therefore, the applied rates are low enough to ensure pore water pressure equilibrium throughout the specimens during monotonic tests.

As listed in Table 5.8, total of 12 strain controlled monotonic triaxial tests were performed on samples recovered from Adapazarı. The primary intention in performing of the static tests is to evaluate the strength of the soils prior to cyclic loadings and to understand the correlation between the static and the cyclic strength behaviors. It was recognized that the specimens monotonically tested were at NC state considering the consolidation response of the samples. As it is seen in the table, all the specimens have an initial shear stress with various ratios of $\Delta\sigma_i/p'_i$. Since the boring locations are very close or adjacent to the existing buildings, the soil samples retrieved from those points inherently sustain a shear stress. It must be noted that the initial stress states arranged for monotonic tests do not perfectly match with those used in cyclic tests of Adapazarı soils. Nevertheless, there are cyclic tests conducted on the specimens having isotropic initial stress states as well. In order to identify a possible correlation between monotonic and cyclic behavior of the samples, the monotonic and cyclic tests having the most similar initial stress states are taken into consideration.

The initial stress conditions of the specimens were arranged as to provide in-situ stress states that may exist under or near structures. Prior to

testing, the specimens were first subjected to certain confining pressures (σ'_{3c}), and then the axial stress was increased incrementally by allowing drainage of the specimen until a particular stress state was reached. Variation of the axial stress applied at this stage imposed an initial sustained deviator stress ($\Delta\sigma_i$). Accordingly, the stress ratio ($\Delta\sigma_i/p'_i$) sustained initially ranges between 0.2 and 1.5. Here, $\Delta\sigma_i$ is the initial deviator stress and p'_i is the initial mean effective stress.

Table 5.8 Initial states and loading rates of monotonic tests conducted on soils of Adapazarı.

Test	σ'_{1c} (kPa)	σ'_{3c} (kPa)	Initial p'_i (kPa)	Rate of ε_a (%/min)	OCR	$\Delta\sigma_i/p'_i$
STA1	100	30	53.33	0.07	1	1.31
STA2	100	30	53.33	1.4	1	1.31
STA3	45	30	35.00	1.4	1	0.43
STA4	90	60	70.00	1.4	1	0.43
STA5	120	80	93.33	1.4	1	0.43
STA6	75	60	65.00	1.4	1	0.23
STA7	60	45	50.00	1.4	1	0.30
STA8	150	60	90.00	1.4	1	1.00
STA9	80	40	53.33	1.4	1	0.75
STA10	170	80	110.00	1.4	1	0.82
STA11	110	30	56.67	1.4	1	1.41
STA12	115	30	58.33	1.4	1	1.46

5.7 Cyclic Triaxial Tests on Adapazari Soils

A total of 17 load controlled cyclic tests were conducted over Adapazari soils which were isotropically and anisotropically consolidated under stresses close to states they sustain in-situ. The initial stress states reached during the tests provide the specimens to remain in NC state. Due to the CSR_{tx} values ranging between 0.30 and 0.60, different cyclic stress amplitudes were applied during the tests. The cyclic tests with Adapazari soils were performed under a frequency of 0.5 Hz, which is considered as representative of the typical frequency range for earthquake loading. The CSR_{tx} values, stress states just before cyclic phase, void

ratios and the ratios of water content (w_c) to LL at the beginning of cyclic shearing are given in Table 5.9.

Table 5.9 Initial conditions of Adapazarı soil samples subjected to cyclic triaxial tests

Test	SAMPLE		USCS	σ'_{1c} (kPa)	σ'_{3c} (kPa)	τ_s/p'_i	CSR_{tx} ($\Delta\sigma_{cyc}/2p'_i$)	e_i	w_c/LL
	BORING NO	DEPTH (m)							
CYCA1	SK-4	3.00-3.70	CL	84	30	0.56	0.5	0.80	0.87
CYCA2	SK-6	2.50-3.20	SM	75	30	0.50	0.6	0.59	NP
CYCA3	SK-6	2.50-3.20	SM	30	30	0.00	0.3	0.66	NP
CYCA4	SK-1	6.00-6.70	CL	70	70	0.00	0.43	1.06	1.08
CYCA5	SK-2	5.50-6.20	ML	60	60	0.00	0.5	0.80	1.01
CYCA6	SK-2	4.00-4.70	ML	45	45	0.00	0.4	1.03	1.25
CYCA7	SK-2	4.00-4.70	ML	65	40	0.26	0.55	1.02	1.24
CYCA8	SK-2	1.50-2.20	ML	30	30	0.00	0.5	0.93	1.14
CYCA9	SK-2	5.50-6.20	ML	140	60	0.46	0.6	0.83	1.06
CYCA10	SK-3	2.50-3.20	ML	40	40	0.00	0.4	0.88	1.07
CYCA11	SK-2	5.50-6.20	ML	110	60	0.33	0.52	0.84	1.07
CYCA12	SK-2	1.50-2.20	ML	75	30	0.50	0.38	0.91	1.10
CYCA13	SK-3	2.50-3.20	ML	55	30	0.33	0.6	0.85	1.04
CYCA14	SK-3	6.00-6.70	SM	80	80	0.00	0.52	0.64	NP
CYCA15	SK-3	4.00-4.70	SM	60	60	0.00	0.5	0.82	1.10
CYCA16	SK-3	6.00-6.70	SM	140	80	0.30	0.5	0.63	NP
CYCA17	SK-3	4.00-4.70	SM	135	60	0.44	0.5	0.81	1.10

In order to investigate the influence of initial stress state on cyclic response of Adapazarı soils, the tests were performed with the specimens having various initial shear stress ratios (τ_s/p'_i). As indicated in Table 5.9, the initial shear stress ratio sustained by the specimens is ranging between 0 and 0.56. It should be noted that $\tau_s/p'_i=0$ condition refers to the isotropic state. The testing procedure implemented before cyclic phase is exactly the same with that used for the reconstituted silt specimens. The sustained initial shear stress was provided by application of axial deviatoric stress ($\Delta\sigma$) after consolidation under confining pressure (σ'_{3c}) only. Then, consolidation was continued under major axial stress ($\sigma'_{1c}=\sigma'_{3c}+\Delta\sigma$) and σ'_3 for 5 or 6 hours. All the specimens were consolidated 24 hours under isotropic conditions although a few hours

were generally sufficient for the consolidation of low plastic soils to be completed. Therefore, the time left for second consolidation phase after loading to obtain an initial shear stress was limited within a few hours.

In Table 5.9, the void ratio following the initial consolidation phase is denoted by e_i. The values of e_i range between 0.59 and 1.06, and accordingly the ratio of w_c/LL is ranging between 0.87 and 1.25. These w_c/LL ratios are relatively high in comparison with those of the reconstituted silt specimens tested in this study. In the table, the non-plastic (NP) samples (i.e., the samples for which the liquid limit values cannot be determined), the ratios of w_c/LL is indicated by "NP".

Table 5.10 Number of cycles (N) and excess pore pressure ratios reached at the axial strains of 3%, 5%, and 10% during cyclic tests

	Number of Cycles (N)			**Excess Pore Pressure Ratio, r_u**					
Test	**3% Ax.St.**	**5% Ax.St.**	**10% Ax.St.**	**3% Ax.St.**	**5% Ax.St.**	**10% Ax.St.**	**Max. Ax.St. (%)**	**N at Max. Ax.St.**	**r_u at Max. Ax.St.**
CYCA1*	15	31	105	0.28	0.3	0.32	18	292	0.36
CYCA2*	38	110		0.32	0.57		6	141	0.63
CYCA3							0.09	28	0.36
CYCA4							2.7	36	0.65
CYCA5			15			1.17	12	41	1.22
CYCA6							0.17	29	0.24
CYCA7*	204	443	609	0.86	0.94	1	10.7	616	1.02
CYCA8							0.3	126	0.41
CYCA9*	5	17	51	0.47	0.6	0.81	37	61	0.9
CYCA10							1.2	125	0.54
CYCA11	1	2	4	0.41	0.56	0.66	19	37	0.72
CYCA12*							2.8	291	0.36
CYCA13*	27	76		0.72	0.78		5.7	262	0.79
CYCA14	1	2	4	0.1	0.66	0.88	15	30	1.2
CYCA15	3	9	36	0.27	0.5	0.88	12	93	1.05
CYCA16	1	4	11	0.08	0.64	0.86	13	27	0.93
CYCA17*	18	40	124	0.67	0.76	0.82	34	214	0.85

*Number of cycles was calculated based on SA axial strains

Corresponding number of cycles (N) needed to reach the axial strains of 3%, 5% and 10% in each test are displayed in Table 5.10. In the case of stress reversal, double amplitude (DA) axial strains; and for non reversal

stress conditions, single amplitude (SA) axial strains were taken into consideration to calculate N.

As it is already observed for the reconstituted silt, cyclic response is again observed to depend on whether the specimens are subjected to stress reversal or not during cyclic loading. In the case of none or slight stress reversals, plastic strains accumulate with almost a constant rate for each cycle. As it can be seen in Figure 5.11, the plastic strain accumulation rate tends to decrease after having reached the point where the peak cyclic stress becomes lower than the monotonic strength for the tests with comparatively low pore water pressure accumulation. It is clearly seen in Figure 5.11 that greater the ratio of the applied peak cyclic stress to the monotonic strength, greater the strain accumulation rate in those tests. However, for the tests where r_u reaches 0.80 and beyond, the strain accumulation rate tends to decrease where the peak cyclic stress falls below the monotonic response, after a while strain accumulation starts to increase again with the r_u exceeding 0.80 (Figure 5.12). Interestingly, in one of the tests where the stress-strain response was dominated on the compression side a sudden increase is observed in the strain accumulation rate after an r_u value of around 0.80 is reached (Figure 5.13). This is the only test result which can be interpreted as flow liquefaction in the entire study. It must be noted that the sample showing such behavior of flow liquefaction is classified as ML according to USCS, whereas no flow liquefaction behavior was observed for the SM samples recovered from Adapazarı within the study.

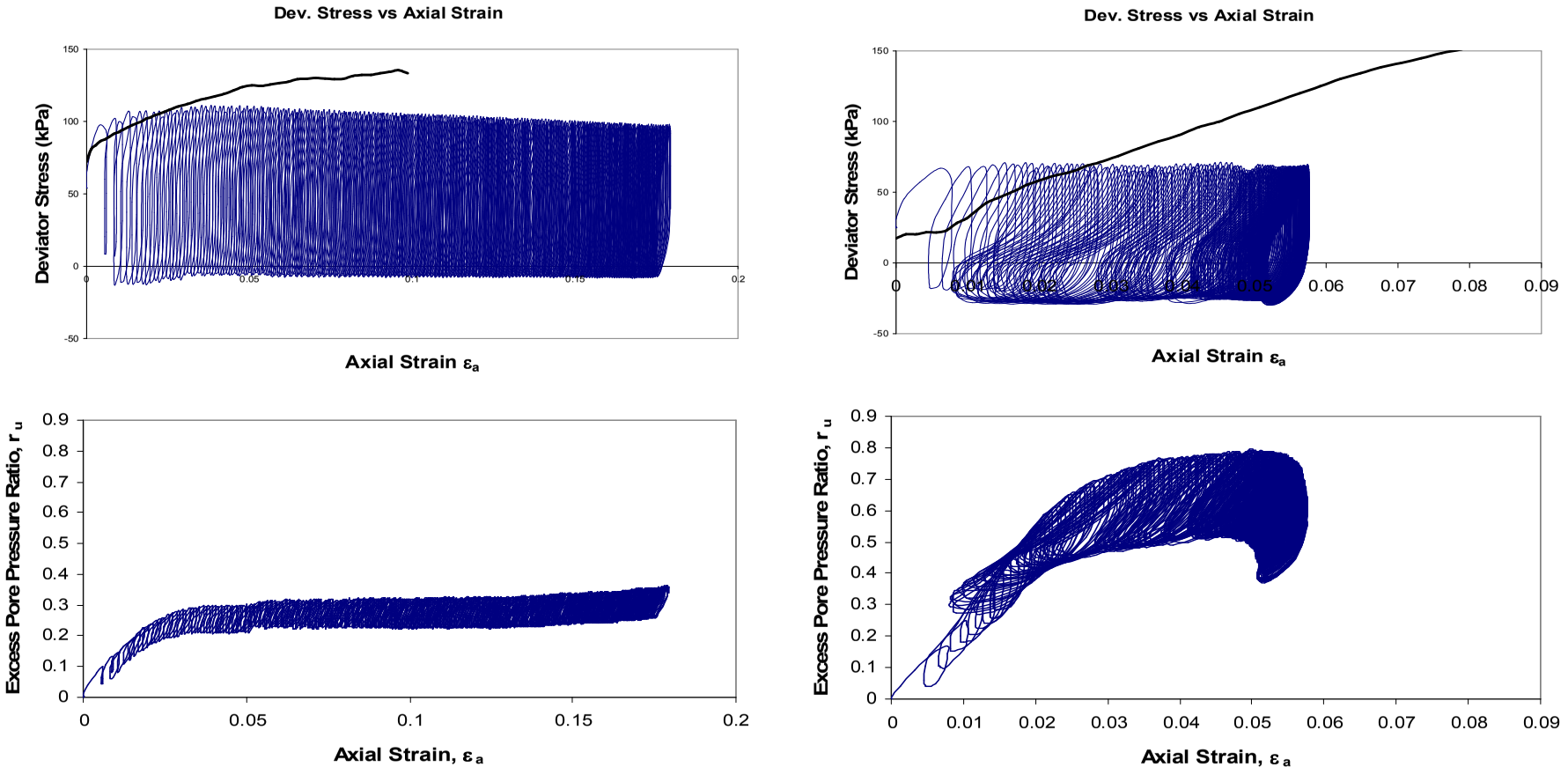

Figure 5.11 Stress-strain behavior and excess pore water pressure accumulation for the samples subjected to τ_s/p'_i values of (a) 0.56 (CYCA1) and (b) 0.33 (CYCA13).

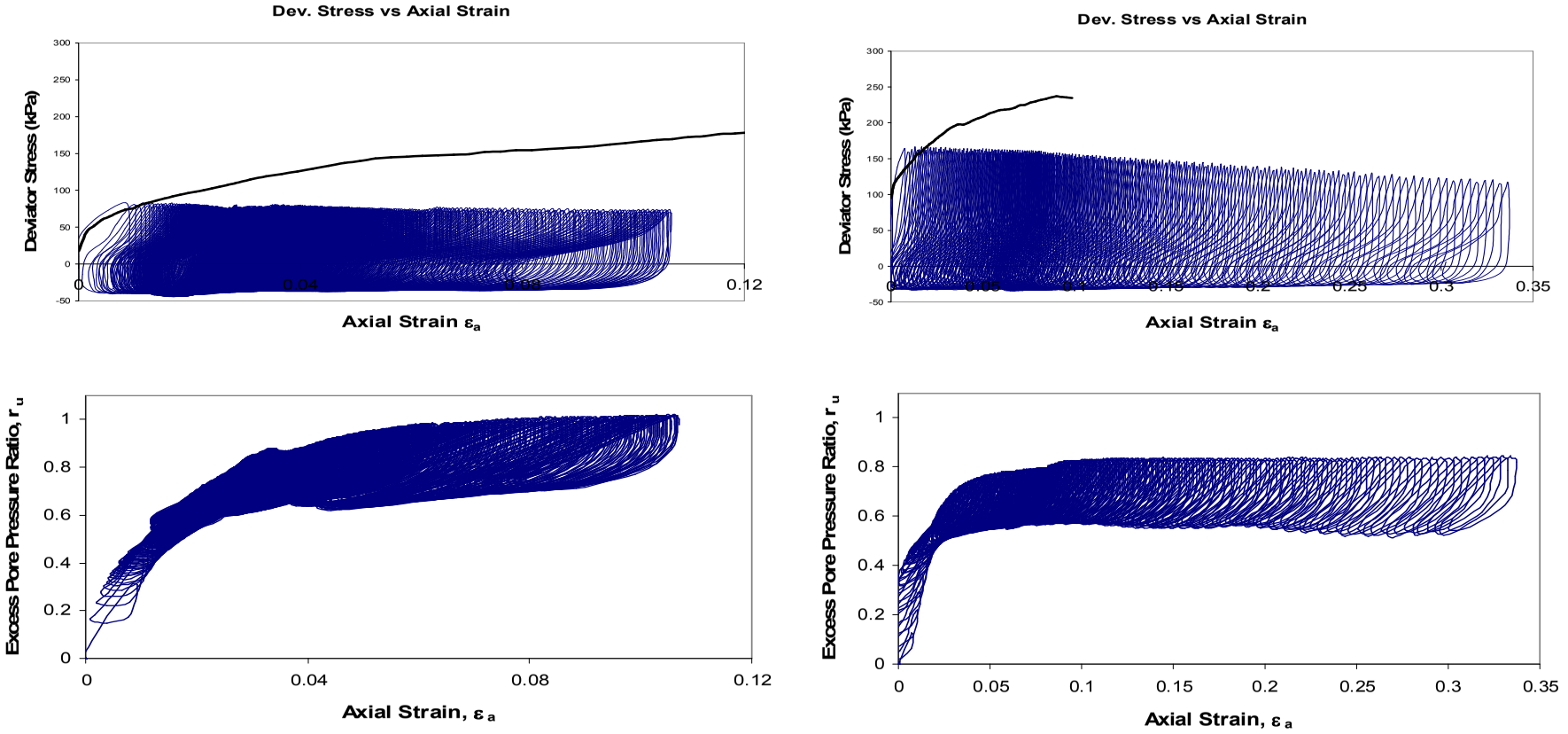

(a) (b)

Figure 5.12 Stress-strain behavior and excess pore water pressure accumulation for the tests (a) CYCA7 and (b) CYCA17

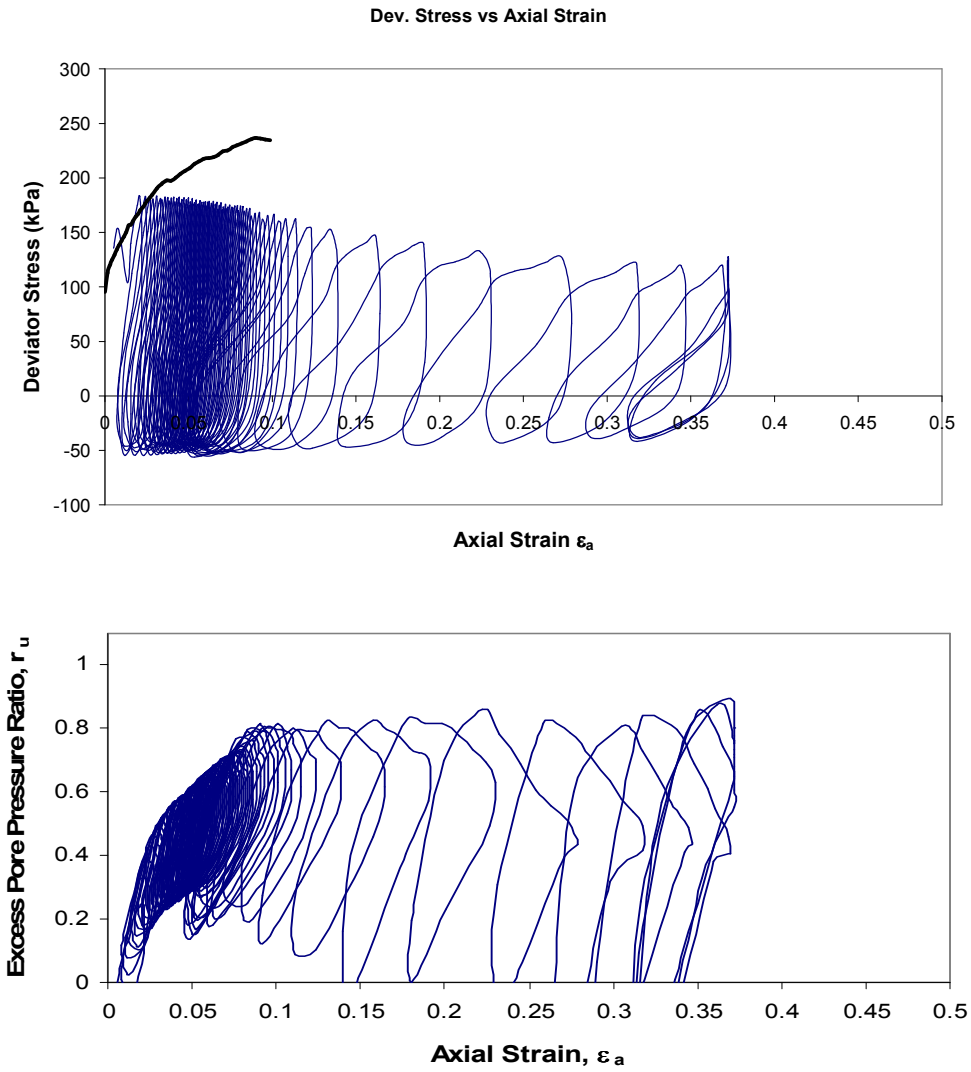

Figure 5.13 Flow liquefaction observed during the test CYCA9

Eight tests were conducted with isotropically consolidated specimens. In these tests, the incremental strains developing in each additional cycle are added to the maximum past strain in compression and extension respectively. The CSR_{tx} range used in the tests did not cause significant strains as reported in Table 5.10. The DA axial strain exceeded 12% in only 3 of the tests performed with isotropically consolidated specimens. In 3 of the remaining 5 tests, the DA axial strain remained even below 1%. In the other two tests, it was 2.7% and 1.2%. As indicated in Tables 5.9 and 5.10, CSR_{tx} values are 0.50, 0.52 and 0.50, respectively, for the tests CYCA5, CYCA14 and CYCA15 in which the DA axial strains exceeded 12%. The stress-strain behavior observed during the tests CYCA5 and

CYCA15 are given in Figure 5.14. The maximum r_u values attained during the tests are in excess of 1.0. The samples used in these tests are classified respectively as ML, SM and SM. This confirms once again that as the grain size increase towards sand size, tendency of excess pore pressure generation and straining increases in the cyclic loading. Nevertheless, there no sudden increase in strain observed during these tests. The excess pore water pressure gradually increases and even exceeds the initial confining stress. Nevertheless, the dilative tendency of such soils prevents excessive loss of strength.

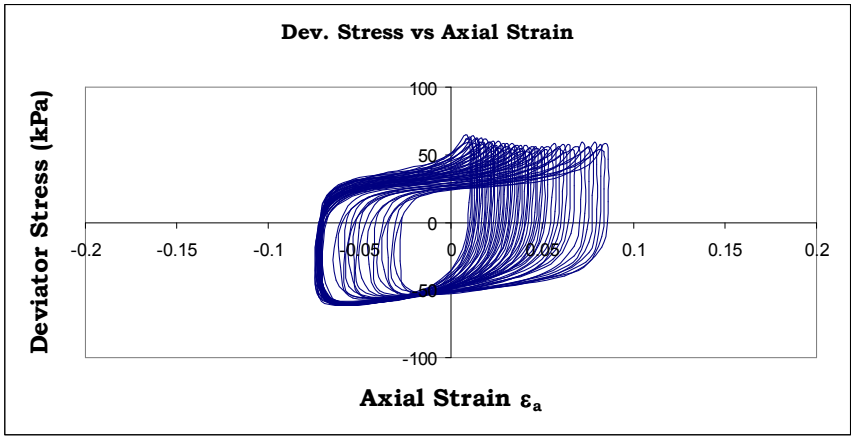

(a)

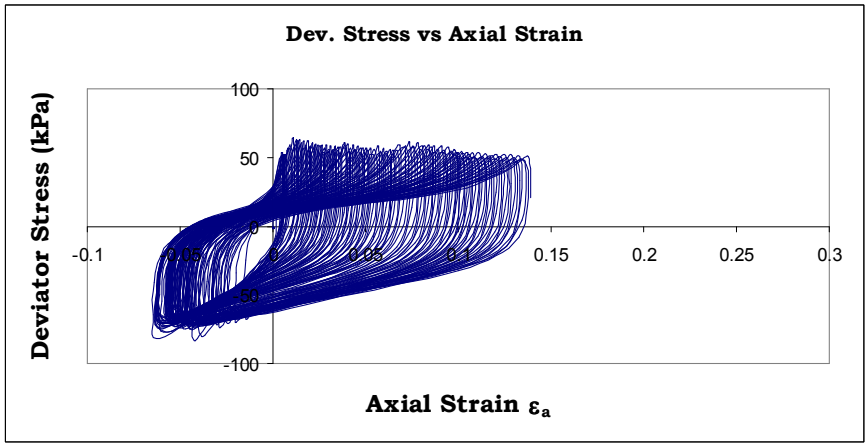

(b)

Figure 5.14 Cyclic stress-strain behavior of isotropically consolidated Adapazarı samples used in the tests of (a) CYCA5 and (b) CYCA15

5.8 Pore Water Pressure Dependent Cyclic Response

As indicated previously, the maximum excess pore pressure (total excess pore water pressure) generated during cyclic tests is to be taken into consideration in evaluation of the pore water pressure response of Adapazarı soils as well. In the tests of reconstituted silt specimens there were a few tests where the maximum DA strains remained at 0.5% and the corresponding r_u values for these tests were around 0.1. This observation was attributed to the strains that are lower than the threshold strain beyond which excess pore water pressure begins to generate (Matasovic and Vucetic, 1995). On the other hand, in the tests conducted with Adapazarı soils, although the DA strains were lower than 0.5%, r_u values exceeded 0.25 (Figure 5.15). This could be attributed to the differences between threshold strains of different soil samples.

The excess pore water pressure generation during cyclic loading is to be examined considering the relationship between total excess pore water pressure and axial strain development. An example of that relationship for one way loading and two way loading is illustrated in Figure 5.16. As it is seen, the logarithmic change of total excess pore water pressure increases gradually with increasing axial strain up to a point beyond which the excess pore water pressure slows down and reaches a constant residual value while the axial strain proceeds to accumulate. Here, this point where the pore water pressure starts to slow down is termed as flexure point as previously stated in chapter 4, while the point where the pore pressure increase remains at negligible levels and r_u reaches a residual value is termed as residual point (Figure 5.17).

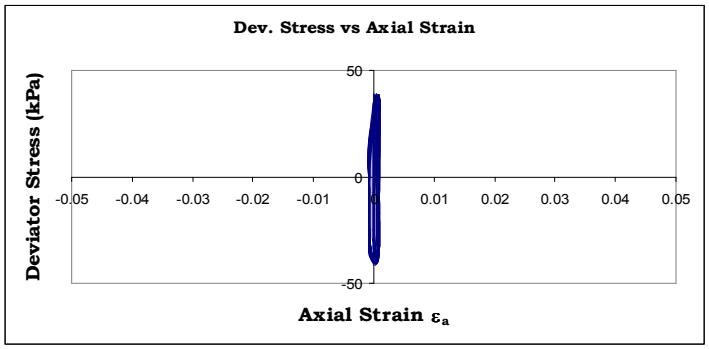

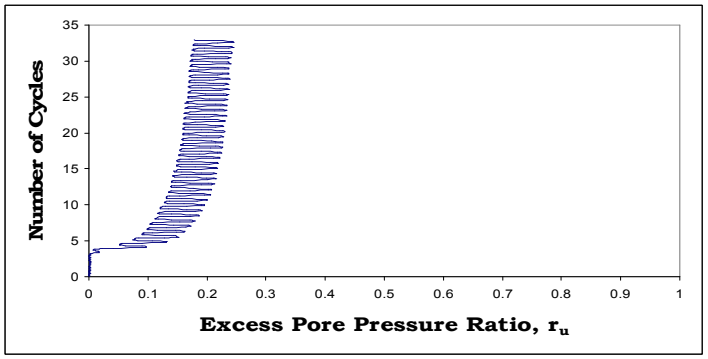

(a)

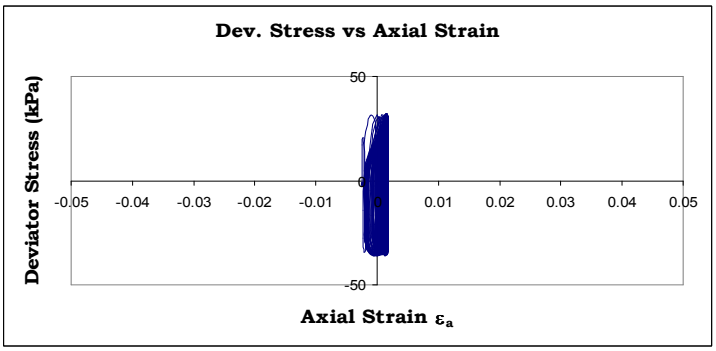

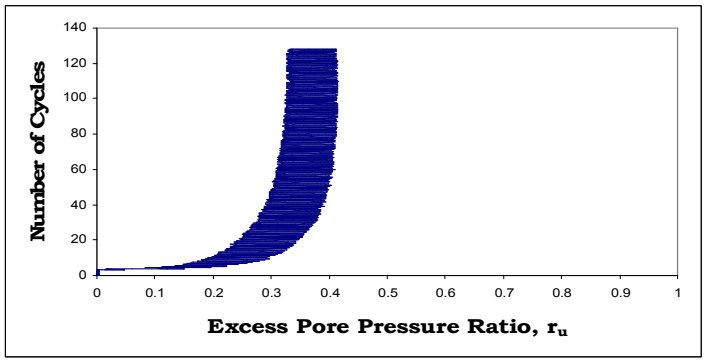

(b)

Figure 5.15 Axial strain and excess pore pressure ratio development with number of cycles in the tests of (a) CYCA6 and (b) CYCA8

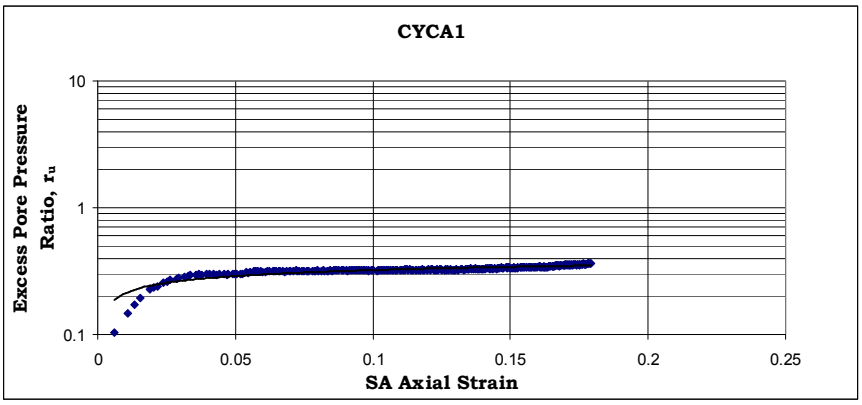

(a)

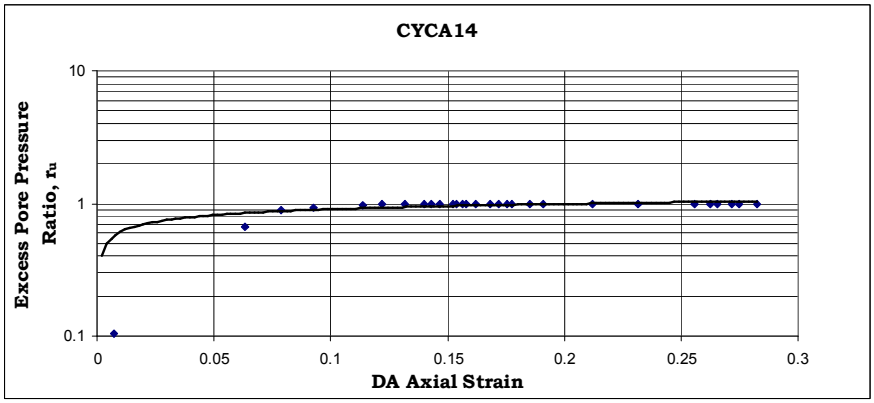

(b)

Figure 5.16 Relationship between r_u and ε_a for the tests of (a) one way and (b) two way loading

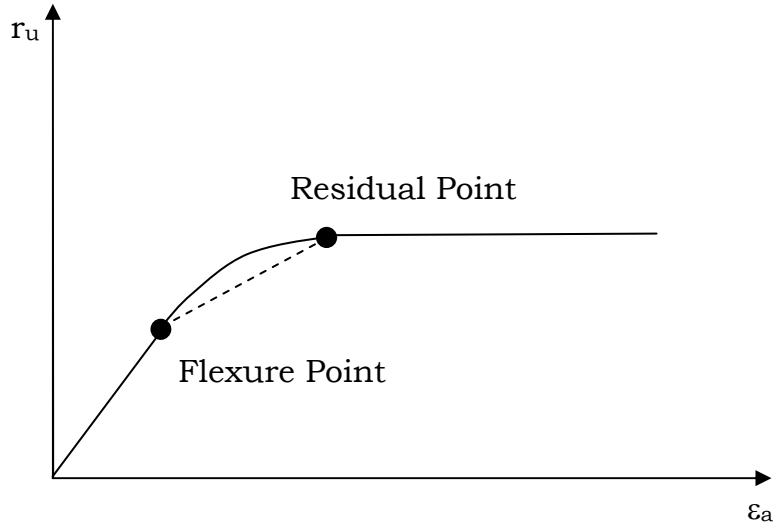

Figure 5.17 The illustration of characteristic points on the curve representing the relationship between r_u and ε_a

The r_u and ε_a values developed at flexure and residual points of each test are given in Table 5.11. The ε_a value is determined as SA or DA axial strain corresponding to the loading pattern (one way or two way loading) used in the test. As it is seen in Table 5.11, there is no flexure point observed for majority of the tests conducted with no initial shear stress. Those are the tests in which DA axial strain and r_u remained significantly low, without a conceivable relationship between r_u and ε_a. Also, a flexure point is not observed. Additionally, the number of cycles (N) reached at those characteristic points are given in Table 5.11. In some tests the trendlines do not match with the real response for the first cycles. Since the flexure point is determined according to the fitted trendline, N at the flexure point is presumed as the one needed to reach the same amount of r_u over the real curve. N required to reach at such characteristic points seems to depend on whether the cyclic response is dominated at compression or extension side. The cyclic response is dependent on the initial static shear stress (τ_s) and the amplitude of cyclic load ($\Delta\sigma_{cyc}$). The relationship between total initial shear stress ratio ($(\tau_s+\tau_{cyc})/p'_i$) and number of cycles ratio ($N_{residual}/N_{flexure}$) is given in Figure 5.18. It can be inferred from the Figure that the ratio $N_{residual}/N_{flexure}$ increases with increasing $(\tau_s+\tau_{cyc})/p'_i$. It must be also noted that the maximum N applied in the tests is fairly sufficient to observe residual excess pore water pressure after the residual point.

The influence of CSR_{tx} on pore pressure generation is also examined in Figure 5.19. As it can be observed, r_u at flexure point increases with increasing CSR_{tx}, whereas the one at residual point interestingly decreases with increasing CSR_{tx}. A possible reason could be the increasing loading rate with increasing CSR_{tx} which results in an uneven pore water pressure distribution throughout the specimen, especially at the early cycles where flexure points plot very near. Since the excess pore water pressure tends to be equalized after a certain number of cycles, the tendency observed for r_u at flexure point and CSR_{tx} becomes reversed for r_u at residual point and CSR_{tx}.

Table 5.11 The r_u and ε_a values observed at flexure and residual points for the cyclic tests of Adapazarı soils

	At flexure point		At residual point		Number of Cycles at Flexure Point	Number of Cycles at Residual Point	Max. Number of Cycles	$(\tau_s+\tau_{cyc})/p'_i$	$r_{u\text{-residual}}/r_{u\text{-flexure}}$	$N_{residual}/N_{flexure}$
Test No	**r_u (%)**	**ε_a (%)**	**r_u (%)**	**ε_a (%)**						
CYCA1*	19	0.6	30.0	3.8	4	26	291	1.06	1.58	6.50
CYCA2*	50	3.8	60.0	5.2	92	158	191	1.10	1.20	1.72
CYCA3	No flexure	No flexure	No flexure	No flexure	No flexure	No flexure	28	0.30	No flexure	No flexure
CYCA4	22.7	0.1	50.0	1.0	2	3	36	0.50	2.20	1.50
CYCA5	39	0.1	100.0	1.6	5	12	81	0.54	2.85	2.40
CYCA6	No flexure	No flexure	No flexure	No flexure	No flexure	No flexure	29	0.40	No flexure	No flexure
CYCA7*	41	0.2	92.0	4.6	5	553	615	0.81	2.24	110.60
CYCA8	No flexure	No flexure	No flexure	No flexure	No flexure	No flexure	126	0.50	No flexure	No flexure
CYCA9*	40	1.5	79.0	9.0	3	49	60	1.06	1.98	16.33
CYCA10	No flexure	No flexure	No flexure	No flexure	No flexure	No flexure	125	0.40	No flexure	No flexure
CYCA11	28	0.1	66.0	11.4	4	10	41	0.90	2.36	2.50
CYCA12*	25	1.4	36.0	2.3	15	220	291	0.88	1.44	14.67
CYCA13*	45	1.4	73.0	3.2	5	40	107	0.93	1.62	8
CYCA14	37	0.2	100.0	12.2	4	8	31	0.52	2.73	2.00
CYCA15	43	1	96.0	11.6	9	65	97	0.50	2.23	7.22
CYCA16	35	0.2	84.0	7.3	5	19	31	0.86	2.40	3.80
CYCA17*	32	0.1	76.0	4.5	6	105	214	0.99	2.38	17.5

*Number of cycles was calculated based on SA axial strains

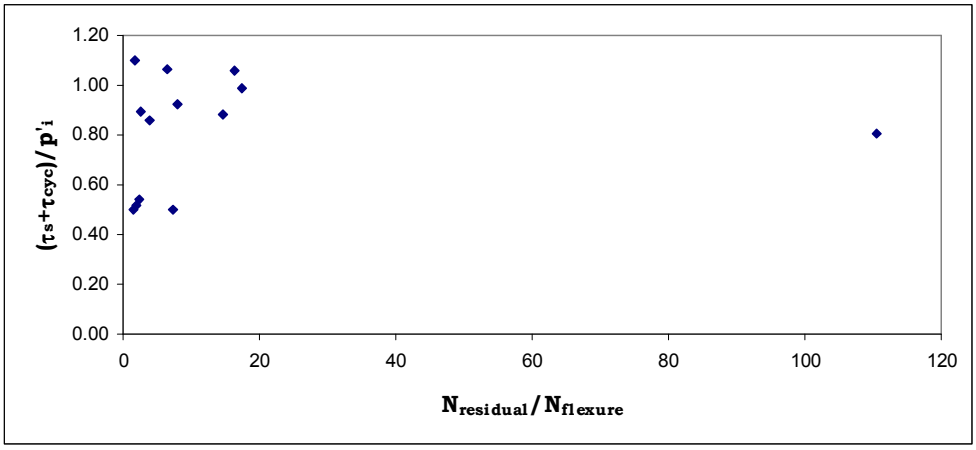

Figure 5.18 The relationship between total initial shear stress ratio ($(\tau_s+\tau_{cyc})/p'_i$) and number of cycles ratio ($N_{residual}/N_{flexure}$)

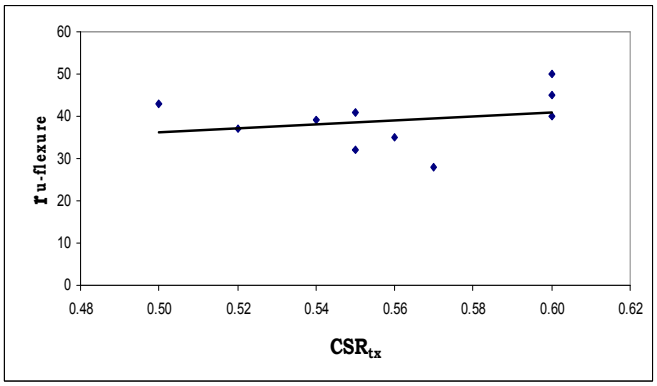

(a)

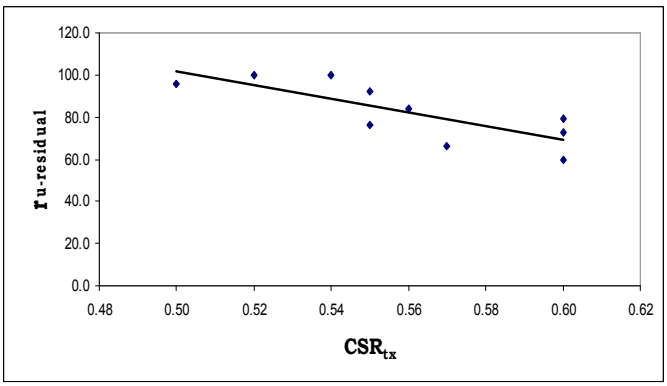

(b)

Figure 5.19 The relationship between r_u and CSR_{tx} for (a) flexure and (b) residual points

As indicated in Table 5.11, the excess pore water pressure ratio increases rapidly within initial axial strain levels mostly up to about 0.1-1% DA for the tests with stress reversals, and 0.1-3% SA for the tests without stress reversals. These values are relatively less those observed for the tests conducted with reconstituted specimens. After such axial strain levels are reached, the gradient of the curve representing begins to decrease within the interval between flexure and residual points as seen in Figure 5.17. Although r_u is observed to be generally between 0.30-0.50 at the flexure point, there are 3 tests in which r_u is around 0.20. Although these values are less than those observed in the tests conducted over reconstituted silt specimens, the residual state value of r_u ranging between 0.60 and 1.00 is generally higher than those observed for the reconstituted silt specimens. The range of r_u at flexure points is well below those generally accepted as a criterion for initiation of liquefaction in the literature. As mentioned in the Chapter on literature review, the initiation of liquefaction is defined as the state where excess pore water pressure ratio reaches 1.00 for sands, whereas the value of r_u between 0.70 to 0.90 is generally accepted as a maximum for failure for the fine grained soils. Although the r_u values observed in this study at flexure points remain well below this range, those observed at residual points are observed to be consistent within the specified range for liquefaction initiation.

In Chapter 4, the data acquired during the cyclic tests carried out with reconstituted silt are used to construct models to estimate r_u as a function of the applied CSR_{tx} and N. Different models were introduced for different stress states and loading frequencies. As the soils samples recovered from Adapazarı were tested in NC state and under a frequency of 0.5 Hz, the models introduced for NC soils having τ_s/p'_i of 0 (isotropically consolidated), 0.35 and 0.60 are used to see how compatible these models are for Adapazarı soils. The models and r_u values observed at relevant cycles in the tests conducted with Adapazarı soils are given in Figure 5.20.

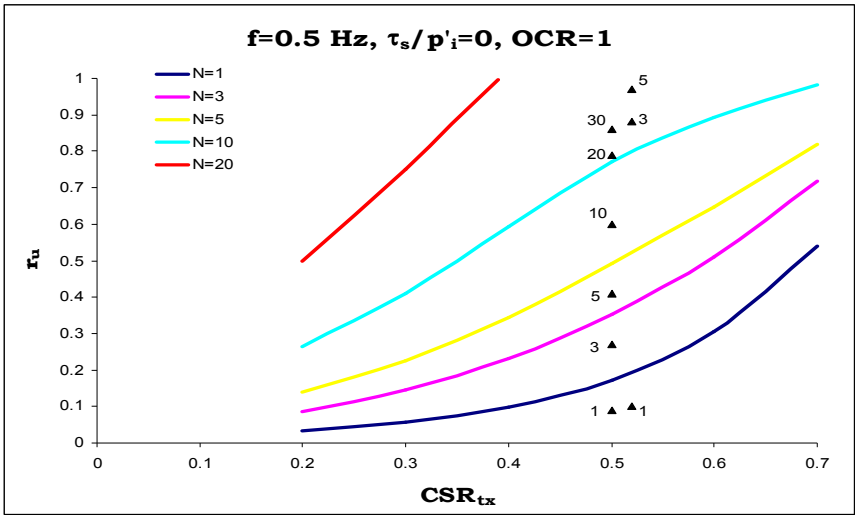

(a)

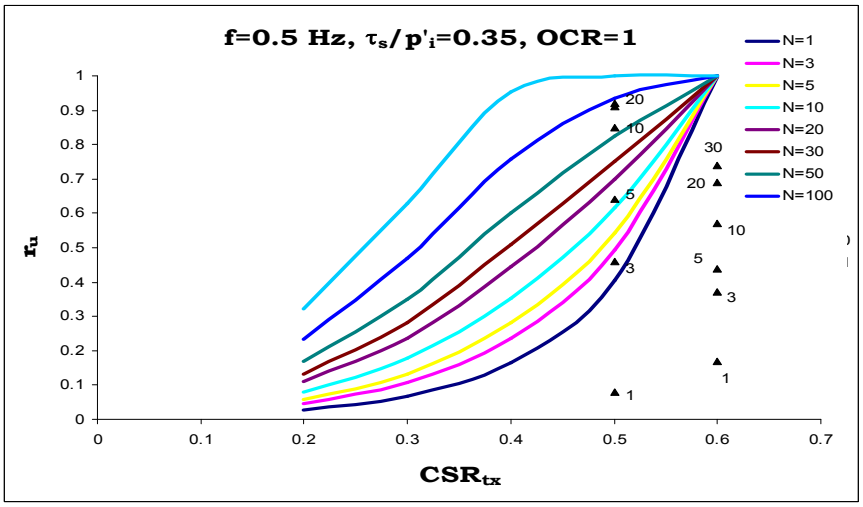

(b)

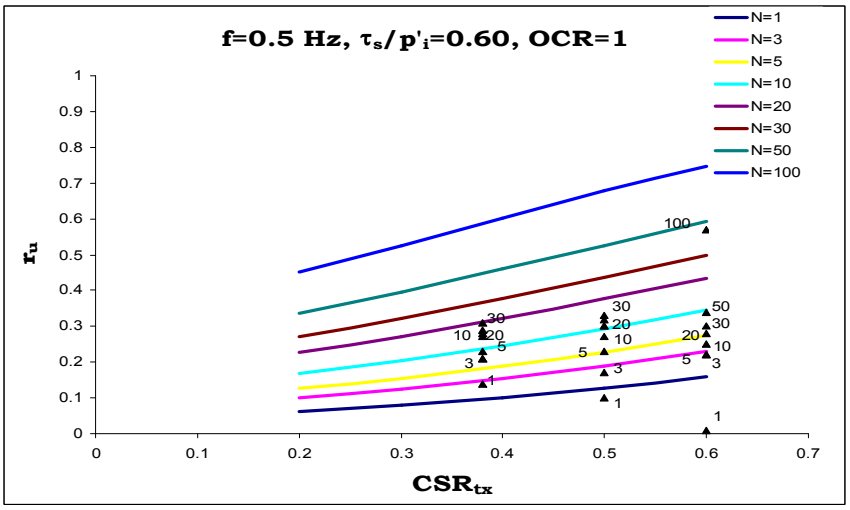

(c)

Figure 5.20 Observed r_u values at corresponding cycles of Adapazarı tests on the models introduced for reconstituted silt having τ_s/p'_i of (a) 0, (b) 0.35 and (c) 0.60

It is observed in Figure 5.20a. that although the pore pressure response of CYCA15 can be approximated quite well by the model, the pore pressure response of CYCA14 is not consistent with the model prediction. None of the tested samples of Adapazarı have τ_s/p'_i of 0.35 or 0.60. Therefore, the tests conducted on the samples having τ_s/p'_i values around 0.35 and 0.60 were taken into consideration during comparison. The results of the tests CYCA13 and CYCA16 which were carried out with samples having τ_s/p'_i of 0.33 and 0.30 are given on the chart in Figure 5.20b. Although the pore pressure response of CYCA16 can be closely predicted, the pore pressure response of CYCA13 is totally out of the estimation range introduced by the model. The results of the tests CYCA1, CYCA2 and CYCA12 which were carried out with samples having τ_s/p'_i of 0.56, 0.50 and 0.50 are given on the chart in Figure 5.20c. As it is seen, the model prediction and the observed values are fairly compatible with each other. Accordingly, as a conclusion, the models do not closely estimate all the results observed during the tests conducted with Adapazarı soils.

Nevertheless, it must be remembered that the models were constructed on the data acquired from the slurry deposited silt samples having initial void ratios (e_i) ranging between 0.68 and 0.77. On the other hand, the samples retrieved from Adapazarı consisted of river deposited alluvia with e_i values ranging between 0.59 and 1.06. Hence, the inconsistencies between the model predictions and the test results Adapazarı soils can be attributed to the differences in soil fabrics of slurry deposited silt and alluvial soils of Adapazarı.

The soil fabric, which basically depends on the nature of deposition is an important aspect in cyclic response of soils. The void ratio (e), and consequently the water sustaining capability of the soil directly depends on the fabric. It has been reported that the liquefaction susceptibility highly depends on the initial void ratio (e_i) and accordingly w_c/LL ratio. In addition, it has been widely accepted that irrespective of liquefaction occurrence, saturated soils undergo cyclically accumulated strains due to the degradation effect induced by increasing pore water pressure.

Although in some of the tests strains exceeded 10% with no significant pore water pressure generation, it can be stated in general that the soil samples recovered from Adapazarı exhibit a greater tendency of pore water generation and subsequent strain accumulation when compared with the reconstituted silt specimens which have relatively less initial w_c/LL ratios. Nonetheless, straining capability of the reconstituted specimens were relatively higher, although the pore water pressure generation trend was not as prevalent as that observed in Adapazarı samples.

5.9 Effect of Initial Characteristics and Applied Stress on the Relationship between r_u and ε_a of Adapazarı Soils

Yılmaz et al. (2004) suggested a method to calculate the plastic strain accumulation due to cyclic loading. The method is based on the equation given by Hyde and Brown (1976), which utilizes the similarity in the behavior of clay under repeated loading compared with that under creep loading. The equation associates logarithm the of strain rate (ln(έ)) with the applied stress (σ) and logarithm of time (ln(t)) as follows:

$$\ln(\acute{\varepsilon})=A+B\sigma+C\ln(t) \qquad (5.1)$$

Hence, the accumulated strains can be estimated through numerical integration for a given load history of repeated loading once the coefficients of A, B and C are known. In that study, neglecting the explicit dependency on time, equation 5.1 was modified for the load-histories (σ(t)) that exert stresses beyond shear strength in the following form:

$$\ln(\acute{\varepsilon})=\alpha+\beta.\sigma(t) \qquad (5.2)$$

The parameters α and β were reported to be dependent on the specimen mechanical properties associated with deformation response and the

characteristics of the imposed load. Accordingly, it was stated that the strain rates calculated by equation 5.2 shows an increasing trend with increasing plasticity index and a decreasing trend with increasing water content, which is proportionally related to void ratio in the case of saturated soils. However, the proposed equation does not explicitly take the pore pressure accumulation into account in calculation of strain rate despite the fact that the saturated soils undergo cyclically accumulated strains which are induced by the degradation effect of increasing pore water pressure.

In this study, the relationship between r_u and ε_a has been introduced for both reconstituted silt and the soils recovered from Adapazarı. It is aimed to understand the mechanism leading to the development of pore water pressure and strain in saturated fine soils. The effects of τ_s/p'_i, OCR, loading rate and CSR_{tx} on excess pore pressure development were explained within the models that were introduced as depending on the data acquired from the tests carried out with reconstituted silt specimens. Depending on the reconstitution technique used during silt deposition, initial void ratio of the specimens had a range between 0.68 and 0.77. Due to this limited range, the effect of e_i on the development of excess pore water pressure and strain accumulation could not be reflected in the proposed models. Additionally, the limitation on range makes the reconstituted silt become a boundary material regarding susceptibility to liquefaction based on the susceptibility criteria discussed in chapter 4. Therefore, here, the tests conducted with Adapazarı soils are used to reflect the effect of e_i as well as those of τ_s/p'_i and CSR_{tx} on the cyclic response of saturated fine soils.

The relationship between r_u and ε_a observed for Adapazarı soil samples is given in Figure 5.16. The points representing the relationship are best fitted with logarithmic regression. R^2 for the regression of that relationship has values between 0.60 and 0.96 with an average of around 0.85. The general form of these curves is given with equation 5.3. The coefficients a and b for the corresponding tests in which the relationship between r_u and ε_a has an apparent trend are given in Table 5.12.

$$r_u = a \ln(\varepsilon_a) + b \qquad (5.3)$$

Table 5.12 The characteristic coefficients a and b for r_u-ε_a relationship observed for Adapazarı soils

Test No	a	b
CYCA1	0.0478	0.432
CYCA2	0.1561	0.9412
CYCA5	0.2308	1.8484
CYCA7	0.1701	1.4258
CYCA9	0.1721	1.1217
CYCA11	0.0881	0.8726
CYCA12	0.1497	0.8915
CYCA13	0.2646	1.5839
CYCA14	0.1495	1.365
CYCA15	0.163	1.2537
CYCA16	0.1245	1.1096
CYCA17	0.1081	1.0472

There are 12 cyclic tests in which the r_u-ε_a relationship displays a trend like those observed for the reconstituted silt specimens. The coefficients of a and b are dependent on mechanical properties of the samples and applied CSR_{tx}. The mechanical properties influencing cyclic response can be generalized as the initial stress state, initial void ratio and CSR_{tx}. Since all the cyclic tests of Adapazarı samples were performed with a loading frequency of 0.5 Hz, the influence of loading frequency could not be reflected on the cyclic behavior of these soils. All the samples recovered from Adapazarı are observed to be either NC or lightly OC. Therefore, the stress history of the samples are not taken into consideration, and initial stress state is expressed with only τ_s/p'_i. As the e_i of samples change in a wide range, the relationship of r_u-ε_a involves the influence due to e_i. Lastly, as the soils are obviously influenced by the magnitude of cyclic load, the effect of CSR_{tx} on the relationship of r_u-ε_a is also expected to be reflected. Thus, the effects of τ_s/p'_i, e_i and CSR_{tx} on the r_u-ε_a relationship are considered to be involved in equation 5.3.

The effect of mechanical properties of the samples and applied cyclic load on the relationship between r_u and ε_a are to be reflected within the coefficients a and b. Hence, the contribution (weight) of the influencing factors on each coefficient is expected to be determined. For the sake of ease in implementation, the factors are presumed to be linearly associated to the coefficients. Accordingly, the relationships between the coefficients (a and b) and the factors (τ_s/p'_i, e_i and CSR_{tx}) are defined as follows.

$$a = A.e_i + B.CSR_{tx} + C.(\tau_s / p'_i) \tag{5.4}$$

$$b = D.e_i + E.CSR_{tx} + F.(\tau_s / p'_i) \tag{5.5}$$

The coefficients A, B, C, D, E and F that represents the contribution of the factors would not have different values for different cyclic tests. There are 12 equations to determine the coefficients A, B, C (for a) and D, E, F (for b) separately. The three unknown parameters for each equation can be determined by solving the 3x3 system of equations in the following.

$$\begin{bmatrix} e_{i-k} & CSR_{tx-k} & \tau_s / p'_{i-k} \\ e_{i-l} & CSR_{tx-l} & \tau_s / p'_{i-l} \\ e_{i-m} & CSR_{tx-m} & \tau_s / p'_{i-m} \end{bmatrix} * \begin{bmatrix} A \\ B \\ C \end{bmatrix} = \begin{bmatrix} a_k \\ a_l \\ a_m \end{bmatrix} \tag{5.6}$$

$$\begin{bmatrix} e_{i-k} & CSR_{tx-k} & \tau_s / p'_{i-k} \\ e_{i-l} & CSR_{tx-l} & \tau_s / p'_{i-l} \\ e_{i-m} & CSR_{tx-m} & \tau_s / p'_{i-m} \end{bmatrix} * \begin{bmatrix} D \\ E \\ F \end{bmatrix} = \begin{bmatrix} b_k \\ b_l \\ b_m \end{bmatrix} \tag{5.7}$$

Since there exist 12 equations in accordance with the number of cyclic tests, the combinations of 3 equations out of 12 becomes 220. Hence, k, l, m in equations 5.6 and 5.7 indicate the number of equation identified with a number from 1 to 12. By solving those equation system combinations 220 solutions result for each coefficient (i.e. A, B, C, D, E, F). Since a single theoretical value is required for each coefficient, the

solutions are expected statistically to approach to an average to be used as the theoretical value.

Quality of the calculated values for each coefficient is examined through data scattering plot and histogram presented for the values of coefficient A, respectively in Figures 5.21 and 5.22 The plots and histograms for the rest of the coefficients are given in Appendix.

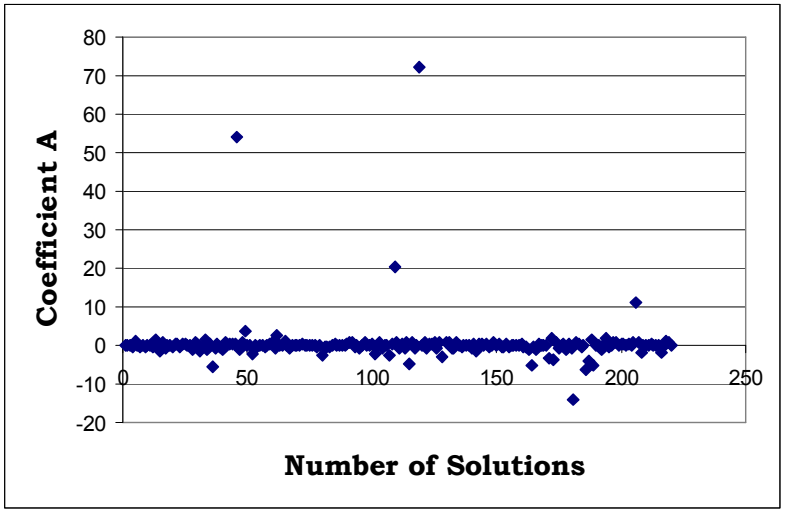

Figure 5.21 Data scattering plot for the values of coefficient A

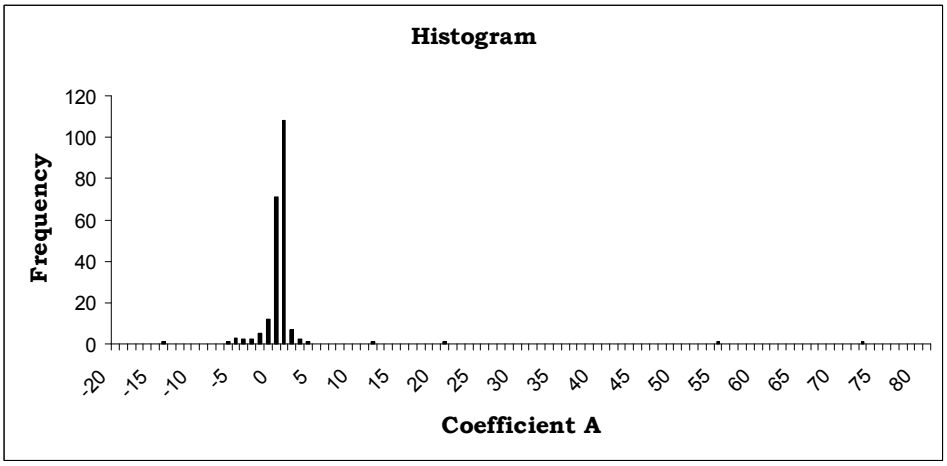

Figure 5.22 Histogram of coefficient A

The values obtained for the coefficients scatter in a wide range as observed in the figures 5.21 and 5.22. The outlying points are discarded and the rest of the data is used to calculate the average. Although, the outliers can be identified through a number of ways, inter-quartile range is the statistical parameter frequently used for this purpose. In descriptive statistics, quartile is one of three points that separate the data set into four equal parts. First quartile (Q_1) cuts off lowest 25% of data, second quartile (Q_2) cuts data set in half, and third quartile (Q3) cuts off highest 25% of data. Inter-quartile range is defined as the difference between the highest and the lowest quartiles (Q_3-Q_1). The outliers are defined as the values remaining outside of the range [Q_1-k*(Q_3-Q_1), Q_3+k*(Q_3-Q_1)] where k is a constant chosen depending on the data distribution. A value of 2 is found to be suitable for the constant k for the data set utilized. The quartiles, the range for identification of outliers and the average for data without outliers of the coefficients are given in Table 5.13. After discarding the outliers, the data scattering plot for coefficient A is shown in Figure 5.23. The plots for the other coefficients are given in Appendix.

Table 5.13 Statistical parameters calculated to determine average values of the coefficients

Statistical Parameters	**Coefficients**					
	A	**B**	**C**	**D**	**E**	**F**
Q_1	-0.28	-0.12	-0.37	-0.67	1.03	-2.55
Q_3	0.37	0.90	0.10	1.78	3.94	-0.52
Q_3-Q_1	0.65	1.02	0.46	2.45	2.90	2.02
k*(Q_3-Q_1)	1.30	2.05	0.93	4.90	5.81	4.05
Q_1-k*(Q_3-Q_1)	-1.57	-2.17	-1.29	-5.57	-4.77	-6.59
Q_3+k*(Q_3-Q_1)	1.67	2.95	1.02	6.68	9.74	3.52
Average	**0.009**	**0.397**	**-0.150**	**0.564**	**2.075**	**-1.433**

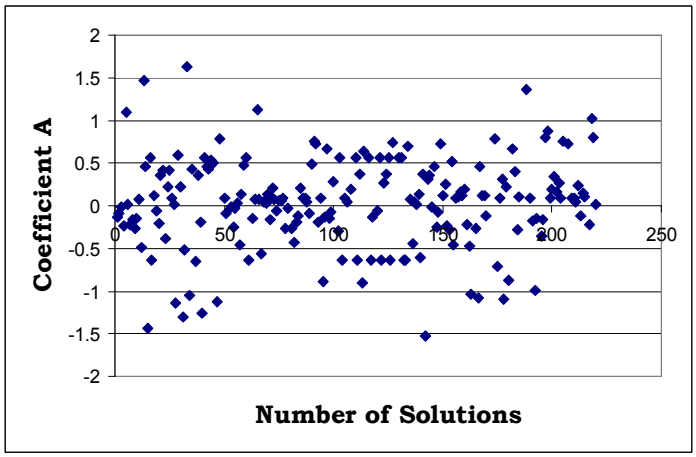

Figure 5.23 Data scattering plot for the values of coefficient A after discarding the outliers

The averages determined for the coefficients are rounded as to be 0 for A, 0.40 for B, -0.15 for C, 0.56 for D, 2.08 for E and -1.43 for F. After determining the values representing the weights of the factors, the characteristic coefficients a and b calculated to estimate the relationship between r_u and ε_a are given in Table 5.14.

Table 5.14 The characteristic coefficients a and b calculated for r_u-ε_a relationship of Adapazarı soils

Test No	a	b	$a_{estimated}$	$b_{estimated}$
CYCA1	0.0478	0.432	0.1156	0.6824
CYCA2	0.1561	0.9412	0.1650	0.8624
CYCA5	0.2308	1.8484	0.2000	1.4854
CYCA7	0.1701	1.4258	0.1812	1.3436
CYCA9	0.1721	1.1217	0.1708	1.0543
CYCA11	0.0881	0.8726	0.1591	1.0874
CYCA12	0.1497	0.8915	0.0770	0.5841
CYCA13	0.2646	1.5839	0.1911	1.2581
CYCA14	0.1495	1.365	0.2080	1.4404
CYCA15	0.163	1.2537	0.2000	1.4965
CYCA16	0.1245	1.1096	0.1550	0.9653
CYCA17	0.1081	1.0472	0.1338	0.8641

The intention of the approach introduced above is to examine the effects of initial properties of soil and applied stress on the cyclic relationship between r_u and ε_a. The weights obtained through the approach bear the

effect of each factor on the cyclic response of Adapazarı soils. Representative plots showing the actual, fitted and estimated r_u-ε_a relationships are given in Figure 5.24. The plots obtained for all the tests are given in Appendix. As the actual relationship was firstly fitted with logarithmic regression, the approach provides estimations close to the curve obtained via logarithmic regression. In parallel with this, the estimations are also close to the real values for the tests with R^2 values greater than 0.80. On the other hand, the approach estimates r_u comparatively higher or lower than the real value only for the first few cycles in some of the tests with R^2 values of about 0.65.

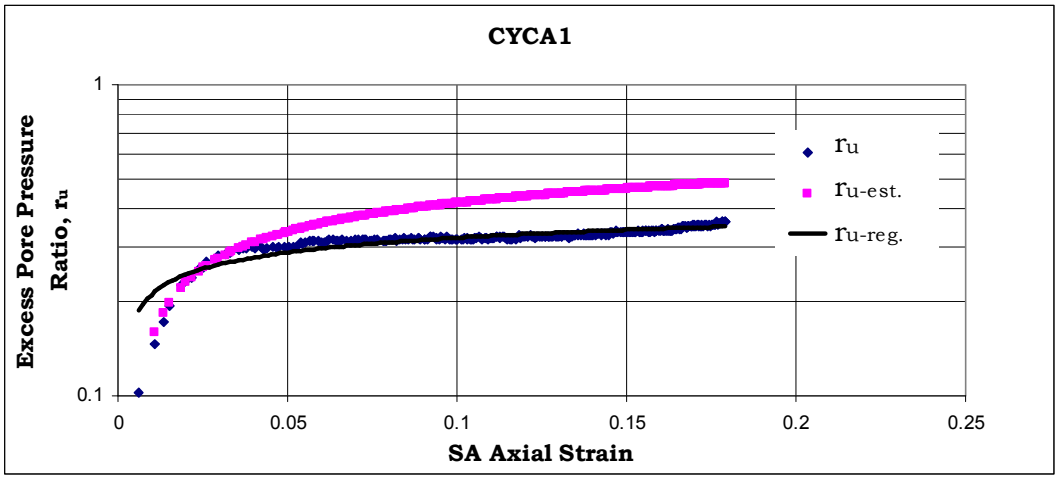

(a)

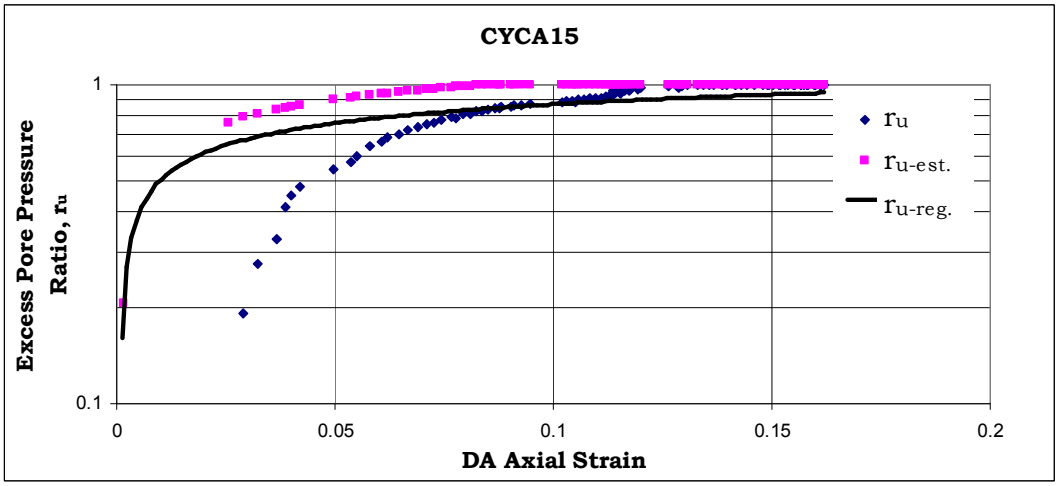

(b)

Figure 5.24 Real, fitted and estimated r_u-ε_a relationships for the tests of (a) CYCA1 with R^2 of 0.84 and (b) CYCA15 with R^2 of 0.67

5.10 Compatibility of Adapazarı Data with the Model of Initial Shear Stress Effect

In Chapter 4, the data acquired during the cyclic tests carried out with reconstituted silt are used to model the relationship between cyclic deviator stress ratio and initial shear stress ratio with respect to N required to reach 5% ε_a. The test results of Adapazarı soils are used to see how compatible the models are for Adapazari soils. 5% ε_a was not reached in some of the tests conducted with Adapazarı soil samples. Therefore, the value of N required to reach 5% ε_a is plotted on the model illustration for the tests of Adapazarı soils in which 5% ε_a was reached. As it is seen, although most of the tests on Adapazarı soils fit fairly well with the model based on reconstituted silt, there are two tests in which N required to reach 5% ε_a is 76 and 110, which totally contravene the model. This could be caused by the differences inherently sustained in non-uniform in-situ soils.

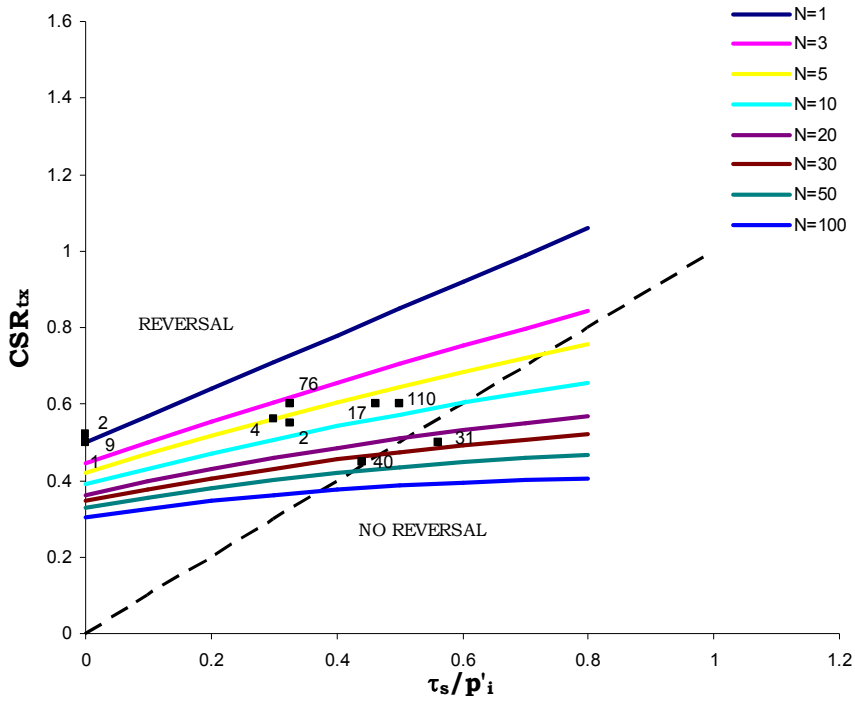

Figure 5.25 Demonstraion of N required to reach 5% ε_a for the tests of Adapazarı soils on the model representing the effect of initial shear stress on cyclic response of reconstituted silt

5.11 Liquefaction Susceptibility Examination of Adapazarı Soils via Existing Criteria

Chinese criteria is represented graphically in Figure 5.26 for the soils having 0.005 mm and smaller particle sizes less than 15%. The corresponding parameters for the cyclically tested 17 samples recovered from Adapazari are plotted on the same figure. As it is observed in Figure 5.26, most of the samples plot on the "susceptible to liquefaction" side. The assessment of the criteria does not meet the test results when considering there is just one test with flow liquefaction. The samples mostly showed cyclic mobility despite the fact that they had e_i values greater than 0.80.

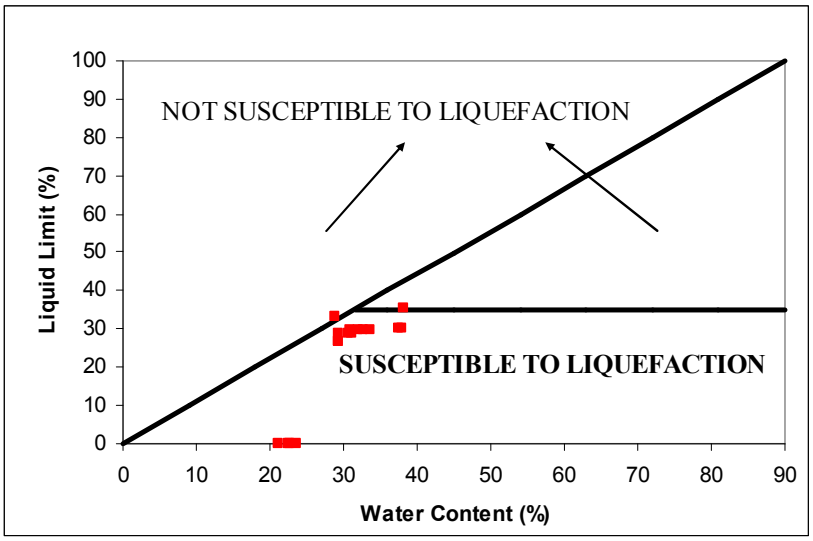

Figure 5.26 The data of Adapazarı samples compared to Chinese criteria for the soils having 0.005 mm and smaller particle sizes less than 15 %.

The properties of the Adapazari samples are also plotted on the graphical representation of the criteria proposed by Andrews and Martin (2000) in Figure 5.27. As it is observed, majority of the points remain in the area defined as "susceptible to liquefaction".

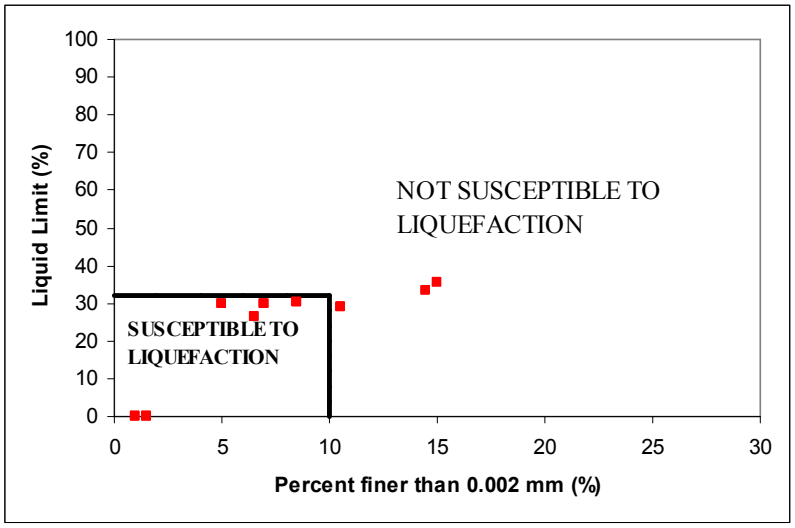

Figure 5.27 The data of Adapazarı samples compared to the liquefaction susceptibility criteria proposed by Andrews and Martin (2000)

As similar to the above, the characteristics of the Adapazari samples are plotted with respect to the criteria proposed by Bray et al. (2004) in Figure 5.28. The samples are classified as "susceptible to liquefaction or cyclic mobility". This assessment is in conformity with the "cyclic mobility" observed for the Adapazari soil samples.

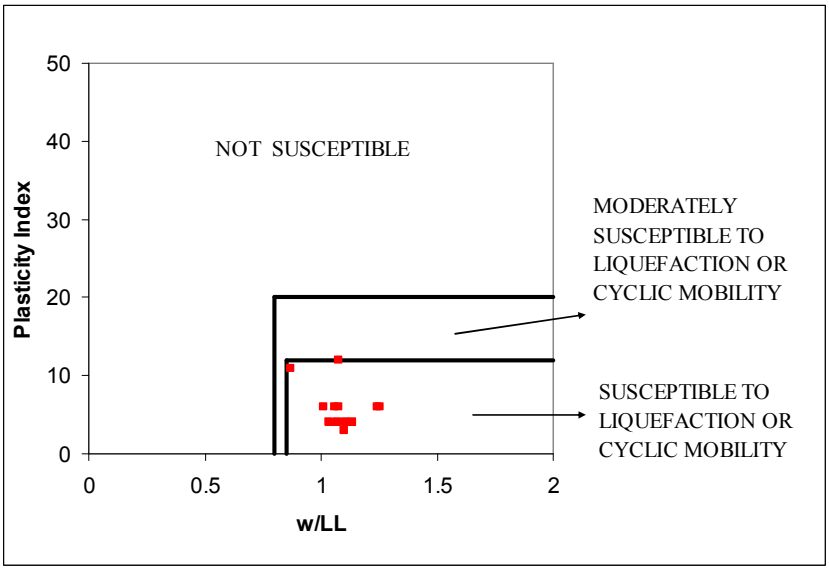

Figure 5.28 The data of Adapazarı samples over the plot showing liquefaction susceptibility criteria proposed by Bray et al. (2004)

Boulanger and Idriss (2004) suggested that the fine-grained soils of PI < 7 have been classified as “sand-like” (i.e. susceptible to liquefaction) and soils of PI ≥ 7 classified as “clay-like” materials. In accordance with this characterization, all the samples but two having PI less than 7 would be classified as “sand-like” material and susceptible to liquefaction. The other two samples that have PI values greater than 7 are classified as not-susceptible to liquefaction.

Most of the samples recovered from Adapazari are classified as susceptible to liquefaction. However, the term liquefaction is used to define both flow liquefaction and cyclic mobility although the cyclic behaviors for these two phenomena have been observed to be different from each other for both in-situ and reconstituted samples. It must be noted that the samples of Adapazari mostly showed cyclic mobility even though the samples had relatively high w_c/LL ratios and the tests were conducted with high levels of CSR_{tx}.

CHAPTER 6

SUMMARY AND CONCLUSIONS

6.1 Summary

The saturated soils display strength and stiffness degradation with increasing excess pore water pressures under repeated loads. The cyclic loads induced by the wave action affecting offshore platforms and by the earthquakes are likely causes which may lead soils to weaken. Weakening and liquefaction of sands under repeated loads is well-known. However, extensive damage to the built environment experienced at the sites underlain by fine soils during earthquakes have led researchers to focus on the seismic response of such soils more recently. Based on this motive, the characteristics affecting cyclic behavior of fine grained soils are investigated through laboratory testing in this study.

In order to provide a systematic and controlled investigation and to minimize the effects based on the inherent variability of naturally deposited soils, reconstituted silt size material is used in the study. The method of slurry deposition is decided to be the most suitable method to reconstitute the material, which is consisted of 68.5% silt, 4.5% clay, and 27% fine sand. The basic characteristics of the material, which is classified as low plastic silt (ML) according to the USCS, are: specific gravity G_s=2.69; LL=31; PL=24; PI=7,.

The specimens were subjected to load controlled cyclic and strain controlled monotonic triaxial tests via consolidated-undrained (CU) procedure. During the tests, 25 monotonic and 69 cyclic triaxial tests were performed on the reconstituted specimens. The tests were carried out with specimens having various initial stress states and stress

histories under various CSR_{tx} values with loading rates of 0.5 and 0.05 Hz. The intention of performing the static tests was to evaluate the strength of the soils prior to cyclic loadings and to understand the correlation between the static and the cyclic strength behavior.

The influence of excess pore water pressure generation during cyclic tests is examined through the relation between total (residual + transient) excess pore water pressure and axial strain. The reconstituted silt specimens were mostly tested under CSR_{tx} values exceeding the threshold strains beyond which the excess pore water pressure starts to generate. As a result, the excess pore water pressure generation was observed starting at the first cycles in a great majority of the tests. In order to observe the effects of the soil and the test characteristics on pore water pressure generation, the cyclic tests were separated into 10 groups based on these characteristics, and the effects are examined separately.

Since the amplitude and the exposure time of the loading have significant effect on the cyclic response of soils, the total excess pore pressure generation is investigated via examination of effect of CSR_{tx} and N on r_u. Then the responses are modeled to represent the relationship between r_u and CSR_{tx} as a function of N. The variation in r_u is plotted against N for each cyclic test. The curve showing the relationship between r_u and N is observed to have a gradually decreasing gradient after a certain r_u value. Such curves are fitted as power functions with satisfactory R-squared values ranging between 0.80 and 0.99. As the relationship between r_u and N depends on the loading frequency, CSR_{tx} and soil characteristics, the relationship between r_u, N and CSR_{tx} is modeled separately according to the loading frequencies of 0.5 and 0.05 Hz. Nevertheless, since the behavior is also influenced by the initial stress state, the models are formed according to the initial stress ratios (τ_s/p'_i) as well. The pore pressure response of all OC specimens can not be modeled. The specimens having an OCR of 2 are modeled, whereas those having an OCR of 4 did not display a consistent relationship. Accordingly, 8 models are introduced to estimate the relationship between r_u, N and CSR_{tx} for the silt tested under various conditions.

The influence of initial confining stress on cyclic response of reconstituted silt is investigated. In order to eliminate the influence of initial shear stresses, the tests performed with isotropically consolidated specimens are used to evaluate the effects of initial confining stress. Isotropic consolidation phase during triaxial tests was carried out mostly with confining pressures of 50, 80 and 100 kPa. The effect of confining stress is examined for NC specimens and for the specimens having OCR of 2. The tests performed with specimens having OCR values greater than 2 were carried out only with σ'_{3c} of 50 kPa. Accordingly, the effect of confining pressure of specimens with OCR greater than 2 can not be evaluated.

The soil elements beneath or around foundations sustain a shear stress due to the induced weight of the structure. The investigations so far have revealed that magnitude of the initially sustained shear stress has a significant effect on cyclic behavior of soils. The tests conducted with frequency of 0.5 Hz are to be taken into consideration for examination of initial shear stress effect, because the number of tests with 0.05 Hz is comparatively rather limited. However, in order to understand how the initial shear stress affects basic stress-strain relationship of reconstituted silt, the monotonic tests performed with specimens consolidated to varying initial shear stresses are also examined. Some of the monotonic tests are carried out with varying initial shear stresses under a number of different loading rates. The pore water pressure generation response investigated during monotonic shearing revealed that the reconstituted silt is highly dilative. This tendency becomes more pronounced with increasing initial shear stress. The initial shear stress effect on cyclic strength is examined by means of the relationship between CSR_{tx} and N required to reach ε_a of 5%. In the cyclic tests the axial strains mostly reach or exceed 10%. However in some tests the cyclic strain remains below a certain value and even below 5%. Therefore ε_a of 5% was chosen as a reference strain to examine initial shear stress effect. The relationship between pore pressure generation and τ_s during cyclic tests is similar to that observed in the monotonic tests.

The relationship between cyclic deviatoric stress ratio (CSR_{tx}) and initial shear stress ratio (τ_s/p'_i) is modeled as a function of N required to reach 5% ε_a. It is observed that the cyclic resistance increases more significantly for the tests with stress reversal, and no appreciable influence of increasing initial shear stress is detected for the case of no stress reversal. The predictions of the introduced model were in good agreement with the observed effect of initial shear stress on cyclic response of the reconstituted silt.

Stress history of the soils has a strong influence on the stress-strain response under both monotonic and dynamic loading conditions. Accordingly, the effect of stress history is examined through the specimens having OCR of 1, 2, 3 and 4. The effect of OCR on monotonic and cyclic behavior of reconstituted silt is investigated and discussed for the specimens sustaining no initial shear stress. The OCR effect on monotonic stress-strain response is explored with monotonic tests performed under OCR of 1, 2 and 4. Although most of the monotonic tests were conducted with NC specimens, two more tests were conducted with specimens having OCR of 2 and 4. Effect of OCR on cyclic response is examined via relationship between CSR_{tx} and N required to reach at 5% ε_a. Again, ε_a of 5% is chosen as a reference value to compare resistance of the specimens having different OCR values.

Loading rate is another factor with a significant effect on the stress-strain behavior of soils. The effect of loading rate is examined through the monotonic tests carried out with loading rates of 0.07%/min and 0.1%/min. Loading rate effect on the cyclic behavior is evaluated via the tests conducted under two different frequencies of 0.5 and 0.05 Hz.

The cyclic degradation observed in reconstituted silt specimens is quantified based on the tests conducted with isotropically consolidated specimens, and expressed by the ratio of secant modulus (E) at the first cycle to that at the N^{th} cycle. E is calculated according to the peak $\Delta\sigma_{cyc}$ and ε_a observed at that peak stress for the relevant cycle. Degradation index (δ_D) is calculated for each cycle by considering SA ε_a values observed

on the compression side. The relationship between δ_D and N is plotted as a function of the applied CSR_{tx}. Cyclic degradation for silt specimens with different OC states were evaluated separately.

Surface rupture of the fault that emerged during the 17 August 1999 İzmit (Kocaeli) earthquake (M_w=7.4) was at a mere average distance of 5 km from the City of Adapazarı. The surface soils at the sites in the City, where foundation displacements commonly occurred, have been reported to be consisting of fine-grained soils (CL/ML). Due to the redundancy in foundation displacement cases, the city of Adapazarı was preferred for investigation of cyclic response of undisturbed fine soils within the context of this study.

Five sites at two different districts (Tığcılar and Yenigün) of the city where foundation displacements were commonly observed during 1999 earthquake were selected for detailed investigations. Boreholes were drilled to depths ranging between 6 m and 8 m at these sites and 1 or 3 tubes of undisturbed soil samples were extruded from various depths in each borhole. The GWT observed in the boreholes were ranging between 1.60 m and 2.60. Extruded samples consisted of low plastic silt-clay mixtures and silty fine sand.

A series of undrained monotonic tests were conducted over Adapazarı samples to examine the static response of those soils, and to identify any conceivable relationship between monotonic and cyclic responses. It must be noted that the initial stress states imposed over the specimens for monotonic tests do not perfectly matched with those used in cyclic tests of Adapazarı soils. However, cyclic tests were also conducted on specimens with isotropic initial stress states.

Total of 17 cyclic tests were conducted over isotropically and anisotropically consolidated Adapazarı soil sample under stresses representative of those in-situ. The initial stress states applied during the tests provide the specimens to remain in NC state. Different cyclic stress amplitudes were applied during the tests so as to provide values of CSR_{tx} ranging between 0.30 and 0.60. The cyclic tests on Adapazari soils were

performed under a frequency of 0.5 Hz, which is considered to be the typical frequency representative of earthquake loading.

The values of initial void ratio (e_i) ranged between 0.59 and 1.06, and accordingly the ratio of w_c/LL ranged between 0.87 and 1.25. These w_c/LL ratios are relatively high when compared with those of the reconstituted silt specimens, which is the main difference between the undisturbed and the reconstituted specimens used throughout the study.

The excess pore water pressure generation during cyclic tests is again examined through the relation between total excess pore water pressure and increasing axial strain. The logarithmic change of total excess pore water pressure increased gradually with increasing axial strain up to a point beyond which the excess pore water pressure development begins to slow down and reaches a constant residual value while the axial strain proceeds to accumulate. In the study, this point where the pore water pressure begins to slow down is termed as the flexure point, and the point where the pore pressure increase remains at negligible levels and r_u reaches a residual value is termed as the residual point. No flexure point is observed for the majority of tests conducted without an initial shear stress. Those tests are the ones in which DA axial strain and r_u remained significantly low, and the relationship between r_u and ε_a does not show a conceivable trend or a flexure point.

In this study, the relationship between r_u and ε_a has been introduced for both reconstituted silt and the soils recovered from Adapazari. It is aimed to understand the mechanism leading to the development of pore water pressure and strain in saturated fine soils. The effects of τ_s/p'_i, OCR, loading rate and CSR_{tx} on excess pore pressure development were explained through the models that were introduced depending on the data acquired from the tests carried out with reconstituted silt specimens. Depending on the reconstitution technique used during silt deposition, initial void ratio of the specimens had a range between 0.68 and 0.77. Due to this limited range, the effect of e_i on the development of excess pore water pressure and strain accumulation could not be reflected in the models constituted based on the test data of reconstituted silt. Therefore,

the tests conducted with Adapazari soils are used to reflect the effect of e_i as well as that of τ_s/p'_i and CSR_{tx} on cyclic response of saturated fine soils. The samples recovered from Adapazarı are observed as to be either NC or lightly OC. Therefore, the stress history of the samples is not taken into consideration, and initial stress state is expressed with only the ratio τ_s/p'_i. As the e_i of samples varied in a wide range, the relationship of r_u-ε_a involves the influence exerted by e_i. Lastly, as the soils are obviously influenced by the magnitude of cyclic load, the effect of CSR_{tx} on the relationship of r_u-ε_a is also expected to be reflected. For the sake of practicality in implementation, the factors are presumed as to be linearly related to the coefficients in the equation representing the relationship between r_u and ε_a. Accordingly, the weight of each factor is determined by means of a statistical approach.

The data acquired during the tests carried out with Adapazari soil samples are compared with the models introduced to estimate r_u-ε_a relationship and the effect of initial shear on cyclic response, which are established with the data of reconstituted silt.

6.2 Conclusions

An extensive laboratory testing program including conventional soil mechanics tests, consolidation tests, reconstitution procedure for soil deposition, monotonic and cyclic triaxial tests was performed to evaluate the cyclic behavior of saturated low plastic fine grained soils. Laboratory program was conducted within two parts, one of which includes the tests performed with the silt specimens reconstituted in the laboratory and the other includes the tests performed with the undisturbed soil samples retrieved from five different sites in Adapazari. Based on the results obtained through the laboratory tests, the key findings are as follows:

- Cyclic response is observed to significantly depend on whether the specimens are subjected to stress reversal or not during cyclic loading.

- In the case of no stress reversal, plastic strains accumulate with almost a constant rate in each cycle. The plastic strain accumulation rate tends to decrease after having reached the point where the peak cyclic stress becomes lower than the monotonic strength. It is observed that the greater the ratio of the applied peak cyclic stress to the monotonic strength, the greater the strain accumulation rate. No significant cyclic degradation was observed in stiffness of the specimens under loading without stress reversals although the axial strains exceeded 5%.
- In the case of stress reversal, the strain accumulation is predominant either in compression or in extension depending on the initial stress state. The incremental strains developed in each additional cycle are added to the maximum past strains in compression and extension respectively. The strain accumulation rate becomes more pronounced in extension with increasing N, which is attributed to lower strength of soils in extension.
- The axial strain accumulation starts to increase at levels of lower r_u with increasing CSR_{tx} for the specimens sustaining no initial shear stress, whereas it starts to increase at levels of higher r_u with increasing CSR_{tx} for the specimens with an initial shear stress. At the flexure points determined through the relationship between r_u and ε_a, the highest r_u values are observed at lowest ε_a values for the tests with lower CSR_{tx} values.
- The results of the tests performed with reconstituted specimens show that the excess pore water pressure ratio increases rapidly within early axial strain levels mostly up to about 5-6% DA for the tests with stress reversals, and 2-4% SA for the tests without stress reversals. Following such axial strain levels, the gradient of the curve representing the relationship between excess pore water pressure ratio and axial strain starts to decrease. At the flexure point, the excess pore pressure ratio is observed as to be mostly between 40% - 60%. This range of excess pore water pressure ratio is well below those reported as a criterion for initiation of liquefaction in the literature.

- The results of the tests performed with soil samples recovered from Adapazarı show that the excess pore water pressure ratio increases rapidly in the early axial strain levels mostly up to about 0.1-1% DA for the tests with stress reversals, and 0.1-3% SA for the tests without stress reversals.
- Increasing confining stress has a detrimental effect on the cyclic resistance of reconstituted NC and lightly OC silt.
- An initial shear stress up to 60% - 70% of p'_i causes cyclic strength to increase. On the one hand, cyclic strength was observed to decrease with the initial shear stress exceeding 60% - 70% of p'_i for the reconstituted silt specimens. Additionally, the maximum pore pressure ratio observed during shearing significantly decreases with increasing τ_s/p'_i.
- The monotonic tests revealed that the undrained shear strength (s_u) increases with increasing OCR. Nevertheless, the increase in resistance with increasing OCR observed during cyclic tests is not as significant as that observed in monotonic tests.
- The loading rate effect differs depending on whether initial shear stress exists or not. An increase in the loading rate obviously causes an increase in the cyclic resistance of silt specimens that do not sustain initial shear stress. On the other hand, loading rate does not influence the cyclic resistance if the cyclic behavior is dominated in the compression side. The loading frequency effect on total pore water pressure response is significant for the isotropically consolidated specimens. A 10 times increase in loading frequency causes significant decrease in the excess pore water pressure generation for the isotropically consolidated specimens, whereas it is negligible for the case of no stress reversals.
- The cyclic degradation increases with increasing CSR_{tx} for all OC levels applied during the tests. An increase in OCR reduces the stiffness degradation as indicated by Vucetic and Dobry (1988). However, this reduction is not as significant as that for clays as shown earlier by Vucetic and Dobry (1988).

- According to the Chinese criteria, the reconstituted silt is evaluated as “not susceptible to liquefaction”. The assessment of the criteria meets the test results when considering no observed flow liquefaction. However, this assessment can be regarded as somewhat conservative when considering the response of cyclic mobility that has frequently occurred during the cyclic tests. The reconstituted silt is classified in the range from “moderately susceptible to liquefaction or cyclic mobility” to “susceptible to liquefaction or cyclic mobility” according to the criteria proposed by Bray et al. (2004). This assessment is in conformity with the “cyclic mobility” observed for the reconstituted silt during cyclic triaxial tests. The area defined as “moderately susceptible to liquefaction or cyclic mobility” gives a room for evaluation of liquefaction susceptibility of borderline materials, especially for low plasticity silts. However, the criteria do not provide a clear distinction between the phenomena of “liquefaction” and “cyclic mobility”.
- The w_c/LL ratios of the samples recovered from Adapazari are relatively high in comparison with those of the reconstituted silt specimens. The r_u values observed at flexure points for Adapazari soils are consistent with those observed in the tests of reconstituted silt specimens. Nevertheless, the r_u values at flexure point range between 0.60 and 1.00 which is generally higher than those observed for the reconstituted silt specimens.
- The r_u values were observed to reach, and even exceed 0.9 at different cycles. Although the excess pore water pressure reaching initial confining stress lead to the loss in effective stress and thus to cyclic strain softening, the dilative tendency of the silt prevents excessive loss of strength. No instantaneous increase is observed either in pore water pressure or strain accumulation, except one test in the entire study. Accordingly, it can be stated that the flow liquefaction was observed only in one of the tests during the study.
- Although the results of many tests performed over Adapazarı soils are compatible with the models introduced through the data of the reconstituted silt, the models do not closely estimate all the results observed during the tests conducted with these soils.

- Most of the samples recovered from Adapazarı are classified as susceptible to liquefaction. However, the term liquefaction is used to define both flow liquefaction and cyclic mobility, despite the fact that these two phenomena have been substantially different from each other regarding the response in both in-situ and reconstituted samples. It must be pointed out that the samples of Adapazari mostly showed cyclic mobility even though the samples had relatively high w_c/LL ratios and the tests were conducted with high CSR_{tx} levels.

REFERENCES

Ambraseys N. N. and Zapotek A. (1969) "The Mudurnu valley (West Anatolia, Turkey) earthquake of 22 July 1967," Bull. of the Seis. Soc., Vol.59, No.2, pp. 521-589.

Andersen K. H., Pool J. H., Brown S. F., and Rosenbrand w. F. (1980) "Cyclic and static laboratory tests on Drammen clay," *Journal of the Geotechnical Engineering Division*, ASCE, Vol.106, No.GT5, pp. 499-529.

Andersen K. H. and Lauritzsen R. (1988). "Bearing capacity for foundations with cyclic loads," *Journal of Geotechnical Engineering*, Vol.114, No.5, pp.540-555.

Andersen K. H., Kleven A., Heien D. (1988). "Cyclic soil data for design of gravity structures," *Journal of Geotechnical Engineering*, Vol.114, No.5, pp.517-539.

Anderson J., Sucuoglu H., Erberik A., Yilmaz T., Inan E., Durukal E., Erdik M., Anooshehpoor R., Brune J., Ni S. (2000) "Strong ground motions from the Kocaeli and Duzce, Turkey, earthquakes and possible implications for seismic hazard anaysis," *Earthquake Spectra*, Supplement A to Volume 16, pp. 113-137.

Andrews D. C. A., and Martin G. R. (2000). "Criteria for liquefaction of silty soils," *Proc., 12th World Conf. On Earthquake Engineering*, Auckland, New Zealand.

Ansal A. M., and Erken A. (1989) "Undrained behavior of a normally consolidated clay under cyclic shear stresses," *Journal of Geotechnical Engineering*, ASCE, Vol.115, No.7, pp. 968-983.

Azzouz A. S., Malek A. M., and Baligh M. M. (1989) "Cyclic behavior of clays in undrained simple shear," *Journal of Geotechnical Engineering*, ASCE, Vol.115, No.5, pp. 637-657.

Bakır B. S., Sucuoğlu H., and Yılmaz T. (2002) "An overview of local site effects and the associated building damage during the 17 August İzmit earthquake," *Bulletin of Seismological Society of America,* Vol.92, No.1, pp.509-526.

Bakir B. S., Yilmaz, M. T., Yakut A., and Gulkan P. (2005) "Re-examination of damage distribution in Adapazari: Geotechnical considerations," *Engineering Structures*, Vol.27, No.7, pp. 1002-1013.

Bishop A. W. and Henkel D. J. (1957) *The measurement of soil properties in the triaxial test,* Edward Arnold Publishers LTD, London, England, 190p.

Boulanger R. W., Meyers M. W., Mejia L. H., and Idriss I. M. (1998). "Behavior of a fine grained soil during the Loma Prieta earthquake," *Canadian Geotechnical Journal*, Vol.35, pp.146-158.

Boulanger R. W., and Idriss I. M. (2004). "Evaluating the potential for liquefaction or cyclic failure of silts and clays," Rep. No. *UCD/CGM-04/01*, Center of Geotechnical Modeling, Dept. of Civil and Environmental Engineering, University of California, Davis, California.

Boulanger R. W., and Idriss I. M. (2006). "Liquefaction susceptibility criteria for silts and clays," *Journal of Geotechnical and Geoenvironmental Engineering*, Vol.132, No.11, pp.1413-1426.

Boulanger R. W., and Idriss I. M. (2007). "Evaluation of cyclic softening in silts and clays," *Journal of Geotechnical and Geoenvironmental Engineering*, Vol.133, No.6, pp.641-652.

Brandon T. L., Rose A. T., Duncan J. M. (2006). "Drained and undrained strength interpretation for low plasticity silts," *Journal of Geotechnical and Geoenvironmental Engineering*, Vol.132, No.2, pp.250-257.

Bray J. D. and Sancio R. B. (2006) "Assessment of the liquefaction susceptibility of fine grained soils," *Journal of Geotechnical and Geoenvironmental Engineering*, Vol.132, No.9, pp.1165-1177.

Bray J. D., Sancio R. B., Durgunoğlu T., Önalp A., Youd T. L., Stewart J. P., Seed R. B., Çetin K. Ö., Bol E, Baturay M. B., Christensen C., and Karadayılar T. (2004) "Subsurface characterization at ground failure sites in Adapazarı, Turkey," *Journal of Geotechnical and Geoenvironmental Engineering*, Vol.130, No.7, pp.673-685.

Campanella R. G. and Lim B. S. (1981) "Liquefaction characteristics of undisturbed soils," *Proceeding of the International Conference on Recent Advances in Geotechnical Earthquake Engineering and Soil Dynamics,* Vol.1, pp.227-230.

Casagrande A. (1936) "Characteristics of cohesionless soils affecting the stability of slopes and earth fills", *Journal of Boston Society of Civil Engineers,* reprinted in *Contributions to Soil Mechanics*, BSCE, 1940 pp.257-276.

Casagrande A. (1938) "The shearing resistance of soils and its relation to the stability of earth dams", Soils and Foundation Conference of the U. S. Engineer Dept., June 17-21, 1938. US ACE, Pub. Boston.

Castro G. (1969) *Liquefaction of sands*, Harvard Soil Mechanics Series, No.81, Pierce Hall.

Castro G. (1975) "Liquefaction and cyclic mobility of saturated sands", *Journal of the Geotechnical Engineering Division*, ASCE, Vol.101, No.GT6, pp. 551-569.

Castro G. and Poulos S. J. (1977) "Factors affecting liquefaction and cyclic mobility", *Journal of the Geotechnical Engineering Division*, ASCE, Vol.103, No.GT6, pp. 501-516.

Chang N. Y., Yeh S. I. and Kaufman L. P. (1982) "Liquefaction potential of clean and silty sands", *Proceedings of Third International Earthquake Microzonation Conference*, Seattle, Washington, Vol.2, pp. 1017-1032.

Craig W. H. (1982) "Strain rate and viscous effects in physical models," Proceedings of International Conference on Soil Dynamics and Earthquake Engineering, Southampton, England, Vol.1, pp. 351-365.

DeAlba P., Seed H. B. and Chan C. K. (1976) “Sand liquefaction in large-scale simple shear tests”, *Journal of the Geotechnical Engineering Division*, ASCE, Vol.102, No.GT9, pp. 909-927.

Dobry R., Ladd R., Yokel F., Chung R., and Powell D. (1982) “Prediction of pore water pressure buildup and liquefaction of sands during earthquakes by the cyclic strain method,” *NBS Building Science Series 138, National Bureau of Standards, US Dept. of Commerce*.

Donahue J., Bray J., and Reimer M. (2007) “Liquefaction testing of fine grained soil prepared using slurry deposition”, *4th International Conference on Earthquake Geotechnical Engineering,* Paper No:1226.

Finn W. D. L., Lee K. W. and Martin G. R. (1977) “An effective stress model for liquefaction”, *Journal of the Geotechnical Engineering Division*, Vol.103, No.GT6, pp. 517-533.

Germaine J. T. and Ladd C. C. (1988) “Triaxial testing of saturated cohesive soils”, Adv. Triaxial Testing of Soil and Rock ASTM pp.421-459

Haldar A. and Miller F. J. (1984) “Statistical evaluation of cyclic strength of sand”, *Journal of Geotechnical Engineering*, Vol.110, No.12, pp. 1785-1802.

Hanzawa H., Itoh Y. and Suzuki K. (1979) “Shear characteristics of a quick sand in the Arabian Gulf”, *Soils and Foundations*, Vol.19, No.4, pp. 1-15.

Hardin B. O. and Drnevich V. P. (1972) “Shear modulus and damping in soils: design equations and curves”, *Journal of Soil Mechanics and Foundation Division*, ASCE, Vol.98, No.7, pp. 667-692.

Holtz R. D. and Kovacs W. D. (1981) *An introduction to geotechnical engineering*, Englewood Cliffs, N. J.: Prentice Hall, 733p.

Hyde A. F. L. and Ward S. J. (1985) “A pore pressure and stability model for a silty clay under repeated loading”, *Geotechnique*, Vol.35, No.2, pp. 113-125.

Hyde A. F. L., Higuchi T., and Yasuhara K. (2006) "Liquefaction, cyclic mobility and failure of silt," *Journal of Geotechnical and Geoenvironmental Engineering*, Vol.132, No.6, pp.716-735.

Hynes M. E. and Olsen R. S. (1999) "Influence of confining stress on liquefaction resistance" *Physics and Mechanics of Soil Liquefaction*, Lade and Yamamuro eds., Balkema, Rotterdam, pp.145-152.

Hyodo M., Yasuhara K, and Hirao K. (1992) "Prediction of clay behaviour in undrained and partially drained cyclic triaxial tests," *Soils and Foundations*, Japanese Soceity of Soil Mechanics and Foundation Engineering, Vol.32, No.4, pp.117-127.

Hyodo M., Yamamoto Y., Sugiyama M. (1994). "Undrained cyclic shear behaviour of normally consolidated clay subjected to initial static shear stress", *Soils and Foundations*, Japanese Soceity of Soil Mechanics and Foundation Engineering, Vol.34, No.4, pp.1-11.

Hsu C. C., and Vucetic M. (2006) "Threshold shear strain for cyclic pore-water pressure in cohesive soils," *Journal of Geotechnical and Geoenvironmental Engineering*, Vol.132, No.10, pp.1325-1335.

Idriss I. M., Dobry R. and Singh R. D. (1978) "Non-linear behavior of soft clays during cyclic loading", *Journal of the Geotechnical Engineering Division*, Vol.104, No.GT12, pp.1427-1447.

Ishibashi I., Kawamura M. and Bhatia S. (1985) "Effect of initial shear on cyclic behavior of sand", *Journal of Geotechnical Engineering*, ASCE, Vol.111, No.12, pp. 1395-1410.

Ishihara K., Troncoso J., Kawase Y. and Takahashi Y. (1980) "Cyclic strength characteristics of tailings materials", Soils and Foundations, Vol.20, No.4, pp. 127-142.

Ishihara K. (1993) "Liquefaction and flow failure during earthquakes", *Geotechnique*, Vol.43, No.3, pp. 351-415.

Ishihara K. (1996). *Soil Behavior in Earthquake Geotechnics*, Clarendon Press, Oxford, 350 p.

Ishihara K., Tatsuaoka F., and Yasuda S., (1975). “Undrained deformation and liquefaction of sand under cyclic stresses”, *Soils and Foundations*, Japanese Society of Soil Mechanics and Foundation Engineering, Vol.15, No.1, pp. 29-44.

Jiang M., Cai Z., Cao P., and Liu D (2010) “Effect of cyclic loading frequency on dynamic properties of marine clay,” *Proceedings of GeoShangai 2010 International Conference*, Geotechnical Special Publications No.201, ASCE, pp.240-245.

Karaca G. (2001). *An investigation into the large vertical displacements experienced by the structures in Adapazarı during 17 August 1999 Earthquake,* MS Thesis, METU, 155p.

Kimura T., and Saitoh K. (1983) “The influence of strain rate on pore pressures in consolidated undrained triaxial tests on cohesive soils,” *Soils and Foundations*, Japanese Society of Soil Mechanics and Foundation Engineering, Vol.23, No.1, pp. 80-90.

Kodaka T., Itabashi K., Fukuzawa H., and Kato S. (2010) “Cyclic shear strength of clay under simple shear condition,” *Proceedings of GeoShangai 2010 International Conference*, Geotechnical Special Publications No.201, ASCE, pp.234-239.

Koester J. P. (1994) “The influence of fines type and content on cyclic strength”, *Ground Failures Under Seismic Conditions*, Geotechnical Special Publication No.44, Prakash and Dakoulas eds., ASCE, Atlanta-Georgia, pp. 17-33.

Konrad J.M., and Wagg B.T. (1993). “Undrained cyclic loading of anisotropically consolidated clayey silts,” *Journal of Geotechnical Engineering*, A.S.C.E., Vol.119, No.5, pp.929-947.

Kramer S. L. (1996) *Geotechnical Earthquake Engineering*, Publ. Prentice Hall.

Krizek R. J., McLean F. G. and Giger M. W. (1974) “Effect of particle characteristics on wave velocity”, Journal of Geotechnical Engineering Division, ASCE, Vol.100, No.1, pp. 89-94.

Ku C. S., Lee D. H. and Wu J. H. (2004) "Evaluation of soil liquefaction in the Chi-Chi, Taiwan earthquake using CPT", *Soil Dynamics and Earthquake Engineering*, Vol.24, No.9-10, pp. 659-673.

Kuerbis R. and Vaid Y. P. (1988) "Sand sample preparation-the slurry deposition method", *Soils and Foundations,* Vol.28, No.4, pp.107-118.

Kuribuyashi E., Iwasaki T. and Tatsuoka F. (1974) "Effects of stress conditions on dynamic properties of sands", *Bulletin of the International Institute of Seismology and Earthquake Engineering*, Vol.12, pp. 117-130.

Kuerbis R., Nequssey D. and Vaid Y. P. (1988) "Effect of gradation and fines content on the undrained response of sand", *Proceedings of the ASCE Geotechnical Division Specialty Conference on Hydraulic Fill Structures*, Colorado State University, Fort Collins, Colorado, USA.

Ladd C. C., and Foott R. (1974) "New design procedure for stability of soft clays," *Journal of the Geotechnical Engineering Division*, ASCE, Vol.100, No.GT7, pp. 763-786.

Ladd R.S. (1974) "Specimen preparation method and liquefaction of sands", *Journal of the Geotechnical Engineering Division,* Vol.100, No.GT10, pp.1180-1184.

Lade P. V. and Yamamuro J. A. (1997) "Effects of non-plastic fines on static liquefaction of sands", *Canadian Geotechnical Journal*, Ottawa, Vol.34, No.6, pp. 918-928.

Lambe T. W., and Whitman R. V. (1979) *Soil Mechanics SI Version*, John Wiley and Sons.

Lee D. H., Juang C. H. and Ku C. S. (2001) "Liquefaction performance of soils at the site of a partially completed ground improvement project during the 1999 Chi-Chi earthquake in Taiwan", *Canadian Geotechnical Journal*, Vol.38, pp. 1241-1253.

Lee K. L. and Seed H. B. (1967a) “Cyclic stress conditions causing liquefaction of sand”, *Journal of the Soil Mechanics and Foundations Division,* Vol.93, No.1, pp.47-70.

Lee K. L. and Seed H. B. (1967b) “Dynamic strength of anisotropically consolidated sand”, *Journal of the Soil Mechanics and Foundations Division,* Vol.93, No.5, pp.169-190.

Lefebvre G. and Pfendler P. (1996). “Strain rate and preshear effects in cyclic resistance of soft clay”, *Journal of Geotechnical Engineering,* ASCE, Vol.122, No.1, pp.21-26.

Lefebvre G., and LeBouef D. (1987) “Rate effects and cyclic loading of sensitive clays,” *Journal of Geotechnical Engineering,* ASCE, Vol.113, No.5, pp. 476-489.

Li S. and Huang M. (2010) “Undrained long-term cyclic degradation characteristics of offshore soft clay”, *Proceedings of GeoShanghai 2010 International Conference*, Shanghai, China, pp. 263-271.

Liou C. P., Streeter V. L. and Richart F. E. (1977) “A numerical model for liquefaction”, *Journal of the Geotechnical Engineering Division*, Vol.103, No.GT6, pp. 589-606.

Matesic L. and Vucetic M. (2003) “Strain-rate effect on soil secant shear modulus at small cyclic strains”, *Journal of Geotechnical and Geoenvironmental Engineering*, Vol.129, No.6, pp. 536-549.

Matasovic N., and Vucetic M. (1995) “Generalized cyclic-degradation-pore-pressure generation model for clays,” *Journal of Geotechnical Engineering*, ASCE, Vol.121, No.1, pp. 33-42.

Matsui T., Ohara H., and Ito T. (1980) “Cyclic stress-strain history and shear characteristics of clay,” *Journal of the Geotechnical Engineering Division*, ASCE, Vol.86, No.GT10, pp. 1101-1120.

Mitchell J. K. (1993) *Fundamentals of soil behavior*, 2nd ed., New York: Wiley, 437p.

Mitchell R. J., and King R. D. (1977) “Cyclic loading of an Ottawa area Champlain Sea clay,” *Canadian Geotechnical Journal*, Vol.14, pp.52-63.

Miura S. and Toki S. (1982) “A sample preparation method and it effect on static and cyclic deformation-strength properties of sand”, *Soils and Foundations,* Vol.22, No.1, pp.61-77.

Mohamad R. and Dobry R. (1986) “Undrained monotonic and cyclic triaxial strength of sand”, *Journal of Geotechnical Engineering*, ASCE, Vol.112, No.10, pp. 941-958.

Mulilis J. P., Seed H. B., Chan C. K., Mitchell J. K., and Arulanandan K. (1977) “Effects of sample preparation on sand liquefaction”, *Journal of the Geotechnical Engineering Division*, Vol.103, No.GT2, pp.91-108.

Pekcan O. (2001) *Cyclic Behavior of Adapazarı Clayey Silts*, MS. Thesis, METU, 83p.

Polito C. P., Green R. A., and Lee J. (2008) “Pore pressure generation models for sands and silty soils subjected to cyclic loading,” *Journal of Geotechnical and Geoenvironmental Engineering*, ASCE, Vol.134, No.10, pp.1490-1500.

Procter D. C., and Khaffaf J. H. (1984) “Cyclic triaxial tests on remoulded clays,” *Journal of Geotechnical Engineering*, ASCE, Vol.110, No.10, pp.1431-1445.

Oda M., Koishikawa I., and Higuchi T. (1978) “Experimental study of anisotropic shear strength of sand by plane strain test”, *Soils and Foundations,* Vol.18, No.1, pp.25-38

Ohara S., and Matsuda H. (1988) “Study on the settlement of saturated clay layer induced by cyclic shear,” *Soils and Foundations*, Japanese Soceity of Soil Mechanics and Foundation Engineering, Vol.28, No.3, pp.103-113.

Ohsaki Y. (1966) “Niigata Earthquakes, 1964, Building damage and soil conditions”, *Soils and Foundations*, Vol.6, No.2, pp.14-37.

Okur D. V. and Ansal A. (2007) "Stiffness degradation of natural fine grained soils during cyclic loading", *Soil Dynamics and Earthquake Engineering*, Vol.27, pp. 843-854.

Okur V., Altun S., and Ansal A. (2008) "The variation of pore pressure related with failure in fine-grained soils under uniform cyclic loadings," Proceedings of GeoCongress 2008, ASCE, pp. 149-156.

Riemer M. F. and Seed R. B. (1997) "Factors affecting apparent position of the steady state line", *Journal of Geotechnical Engineering*, Vol.123, No.3, pp. 281-288.

Rogers J. D., Wills C. J., and Manson M. W. (1991) "Two sequences of fine grained soil liquefaction at Soda Lake, Pajaro River Valley, Santa Cruz County, California", *Proceedings of the Second International Conference on Recent Advances in Geotechnical Engineering and Soil Dynamics,* Vol.3, pp.2295-2308.

Rollins K. M. and Seed H. B. (1988) "Influence of buildings on potential liquefaction damage", *Journal of Geotechnical Engineering*, ASCE, Vol.116, No.GT2, pp. 165-185.

Roscoe K. H., Schofield A. N., and Wroth C. P. (1958) "On the yielding of soils", *Geotecnique,* Vol.8, pp.22-53.

Sancio R. B., Bray J. D., Stewart J.P., Youd T. L., Durgunoğlu H. T., Önalp A., Seed R. B., Christensen C., Baturay B., and Karadayılar T. (2002) "Correlation between ground failure and soil conditions in Adapazarı, Turkey", *Soil Dynamics and Earthquake Engineering*, Vol.22, pp.1093-1102.

Sanin M. V., and Wijewickreme D. (2006) "Cyclic shear response of channel-fill Fraser River Delta silt," *Soil Dynamics and Earthquake Engineering*, Vol.26, pp. 854-869.

Seed H. B. and Lee K. L. (1966) "Liquefaction of saturated sands during cyclic loading", *Journal of Soil Mechanics and Foundations Division,* Vol.92, No.6, pp.105-134.

Seed H. B. and Idriss I. M. (1970) *Soil moduli and damping factors for dynamic response analyses*, Report No:EERC 70-10, Earthquake Engineering Research Center, Univ. of California, Berkeley, California, USA.

Seed H. B. and Idriss I. M. (1971) "Simplified procedures for evaluating soil liquefaction potential." *Journal of Soil Mechanics and Foundations Division*, ASCE, Vol.97, No.SM9, pp. 1249-1273.

Seed H. B. and Idriss I. M., Makdisi F., and Banerjee N. (1975). *Representation of irregular stress time histories by equivalent uniform stress series in liquefaction analysis,* Report No. EECR-75-29, Berkeley, California.

Seed H. B., Martin P. P. and Lysmer J. (1976) "Pore-water pressure changes during soil liquefaction", *Journal of the Geotechnical Engineering Division*, Vol.102, No.GT4, pp. 323-346.

Seed H. B. and Idriss I. M. (1982). *Ground Motions and Soil Liquefaction during Earthquakes,* Earthquake Engineering Research Institute, MNO-5 Berkeley, California, USA.

Seed H. B., Wong R. T., Idriss I. M. and Tokimatsu K. (1986) "Moduli and damping factors for dynamic analyses of cohesionless soils", *Journal of Geotechnical Engineering*, ASCE, Vol.112, No.11, pp. 1016-1032.

Seed H. B., Romo M. P., Sun J. I., Jaime A, and Lysmer J. (1988) "The Mexico Earthquake of September 19, 1985- relationship between soil conditions and earthquake ground motions", *Earthquake Spectra*, Vol.4, No.4, pp.687-729.

Seed R. B. and Harder L. F. (1990) "SPT-based analysis of cyclic pore pressure generation and undrained residual strength", *Proceedings of the B. Seed Memorial Symposium*, Vol.2, pp. 351-376.

Silver M. L., Chan C. K., Ladd R. S., Lee K. L., Tiedmann D. A., Townsend F. C., Valera J. E., and Wilson J. H. (1976) "Cyclic triaxial strength of standard test sand", *Journal of Geotechnical Engineering Division,* Vol.120, No.GT5, pp.511-523.

Sitharam T. G., GovindaRaju L. and Sridharan A. (2004) "Dynamic properties and liquefaction potential of soils", *Current Science*, Vol.87, No.10, pp. 1370-1378.

Sitharam T. G. and Dash H. K. (2008) "Effect of non-plastic fines on cyclic behavior of sandy soils", GeoCongress 2008: Geosustainability and Geohazard Mitigation, pp. 319-326.

Steedman R. S., Ledbetter R. H. and Hynes M. E. (2000) "The influence of high confining stress on the cyclic behavior of saturated sand", *Soil Dynamics and Liquefaction 2000*, Geotechnical Special Publication No.107, Pak and Yamamuro eds., ASCE, Denver-Colorado, pp. 35-57.

Tatsuoka F., Ochi K., Fujii S., and Okamoto M. (1986) "Cyclic undrained triaxial and torsional shear strength of sands for different sample preparation methods", *Soils and Foundations*, Vol.26, No.3, pp.23-41.

Tatsuoka F. (1988) "Some recent developments in triaxial testing systems for cohesionless soils", Rep. No. 977., *Advanced Triaxial Testing of Soil and Rock*, ASTM STP., Philadelphia, PA.

Taylor D. W. (1948) *Fundamentals of Soil Mechanics*, Wiley, New York.

Terzaghi K. and Peck R. B. (1948) *Soil Mechanics in Engineering Practice*, John Wiley and Sons, New York.

Thevanayagam S., Fiorillo M. and Liang J. (2000) "Effect of non-plastic fines on undrained cyclic strength of silty sands", *Soil Dynamics and Liquefaction 2000*, Geotechnical Special Publication No.107, Pak and Yamamuro eds., ASCE, Denver-Colorado, pp. 77-91.

Tohno I., and Yasuda S. (1981) "Liquefaction of the ground during the 1978 Miyagiken-Oki earthquake," Soils and Foundations, Vol.21, No.3, pp.18-34.

Vaid Y. P. and Chern J. C. (1983a) "Effect of static shear on resistance of liquefaction", *Soils and Foundations*, Vol.23, No.1, pp. 47-60.

Vaid Y. P. and Chern J. C. (1983b) “Mechanism of deformation during cyclic undrained loading of saturated sands”, *Soil Dynamics and Earthquake Engineering*, Vol.2, No.3, pp. 171-177.

Vaid Y. P. and Negussey D. (1988) “Preparation of reconstituted sand specimens”, Adv. Triaxial Test. Soil and Rock ASTM STP 977:pp.405-417.

Vaid Y. P., Chung E. K. F. and Kuerbis R. H. (1990) “Stress path and steady state”, *Canadian Geotechnical Journal*, Vol.27, No.1, pp. 1-7.

Vaid Y. P. (1994) “Liquefaction of silty soils”, *Ground Failures Under Seismic Conditions*, Geotechnical Special Publication No.44, Prakash and Dakoulas eds., ASCE, Atlanta-Georgia, pp. 1-16.

Vaid Y. P. and Thomas J. (1995) “Liquefaction and postliquefaction behavior of sand”, *Journal of Geotechnical Engineering*, Vol.121, No.2, pp.163-173.

Vaid Y. P., Uthayakumar M., Sivathayalan S., Robertson P. K. and Hoffman B. (1995) “Laboratory testing of Syncrude sand”, *Proceedings of 48th Canadian Geotechnical Conference*, Vancouver, B. C., Vol.1, pp. 223-232.

Vaid Y. P. and Sivathayalan S. (1999) “Fundamental factors affecting liquefaction susceptibility of sands” Physics and Mechanics of Soil Liquefaction, Lade and Yamamuro eds., Balkema, Rotterdam, pp.105-120.

Vaid Y. P., Sivathayalan S. and Stedman D. (1999) “Influence of specimen reconstituting method on the undrained response of sand”, Geotechnical Testing Journal, Vol.22, No.3, pp. 187-195.

Vessely D. A., Reimer M., and Arango I. (1996) “Liquefaction susceptibility of soft alluvial silts in the Willamette Valley”, *Oregon Geology*, Vol.58, No.6, pp.142-145.

Voznesensky E. A., and Nordal S. (1999) “Dynamic instability of clays: an energy approach,” *Soil Dynamics and Earthquake Engineering*, Vol.18, pp. 125-133.

Vucetic M. (1988) “Normalized behavior of offshore clay under uniform cyclic loading,” *Canadian Geotechnical Journal,* Vol.25, pp. 33-41.

Vucetic M. (1994) “Cyclic threshold shear strains in soils,” *Journal of Geotechnical Engineering*, ASCE, Vol.120, No.12, pp. 2208-2228.

Vucetic M. and Dobry R. (1988) “Degradation of marine clays under cyclic loading”, *Journal of Geotechnical Engineering*, Vol.114, No.2, pp. 133-149.

Vucetic M. and Dobry R. (1991) “Effect of soil plasticity on cyclic response”, *Journal of Geotechnical Engineering*, Vol.117, No.1, pp. 89-107.

Wang S., Lu X. and Shi Z. (2010) “The effects of grain size distribution and structure on mechanical behavior of silty sand”, The *Open Ocean Engineering Journal*, Vol.3, pp.82-85.

Wang W. (1979), *Some findings in soil liquefaction,* Water Conservancy, and Hydroelectric Power Scientific Research Institute, Beijing, China.

Wijewickreme D., and Sanin M. V. (2010) “Postcyclic reconsolidation strains in low-plastic Fraser River silt due to dissipation excess pore-water pressures,” *Journal of Geotechnical and Geoenvironmental Engineering*, Vol.136, No.10, pp. 1347-1357.

Wu, J. (2002) *Liquefaction triggering and post-liquefaction deformation of Monterey 0/30 sand under uni-directional cyclic simple shear loading*, Ph.D. Dissertation, University of California, Berkeley, California, USA.

Yamamuro J. A. and Lade P. V. (1999) “Experiments and modeling of silty sands susceptible to static liquefaction”, *Mechanics of Cohesive-Frictional Materials*, Vol.4, No.6, pp. 545-564.

Yamamuro J. A., Covert K. M. and Lade P. V. (1999) “Static and cyclic liquefaction of silty sands” Physics and Mechanics of Soil Liquefaction, Lade and Yamamuro eds., Balkema, Rotterdam, pp.55-66.

Yamamuro J. A. and Covert K. M. (2001) “Monotonic and cyclic liquefaction of very loose sands with high silt content”, *Journal of Geotechnical and Geoenvironmental Engineering*, Vol.127, No.4, pp.314-324.

Yamamuro J. A. and Wood F. M. (2004) “Effect of depositional method on the undrained behavior and microstructure of sand with silt”, *Soil Dynamics and Earthquake Engineering,* Vol.24, pp.751-760.

Yasuda S., Wakamatsu K. and Nagase H. (1994) “Liquefaction of artificially filled silty sands”, *Ground Failures Under Seismic Conditions*, Geotechnical Special Publication No.44, Prakash and Dakoulas eds., ASCE, Atlanta-Georgia, pp. 91-104.

Yasuhara K., Yamanouchi T., and Hirao K. (1982) “Cyclic strength and deformation of normally consolidated clay,” *Soils and Foundations*, J.G.S., Vol.22, No.3, pp.77-91.

Yasuhara K., Hirao K., and Hyde A. F. L. (1992) “Effects of cyclic loading on undrained strength and compressibility of clay,” *Soils and Foundations*, J.G.S., Vol.32, No.1, pp.100-116.

Yasuhara K., Murakami S., Toyota N., Hyde A.F.L. (2001). “Settlements in fine grained soils under cyclic loading”, *Soils and Foundations*, J.G.S., Vol.41, No.6, pp.25-36.

Yasuhara K., Murakami S., Song B. W., Yokokawa S. and Hyde A. F. L. (2003) “Postcyclic degradation of strength and stiffness for low plasticity silt”, *Journal of Geotechnical and Geoenvironmental Engineering*, Vol.129, No.8, pp. 756-769.

Youd T. L., Harp E. L., Keefer D. K., and Wilson R. C. (1985) “The Borah Peak, Idaho earthquake of October 28, 1983—liquefaction,” Earthquake Spectra, EERI, Vol.2, No.1, pp.71-89.

Youd T. L., Idriss I. M., Andrus R. D., Arango I., Castro G., Christian J. T., Dobry R., Finn W. D. L., Harder L. F., Hynes M. E., Ishihara K., Koester J. P., Liao S. C., Marcuson W. F., Martin G. R., Mitchell J. K., Moriwaki Y., Power M. S., Robertson P. K., Seed R. B., Stokoe K. H. (2001) "Liquefaction resistance of soils: summary report from the 1996 NCEER and 1998 NCEER/NSF workshops on evaluation of liquefaction resistance of soils", *Journal of Geotechnical and Geoenviromental Engineering*, ASCE, Vol.127, No.10, pp. 817-833.

Yılmaz M. T., Pekcan O., Bakır B. S. (2004). "Undrained cyclic shear and deformation behavior of silt-clay mixtures of Adapazarı, Turkey", *Soil Dynamics and Earthquake Engineering,* Vol.24, Issue.7, pp.497-507.

Yilmaz M. T. and Bakir B. S. (2009) "Capacity of shallow foundations on saturated cohesionless soils under combined loading," *Canadian Geotechnical Journal, Vol.46*, pp. 639-649.

Zeevaert L. (1991) "Seismosoil dynamics of foundations in Mexico City Earthquake, 1985", *Journal of Geotechnical Engineering*, Vol.117, No.3, pp.376-427.

Zhou J. and Gong X. (2001) "Strain degradation of saturated clay under cyclic loading", Can. Geotech. Journal, Vol.38, pp. 208-212.

Zlatovic S. and Ishihara K. (1997) "Normalized behavior of very loose non-plastic soils: effects of fabric", *Soils and Foundations,* Vol.37, No.4, pp.47-56.

APPENDIX

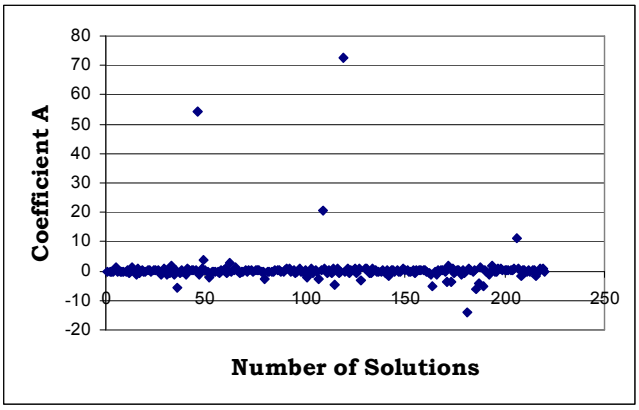

(a)

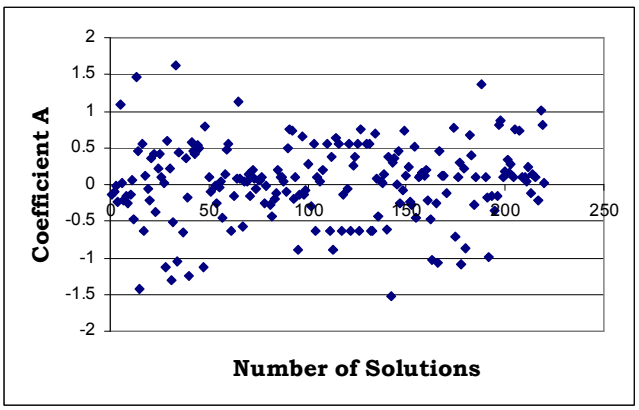

(b)

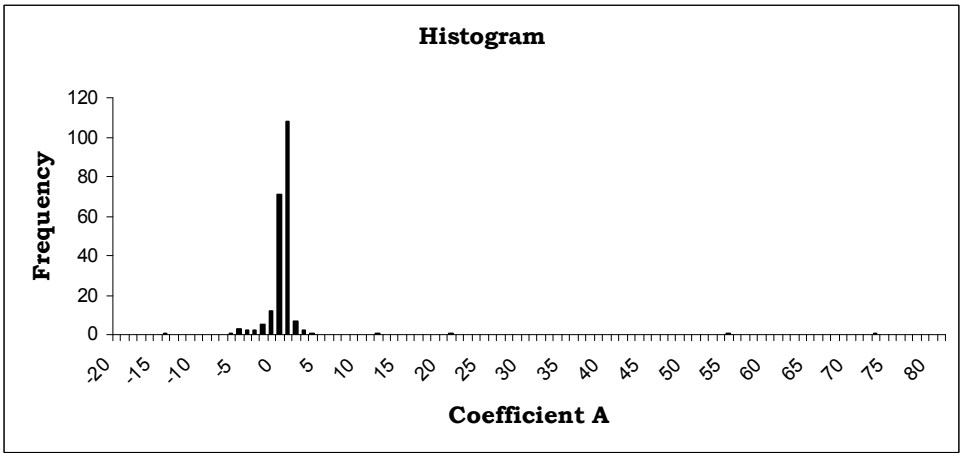

(c)

Figure A.1 Coefficient A: data scattering plot (a) before filtering the outliers and (b) after filtering the outliers, (c) histogram.

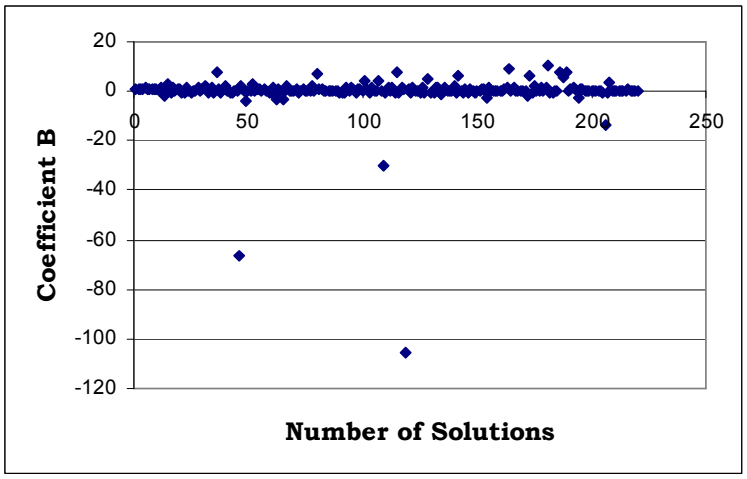

(a)

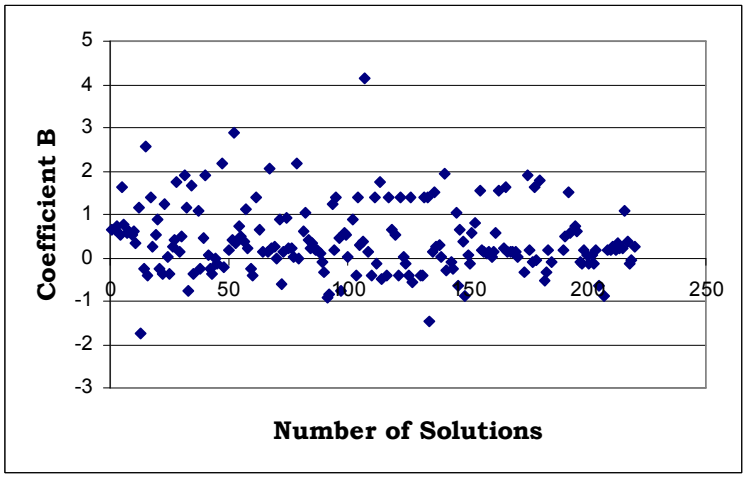

(b)

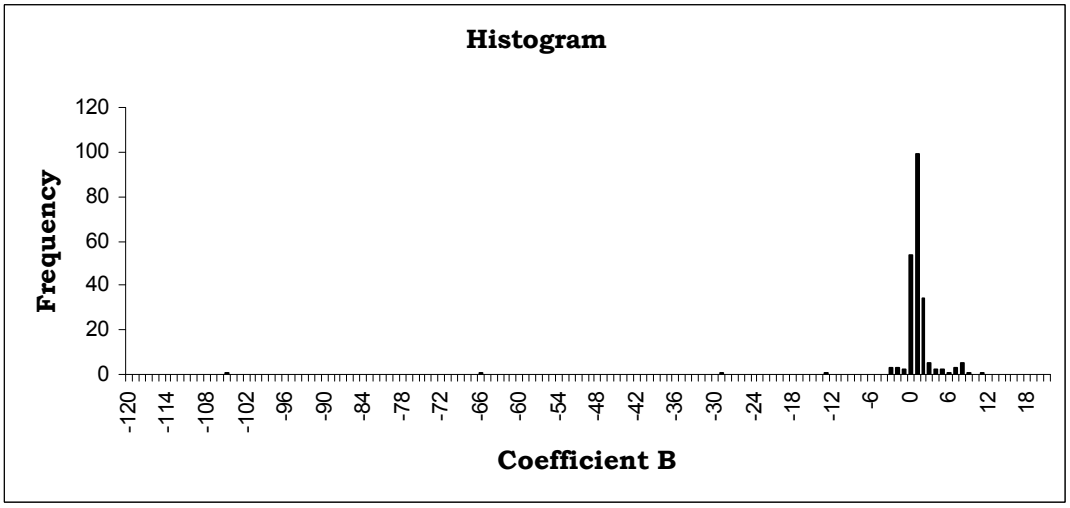

(c)

Figure A.2 Coefficient B: data scattering plot (a) before filtering the outliers and (b) after filtering the outliers, (c) histogram.

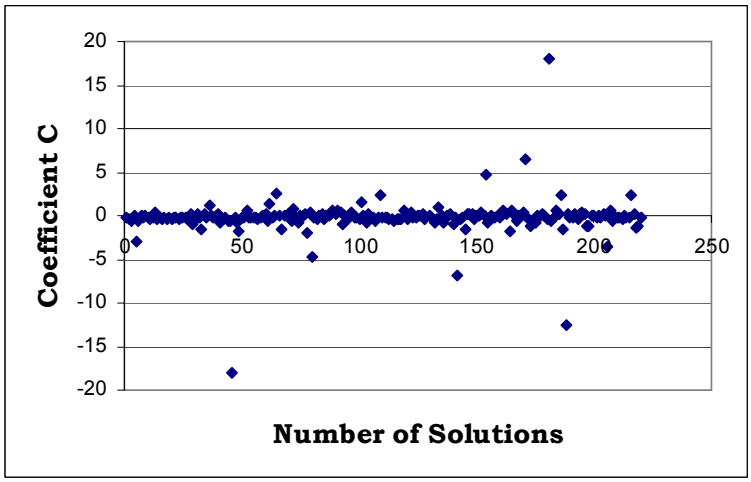

(a)

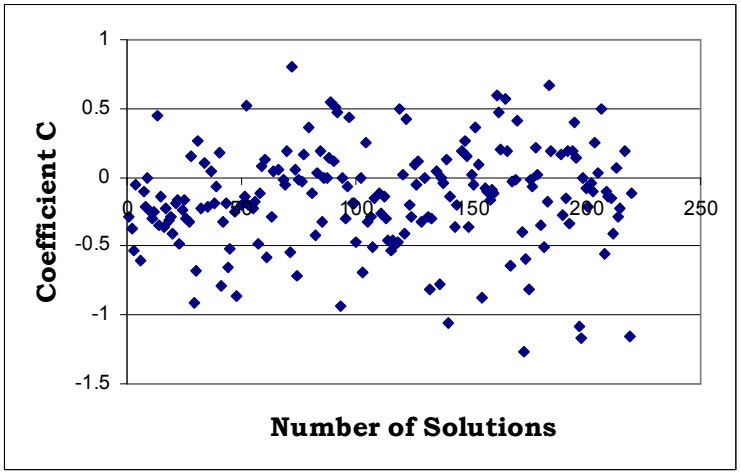

(b)

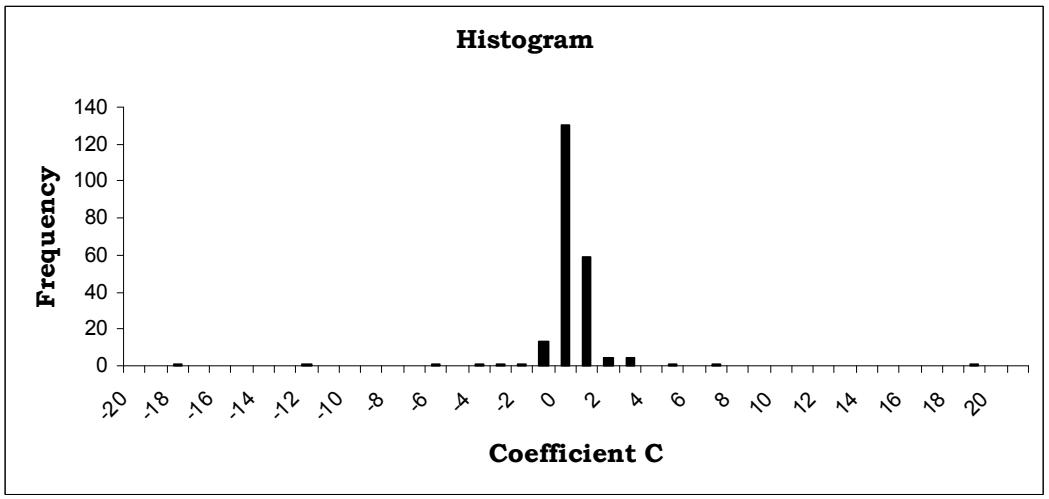

(c)

Figure A.3 Coefficient C: data scattering plot (a) before filtering the outliers and (b) after filtering the outliers, (c) histogram.

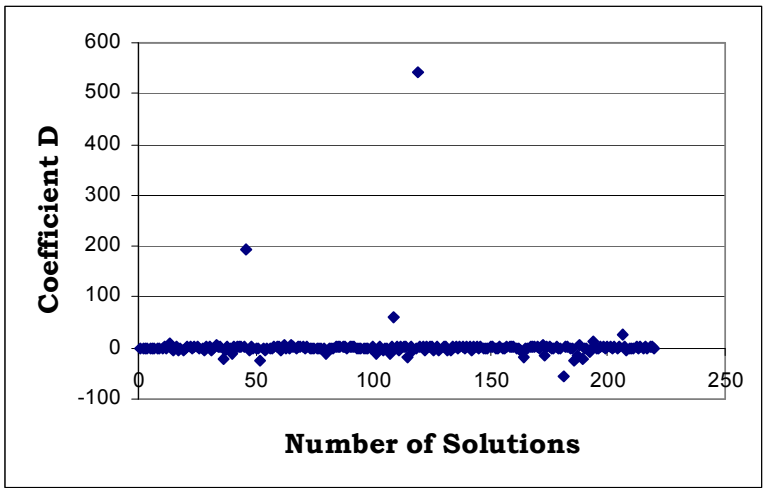

(a)

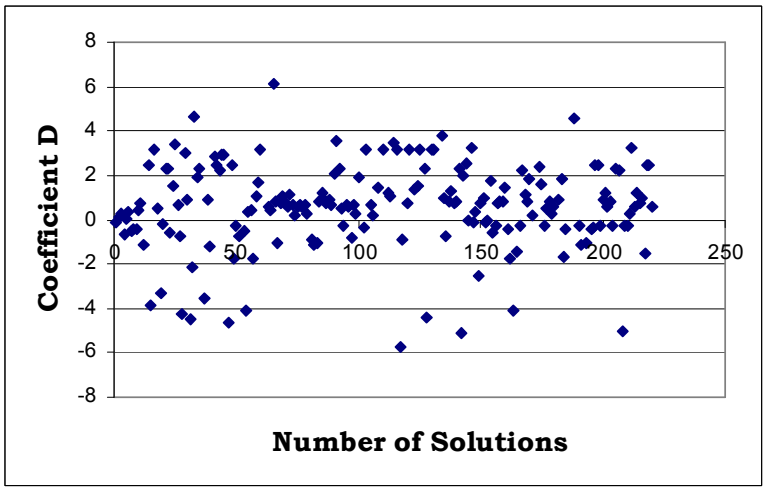

(b)

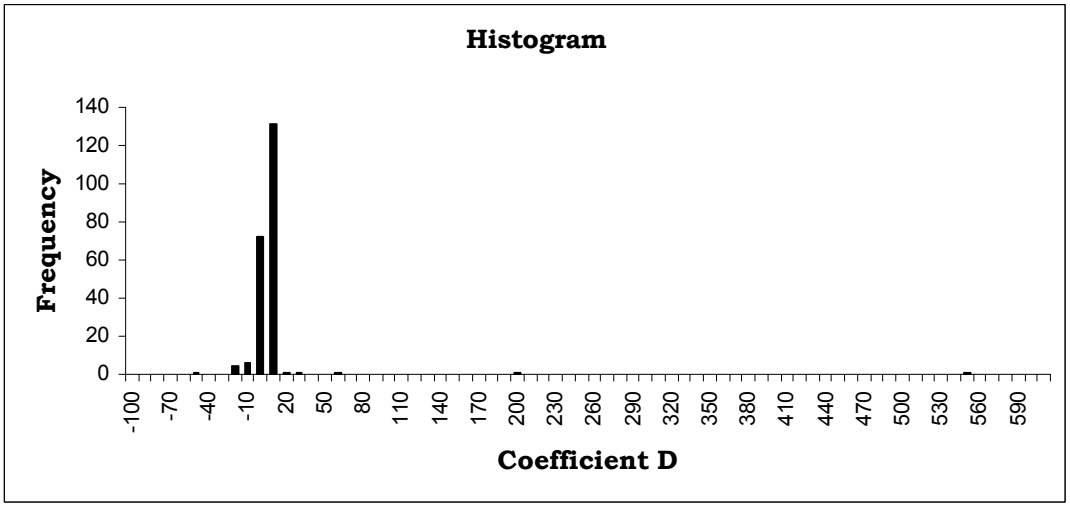

(c)

Figure A.4 Coefficient D: data scattering plot (a) before filtering the outliers and (b) after filtering the outliers, (c) histogram.

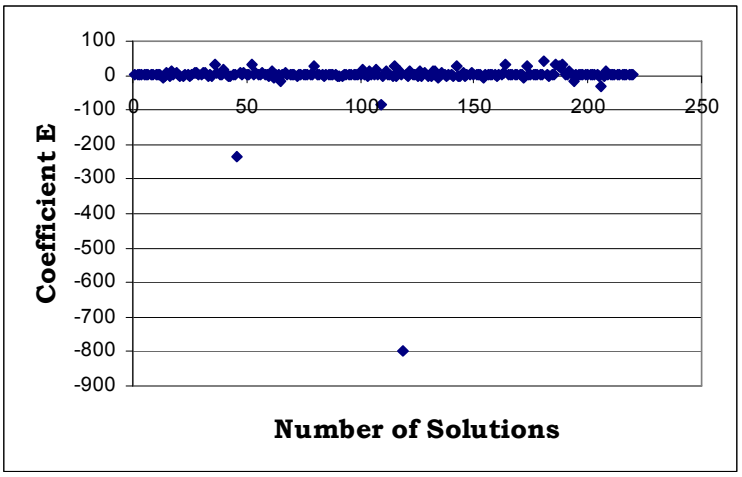

(a)

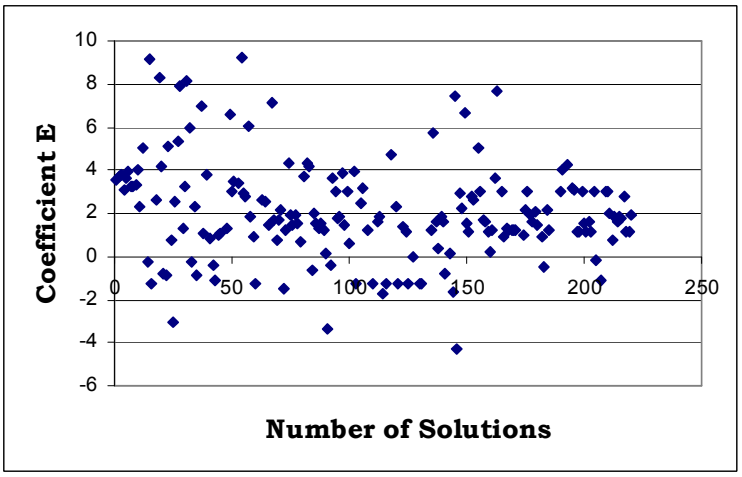

(b)

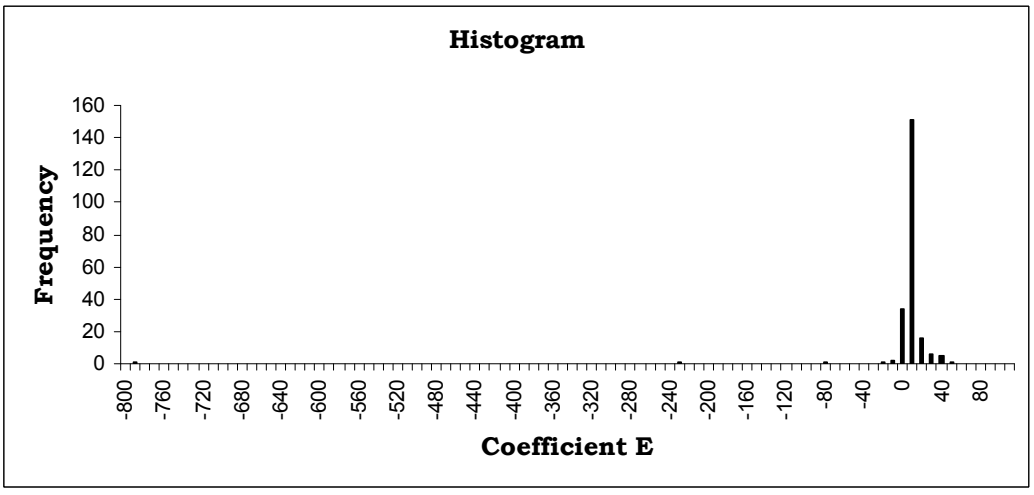

(c)

Figure A.5 Coefficient E: data scattering plot (a) before filtering the outliers and (b) after filtering the outliers, (c) histogram.

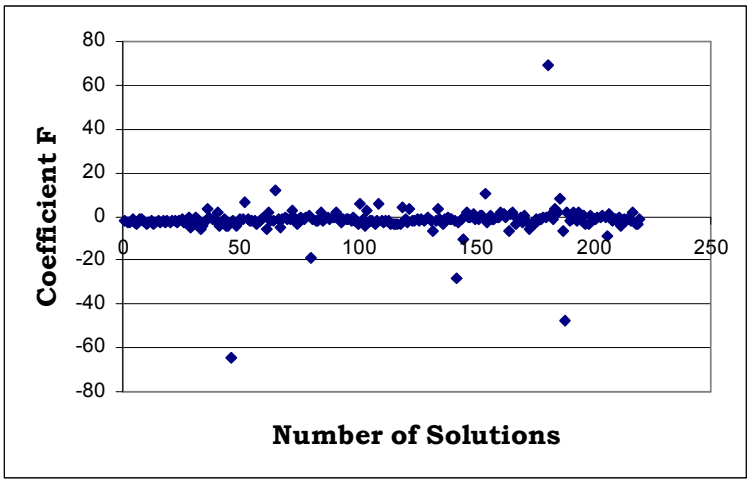

(a)

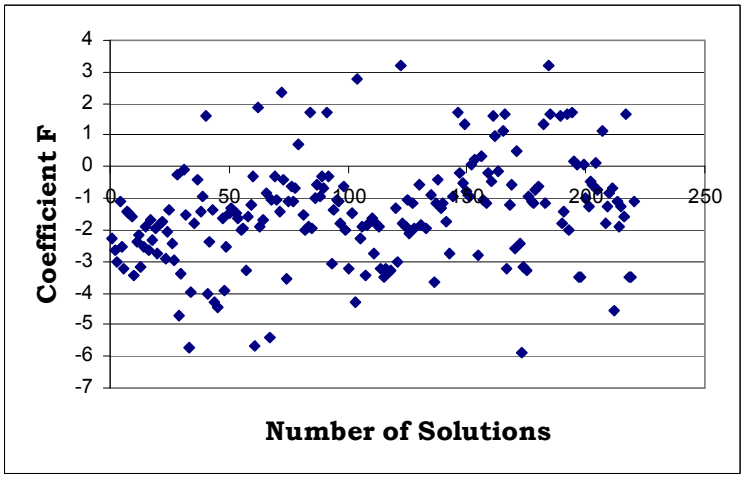

(b)

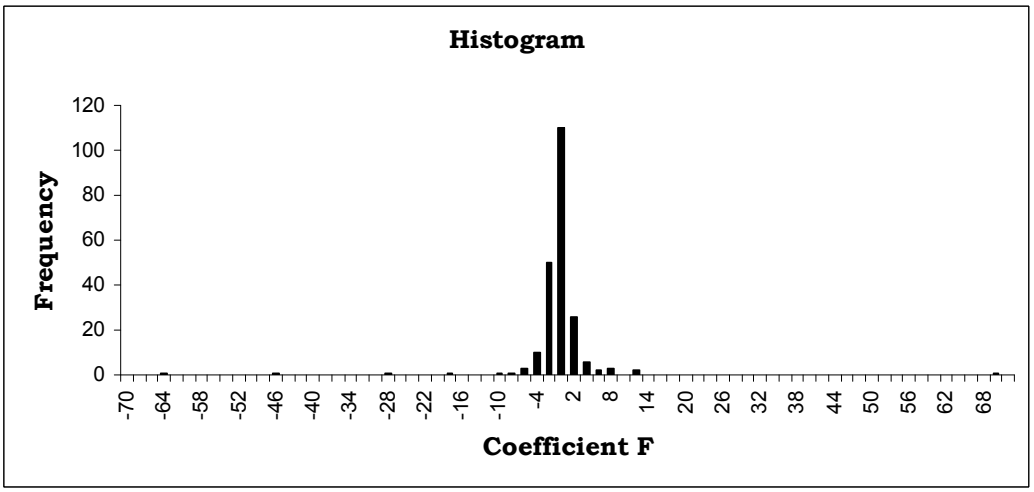

(c)

Figure A.6 Coefficient F: data scattering plot (a) before filtering the outliers and (b) after filtering the outliers, (c) histogram.

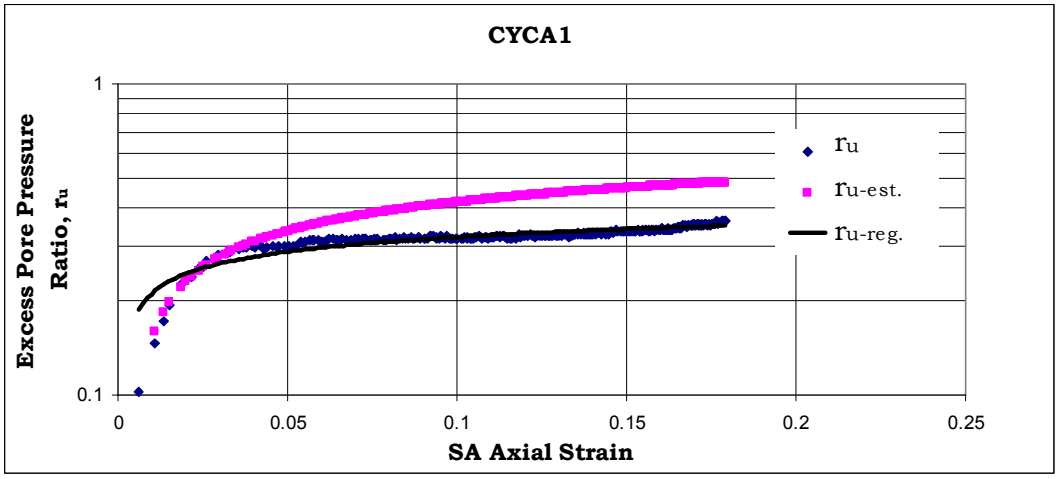

Figure A.7 Actual, fitted and estimated r_u-ε_a relationships for the test CYCA1

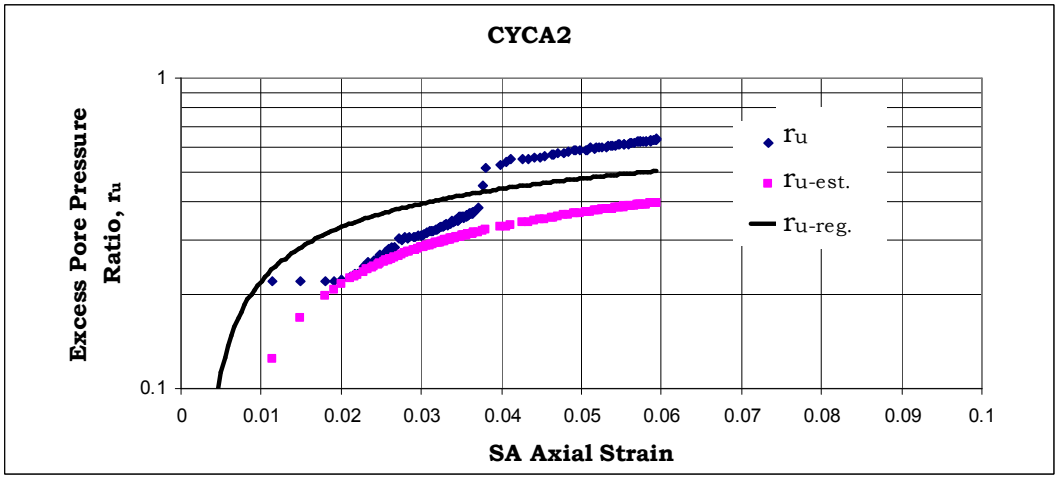

Figure A.8 Actual, fitted and estimated r_u-ε_a relationships for the test CYCA2

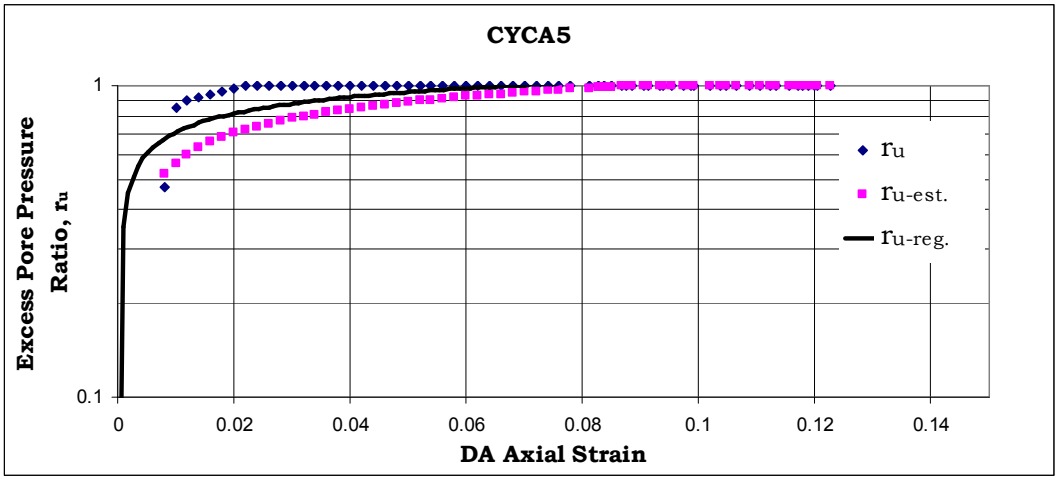

Figure A.9 Actual, fitted and estimated r_u-ε_a relationships for the test CYCA5

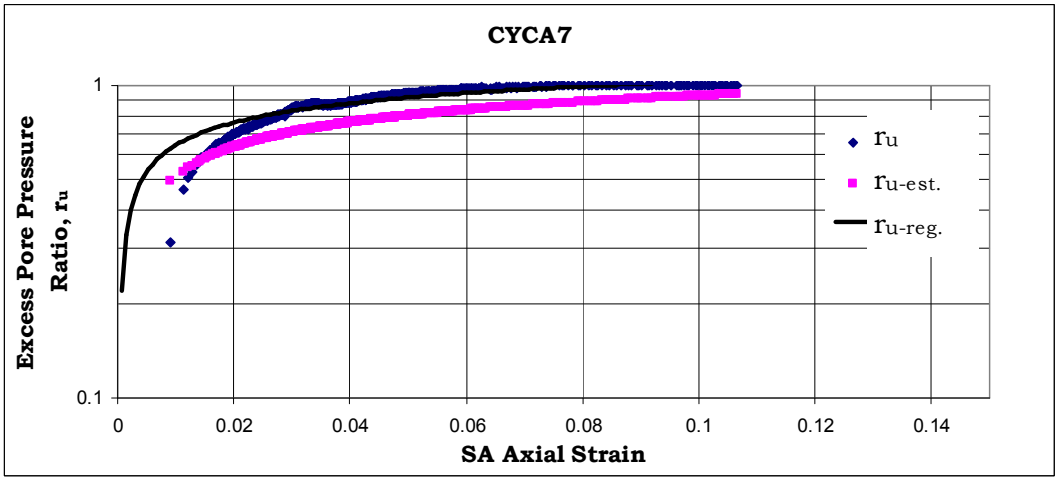

Figure A.10 Actual, fitted and estimated r_u-ε_a relationships for the test CYCA7

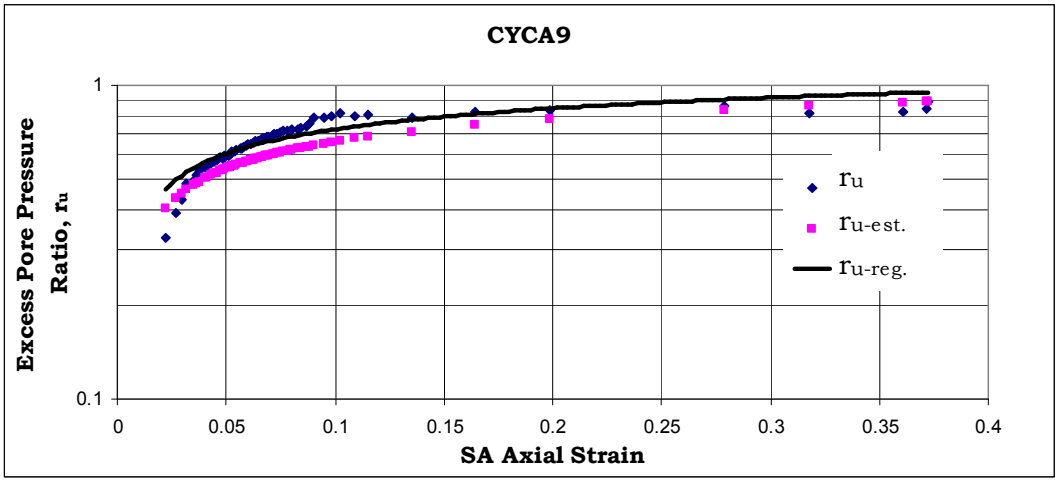

Figure A.11 Actual, fitted and estimated r_u-ε_a relationships for the test CYCA9

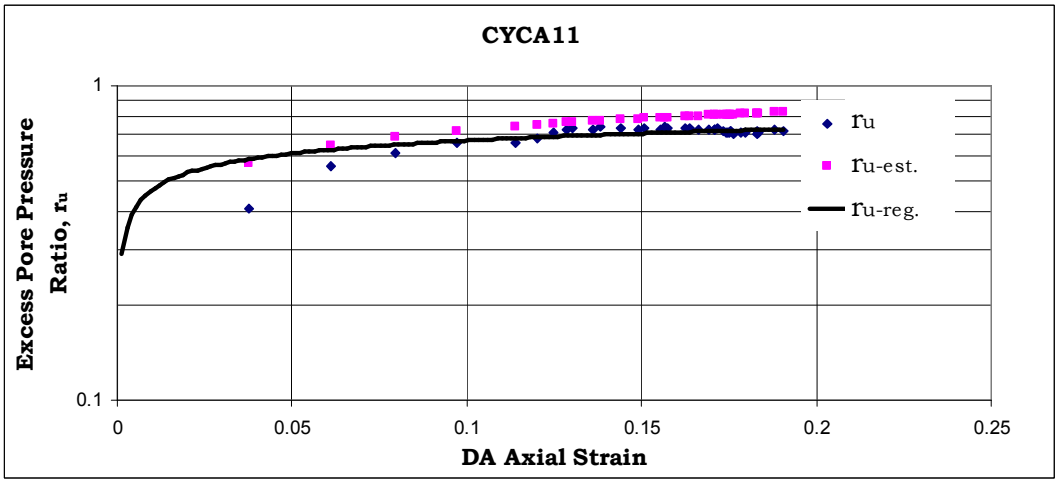

Figure A.12 Actual, fitted and estimated r_u-ε_a relationships for the test CYCA11

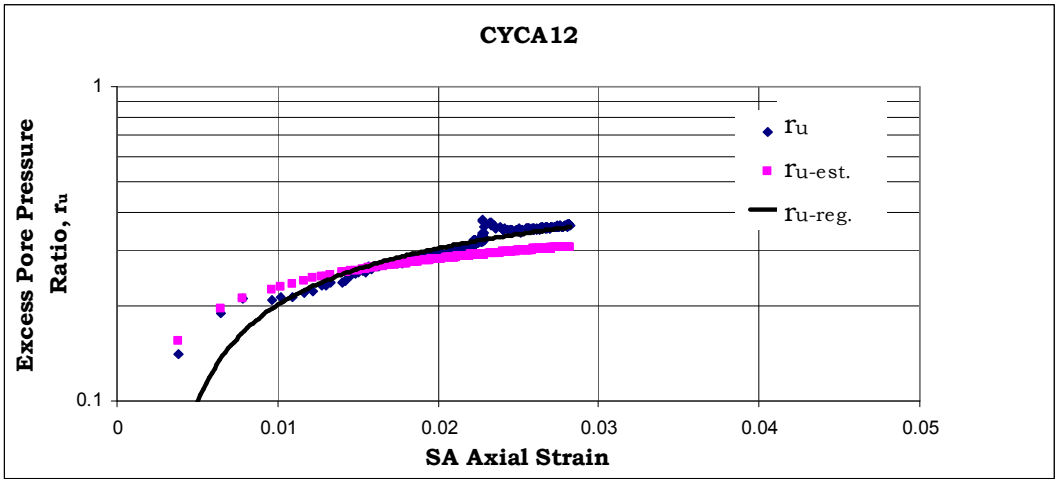

Figure A.13 Actual, fitted and estimated r_u-ε_a relationships for the test CYCA12

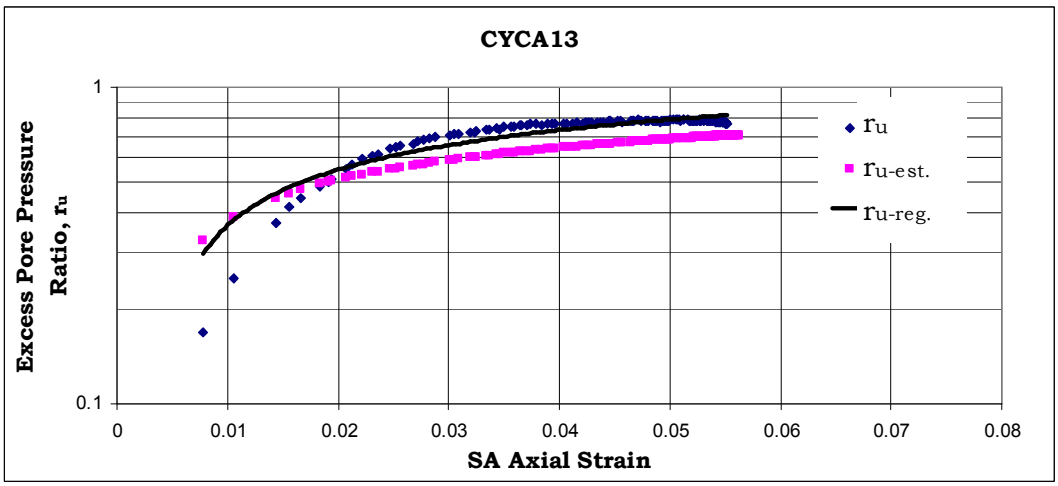

Figure A.14 Actual, fitted and estimated r_u-ε_a relationships for the test CYCA13

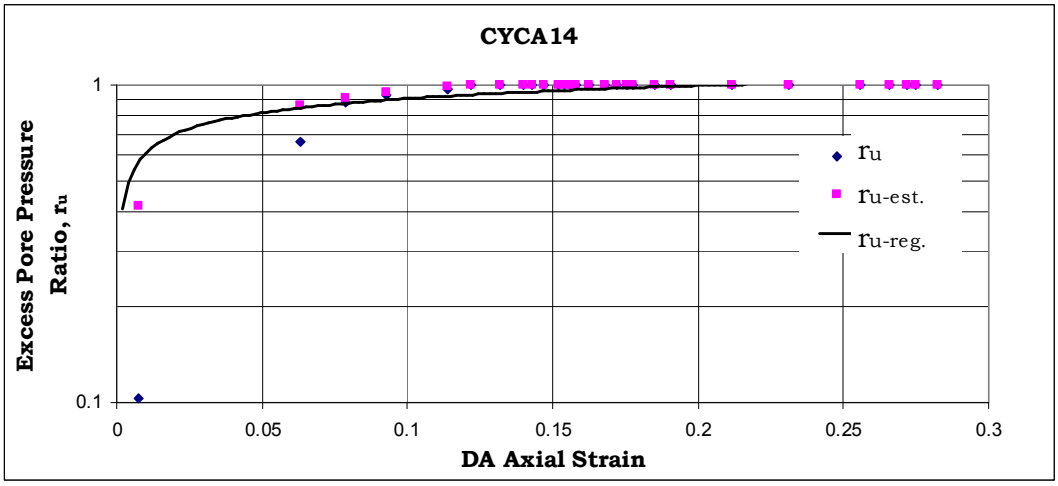

Figure A.15 Actual, fitted and estimated r_u-ε_a relationships for the test CYCA14

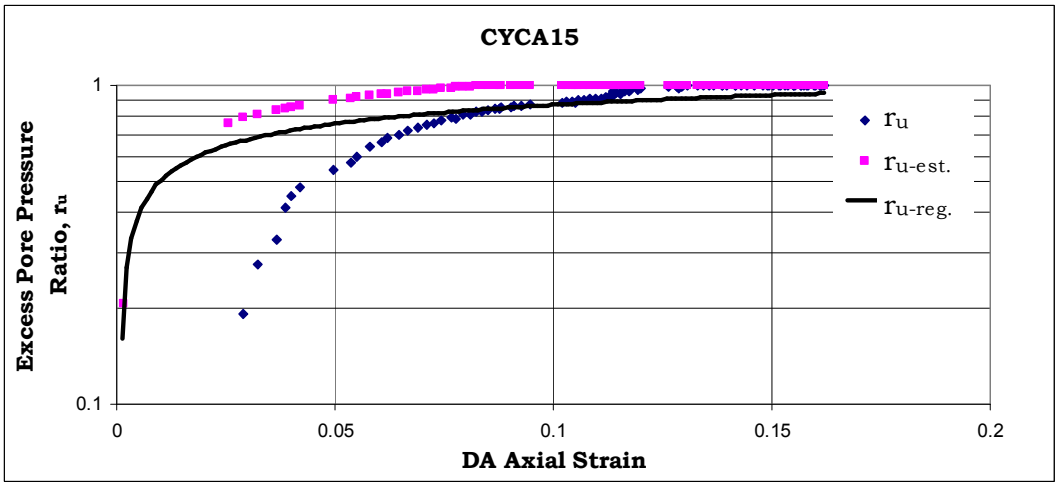

Figure A.16 Actual, fitted and estimated r_u-ε_a relationships for the test CYCA15

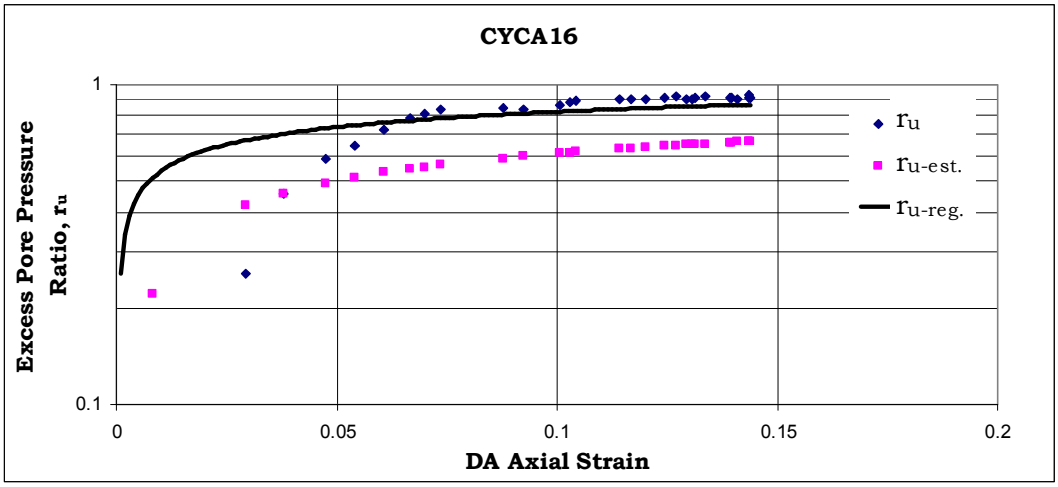

Figure A.17 Actual, fitted and estimated r_u-ε_a relationships for the test CYCA16

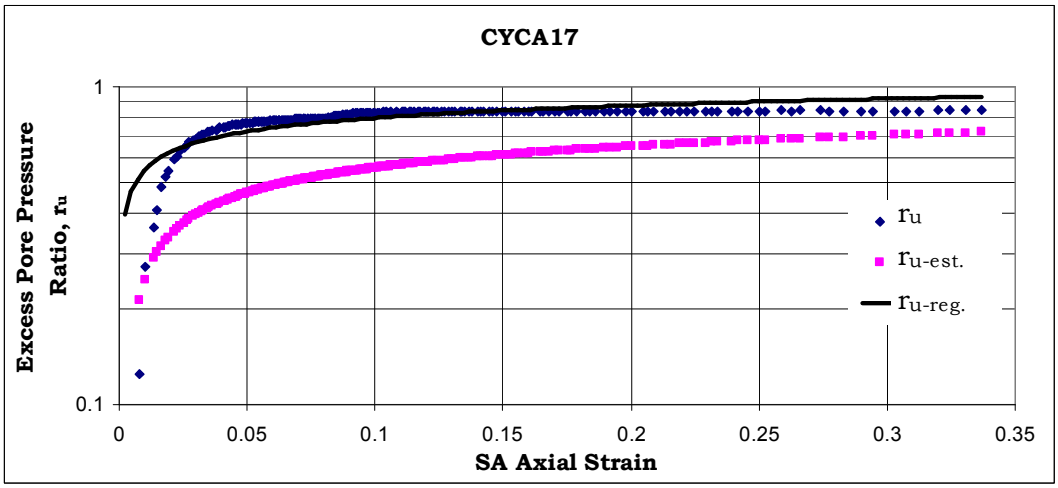

Figure A.18 Actual, fitted and estimated r_u-ε_a relationships for the test CYCA17

CURRICULUM VITAE

PERSONAL INFORMATION

Surname, Name: Saglam, Selman
Nationality: Turkish (TC)
Date and Place of Birth: 20 August 1978, Elazig.
Marital Status: Married
Phone: +90 312 210 5469
email: selman@metu.edu.tr

EDUCATION

Degree/Interval	Institution
Visiting Scholar /2010-2011	University of Southern California, LA, CA, USA.
MS/ 2001-2003	Geotechnical Engineering, Dokuz Eylul University, Izmir
BS/1997-2001	Civil Engineering, Dokuz Eylul University, Izmir

SCHOLARSHIP and AWARDS

TUBITAK-GRANT FOR DOCTORAL FELLOWSHIP (2007-2009)
AWARD FOR EXCELLENCE in UNDERGRADUATE EDUCATION (Given for the students graduated with a level in the first 10%)

WORK EXPERIENCE

Year	**Place**	**Enrollment**
2004-Present	METU	Research Assistant
July-Sept., 2002	Calis Engineering Design Office	Engineer
2001-2003	Dokuz Eylul University, Works of Revolving Funds	Engineer
July-Aug., 2000	Kutlutas AS	Intern Engineering Student
July-Aug., 1999	Guris AS	Intern Engineering Student

RESEARCH PROJECTS

EUROPEAN UNION SERIES PROJECT-Dynamic Response of Box Shaped Underground Structures.

- *Date:* September 2009-January 2012
- *Title:* Researcher
- *Project Partners:* METU, IFFSTAR (LCPC) Laboratories Nantes-France, Technical University of Kaiserslautern-Germany

PUBLICATIONS

- **Sağlam, S.,** Özden, G. (2004) "Geoteknik mühendisliği eğitiminde zorluklar ve çözüm yolları", İMO, Türkiye İnşaat Mühendisliği XVII Teknik Kongre ve Sergisi, 15-17 Nisan 2004, İstanbul.
- Bakır, B. S., **Sağlam, S**. (2006), "Discussion of "Liquefaction-induced lateral spreading at İzmit Bay during the Kocaeli (İzmit) Earthquake" by K. Onder Cetin, T. Leslie Youd, Raymond B. Seed, Jonathan D. Bray, Jonathan P. Stewart, H. Duran Durgunoglu, W. Lettis, and M. Tolga Yılmaz", *Journal of Geotechnical and Geoenviromental Engineering*, ASCE, Vol.132, No.7, pp. 953-955.

- Erdemgil, M., **Sağlam, S.**, Bakır, B. S. (2007) "Utilization of highly expansive polymer injection to mitigate seismic foundation failure for existing structures", 8th Pasific Conference on Earthquake Engineering, 5-7 Dec. 2007, Singapore.
- Ertuğrul, Ö. L., **Sağlam, S.**, Özkan, M. Y. (2008) "Excitation and flexibility effects on dynamic response of cantilever retaining walls", ASCE GEESD IV, Geotechnical Earthquake Engineering and Soil Dynamics Conference, 2008, Sacremento, USA.
- Üçer, S., **Sağlam, S.,** Bakır, B. S. (2009) "Seismic slope stability assessment of a construction site at Bandırma, Turkey", 2nd International Conference on New Developments in Soil Mechanics and Geotechnical Engineering, 28-30 May 2009, Near East University, Nicosia, North Cyprus.
- Ülgen, D., **Sağlam, S.** (2009) "Seismic stability assessment of an existent countermeasure against landslide in an urban area", 2nd International Conference on New Developments in Soil Mechanics and Geotechnical Engineering, 28-30 May 2009, Near East University, Nicosia, North Cyprus.
- **Sağlam, S.,** Bakır, B. S. (2009) "Coastal ground failures at İzmit Bay during the 1999 Kocaeli (İzmit) Earhquake", Sakarya International Symposium of Earthquake Engineering, Oct.1-3, Sakarya, Turkey.
- **Sağlam, S.,** Bakır, B. S. (2010) "Cyclic response of reconstituted low plasticity silt", 5th International Conference on Recent Advances in Geotechnical Earthquake Engineering and Soil Dynamics and Symposium in Honor of Professor I. M. Idriss, May 24-29 2010, San Diego, USA.